eman ta zabal zazu

Universidad del País Vasco
Euskal Herriko Unibertsitatea

Facultad de Ciencia y Tecnología
Departamento de Biología Molecular y Biomedicina

IDENTIFICATION OF TICK SALIVA ANTIGENS AS VACCINE CANDIDATES AND IMMUNOTHERAPEUTICS

TESIS DOCTORAL

Julen Tomás Cortázar

2017

This thesis has been possible thanks to a contract from CIC bioGUNE from 2013 through 2017, as well as funds from the European Union through the ANTIDotE project.

The experimental work has been financed by the European Union in collaboration with the ANTIDotE consortium (agreement number 602272) and the Department of Education of the Basque Government (grant number PI-2013-49).

ACKNOWLEDGEMENTS

*Ocasionalmente, solemos pecar de soberbia y de arrogancia. Sin embargo, en esta historia escaso es el narcisismo y mucho es aquello que elogiar y que agradecer a todas las personas que voy a citar a continuación. Principalmente a mi director de tesis, Juan Anguita, quien me dio esta ansiada y tan buscada oportunidad de llevar a cabo un proyecto que espero culminar pronto. (**Gracias Juan)**. Gracias por tu confianza, ayuda y apoyo. He aprendido mucho de ti. Ciertamente, cuatro años y medio dan para muchas discusiones, pero también muy buenos momentos y risas. De un amigo: Te debo una vida que no sé cómo devolvértela. Y este pedazo de vida la he compartido en "JA lab" con gente muy especial con la que he reído, aprendido, disfrutado, peleado y querido. De cada uno me llevo algo. Entre ellos, como no, "mami Itzi". (**Mila esker Itzi)**, por todo tu apoyo, ayuda y por ser tan buena profesora. Gracias por esos días de jarana que tanto me gustan, vaso en mano, bocata, cena o talo y fiesta. Nico, y las interminables risas que nos hemos echado, con sus fábulas y anécdotas del pueblo y por tus consejos en épocas de crisis. Cantábamos canciones tan dispares como Mr. Tambourine Man de Bob Dylan o Fosa común de Gatillazo a esas horas intempestivas en las que de repente aparece Santa o Salva con la escoba. ¡Vete para casa, sinvergüenza! Decían. Siempre haciéndolo bien. (**Gracias Nico)**. ¡A ver Atondo! A ti creo que te conquisto mejor con esto: Egin nahi dodazan gauza guztixek egin, erratzeko aukera bat eduki nahi dot, ta indarra dagoen artien, bidiek zabalduz, bai!!!! zugan sinestu!!!! Mila esker por toda tu ayuda**.** Benetan. Espero que haya muchos más conciertos de Amaral, y de Gatibu por supuesto **(Eskerrik asko Esti)**. Como no, Ana. Será por algo que estos tres meses que has estado fuera te he echado menos. Aunque realmente creo que hablo en nombre de todo el laboratorio. Esa felicidad contagia a todo el mundo, no cambies nunca. Gracias por esos abrazos y por estar ahí en momentos en los de poca cordura. (**Eskerrik asko, Ana)**. Leti A., simplemente gracias por tu sinceridad, tus consejos y ayuda en las presentaciones, charlas, publicaciones, tesis y demás historias serias. (**Eskerrik asko Leti A.**). Gracias por esas avellanas, almendras y nueces que tu ama con mucho cariño nos pela. Por cierto, un día de extremo ayuno abrí ese cajón de vicio y pecado. Sin duda iré al infierno, si llego. Burla. Miguel, claro que sí. Yo soy de Miguel. Gracias por toda tu ayuda con el papel de Salp15. Sin ti no hubiera sido lo mismo. La gente de Barakaldo nos entendemos a la perfección. Hemos transitado las mismas calles durante muchos años y simplemente*

*una mirada lo dice todo (**Mila esker Miguel**). Rafa, gracias por enseñarme nuevas técnicas, las emplearé siempre que pueda. Gracias por tus cervezas artesanas que me traes de vez en cuando y por proveerme de otras cosas que sólo tú y yo sabemos. Risas. Héctor, gracias por la tanasa y por tanto bicho que has traído al laboratorio. La tanasa es una historia de amor que nunca va a acabar. Un beso. (**Gracias Héctor**). Realmente no lo sabe nadie, pero compartimos cama todos los días. Es un secreto a voces. Leti S., Leti reina, gracias por preguntarme todos los días si necesito algo como un gel. ¡Ah, sí! Luego te canto la canción de la mosca ji ji, ja ja. Yo también me voy de aquí en coche de cristal. Eso sí, espero no enfermar y morir como ella. Guiño. (**Gracias Leti S.**). Ainize, gracias por salvarme la vida tantas veces, tirarme el flotador y acercarme hasta la orilla. Ahí no me ahogo (**Gracias Ainize**). Diegu gallu, qué chiste más simple. Admito que fui yo. Los primeros días me daba cosa soltártelo. Ahora, en cambio, nos echamos unas risas. Es lo que tiene esa complicidad que nos hace ser fuertes. Gracias por los ELISAs, clonajes y demás marrones. Gracias por tus ánimos y por aquella charla filosófica-sicológica que tuvimos hace poco. (**Gracias Diego**). Ainhoa, aunque me hubiese gustado más, poco tiempo nos ha quedado. Que te vaya todo muy bien y espero que consigas la beca y saques muchos artículos y cositas (**Gracias Ainhoa**).*

*Arkaitz, aquí se acaba el camino. Aunque como decía Machado, no hay camino, sino convicción. Gracias por todos tus ánimos y por preguntarme con tanta asiduidad por el proyecto. Gracias por tu confianza para ese maravilloso papel (**Eskerrik asko Arkaitz**). Gracias a todo el labo de AC, y a la gente con la que tuve más contacto cuando éramos JAC: Lore, Amatxu, Alfredo, Nati, Leire, Pili, Soni, Amaia y Patri (**Eskerrik asko, chic@s**, se os quiere)*

*Gracias al laboratorio de Rosa Barrio por el papel de Salp15. En especial a Jim, que me enseñó a mimar las células S2 y producir kilos de proteína activa. (**Thank you Jim et ipsum**). Pero también a Cora, que te debo una foto, y a Lutxi, Imma y Maria.*

*Gracias a Encarni por la organización de todas esas sidrerías que nos lo passamos tan bien (**Mila esker, Encarni**). Y como no, gracias Marta, por esas quedadas por las calles de Bilbao o esas comidas en ese pedazo de terraza con el Guggenheim al fondo. También porque siempre estás dispuesta para hablar de cualquier cosa, sea relativo al laboratorio o no (**Eskerrik asko, Marta**).*

*Thanks also to Dr. Utpal Pal and his group for those three months that I was in the Department of Veterinary Medicine at University of Maryland (**Thanks Utpal**).*

*Thanks to Juraj, Quentin, Meghna, Xuran, Shelby, Preety, Kamoltip and Xiuli (**Thanks guys**).*

*Gracias a todo el edificio 800 por acogerme tan bien. Gracias Adriana. Que aunque no consiguiésemos sacar ni un maldito cristal, esas proteínas me hicieron sacar de ti todo lo que ahora sé de purificación de proteínas (**Gracias Adriana**). Gracias Alberto por lo mismo, y por tu paciencia (**Gracias Alberto**). Agradecer también a la gente de Aitor Hierro y Alfonso Martínez que tanto me han ayudado, aconsejado y enseñado: Ander, Maria, Miguel, Carlos, Iker y Paula. Gracias a Paco y Nekane también y a la gente de su labo, Geor y Amaia, por ese papel de Salp15 y por iniciarme en la purificación de proteínas insolubles. Poco a poco voy haciendo una montañita (**Gracias chic@s**). Gracias por esas cenas y comidas en el txoko o en alguna casa. Gracias Bea y gracias Bego.*

Como no pueden faltar también en estos agradecimientos. Gracias a:

- *A mi cuadrilla de Barakaldo, en especial a Kirtsan, Gorka, Izas, Iker y Jon, por haberme aguantado este año tan raro.*
- *Gracias a un tipo llamado Yoga, y sus ejercicios de relajación.*
- *A todo el pueblo de Godojos, amig@s, prim@s, ti@s y como no, a ese pedazo de castillo que todo lo ve.*
- *Al trio calavera, Iskander y Pablo.*
- *Al grupo Lab Meetings for Nobel Prize: Marta, Maria y Joana.*
- *A Ekaitz Agirregoitia por sus consejos.*
- *A Aritz Garcia por esa maravillosa portada.*
- *A toda mi familia, Tomás-Cortázar. En especial a mis prim@s Lander, Luis, Marta, Kristina, Jon, Oihane, Irati, Ibai, Eder y Jagoba*

AITA, AMA, TXABI, AITZIBER, UXUE ETA NAROA, ESKERRIK ASKO. MAITE ZAITUZTET.

NON GOGOA, HAN ZANGOA

Hau da ene ondasun guzia

Hau da ene etxea, hau da
ene aulkia, hau da ene ohea,
hau da ene ondasun guzia.
Bakardade eta isiltasun
hau da ene jabego bakarra.
Mila jostorratz herdoildu aldean,
leihorik gabeko begirada,
zafrada garratz bat bihotzean,
hauxe da nik dudan guzia:
hilda nagoela esan dezaket?
Amagandik irten nintzen bezala
irtengo naiz endredo honetatik.
Aterik zabaldu ezin eta
—ba ote da hilobi estuagorik?—
funtzionarioen begi kliskak
mirillan igartzean ohartzen naiz
bizirik nagoela.

Joseba Sarrionaindia

COMO TÚ

Así es mi vida,
piedra,
como tú. Como tú,
piedra pequeña;
como tú,
piedra ligera;
como tú,
canto que ruedas
por las calzadas
y por las veredas;
como tú,
guijarro humilde de las carreteras;
como tú,
que en días de tormenta
te hundes
en el cieno de la tierra
y luego
centelleas
bajo los cascos
y bajo las ruedas;
como tú, que no has servido
para ser ni piedra
de una lonja,
ni piedra de una audiencia,
ni piedra de un palacio,
ni piedra de una iglesia;
como tú,
piedra aventurera;
como tú,
que tal vez estás hecha
sólo para una honda,
piedra pequeña
y
ligera...

León Felipe

TABLE OF CONTENTS

TABLE OF CONTENTS

ABBREVIATIONS

ABBREVIATIONS

>20TBY: More than 20 Tick Bites per Year.
64TRP: 64 Truncated Protein.
AAALAC: Association for Assessment and Accreditation of Laboratory Care Animal International
Actb: Actin Beta.
AKR: Akirins.
ANOVA: Analysis Of Variance.
APC: Antigen Presenting Cells.
Balb/c mice: Derived from albino mice stocks originally disseminated by Bagg (1913) to Snell in 1932 that has an albino coat with genotype c.
BAM: Binary Alignment/Map.
BC: Bottom of the Capsule.
BCA: Bicinchoninic Acid Assay.
BD: Becton Dickinson.
BLAST: Basic Local Alignment Search Tool.
BM86: *Boophilus microplus* 86.
BM95: *Boophilus microplus* 95.
C57BL/6: C57 black 6.
CB6F1: Charles River breeds hybrid mouse model.
CD11b: Cluster of Differentiation 11.
CD16: Cluster of Differentiation 16.
CD23: Cluster of Differentiation 23.
CD25: Cluster of Differentiation 25.
CD28: Cluster of Differentiation 28.
CD32: Cluster of Differentiation 32.
CD3ε: Cluster of Differentiation 3 epsilon.
CD4: Cluster of differentiation 4.
CD44: Cluster of Differentiation 44.
CD45: Cluster of Differentiation 45.
CD69: Cluster of Differentiation 69.
CD73: Cluster of Differentiation 73.
CD8: Cluster of Differentiation 8.
CD80: Cluster of Differentiation 80.
CD86: Cluster of Differentiation 86.
CD93: Cluster of Differentiation 93.
CDC: Center for Disease Control and Prevention.
cDNA: Complementary Desoxyribonucleic Acid.
CFA: Complete Freund's Adjuvant.
CIC: Centro de Investigación Cooperativa.
CID: Collision-Induced Dissociation.
CRAC: Calcium Release-Activated Channels.
DAB: Diaminobencidine.
DAG: Diacylglycerol.
DDA: Data-Dependent Acquisition.
DTT: Dithiothreitol.
EAE: Experimental Autoimmune Encephalomyelitis.

EDTA: Ethylenediaminetetraacetic acid.
EGF: Epidermal Growth Factor.
ELISA: Enzyme-Linked Immunosorbent Assay.
ER: Endoplasmic reticulum.
EVA: Ethylene Vinyl Acetate.
F4/80: EGF-like module-containing mucin-like hormone receptor-like 1.
FCS: Fetal Calf Serum.
FDR: False Discovery Rate.
Foxp3: Forkhead box P3
FR4: Folate Receptor 4.
GC: Gas Chamber.
GEO: Gene Expression Omnibus.
GOBP: Gene ontology analysis of Biological Processes.
GR-1: Granulocytic marker 1.
GvHD: Graft-versus-Host Disease.
GvT: Graft-versus-Tumor effect.
H-$2^{b,d}$: MHC haplotype H b and d.
H-2^{b}: MHC haplotype H b.
H&E: Hematoxylin&Eosin
HGA: Human Granulocytic Anaplasmosis.
HIS: 6 x Histidine tag.
HLA: Human Leukocyte Antigens.
HMMTOP: Transmembrane Topology Prediction server.
HP: Heating Pad.
HRP: Horseradish Peroxidase.
HSCT: Hematopoietic Stem Cell Transplantation
IACUC: Institutional Animal Care and Use Committee.
IFA: Incomplete Freund's Adjuvant.
IFN-γ: Interferon gamma.
IgG: Immunnoglobulin G.
IgM: Inmunglobulin M.
IL-2: Interleukin 2.
IL-4: Interleukin 4.
IL-6: Interleukin 6.
IP3: Inositol 1,4,5-trisphosphate.
IPTG: Isopropyl-β-D-thiogalactoside.
IrHRF: *Ixodes ricinus* Histamine Release Factor.
IsHRF: *Ixodes scapularis* Histamine Release Factor.
ITAMs: Immunoreceptor Tyrosine-based Activation Motif.
KLH: Keyhole Limpet Hemocyanin.
Lat: Linker for Activation of T cells.
LC-MS/MS: Liquid Chromatography-Mass Spectometry/Mass Spectometry.
Lck: Lymphocyte-specific protein tyrosine kinase.
LPS: Lipopolysacharide.
LRR: Leucine-Rich Repeat.
Ly6C: Lymphocyte antigen 6 complex.
MDSC: Myeloid-Derived Suppressor Cells.
ME: Midgut Extract.
SGE: Salivary Gland Extract.
Met: Metionine.

MHCII: Major Histocompatibility Complex II.
miHA: minor Histocompatibility Antigens.
MP: Mouth Piece.
MW: Molecular Weight.
NCBI: National Center for Biotechnology Information.
NF-AT: Nuclear Factor of Activated T-cells.
NF-kB: Nuclear Factor Kappa-light-chain-enhancer of activated B cells.
NGS: Next Generation Sequencing.
NRP1: Neuropilin 1.
OspA: Outer surface protein A.
OspC: Outer Surface Protein C.
OVA: Ovalbumin.
PAS: Periodic Acid Schiff.
PBS: Phosphate Buffered Saline.
PCA: Principal Component Analysis.
PCR: Polymerase Chain Reaction.
PLCγ1: Phosphoinositide-specific phospholipase C.
qRT-PCR: quantitative Reverse Transcription Polymerase Chain Reaction.
RN: Redness.
RNAi: Ribonucleic Acid interference.
RP-LC-MS/MS: Reverse Phase-Liquid Chromatography-Mass Spectometry/Mass Spectometry.
Rpl19: Ribosomal Protein L19.
Salp15: Salivary Protein 15.
Salp15ΔP11. Salp15 deletion of Peptide 11.
Salp25D: Salivary Protein 25D.
SDS-PAGE: Sodium Dodecyl Sulfate PolyAcrylamide Gel Electrophoresis.
SE: Standard Error.
SF: Shaved Flanks.
SFG: Spotted Fever Group.
Src: Proto-oncogene tyrosine-protein kinase Src.
SUB: Subolesin.
TBD: Tick-Borne Disease.
TBEV: Tick-Borne Encephalitis Virus.
TBS-T: Tris-Buffered Saline-Tween
TCR: T Cell Receptor.
TFA: Trifluoroacetic Acid.
TGFß: Transcription Growth Factor Beta.
TH: Tissue Homogenate.
Th1: T helper 1 cells.
Th17: T Helper 17.
Th2: T helper 2 cells.
tHRF: Tick Histamine Release Factor.
TLSPI: Tick Salivary Lectin Pathway Inhibitor.
TNF: Tumous Necrosis Factor.
Tris: *Tris*(hidroximetil)aminometano.
TROSPA: Tick Rececptor Outer Surface Protein A.
Val: Valine.
Vav1: Vav guanine nucleotide exchange factor 1.
YSD: Yeast Surface Display.

Zap-70: Zeta-chain-associated protein kinase 70.

SUMMARY / RESUMEN

SUMMARY

Mice are widely used in research. This animal species has also been extensively used to study the relationship between ticks and their mammalian hosts, including the design and test of vaccine candidates, although it is believed that mice do not develop tick immunity. We have established a test system in order to assess protection against tick feeding using this small animal model. We have redesigned containment capsules and tested the use of tissue cement to attach them to the shaved skin of the mice. Our results provide both an improved capsule design and permanent and strong bonding capabilities of the tissue cement. We then assessed the protective capacity of different immunization strategies, both active and passive, against an array of antigens and tissue extracts. We therefore tested active immunization with tick Histamine Release Factor (tHRF), as well as passive transfer of both human and bovine sera against whole tick, midgut or salivary gland extracts. We found that none of the strategies utilized elicited strong and consistent effects on different parameters of tick feeding, such as attachment time, weight at detachment or molting efficiency. These results suggest that, at least for the European tick, *Ixodes ricinus*, mice are not in general a suitable model to test anti-tick vaccines.

On the other hand, in order to identify tick antigens as potential targets for the development of a tick vaccine, salivary gland and midgut extracts were immunoprecipitated with immune antisera raised in cows that had shown protective effects against tick feeding in these animals. We identified antigen with putative metalloprotease, integrin and Apple domain-containing proteins that could function to prevent blood coagulation. Our identification was validated with the protein annotated as *I. ricinus* A0A0K8RQF1, which shares homology with Toll-like receptors and could form part of the immune response of ticks. This antigen, which is differentially recognized by protective anti-tick sera could alone or in combination protect against tick feeding in species such as cows and perhaps humans, and provide the basis for a new anti-tick vaccine.

Salp15, a salivary protein of *Ixodes* ticks, inhibits the activation of naïve CD4 T cells. Treatment with Salp15 results in the inhibition of early signaling events and the

production of the autocrine growth factor, interleukin-2. The fate of the CD4 T cells activated in the presence of Salp15 or its long-term effects are, however, unknown. We now show that Salp15 binding to CD4 is persistent and induces a long-lasting immunomodulatory effect. The activity of Salp15 results in sustained diminished cross-antigenic antibody production even after interruption of the treatment with the protein. Transcriptionally, the salivary protein provokes an acute effect that includes known activation markers, such as *Il2* or *Cd44*, and that fades over time. The long-term effects exerted by Salp15 do not involve the induction of either anergy traits nor increased populations of regulatory T cells. Similarly, the treatment with Salp15 does not result in B cell anergy or the generation of myeloid suppressor cells. However, Salp15 induces the increased expression of the ectoenzyme, CD73, in regulatory T cells and increased production of adenosine. Our study provides a profound characterization of the immunomodulatory activity of Salp15 and suggest that its long-term effects are due to the specific regulation of CD73.

RESUMEN

El modelo de ratón ha sido ampliamente usado en investigación. Esta especie animal ha sido también ampliamente usada para estudiar las relaciones entre las garrapatas y sus huéspedes mamíferos, incluyendo el diseño y evaluación de antígenos para el desarrollo de vacunas, a pesar de la creencia de que los ratones no desarrollan inmunidad frente a garrapatas. En nuestro grupo, hemos establecido un sistema con el fin de poder evaluar la protección frente a la alimentación de las garrapatas usando este modelo animal. Hemos rediseñado capsulas de contención y puesto a prueba el uso de pegamento tisular para fijar las capsulas a la piel del ratón. Nuestros resultados proporcionan tanto un diseño mejorado de la capsula de contención como una fuerte capacidad de adhesión y duración por parte del pegamento tisular. De esta manera, evaluamos la capacidad protectora de las diferentes estrategias de inmunización, tanto activa como pasiva, frente a una variedad de antígenos y extractos tisulares de garrapata. Asimismo, evaluamos la inmunización activa con el Factor de Liberación de Histamina, así como la transferencia pasiva de sueros tanto humanos como bovinos frente a extractos de garrapata total, estomago o glándula salivar. Los resultados mostraron que ninguna de las estrategias utilizadas provocó efectos sólidos y consistentes en cuanto a parámetros relacionados con la alimentación de garrapatas, tales como el tiempo de adhesión al huésped, el peso a la hora de su desprendimiento o la eficiencia en la muda. Estos resultados sugieren que, al menos para la garrapata europea, *Ixodes ricinus*, el modelo de ratón no es un modelo apropiado para el diseño y estudio de vacunas anti-garrapatas.

Por otra parte, con el fin de identificar antígenos de garrapatas como dianas potenciales para el desarrollo de una vacuna, extractos de glándula salivar y estómago fueron inmunoprecipitados con suero inmune elaborado en vacas que previamente mostraron efectos protectores frente a su alimentación en estos animales. De esta forma, identificamos antígenos tales como metaloproteasas, integrinas y proteínas con dominios Apple que podrían actuar previniendo la coagulación de la sangre. Nuestra identificación fue validada con la proteína anotada como *I. ricinus* A0A0K8RQF1, que comparte homología con los receptores Toll y podría formar parte de la respuesta inmune de las garrapatas. Este antígeno, diferencialmente reconocido por el suero inmune contra garrapatas, podría, o bien sólo o bien en combinación con otros antígenos, proteger contra

la alimentación de garrapatas en especies tales como vacas y tal vez humanos, y proporcionar, a su vez, la base para una nueva vacuna frente a estos parásitos.

Salp15, una proteína de la saliva de garrapatas del genero *Ixodes*, inhibe la activación de las células CD4 T. El tratamiento con Salp15 resulta en la inhibición de eventos de señalización celular tempranos y de la producción del factor de crecimiento autocrino, interleuquina-2. El destino de las células CD4 T activadas en presencia de Salp15 o sus efectoras a largo plazo son, sin embargo, desconocidos. En este estudio mostramos que la unión de Salp15 a CD4 es persistente e induce un efecto inmunomodulatorio de larga duración. La actividad de Salp15 provoca una producción reducida de anticuerpos frente a antígenos cruzados que es prolongado en el tiempo, incluso después de la interrupción del tratamiento con Salp15. A nivel transcripcional, la proteína salivar provoca un efecto agudo en la transcripción de varios genes que incluyen marcadores de activación, tales como *Il2* o *Cd44*, y que se desvanece con el tiempo. Los efectos a largo plazo ejercidos por Salp15 no involucran la inducción de marcadores de anergia ni el aumento de la población de células T reguladoras. Similarmente, el tratamiento con Salp15 no resulta en la generación de células B anergicas o de células mieloides supresoras. Sin embargo, Salp15 induce un incremento en la expresión de la ectoenzima, CD73, en las células T reguladoras y un aumento en la producción de adenosina. Nuestro estudio proporciona una caracterización profunda de la actividad inmunomodulatoria de Salp15 y sugiere que su efecto a largo plazo es debido a la regulación específica de CD73.

HYPOTHESIS AND OBJECTIVES

HYPOTHESIS AND OBJECTIVES

Tick populations are increasing worldwide driving a surge in the number of tick-borne infections. This increase is associated with the alteration of their habitat and to factors related to climate change, the distribution of their mammalian hosts and those related to anthropogenic changes. Ticks belonging to the *Ixodes* genus constitute the vectors for several medically important diseases, such as Lyme Disease, Human granulocytic anaplasmosis, Tick-Borne Encephalitis or Babesiosis. The European tick, *I. ricinus* is responsible for the transmission of the highest number of vector borne infections in Europe. Conventional control measures to prevent the expansion of ticks have classically consisted in the employment of acaricides or the unfeasible culling of wildlife reservoirs, which are becoming socially unacceptable due to their environmental harmful effects. As an alternative, the development of environmentally friendly vaccines against ticks would ideally prevent the transmission of tick-borne microorganisms. Therefore, the characterization and identification of new protective antigens that can induce the blockade of tick feeding would form the basis for the development of a tick vaccine that ideally could prevent the transmission of tick-borne pathogens.

The specific objectives of the first part of this thesis were:

1. The establishment of a tick feeding system on mice for the assessment of potential tick vaccine formulations.
2. The identification of new tick vaccine antigens from protective immune antisera as well as the *in silico* characterization of the antigens.

The identification of potentially useful activities among tick salivary antigens can provide the development of novel therapies for different pathological conditions. The activity of Salp15 on CD4 T cells has been tested in different models of immune diseases, including asthma and multiple sclerosis. Since this protein is able to inhibit early T cell signaling events, we hypothesized that the protein could preclude the activation of CD4 T cells and induce a long-term unresponsive or anergic state in disease models in which the activation of these cells is predictable, such as transplantation. Therefore, we sought to establish:

1. The characterization of the long-term effects of Salp15 in CD4 T cells in a murine model of transplantation and graft versus host disease.

2. The identification of short- and long-term transcriptional traits induced by Salp15 on activating CD4 T cells.
3. The study of the induction of populations of anergic and/or regulatory cells by Salp15 *in vitro* and *in vivo*.

CHAPTER 1

IDENTIFICATION OF TICK VACCINE ANTIGENS

1.1. INTRODUCTION

A brief anthropocentric history of ticks. Humans have been aware of ticks since ancient times. Around 1.500 B.C., Egyptians made illustrations representing ticks infesting hyena-like animals (Arthur, 1965) and described "tick fever" in papyrus scrolls (Varma 1993, Hillyard 1996). Later on, Homer left some writings about ticks, and Aristotle (384–322 B.C.) associated tick infestation of animals with high grass in his *Historia Animalium* (Aristotle, 343 B.C). He described them as a "disgusting parasitic animal generated from couch grass" (*Elymus repens*). In those times, ticks were named *ricini* from the Latin name used later to designate the castor oil plant, *Ricinus communis,* due to the high similarity between their seeds and the parasite. Pliny the Elder (23–79 A.D.) in his *Historia Naturalis* referred them as "an animal living on blood with its head always fixed and swelling, being one of the animals which has no exit (i.e., anus) for its food, bursts with over-repletion and dies from actual nourishment" (Arthur, 1965). However, even though the effect of ticks in animals and humans is known since many centuries ago, it was not until 1893 when Smith and Kilbourne demonstrated for the first time that ticks transmit pathogens (Assadian et al., 2002). They showed that the protozoan *Babesia bigemina*, the causative agent of the Texas cattle fever, is transmitted by cattle ticks from the genus *Boophilus*. Nowadays, it is well known that ticks transmit a variety of different pathogens worldwide and since at least 5.300 year ago, the age of mummified human remains found in the Alps (Ötzy; Figure 1.1) that contain genetic material from the bacterium that causes Lyme disease.

Figure 1.1. Remains of Ötzy, a 5.300 year-old mummy recovered from the Alps on the border between Austria and Italy.

Ticks: brief description and taxonomy. Ticks are members of the phylum *Arthropoda* within the kingdom *Animalia*. The phylum *Arthropoda* is divided into six major classes. Ticks belong to the subclass *Acari* within the class *Arachnida*. There are about 900 species of ticks, but while they

are arranged in four families, most of them fall within two major families: *Ixodidae* and *Argasidae*, commonly known as hard and soft ticks, respectively (Fig. 1.2.; Estrada-Peña, 2015). All ticks are obligate blood feeding ectoparasites. However, the two families go through different life cycles and contain several morphological features that separate them. The main distinguishing characteristic is the presence (hard ticks) or absence (soft ticks) of a sclerotized dorsal shield (*scutum*). Apart from this main feature, they are differentiated by another peculiarity. The members of the *Argasidae* family do not contain a prominent mouth and feeding structure (gnathosoma) and they can only engorge up to ten times their body mass in blood during a period of a few hours. On the other hand, members of the *Ixodidae* family exhibit a gnathosoma that is apically located, allowing them to feed for extended periods of time.

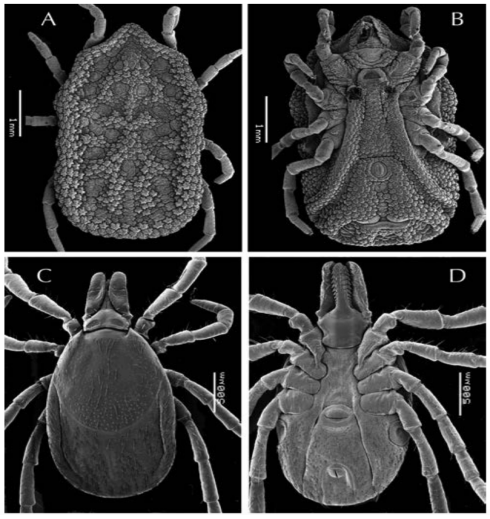

Figure 1.2. **General morphology of the *Argasidae* and *Ixodidae* families.** A and C represent the dorsal views of a soft and hard (*Ixodes ricinus*) tick. B and C represent the ventral views (Estrada-Peña, 2015).

Furthermore, they are able to ingest more than 100 times their body mass in blood. Moreover, soft ticks present a specialized coxal organ that ultrafiltrates the excess of water from the incoming blood meal, whereas hard ticks accomplish their osmoregulation by secreting the excess liquid back into the host as saliva via their salivary glands (Estrada-Peña, 2015), which is precisely the site of development and replication of many pathogens (Kocan et al., 2010; Bishop et al., 2004; Bock et al., 2004; Piesman & Gern, 2004; Mansfield et al., 2009).

Figure 1.3. Sexual dimorphism in *Ixodes ricinus*. Male (left) and female (right).

European *Ixodes* ticks: *Ixodes ricinus*. The genus *Ixodes* is the biggest group within the family *Ixodidae*, containing almost 250 species. They are considered, together with mosquitoes, the most

important vectors of human and animal diseases worldwide. However, only a few species that are potential carriers of pathogens or that indirectly serve as vectors for diseases have been generally studied (Ash et al.; 2017). Thus, the European tick *Ixodes ricinus*, which can harbor a variety of pathogens has been the most studied tick in Europe.

***Ixodes ricinus*.** The castor bean tick, *I. ricinus* is a relatively small tick. It presents sexual dimorphism at the adult stage, being the females slightly larger than males (Fig. 1.3). As other members of the family *Ixodidae*, they show a sclerotized dorsal scutum, which protects and covers the whole body in males and only partially in females. This hard tick has a wide geographical distribution in Europe due to its ability to survive in various environmental conditions, covering a region that extends from Portugal to Russia and from North Africa to Scandinavia.

Life cycle. The life cycle of *I. ricinus* consists of four stages: egg, larva, nymph and adult. They must feed on a host in order to molt into the next life stage. First, the six-legged larvae hatch in summer usually from a batch of around 3,000 eggs. They then climb the vegetation and wait for passing hosts in order to adhere to them. Usually, these are small animals such as mice, voles as well as birds. After feeding for 2-3 days, they fall into the vegetation and begin the molting process into 8-legged nymphs. Nymphs feed on a second host, which usually are small or medium sized animals, including rodents and lagomorphs. After feeding for 4-5 days, nymphs molt to the adult stage, which will mate and feed on a third larger animal (herbivores such as bovids and cervids, carnivores or humans) with the sole purpose of laying eggs, dying afterwards (Fig. 1.4.; Soneshine et al., 2013).

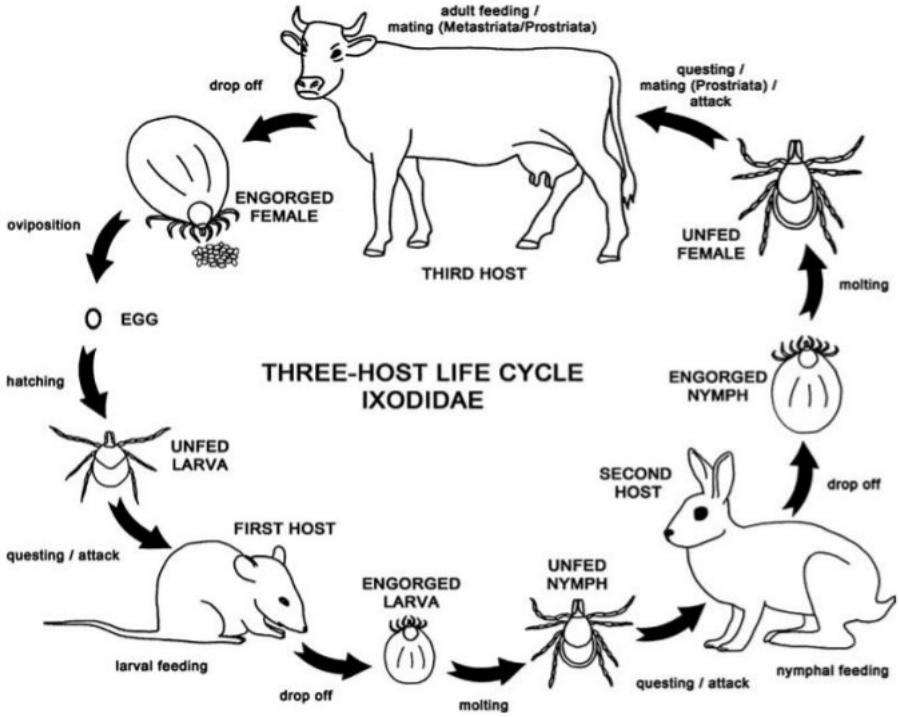

Figure 1.4.Three-host life cycle of the Ixodidae family (Sonenshine et al., 2013).

Stages in which transmission of pathogens occur. At the moment of attachment, larvae, nymphs and adults start to introduce their saliva into the host. Tick saliva contains several compounds with pharmacological functions that help the arthropod during attachment and feeding (See below). Ticks can acquire pathogens while feeding on an infected host, transtadially (across life stages) or transovarially (from the female to the offspring). Apart from the introduction of the cocktail of functional proteins into the host, ticks also introduce pathogens via their saliva. However, the life stage that can transmit pathogens vary depending on both the tick species and the pathogen. Even though transmission of pathogens is most common by nymphs, followed by adults (because of the amount of bites per year in comparison to larva bites), larvae are also known to transmit *B. afzelii and B. miyamotoi* to humans, which is a direct consequence of transovarial transmission of these bacteria in this species (Duijvendijk et al., 2016).

***Ixodes ricinus* as vectors of pathogens.** The European castor bean tick is able to transmit a great variety of pathogenic microorganisms, ranging from virus to protozoans, thus causing the highest number of human vector-borne diseases in Europe (Rizzoli et al. 2014). Among all the vector-borne diseases, the most prevalent is Lyme disease or Lyme borreliosis. Lyme borreliosis is caused by *Borrelia burgdorferi sensu lato* and include the genospecies *B. burgdorferi sensu stricto*, *B. garinii* and *B. afzelii* (Cerar et al., 2016). It accounts for at least 65.000 cases per year in Europe (Sprong et al., 2014). The diseases caused by vector-borne virus such as tick borne encephalitis virus (TBEV) are also clinically important. TBEV is the most pathogenic of all tick-transmitted microorganisms, causing around 1-2% of deaths among all the cases while 50% of infected individuals suffer long term sequelae. Furthermore, several emerging diseases of medical and veterinary importance, caused by obligatory intracellular bacteria belonging to the order *Ricketsiales* have been described. These include Human granulocytic anaplasmosis (HGA), caused by *Anaplasma phagocytophyllum* or the spotted fever group (SFG) caused by members of the *Ricketsia* genus, among others. Finally, protozooans from the genus *Babesia* produce babesiosis in humans (Rizzoli et al., 2014).

- ***Lyme borreliosis***. Upon its deposition into the dermis, *B. burdogferi* stablishes a local infection, which usually initiates a local inflammatory response that can result in the appearance of a slowly expanding skin lesion named *erythema migrans*. At this stage (Stage I), other non-specific, flu-like symptoms can occur, including fever, headache, malaise, myalgia and/or arthralgia. The spirochete then disseminates hematogenously throughout the body by binding to blood components such as plasminogen, platelets and the integrins lining the endothelium of blood vessels (Stage II). The bacterium can colonize different tissues and organs, inducing symptoms such as conduction system abnormalities, meningitis and acute arthritis. Some untreated individuals develop persistent forms of the disease normally associated with the prolonged infection with the spirochete: arthritis, neuroborreliosis or cutaneous lesions such as *acrodermatitis chronica atroficans* (Smith et al., 2002; Steere, 2001; Steere et al., 1983).

- ***Human granulocytic anaplasmosis*** is a ricketsial infection caused by *A. phagocytophyllum*. This pathogen can induce a severe illness and even death. While many patients resolve the infection without any antibiotic treatment, most symptomatic patients need a specific antibiotic therapy, usually doxycycline. Early symptomatology is non-specific, frequently mimicking a viral illness, and tests for early diagnosis are not available (Bakken & Dumler, 2015).

- ***Tick-borne encephalitis*** is an important viral infection of the central nervous system transmitted to humans predominantly by tick bites. Even though it is preventable by vaccination, the incidence is increasing in the last years and is becoming a health problem in Europe and Asia. Symptoms may range from mild meningitis to severe meningoencephalitis with or without paralysis. A post-encephalitic syndrome can develope in up to 50% of patients after acute tick-borne encephalitis (Bogovic & Strie, 2015).

- ***Babesiosis*** is caused by protozoans belonging to the genus *Babesia*. It is considered an emerging parasitic tick-borne disease. More than 100 *Babesia* species have been described so far, but only *B. microti*, *B. divergens* and *B. venatorum* have been associated with human disease. The infection is often asympomatic or mild but it can lead to progressive and more severe illness in immunocompromised individuals.

Effect of habitat alterations in tick populations and tick-borne infectious diseases. Tick populations are increasing due to habitat changes caused by multiple and interacting factors. The drivers of tick expansion can be divided into three groups: those related to changes in climate change, those involved in the distribution of tick hosts, and anthropogenically-induced changes. Climate change is rising the average surface temperatures on Earth, increasing rainfall, decreasing snow cover and extending vegetation. All these conditions make the periods in which ticks can be questing hosts, molting or reproducing longer and more productive, enhancing the survival of the species and its abundance. On the other hand, the effects of climate change can also be identified by the geographical distribution change of tick hosts, including the colonization of higher latitudes and altitudes and ticks are dispersing with them (Medlock et al., 2013). Also important are the changes induced by human

activity. In the last twenty years, urbanized areas have increased worldwide expanding outwards into wildlife areas (Fig. 1.5). Urbanization leads to the fragmentation of ecosystems and loss of biodiversity (Rizzolli et al., 2014), including predators for both ticks and their hosts. Another consequence of this invasion of the tick habitat is the development of new contact opportunities between humans and their pets with ticks (Uspensky, 2014) or with economically important and domesticated grazing animals like cows, sheep, goats or horses, making tick reservoirs increase. All of these factors improve the survival, development and reproduction of ticks.

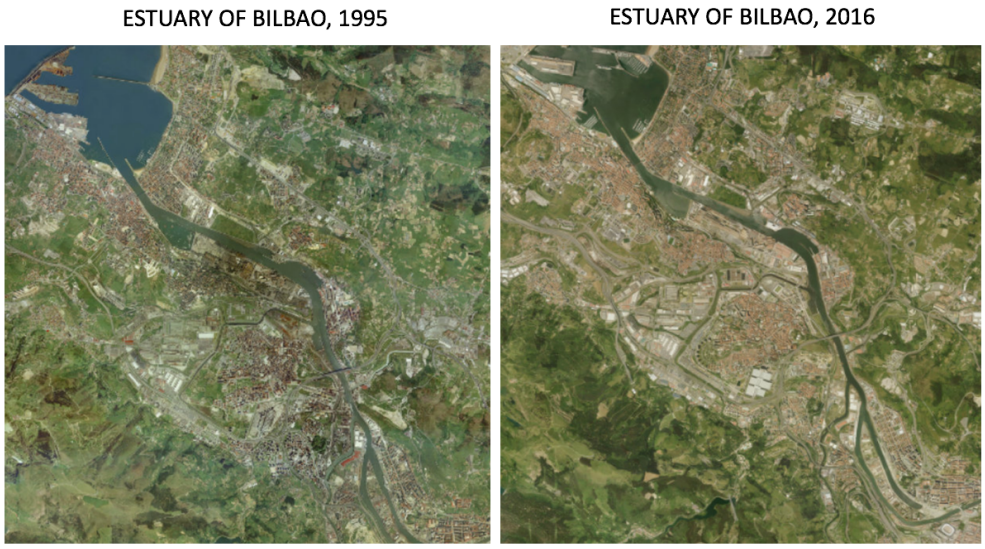

Figure 1.5. **In the last twenty years, urbanized areas have increased worldwide expanding outwards into wildlife areas of ticks.** Satellite images of the Great Bilbao area along the stuary of the river Nervion taken 20 years apart. The images show the expansion of the urban areas around the biggest city in the Basque Country.

From conventional control measures to tick vaccines. Apart from the expensive, impractical and unfeasible culling of wildlife reservoirs, conventional control measures of ticks have been based for many years in the use of acaricides. However, the application of these compounds is becoming socially unacceptable due to their environmentally harmful effects, including the appearance of acaricide-resistance ticks and the contamination of meat and milk products with acaricide residues (Domingos et al., 2013; Gortazar et al., 2014). As an alternative, the use of tick vaccines might be a

cost-effective and environmentally friendly alternative to prevent problems associated with the use of acaricides. A commercially available vaccine for the control of cattle tick infestations by *Rhipicephalus microplus* has been used with success using the tick protective gut antigens, BM86 and BM95. The combination of antigens such as subolesin and BM86 has also been able to reduce *R. microplus* infestations in red deer and white-tailed deer with an overall efficacy of approximately 80% (Gortazar et al., 2014; de la Fuente et al., 2016). The use of this anti-tick vaccine dramatically reduced the incidence of bovine babesiosis in cattle (Sprong et al., 2014). Because of the success in controlling this tick species and the related tick-borne diseases, vaccines are also being considered as an alternative for the control of human tick-borne diseases caused by the European castor bean tick *I. ricinus* (de la Fuente et al., 2016). Indeed, humans with hypersensitivity to ticks have a lower risk of contracting Lyme Disease (Burke et al., 2011). Therefore, the identification of tick antigens that could be developed as vaccines can complement vaccination strategies for individual tick-borne infectious diseases (TBD).

Vaccines for tick-borne diseases. Specific vaccines for some human TBDs are already available or still ongoing. For example, a highly effective inactivated vaccine for TBEV is accessible and licensed for use in Europe and Russia. However, protection requires multiple doses and frequent boosters to maintain the immunity against the virus and therefore, vaccination rates remain still very low in endemic areas (Rumyantsev et al., 2013). A vaccine against Lyme borreliosis is not currently available, even though a vaccine was licensed in the United States in 1998 against *B. burgdorferi sensu stricto* based on the lipidated form of the outer surface protein A (OspA). Nevertheless, the vaccine was removed from the market in 2002 due to poor sales and later unsubstantiated safety concerns (Šmit & Postma, 2016) even though it is still used in pets. The vaccine targeted a surface protein of the spirochete that is only expressed in the tick (de Silva et al., 1996), which required yearly boosts in order to maintain high circulating antibody titers. Even though there is extensive research seeking alternative vaccines against *B. burgdorferi* that target surface antigens expressed in the mammalian host, no single candidate has been clearly identified. On the other hand, no vaccines are currently available for HGA or Babesiosis. Therefore, there is a need to identify novel vaccine targets that protect against one or more TBDs.

Acquired host tick immunity. Usually, tick bites are unnoticeable; however, some individuals show sensitivity and develop local reactions around the bite area. These skin reactions to tick bites have also been known to occur in certain species of animals for over 75 years. In 1939, William Trager described a phenomenon that he called "tick immunity" (Trager, 1965). He observed that *Dermatocentor variabilis* ticks did not engorge efficiently on guinea pigs after several infestations. Tick immunity has been demonstrated in other species, including rabbits (Narasimhan et al., 2007) and may be responsible for the enhanced sensitivity observed in humans that perform activities with increased exposure to ticks, such as forestry workers. Noticeably, tick immunity has not been reproduced in mice, although one manuscript described this phenomenon in Balb/c mice (Borsky et al., 1994) , which, however, has not been replicated. The differential capacity of mammalian species to develop immunity against these arthropods may have ecological implications, since small rodents are important for the maintenance of ticks in Nature.

Tick immunity affects the numbers of ticks feeding on the host, results in delayed time of engorgement, a reduction in tick weight, the inability of the tick to molt and decreased fecundity. Aside from the involvement of some cellular types -such as mast cells, basophils and eosinophils -, antibodies against tick proteins play an important role in tick immunity (Schuijt et al., 2011). Thus, passive transfer of tick immune sera mimics the effect on engorging ticks (Das et al., 2001; Whelen et al.,1993). Thus, the identification and characterization of the antigens that elicit this humoral response has been the subject of extensive investigation (Sprong et al., 2014; Schuijt et al., 2011).

Tick salivary gland proteins as targets for anti-tick vaccines. The tick salivary gland is a multifunctional organ that is critical for the success and survival of ticks. It serves as an osmoregulatory instrument when the tick drops from the host, but during the period of time in which the tick is attached, salivary glands also play a crucial role. Salivary glands maintain the tick attached to the host, help the infection and the transmission of pathogens and facilitate their feeding from the blood meal by the introduction of tick saliva into the host (Bowman and Sauer, 2004). Therefore, tick saliva antigens are the first exposed to the mammalian host during feeding and they can be used as a vaccine targets (Juncadella & Anguita, 2009). Moreover,

immunization with salivary gland extracts is able to trigger anti-tick immune responses in laboratory animals (Hovius et al., 2008).

Tick saliva. Tick saliva contains an array of functional proteins that support tick feeding. The discovery of the activities presented in tick saliva has been expanding from initial limited screening procedures, including its biochemical characterization (Valenzuela, 2004) or the use of antibodies from tick-immune animals (Narasinmhan et al., 2007) to more recently, high throughput screening technologies such as transcriptomics (NGS), proteomics (LC-MS/MS or RP-LC-MS/MS), multiple RNA interference (RNAi) screenings, capillary feeding, functional genomics approaches (Merino et al., 2013), protein arrays (Manzano-Román et al., 2012) or the use of Yeast Surface Display (YSD) expression libraries of tick cDNA probed with immune sera (Schuijt et al., 2011). Several studies have been performed using novel high-throughput technologies in order to elucidate the characterization of salivary protein composition and gene expression dynamics (Chmelar et al., 2016). These technologies are contributing to elucidate the salivary family proteins that are the most represented across tick species, or regulated by feeding or the presence of specific pathogens. The most over-represented tick saliva family proteins in *Ixodes ricinus* during feeding are collagen-like proteins, Kunitz domain-containing proteins, basic tail proteins, Salp15/ixostatin family members, lipocalins, metalloproteases and several new proteins families of unknown function (Chmelar et al., 2008; Kotsyfakis et al., 2015). However, very few studies have been performed in order to characterize the changes in gene expression induced by the presence of pathogens in the tick. For example, most studies have been focused on the interaction between *Ixodes* ticks cell lines and *A. phagocitophillum* and little is known about the genes involved in the immune response by *I. ricinus* to this pathogen (Alberdi et al., 2015; Ayllón et al., 2015). Some studies have, however, described changes in gene expression in TBEV-infected ticks (Villar et al., 2017) or *B. burgdorferi* (Cotté et al., 2014). In response to the infection by the spirochete, the upregulation of proteins used for protein synthesis, processing and cell defense was noted, while cytoskeleton proteins were downregulated. Nevertheless, new protective antigens need to be stablished to enhance vaccine efficacy for the control of TBDs (de la Fuente et al., 2016).

The functional characterization of salivary gland proteins is complicated in the absence of a complete annotated genome. Only around 67% of the non-repetitive sequences of the *I. ricinus* genome have been annotated (Cramaro et al., 2017), even though it has been sequenced (Cramaro et al., 2013). Currently, homology with annotated *I. scapularis* genes is being used to elucidate the function of *I. ricinus* proteins. The problem is compounded by the fact that the genes present in tick salivary glands are subjected to great evolutionary pressure, since these proteins are exposed to immunological responses by the host. Thus, transcriptomic analysis in ticks show that salivary gland gene expression is very diverse especially compared to hematophagous insects (Chmelar et al., 2012) and are evolving rapidly (Gulia-Nuss et al., 2016). For example, the *I. scapularis* genome is the richest source of Kunitz domain-containing proteins, while lipocalins (40 genes) and metalloproteases (34 genes) represent families with gene expansions in the *I. scapularis* genome (Gulia-Nuss et al., 2016).

Despite these challenges, great advances have been made in the determination of the activities associated with these protein families that affect host homeostasis and immune responses. These include vasodilators, inhibitors of platelet aggregation and blood coagulation, inhibitors of angiogenesis, complement inhibitors, chemokine-binding proteins (or evasins) and modulators of immune cell function (Kazimírová & Štibrániová, 2013, Hovius et al., 2008). For example, Salp15, also presented in *I. ricinus* as Iric-1, inhibits the activation of CD4 T cells (Anguita et al., 2002) and the production of pro-inflammatory cytokines by LPS-activated dendritic cells (Hovius et al., 2008). Among the proteins described in the transcriptomics and proteomics studies, only a few of them have been tested in animals as potential antigens to serve as a whole or in part of a tick vaccine.

Specific recombinant tick antigens and their effect on ticks and pathogen transmission.

1. **BM86.** Vaccines exist for the control of *Rhipicephalus microplus* cattle tick infestations since 1990. This vaccine is based on the midgut protein BM86 from *R. microplus* and is able to reduce the number of ticks feeding in cows, their weight, the reproductive capacity of engorging female ticks as well as the incidence of babesiosis while also controling the transmission of *A. marginale* in regions where ticks are their main vector (Merino et al. 2013). Despite the

ability of the BM86-based vaccine to limit cattle tick infestations and pathogen transmission, the vaccine is not universally effective. In fact, homologues of this protein have been tested in other tick species. A negative effect on numbers of engorging ticks or on tick feeding has been shown in ticks such as *R. annulatus*, *R. decoloratus*, *Hyalomma anatolicum*, *H. dromedarii, H. anatolicum* and *H. scupense.* However, no effect has been observed in ticks such *Amblyomma cajennense*, *A. variegatum* or *R. appendiculatus* (Coumou et al. 2015). A BM86 ortholog-based vaccine is also innefective on *I. ricinus* feeding or oviposition (Coumou et al., 2015). Therefore, immunization with BM86 orthologues has varied effects across tick species (Merino et al., 2013).

2. **BM95.** This glycoprotein is a BM86 homologue the also protects cattle against infestations, having a broader range of tick species effectiveness than BM86. Moreover, the combined immunization with BM86 and BM95 is able to induce longer lasting immune responses than BM86 alone (Schetters et al. 2016).
3. **64TRP.** 64TRP is a putative tick cement protein that plays a role in the attachment and feeding of ticks. It helps maintain the tick´s mouthparts attached to the host skin in both adult and immature stages of some tick species, including *I. ricinus*. This antigen induces a strong antibody response and delayed type hypersensitivity responses (Trimnel et al., 2005). Fed ticks in 64TRP-immunized animal models show impaired attachment and feeding as well as cross-reaction with 'concealed' midgut antigens (Trimnel et al., 2002; Trimmel et al., 2005). Vaccination studies in mice prevented the transmission of TBEV by *I. ricinus* (Labuda et al., 2006), establishing that the transmission of this virus can be prevented by interfeering with the efficient feeding of ticks.
4. **Salp25D.** This protein is expressed in salivary glands and midguts and has homology to peroxiredoxin antioxidants (Das et al., 2001). Immuniation with Salp25D reduced *B. burgdorferi* acquisition by *I. scapularis* in mice, suggesting that this antigen is involved in protecting the bacteria from reactive oxygen species produced by neutrophils. However, it did not affect transmission from the tick to the host (Narashimhan et al. 2007).
5. **The tick histamine release factor (tHRF).** tHRF was first described in *I. scapularis* as secreted in the saliva. tHRF-silenced ticks by RNAi showed a decrease in tick feeding and *B. burgdorferi* transmission in mice. Active

immunization and passively transferred tHRF antiserum also protected against tick feeding and *B. burdogferi* infection in mice (Dai et al., 2010).

6. **Tick Salivary Lectin Pathway Inhibitor (TLSPI).** TLSPI was characterized in *I. scapularis* by Schuijt and cols.: the protein is able to inhibit the complement cascade and therefore enhance the transmission of *B. burgdorferi.* Silenced ticks presented a significantly reduction in *B. burgdorferi* acquisition by nymphs and impaired its transmission to mice. However, immunization with the recombinant protein did not completely affect bacterial transmission from the tick to the host (Schuijt et al., 2011; Wagemarkers et al., 2016).
7. **Ferritins** are iron reservoir proteins that maintain the homeostasis of iron during tick feeding. A common heavy chain type ferritin 2 has been recently characterized as a gut-specific protein released into the tick hemolymph, where it acts as an iron transporter (Hajdusek et al., 2009). The knockdown by RNAi and immunization with this protein reduced tick feeding, oviposition and fertility in *I. ricinus, R. microplus* and *R. anulatus.*
8. **TROSPA**. The tick receptor in the midgut for *B. burgdorferi* OspA was identified by Pal and cols. in 2004 (Pal et al., 2004). Silencing TROSPA via RNA interference or the use of TROSPA antisera induced a reduction of *B. burgdorferi* attachment to the *I. scapularis* gut and therefore a reduction in the bacterial burden within the tick and in the transmission of the bacteria to the host (Pal et al., 2004).
9. **Serpins.** This family of structurally related proteins regulates many important functions including coagulation, food digestion, inflammatory and immune responses (Mulenga et al., 2001). Immunization with a mixture of different serpins reduced the engorgement of the ticks after feeding, tick infestations and induced increased mortality of *Haemaphysalis*, *Rhipicephalus* and *Theleria* ticks (Imamura et al., 2005, 2006, 2008).
10. **Subolesin (SUB).** Subolesin was characterized from *I. scapularis* as an orhologue of insect and vertebrate akirins (AKR). SUB is involved in tick innate immune responses and multiple molecular pathways. Immunization with this antigen reduced tick infestations and the transmission of *A. phagocytophillum, A. marginale, B. bigemina* and *B. burdogferi* (de la Fuente et al., 2006b; Merino et al., 2011b; Bensaci et al., 2012). RNA interference of this gene presented contradictory results. It decreased tick innate immunity

resulting in higher infection levels, but also affected genes that are necessary and required for pathogen infection and multiplication (Zivkovic et al., 2010; de la Fuente et al., 2011). Vaccines combining epitopes from SUB/AKR protect against ticks, mosquito and sand fly infestations (Moreno-Cid et al., 2013).

11. **Salp15** inhibits the activation of CD4 T cells (Anguita et al., 2002), complement activity (Schuijt et al., 2008), as well as dendritic cell function (Hovious et al., 2008). The salivary protein binds to *B. burdogferi* OspC (outer surface protein C) and protects the bacteria from antibody mediated killing facilitating the survival of the spirochete, pathogen transmission and host infection (Ramamoorthi et al., 2005; Dai et al., 2009). Salp15-immunized mice showed protection from infection with *B. burgdorferi* (Dai et al., 2009).

1.2. METHODS

Tick capsule assembly. Before developing the final capsule design, several tests were performed from the original design provided by our collaborators at the ANTIDotE project. The capsules were assembled using the following materials: 5 ml syringes from BD (catalogue number:307731); 0.5 ml tubes with screwed caps (Axygen, SCT-050-G) and 2 mm thick EVA foam sheets. A syringe was cut at the top just below the mark 'BD' (Fig. 1.6A). Then, the top, flat part of a screw cap of a 0.5 ml tube was eliminated (Fig. 1.6B) and inserted into the cut syringe (Fig. 1.6C). A piece of 2 mm EVA foam that fits the top of the cut syringe was attached to it with Pattex glue, forming the base of the capsule (Fig. 1.6D). A 0.5 ml tube was then cut below the ribbed rim and closed with an intact cap, as shown in Fig. 1.6E. This modified container would be used for maintaining the ticks before their attachment to the mice, keeping it closed with another screw cap (Fig. 1.6F).

Tick capsule fitting. Six to 10-week-old Balb/c mice were anesthetized with isoflurane using an anesthesia machine (Fig. 1.6G). Then, they were placed on a heating pad to avoid heat loss introducing their head into a mouth piece attached to the anesthesia machine. The right-hand side flank was shaved with an electric trimmer before attaching the capsule, either with Pattex glue or tissue cement (Fig. 1.6H), carefully checking that the capsule does not impede the movement of the legs.

Capsules were always attached to the mice 24 h before placing the ticks, since we observed that the fumes emanating from both Pattex glue or tissue cement would inhibit tick attachment (data not shown).

I. ricinus ticks were placed on ice, counted and maintained inside the capsules until they were placed on the mice. In all the experiments, 10 nymphal ticks were used per mouse. To allow tick attachment, the capsules were gently tapped on a table. The screwed cap was then taken off and the tube was quickly screwed into the skin-attached capsule holding piece (Fig. 1.6I).

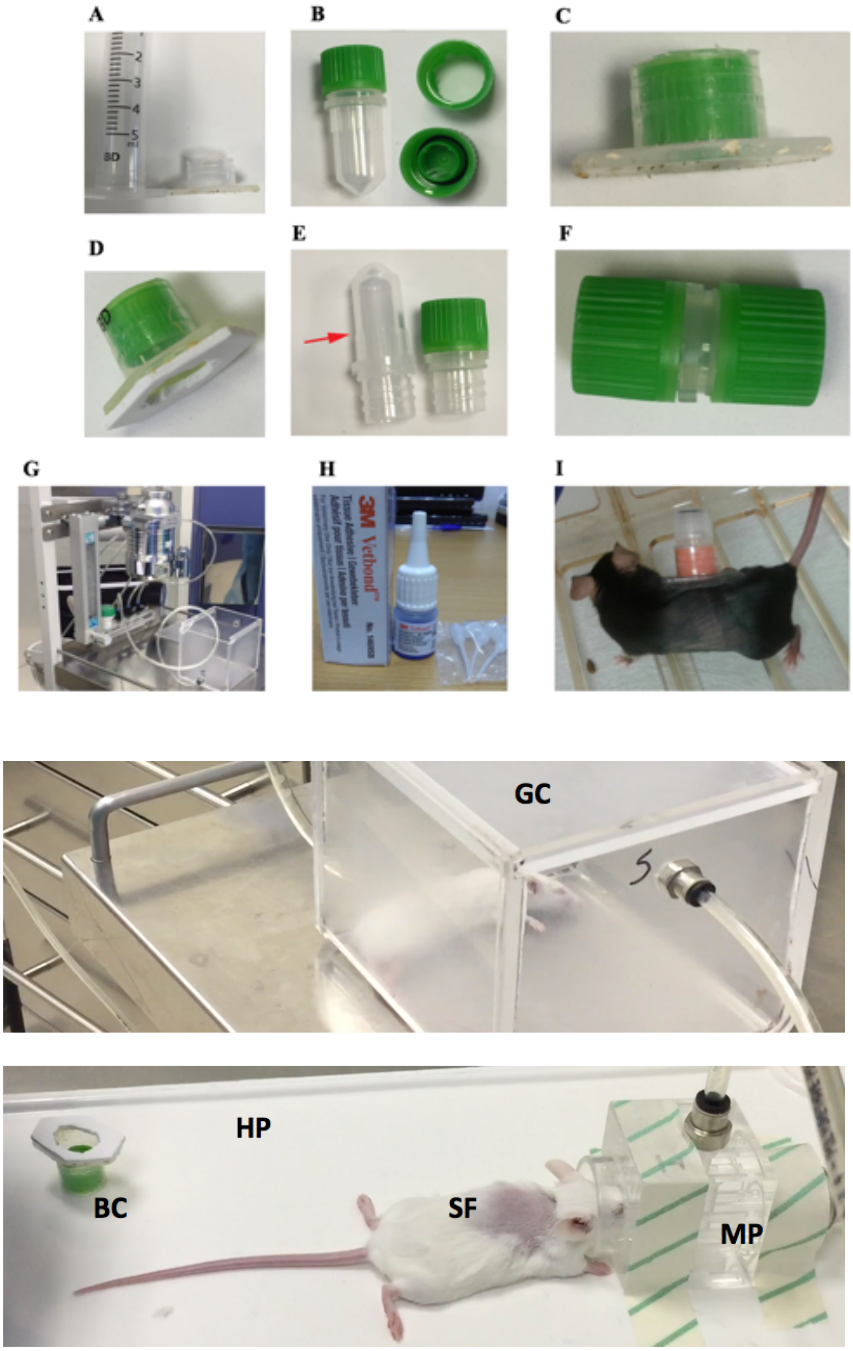

Figure 1.6. **Tick capsule assembly and fitting.** Panels A through F present the steps in the assembly of the tick chambers used throughout these studies. Mice were anesthetized by isoflurane in the gas chamber (GC) of the anesthesia machine. Then, mice were placed in a heating pad (HP) introducing their head into the mouth piece (MP) of the anesthesia machine. SF: Shaved flanks. BC: Bottom of the capsule.

Tick feeding. *I. ricinus* ticks were obtained through BEI Resources, in collaboration with the Centers for Disease Control and Prevention (CDC). Ticks were monitored after 2-3 h of attachment and daily for five days. Tick weight was measured upon detachment. The number of ticks that detached every day was also recorded. All the ticks were saved in order to examine their molting success after at least 4 weeks. All experiments were performed in 4 mice per group (40 ticks) and were performed at least twice. Data from both experiments were combined in order to apply statistical analysis to the results.

Active and passive immunization studies. For active immunizations, the mice were immunized initially with 100 μg OVA (ovalbumin) or tHRF in aluminum hydroxide (Invivogen, USA) or Complete Freund's adjuvant (CFA) as adjuvants. Mice were boosted two times more after the first immunization in aluminum hydroxide or Incomplete Freund's adjuvant (IFA) (Sigma Chemical Co.), respectively, at two weeks intervals. The mice were injected subcutaneously into two different sites. The mice were bled at the beginning of the assay, at day 28 and at the end of the experiment to measure IgG titers against the proteins.

For passive immunizations, mice were injected subcutaneously with 100 μl of sera in two different sites when the capsules were attached. The mice were injected again at the time of tick attachment. At sacrifice (5 days after tick attachment), the mice were bled for the detection of human and bovine antibodies in the murine serum.

IgG titer measurement and detection. To measure IgG titers, purified soluble tHRF or OVA were coated overnight at 4 °C in 96-well plates, at a concentration of 0.5 μg/ml in 0.1 M sodium bicarbonate buffer (pH 9.5). The wells were then blocked with PBS containing 1% fetal calf serum (FCS) for 1 h. Plates were washed and the sera were diluted in blocking solution and applied to the wells in triplicate at dilutions ranging from 1/1,000 to 1/128,000 and incubated at 4°C for 2 h. The plates were then washed, and biotinylated anti mouse IgG antibody (BD Pharmingen) diluted (1/1,000) in 1% FCS/PBS, was added. The plates were incubated at room temperature for 1 h, washed, and streptavidin/peroxidase (Invitrogen), diluted 1/1000 in blocking solution was added. The plates were then incubated at room temperature for 1 h, washed, incubated with a peroxidase substrate, and the optical density at 450 nm was recorded.

For the detection of human and bovine sera, 100-fold diluted sera were coated over-night at 4 °C in 0.1 M sodium bicarbonate buffer (pH 9.5) in 96-well plates. The plates were then washed and incubated at room temperature for 1 h with biotinylated anti-bovine or anti-human IgG at a 1/1,000 dilution (BD Pharmingen) in 1% FCS/PBS. The plates were washed, and incubated with streptavidin/peroxidase and substrate, as before. The optical density at 450 nm was then recorded.

Direct antigen immunoprecipitation. Control and immune calf sera IgG were purified using the Melon Gel IgG Spin Purification Kit (Thermo, USA), following the manufacturer´s protocol. Protein content was then measured in midgut and salivary gland lysates using the Pierce BCA Protein Assay Kit (Thermo, USA). The direct immunoprecipitation was performed using the Pierce Direct IP Kit (Thermo, USA) following the manufacturer's instructions. Enrichment was carried out by incubation of 100 µl of the AminoLink Plus Coupling Resin slurry with 20 µl purified sera that was immobilized onto the aldehyde-activated agarose resin at room temperature for two hours. One mg of the tissue lysates was added to each antibody-coupled resin in a spin column. The column was incubated with gentle shaking at 4 °C overnight to form antibody-antigen complexes. After several washes, the antigens were eluted in 100 µl and analyzed by SDS-PAGE.

Tryptic digestion. SDS-PAGE bands of the immunoprecipitated antigens were cut and washed in milli-Q water. Reduction and alkylation were performed using ditiothreitol (10 mM DTT in 50 mM ammonium bicarbonate) at 56 ºC for 20 min, followed by iodoacetamide (50 mM iodoacetamide in 50 mM ammonium bicarbonate) for another 20 min in the dark. Gel pieces were dried and incubated with trypsin (12.5 µg/ml in 50 mM ammonium bicarbonate) for 20 min on ice. After rehydration, the trypsin supernatant was discarded; Gel pieces were hydrated with 50 mM ammonium bicarbonate, and incubated overnight at 37 ºC. After digestion, acidic peptides were cleaned with 0.1% trifluoroacetic acid (TFA) and dried in an RVC2 25 speedvac concentrator (Christ). The peptides were resuspended in 10 µl 0.1% formic acid and sonicated for 5 min prior to analysis.

LC-MS/MS analysis. Peptide separation was performed on a nanoACQUITY UPLC System (Waters) connected to an LTQ Orbitrap XL mass spectrometer (Thermo Electron) or a Synapt G2 Si (Waters). An aliquot of each sample was loaded onto a

Symmetry 300 C18 UPLC Trap column (180 µm x 20 mm, 5 µm (Waters). The precolumn was connected to a BEH130 C18 column, 75 µm x 200 mm, 1.7 µm (Waters), and equilibrated in 3% acetonitrile and 0.1% FA. Peptides were eluted directly into the nanoelectrospray capillary (Proxeon Biosystems) at 300 nl/min, using a 60 minute-linear gradient of 3–50% acetonitrile.

The LTQ Orbitrap XL ETD automatically switched between MS and MS/MS acquisition in DDA mode. Full MS scan survey spectra (m/z 400–2,000) were acquired in the orbitrap with mass resolution of 30,000 at m/z 400. After each survey scan, the six most intense ions above 1,000 counts were sequentially subjected to collision-induced dissociation (CID) in the linear ion trap. Precursors with charge states of 2 and 3 were specifically selected for CID. Peptides were excluded from further analysis during 60 s using the dynamic exclusion feature.

Data analysis. Searches were performed using the Mascot search engine v2.1 (Matrix Science) through Proteome Discoverer 1.4. (Thermo Electron). Carbamidomethylation of cysteines was set as fixed modification, and oxidation of methionines as variable modification, and 2 missed cleavages were allowed. Ten ppm of peptide mass tolerance and 0.5 Da fragment mass tolerance were used for Orbi acquisitions, whereas 15 ppm peptide mass tolerance and 0.2 Da fragment mass tolerance were used for Synapt G2Si runs. Spectra were searched against the Uniprot/Swissprot database. A decoy search was carried out in order to estimate the false discovery rate (FDR). Only peptides with a false discovery rate < 1% were selected.

Western blotting. For the validation or recognition of tick antigens by bovine immune sera, 5 µg of each extract or purified protein were boiled at 95 °C for 10 minutes, subjected to SDS-PAGE and transferred to a nitrocellulose membrane at 200 V for 1h. The membranes were blocked with 5% non-fat milk in Tris-buffered saline solution containing 0.01% Tween-20 (TBS-T). The membranes were immunoblotted with specific control and/or immune diluted bovine sera (1:500) at 4 °C overnight.

Cloning and purification. The four proteins V5IFB6, A0A131YAQ2, V5HWD5, A0A0K8RQF1 were cloned by overlapping PCR from salivary gland cDNA and cloned as *Nco*I-*Sal*I fragments into the pHIS-parallel 2 expression vector. Sequence-confirmed clones of A0A0K8RQF1 were induced with 1 mM Isopropyl-β-D-

thiogalactoside (IPTG) for 16 h at 20 °C in *E. coli* BL21 C41(DE3). The bacterial cells were then lysed and centrifuged. The expressed protein A0A0K8RQF1 was extracted from the inclusion bodies following the following protocol: the pellet was thoroughly homogenized in 50 mM Tris pH 8; 300 mM NaCl; 1 mM DTT; 2% Triton X-100 followed by an incubation at 37 °C for 30 min. The sample was ultracentrifuged at 96,000 xg for 30 min and the pellet was homogenized again in 50 mM Tris pH 8; 300 mM NaCl; 1 mM DTT and incubated at 37 °C for 30 min. After a second ultracentrifugation, the pellet was homogenized in 50 mM Tris pH 8; 300 mM NaCl; 1 mM DTT; 7 M urea. The denatured proteins were refolded by dialysis in PBS overnight with an intermediate exchange of buffer to a final concentration of 2 M urea.

Statistical analysis. Results are presented as means ± SE, unless otherwise indicated. The differences in means between groups were tested using the Student´s T-test. Differences in antibody titers were assessed by a 2-way ANOVA. Differences in tick molting efficiencies were tested using the Fisher's exact test. All calculations were made in GraphPad Prism, version 7. A p value < 0.05 was considered statistically significant. All experiments were performed at least 3 times. *In vivo* experiments consisted of groups of 4 mice and were performed at least twice.

Ethics statement. All work involving animals was approved by the Institutional Animal Care and Use Committee (IACUC) at CIC bioGUNE and the competent authority (Diputación de Bizkaia). CIC bioGUNE animal facility is accredited by AAALAC Intl. All experiments were performed in accordance with European and Spanish guidelines and regulations.

1.3. RESULTS

Establishment of the tick feeding system on mice. Mice have been routinely used to feed ticks for propagation of tick colonies (Embers et al. 2013), and for the study of tick-host-pathogen interactions (Smith et al. 2016) or the efficacy of vaccines (Dai et al. 2010). These studies require the attachment of all placed ticks, and therefore they are enclosed or retained in glued chambers or capsules (Coumou et al. 2015) mimicking the natural situation in which ticks are grouped together at localized sites (Randolph et a. 1997). Several laboratories use common adhesives to attach the capsules to the mouse skin, including Pattex (Fig. 1.7). However, in order to follow regulations regarding animal welfare stablished by the Association for Assessment and Accreditation of Laboratory Care Animal International (AAALAC) International, we tested tissue cement (Fig. 1.7) as an alternative, clinically accepted adhesive to attach the capsules to the mouse. After several tests to optimize the amount of tissue cement for the proper attachment of the capsule to the shaved flank of the mice, a test was performed to compare tick attachment and feeding when using both types of adhesives (Fig. 1.8).

Figure 1.7. The two type of commercial adhesives tested for tick feeding efficiency.

Four mice were used per group to which 10 ticks were placed within the capsule. The results did not show any difference in the weight of the recovered ticks between both adhesives (Fig. 1.8). These preliminary experiments confirmed that the use of an appropriate veterinary-grade tissue adhesive results in the attachment and feeding of *I. ricinus* ticks.

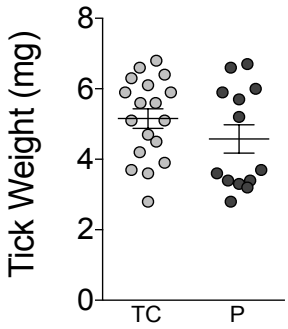

Figure 1.8. Tick weights upon feeding in mice to which the ticks capsules were attached with the two adhesives. The capsules were attached either with tissue cement (TC) or the commercial glue, Pattex (P). The circles represent the weight of individual recovered ticks until day 5 after attachment.

Assessing the use of mice to test tick vaccines. We then proceeded to the immunization of mice with a known antigen originally described as protective against *I. scapularis* feeding. Tick Histamine Release Factor (tHRF) is secreted in the saliva and binds to host basophils stimulating the release of histamine. Immunization with *I. scapularis* tHRF reduced the efficiency of tick feeding. Therefore, we sought to address whether the *I. ricinus* variant would show the same protective effect (Dai et al., 2010).

Using primers specific for *I. scapularis* tHRF, we cloned the *I. ricinus* ortholog in *E. coli*. Even though both orthologs differ in 11 nucleotides, a single mutation encode a non-synonymous substitution. Therefore, the amino acid sequences were almost identical, except for a conserved modification at amino acid 162 (Val162Met) (Fig. 1.9A). The protein was cloned into the pHIS-parallel 2 expression vector with a HIS-tag added at the N-terminus to allow its purification by nickel affinity chromatography (Fig. 1.9B). The expressed protein was soluble and purified by affinity chromatography (Fig. 1.10).

Once purified, we immunized groups of Balb/c mice and tested tick feeding parameters following the approach described in Fig. 1.11. The immunizations were performed with both aluminum hydroxide and CFA. Ovalbumin (OVA) was used as a control in both cases.

A

```
IsHRF                                                          -----------------
IrHRF                                                          ATGTCGTACTACCATCA

IsHRF          ------------------------------------------------------------------
IrHRF          CCATCACCATCACGATTACGATATCCCAACGACCGAAAACCTGTATTTTCAGGGCGCCAT

IsHRF          ----ATGCTGCTTTTCAAGGATATCTTGACCGGTGACGAGATGTTCACCGACTCGGTCAA
IrHRF          GGGAATGCTGCTTTTCAAGGATATCTTGACCGGTGACGAGATGTTCACCGACTCGGTCAA
                   ************************************************************

IsHRF          ATACAAGCTGGTGGATGACTGCATCTTCGAAATCGAGTGCGAGCACGTGACACGGAAGGT
IrHRF          ATACAAGCTGGTGGATGACTGCATCTTCGAAATCGAGTGCGAGCACGTGACGCGCAAGGT
               ************************************************** ** *****

IsHRF          GGGCGAGGTGGCGCTGGACGGCGCCAACCCATCTGCCGAGGAAGTGGAGGAGGGCACGGA
IrHRF          GGGCGAGGTGGCGCTGGACGGTGCCAACCCATCTGCCGAGGAAGTGGAGGAGGGCACGGA
               ********************* ****************************************

IsHRF          GGAGGGCACAGAAAAGCGGCCTGGACCTGGTGCTGAACATGCGCCTGGTGGAGACGGGTTT
IrHRF          GGAGGGCACAGACGAGCGGCCTGGACCTGGTGTTGAACATGCGCCTGGTGGAGACGGGTTT
               ************ ***************** ****************************

IsHRF          CTCCAAGACGGACTACAAGAACTACCTCAAGACTTACACCAAGGCCCTGATGGACAAGTG
IrHRF          CTCCAAGACAGACTACAAGAACTACCTCAAGACGTACACCAAGGCCCTGATGGACAAGTG
               ********* ********************** **************************

IsHRF          GAAGGAGGATGGCAAGTCGGAGGCCGAGGTCAACGAGGCCAAGAGCAAGCTCACAGAGGC
IrHRF          GAAGGAGGACGGCAAGTCGGAGGCCGAGGTCAACGAGGCCAAGAGCAAGCTCACCGAGGC
               ********* ********************************************* *****

IsHRF          CGTCAAGAAGGTGCTGCCCAGGATTGGGGACATGCAGTTCTTCCTCGGAGAATCTTCCAA
IrHRF          CGTCAAGAAGGTGCTGCCCAGGATCGGGGACATGCAGTTCTTCCTCGGAGAATCTTCCAA
               ********************** ***********************************

IsHRF          CCCCGACGGCATTGTTGCCCTCTTGGAGTACCGCCCGAACAAGAGCGGTGGCGAGACGCC
IrHRF          CCCCGACGGCATTGTTGCCCTCTTGGAGTACCGCCCGAACAAGAGCGGTGGCGAGACGCC
               ************************************************************

IsHRF          AGTCGTGATGTTCTTCAAGCACGGGCTCTTGGAAGAGAAGCAGTAA
IrHRF          AGTCATGATGTTCTTCAAGCACGGGCTCTTGGAAGAGAAGCAGTAA
               **** ****************************************
```

B

```
IsHRF          ----------------------------MLLFKDILTGDEMFTDSVKYKLVDDCIFEIECE
IrHRF          MSYYHHHHHHDYDIPTTENLYFQGAMGMLLFKDILTGDEMFTDSVKYKLVDDCIFEIECE
                                           *********************************

IsHRF          HVTRKVGEVALDGANPSAEEVEEGTEEGTESGLDLVLNMRLVETGFSKTDYKNYLKTYTK
IrHRF          HVTRKVGEVALDGANPSAEEVEEGTEEGTESGLDLVLNMRLVETGFSKTDYKNYLKTYTK
               ************************************************************

IsHRF          ALMDKWKEDGKSEAEVNEAKSKLTEAVKKVLPRIGDMQFFLGESSNPDGIVALLEYRPNK
IrHRF          ALMDKWKEDGKSEAEVNEAKSKLTEAVKKVLPRIGDMQFFLGESSNPDGIVALLEYRPNK
               ************************************************************

IsHRF          SGGETPVVMFFKHGLLEEKQ
IrHRF          SGGETPVMMFFKHGLLEEKQ
               *******:************
```

Figure 1.9. Alignment of the nucleotide and amino acid sequences of *I. scapularis* (IsHRF) and *I. ricinus* (IrHRF) tHRF orthologs. (A) Alignment of the nucleotide sequences. The sequence corresponding to the poly His tag attached to the N-terminus of the protein is highlighted in yellow. The synonymous substitutions between both orthologs are noted in green, while the unique non-synonymous substitution is marked in red. **(B)** Alignment of the amino acid sequences of both tHRF orthologs. The amino acid sequence corresponding to the vector (in yellow) and the incorporated HIS-tag (in blue) are noted.

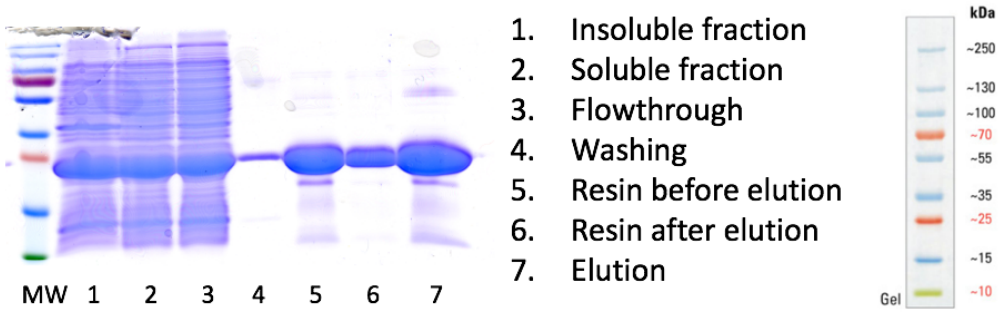

Figure 1.10. **Production of *I. ricinus* tHRF in E. coli.** Steps performed for the erichment of the protein using niquel affinity chromatography. The soluble fraction (2) was bound to a nickel resin, washed and eluted using 250mM of imidazol.

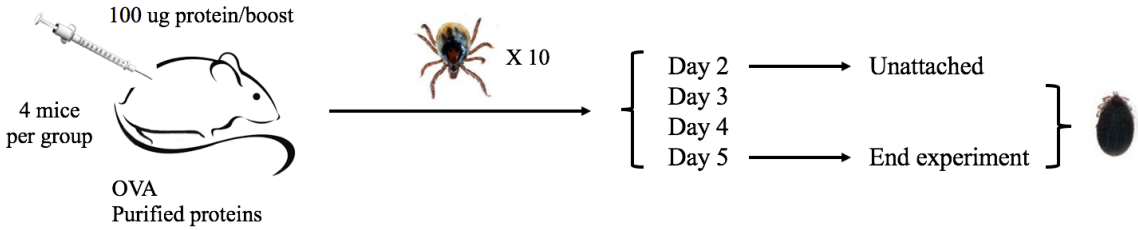

Figure 1.11. Strategy for active immunization. Four Balb/c mice per group were immunized subcutaneously with 100 µg OVA or tHRF. Once the immunization was completed, 10 ticks were attached in each mouse and monitored for 5 days. At the end of the experiment the following parameters were measured: tick weight, dettachment time, engorgement efficiency and molting.

When aluminum hydroxide was used, we performed a first immunization followed by two boosts at two weeks intervals. Mice were bled and antibody titers against tHRF were determined at days 0 and 28, as well as at the end of the experiment (Fig. 1.12A). Once the IgG response against tHRF was recorded after the third boost, 10 ticks were placed in each mouse and parameters related to tick feeding were measured for 5 days (Fig. 1.12B,C,D,E): tick weight, attachment, engorgement time and molting. In a second set of experiments, mice were immunized once with CFA followed by a single boost with IFA (incomplete Freund's adjuvant), since antigen-specific titers were high and similar to the immunization with aluminum hydroxide

(Fig. 1.13A). As in the previous assay, ticks were placed in mice and parameters related to tick feeding were measured over time.

Immunization with aluminum hydroxide did not affect tick weights, feeding or molting efficiency (Fig. 1.12). Similar results were observed when the mice were immunized using CFA/IFA as adjuvants. (Fig. 1.13), except that a small but significant reduction in molting succes was observed in the tHRF-immunized group compared to the OVA-immunized, control group (Fig. 1.13E).

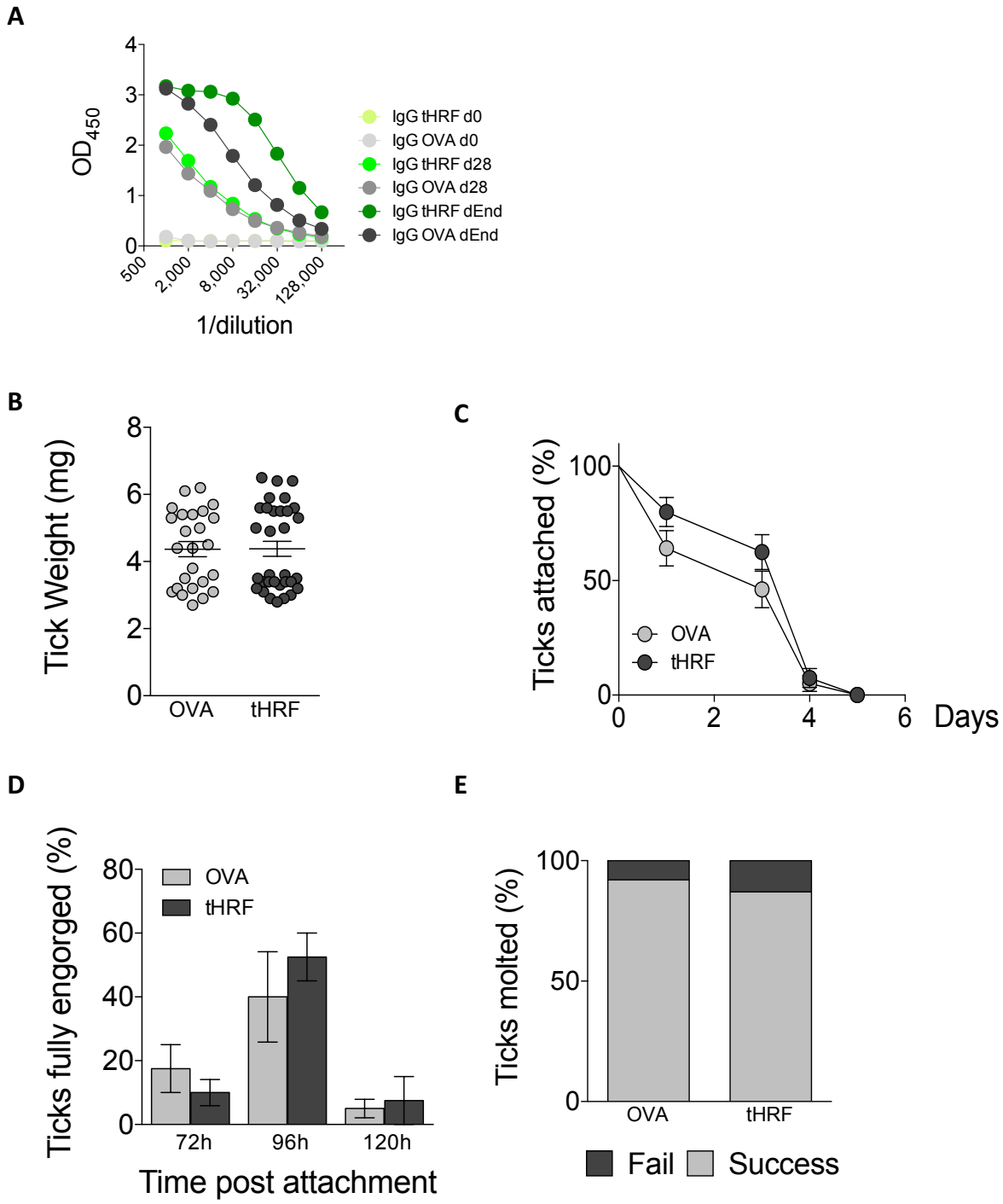

Figure 1.12. Tick feeding parameters in tHRF immunized mice using aluminium hydroxide as adjuvant. (A) IgG titers for OVA (control) and tHRF at the beginning of the assay (IgG d0), after the second boost (IgG d28) and at the end of the experiment (IgG dEnd). The curves represent the mean IgG response from four mice. **(B)** Weights of ticks after feeding on tHRF- and OVA-immunized mice. **(C)** Percentage of ticks remaining attached throughout the experiment. **(D)** Percentage of fully engorged ticks recovered throughout the experiment. **(E)** Rate of success in molting. Percentage of molted ticks relative to those fully engorged.

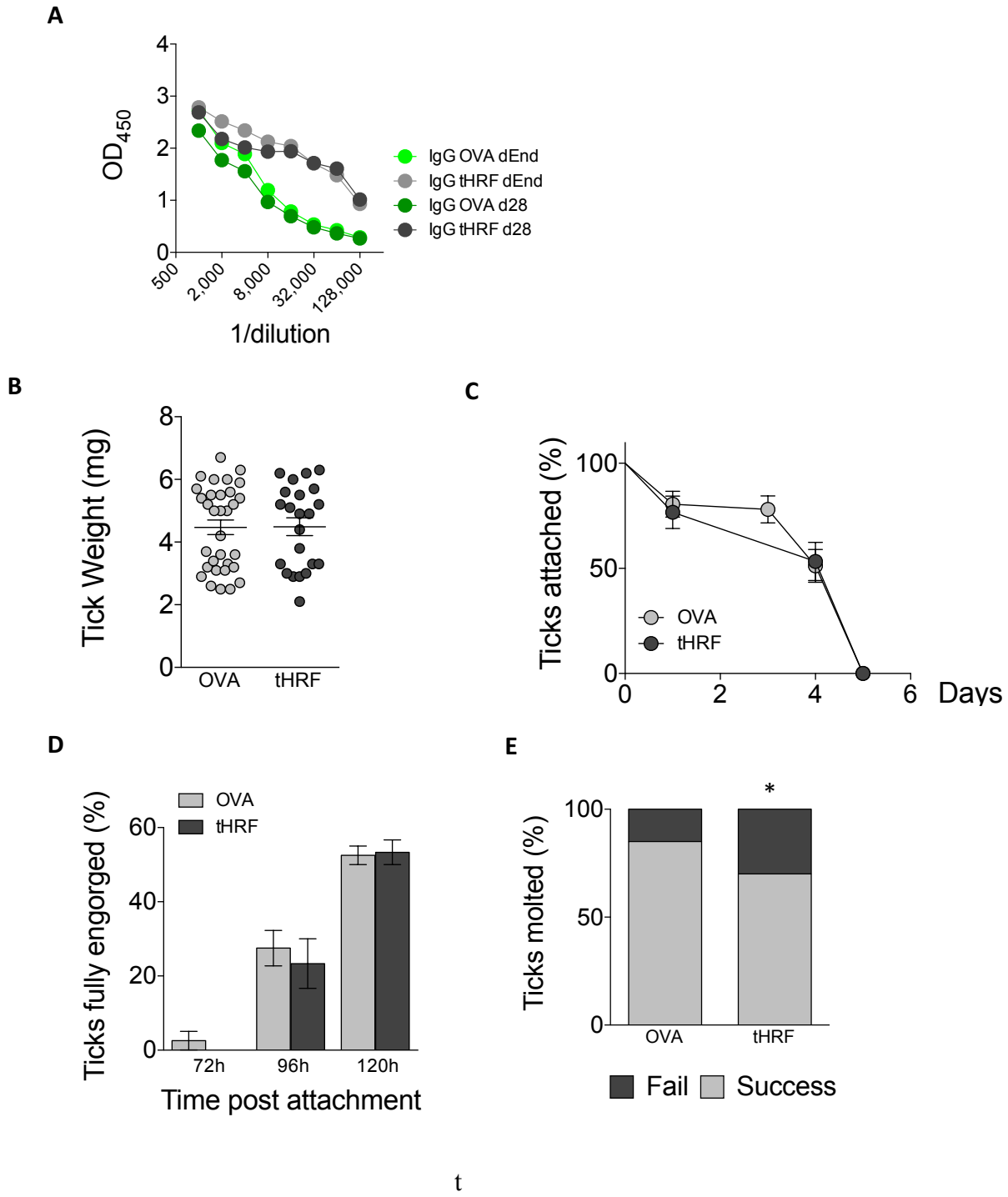

t

Figure 1.13 Tick feeding parameters in tHRF immunized mice using Freunds adjuvant. **(A)** IgG titers for OVA (control) and tHRF at the beginning of the assay (IgG d0), after the second boost (IgG d28) and at the end of the experiment (IgG dEnd). The curves represent the mean IgG response from four mice. **(B)** Weights of ticks after feeding on tHRF- and OVA-immunized mice. **(C)** Percentage of ticks remaining attached throughout the experiment. **(D)** Percentage of fully engorged ticks recovered throughout the experiment. **(E)** Rate of success in molting. Percentage of molted ticks relative to those fully engorged. * Fisher's exact test, $p < 0.05$.

Effect of passive immunization with human and bovine immune sera in tick feeding parameters in mice. We then tested a passive immunization strategy using sera obtained from humans that either had shown a local inflammatory response upon tick attachment or that had reported more than 20 tick bites per year, as well as sera obtained from cows immunized with combinations of tick extracts that had shown effect on the ability of ticks to subsequently feed. The sera used for these experiments are summarized in Fig. 1.14.

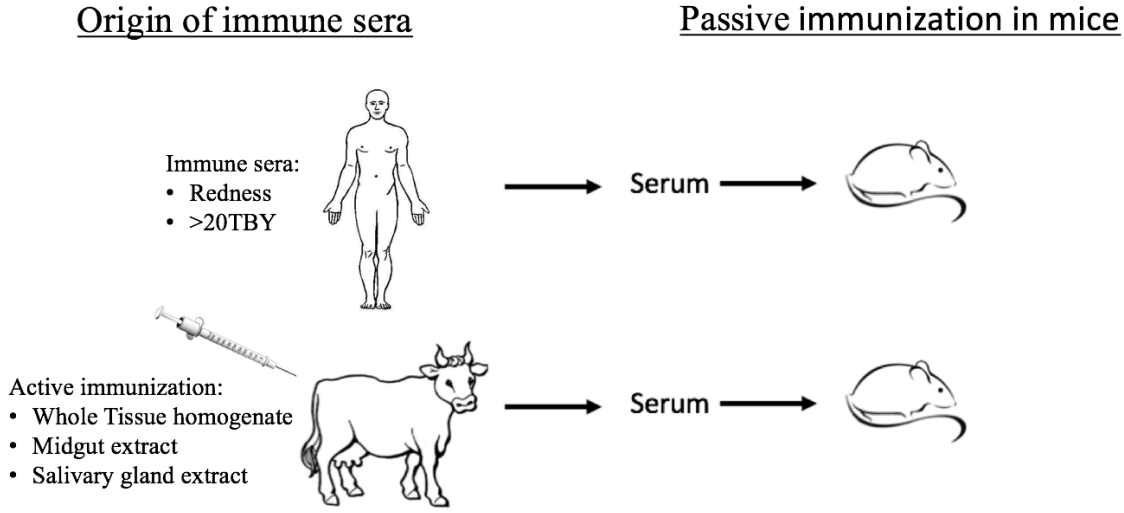

Figure 1.14. Human and bovine tick immune antisera used for the passive immunization of mice. Human sera were obtained from forestry workers reporting a local inflammatory reaction at the site of tick bites (Redness) or more than 20 tick bites per year (>20TBY). Bovine sera were raised against whole tick homogenates, midgut or salivary gland extracts.

First, we used human sera obtained from forestry workers that had developed a local inflammatory reaction to tick bites, indicated by redness on the bite site (RN sera), or reporting more than 20 tick bites per year (>20 sera). As control, we used sera obtained from clerical workers. Mice were passively immunized as described in figure 1.15. All the sera were provided by Dr. Joppe Hovius at Amsterdam Medical College from their collection and as part of the ANTIDotE project.

Four Balb/c mice per group were passively immunized subcutaneously with control, RN or >20 TBY sera the day the tick capsules were attached and the following day, at the time of tick deposition. Parameters of tick feeding were measured

as before. Circulating human IgG were readily detected in the murine sera at the time of sacrifice (day 5 of feeding; Fig. 1.16A). However, no differences in tick feeding were observed regardless of the sera used (Fig. 1.16).

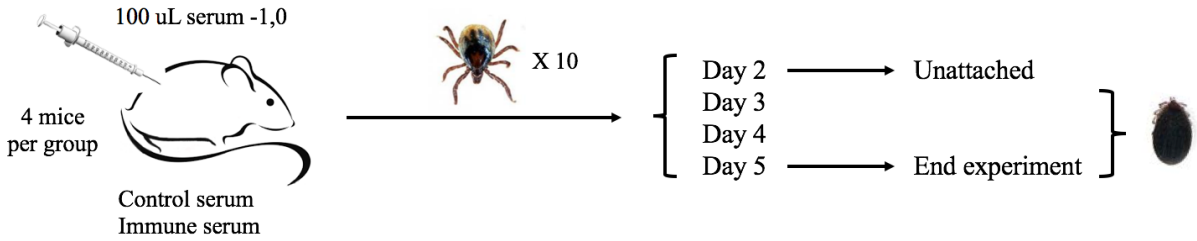

Figure 1.15. Established strategy for passive immunization. Four Balb/c mice per group were immunized subcutaneously with 100 µl control or immune sera one day before and at the time of tick placement. Ticks were monitored during 5 days. At the end of the experiment the following parameters were measured: tick weight at dettachment, attachment period, engorgement time and molting success.

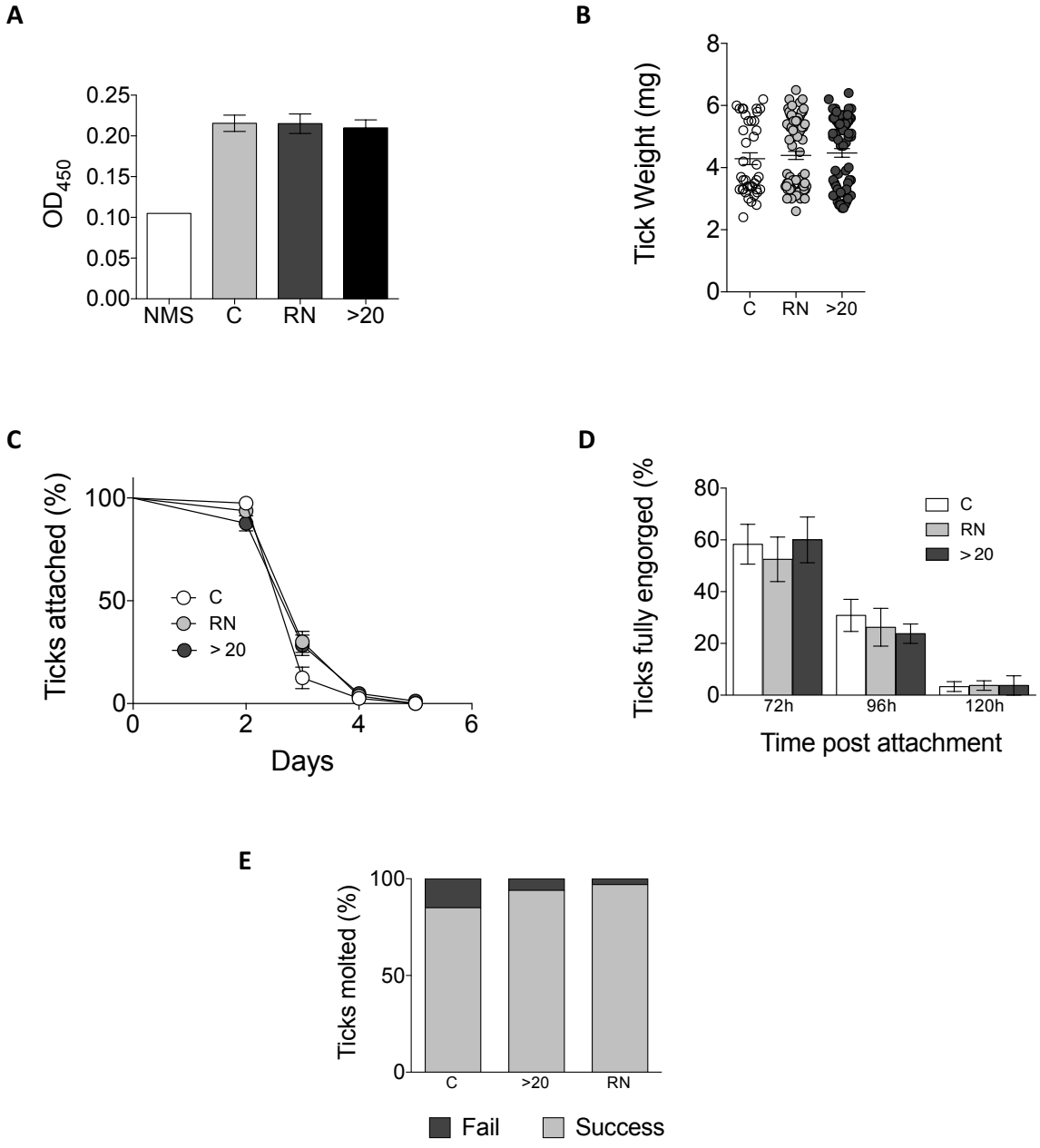

Figure 1.16. Effect of passive immunization with human sera on tick feeding parameters. **(A)** Human sera detection in mice. The bars represent the mean IgG response from four mice. (**B)** Tick weights at the time of dettachment. (**C**) Percentage of attached ticks throughout the experiment. (**D)** Percentage of the fully engorged ticks recovered throughout the course of the experiments. (**E)** Rate of success in molting. Percentage of molted ticks relative to the number of engorged ticks recovered.

Because the perception that humans have on their response to tick bites is subjective and not formal demonstration that tick immunity had occurred in these groups of workers, we also tested sera from cows that had been immunized with whole tick tissue homogenates, midgut extracts or salivary gland extracts. Active immunizations were performed by Dr. Ard Nijhof's group in Berlin (a member in the European ANTIDotE project), and had shown the ability to reduce tick feeding success on cows (data not shown). In those immunization studies sera were collected before immunization (Control sera) or after two rounds of immunization using Montanide® as adjuvant. The groups of sera tested were:

- Serum at day 0 before immunization (Control sera, α-ME d0, α-SGE d0)
- Serum from whole tick tissue homogenate (TH) immunized cows (TH antisera).
- Serum from midgut extract (ME) immunized cows (ME antisera, α-ME d68)
- Serum from salivary gland extract (SGE) immunized cows (SGE antisera, α-SGE d68)

Mice were passively immunized as before (Fig. 1.15) and infested with 10 ticks. Cow IgGs were detected in the murine sera at the end of the experiment (5 days post feeding; Figs. 1.17A, 1.18A). We found that the passive immunization with whole tick homonegate antisera reduced tick weights at dettachment (Fig. 1.17), while no other analyed parameters were affected (see Figs. 1.17). On the other hand, the use of cow sera specific for tick SGE or ME did not replicate the effect observed in tick weights (Fig. 1.18). However, a small delay in tick dettachment was noted as a result of the use of anti-tick ME sera (Fig. 1.18).

Overall, these results show that although some parameters associated with tick rejection can be replicated in mice upon immunization with antigens shown to be protective in other species, the murine model does not provide a robust system to thoroughly test anti-tick vaccines . These data also confirm that mice do not replicate features of tick immunity observed in other species, most predominantly guinea pigs and rabbits, but also those observed in immunized cows, and even under forced (immunization) conditions, the murine immune system does not develop strong anti-tick effector mechanisms.

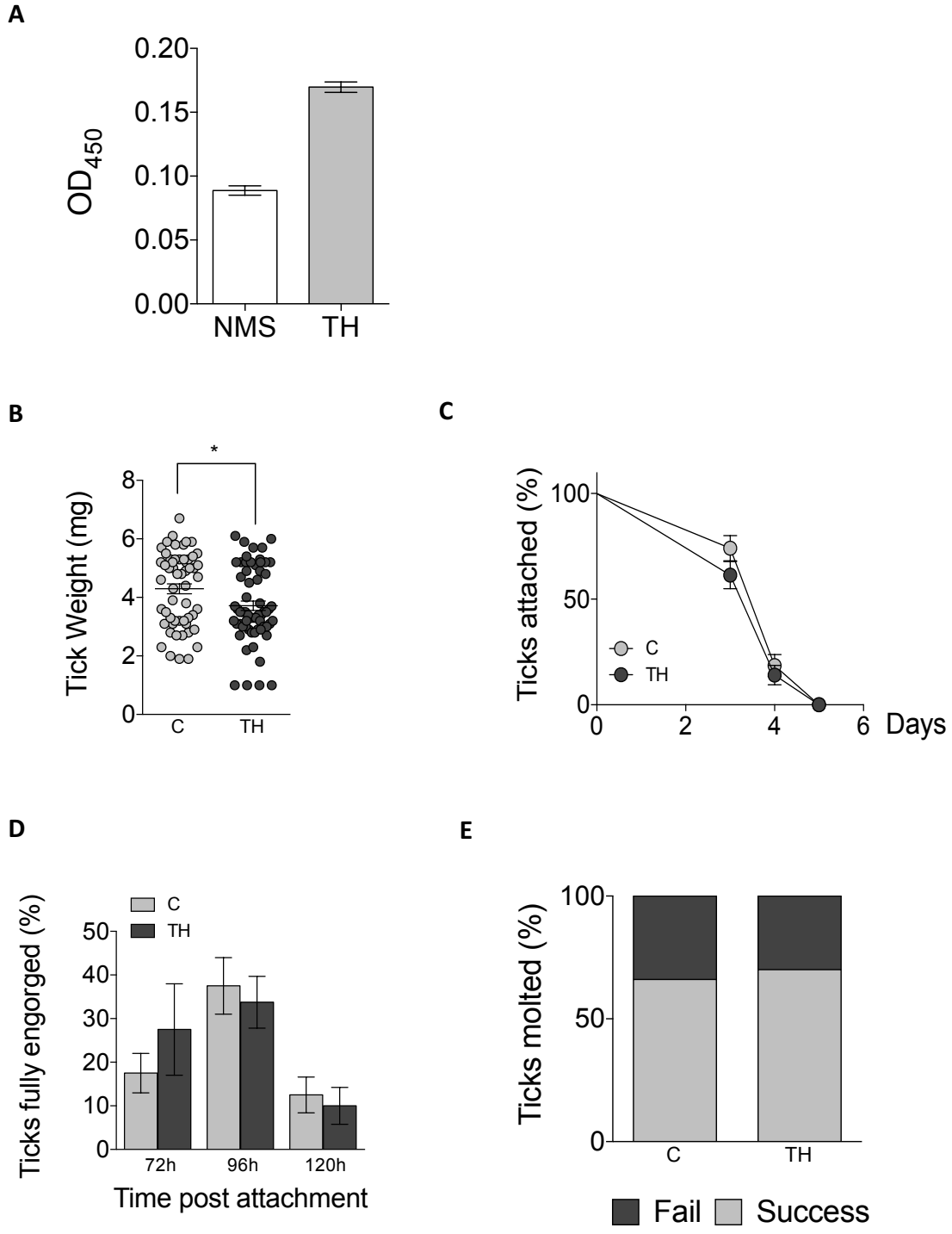

Figure 1.17. Effect of passive immunization with bovine sera raised against whole tick extracts. (A) Cow sera detection in mice. The bars represent the mean IgG response from four mice. (**B)** Tick weights at the time of dettachment. *, Student's T test, $p < 0.05$. (**C**) Percentage of attached ticks throughout the experiment. (**D)** Percentage of the fully engorged ticks recovered throughout the course of the experiments. (**E)** Rate of success in molting. Percentage of molted ticks relative to the number of engorged ticks recovered.

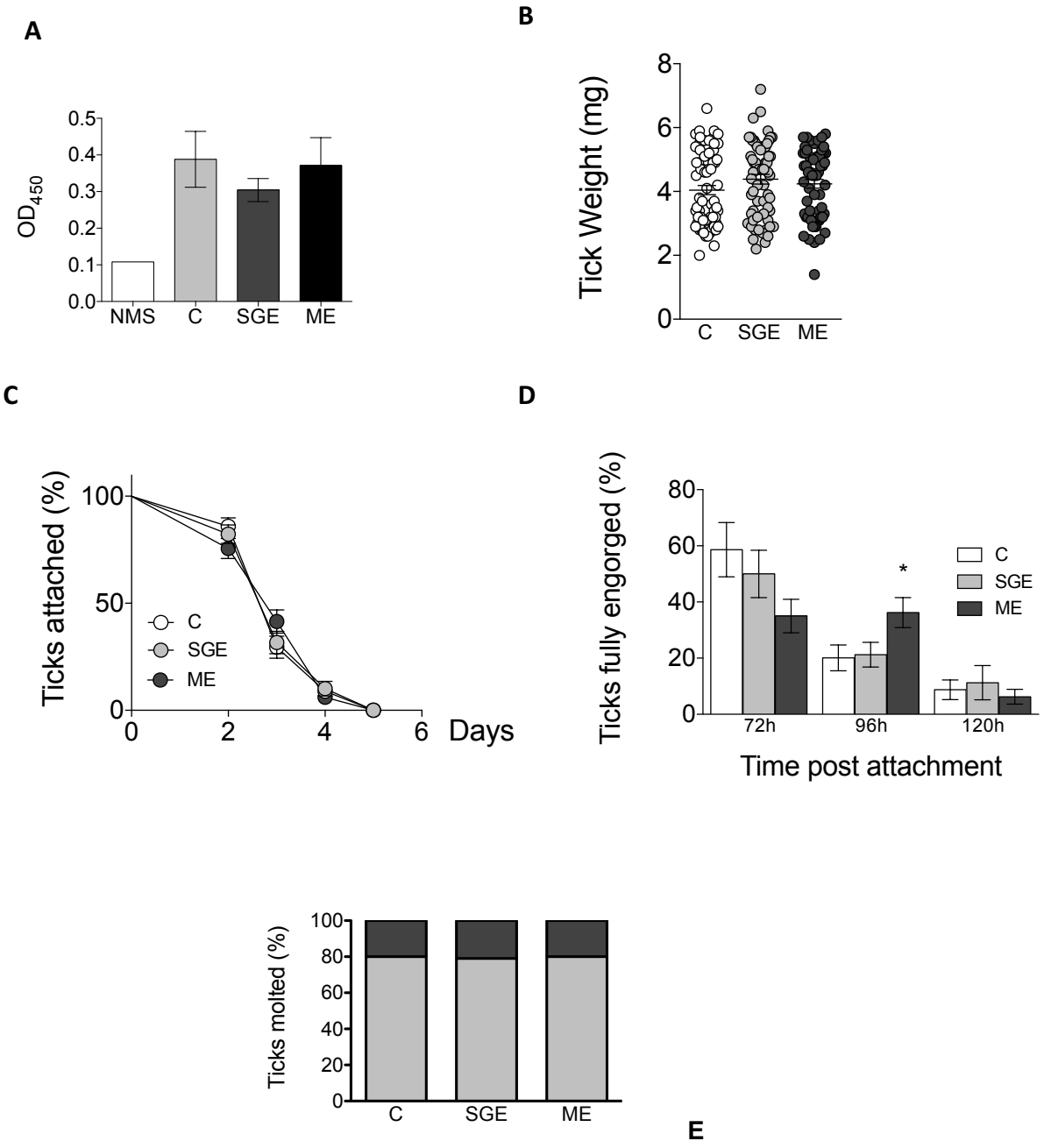

Figure 1.18. Effect of passive immunization with bovine sera raised against salivary gland (SGE) and midgut (ME) extracts. (A) Cow sera detection in control, SGE and ME immunized mice. The bars represent the mean IgG response from four mice. **(B)** Weights of ticks at the time of dettachment. (**C**) Percentage of attached ticks throughout the experiment. (**D)** Percentage of the fully engorged ticks recovered throughout the course of the experiments. *, Student's T test Control vs. ME, $p < 0.05$. (**E)** Rate of success in molting. Percentage of molted ticks relative to the number of engorged ticks recovered.

Identification of tick vaccine antigens from cow hyperimmune sera. In order to determine the specificity of the bovine anti-tick sera used in the previous experiments, we immunoblotted midgut and salivary gland extracts using day 68 hyperimmune and day 0 control sera. Both sera showed specific recognition of proteins in SGE and ME extracts (Fig. 1.19). However, while the anti-SGE sera recognized a limited number of antigens, midgut antisera showed a wide range of proteins that were specifically recognized (Fig. 1.19).

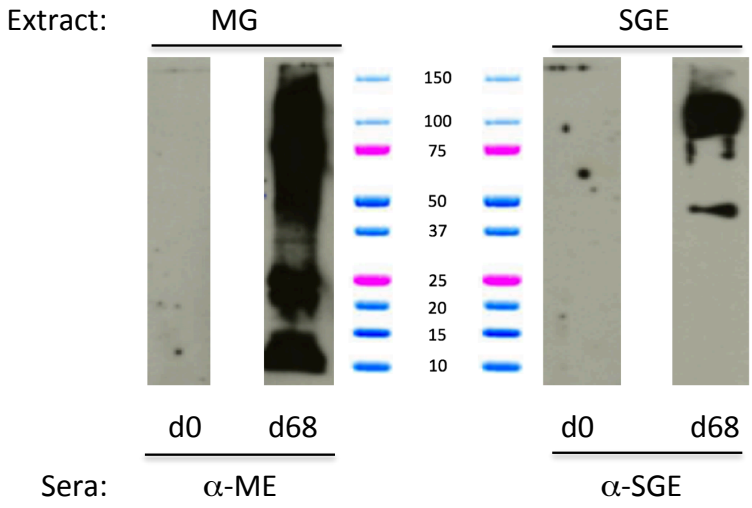

Figure 1.19. Reactivity of bovine sera against midgut and salivary gland extracts. Five μg of midgut (ME) and salivary gland (SGE) extracts were separated on SDS-PAGE and transferred to a nitrocellulose membrane. MG and SGE blots were tested using midgut antisera (α-ME d68) and salivary gland antisera (α-SGE d68), respectively. Pre-immune (d0) sera were used as controls.

We then sought to identify the antigens recognized by the hyperimmune sera because we argued that either alone or in combination, they could provide protection against tick feeding upon immunization and therefore, serve as vaccine candidates. For this purpose, we implemented an approach based on the immunoprecipitation of the antigens contained in both SGE and MG extracts by their specific antisera, followed by the identification of the antigens by Mass Spectrometry (Fig. 1.20).

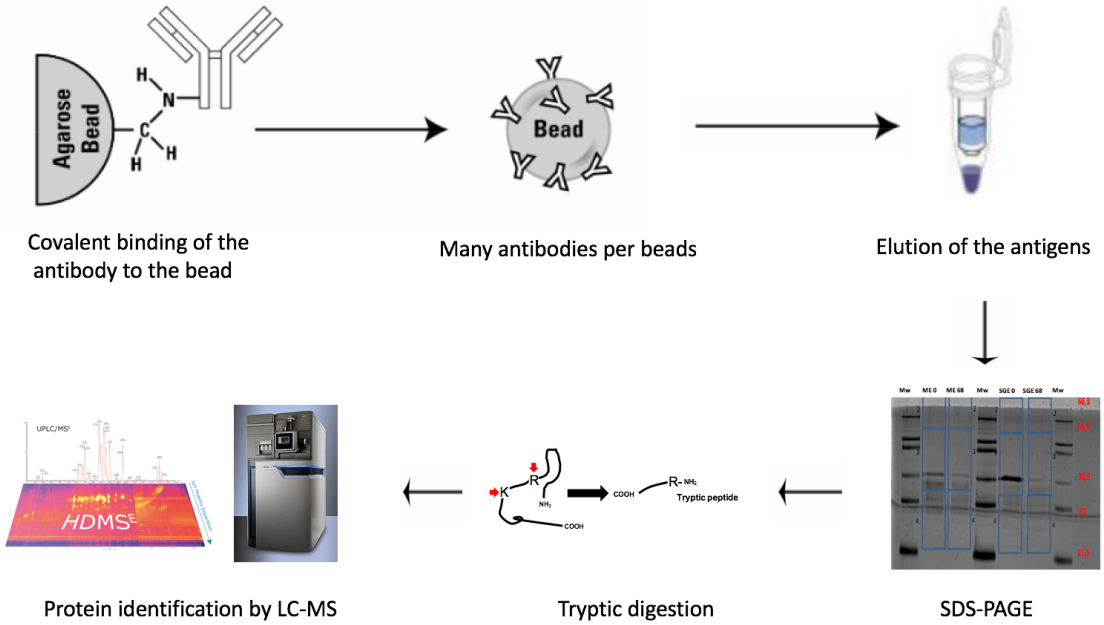

Figure 1.20. Outline of the experimental approach followed to identify antigens specifically recognized by MG and SGE bovine antisera.

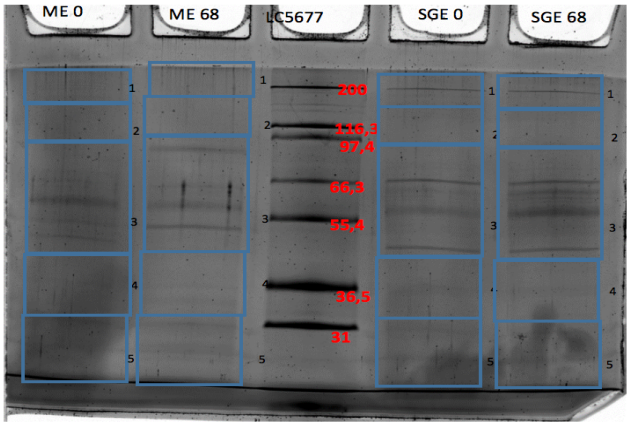

Figure 1.21. SDS-PAGE of the immunoprecipitated MG and SGE antigens. The gel was cut in slices as depicted, followed by in-gel protease digestion.

The immunoprecipitation of the antigens contained in the midgut and salivary gland extracts was performed using a technique that allows the binding of several antibodies per bead and to minimize the co-elution of heavy and light chains of the antibodies, by their direct covalent binding to the beads. This prevents their elution,

obtaining therefore a solution containing only the specific antigens recognized by these antibodies. We performed four immunoprecipitations with the antibodies contained in these sera: α-ME d0, α-ME d68, α-SGE d0, α-SGE d68.

The eluted immunoprecipitated proteins were ran in SDS-PAGE and the gels were excised as shown in Fig. 1.21. Slice number 3 was digested separately due to the higher density of bands. An in-gel tryptic digestion generated peptides that were separated by liquid chromatography and detected by mass spectrometry. The identification of the proteins was performed by Mascot software by comparing the peptides with those in the Uniprot/Swissprot database. The results of this analysis are summarized in Table 1.1.

Table 1.1. Immunoprecipitated proteins detected by LC/MS.

Accession	Description	ΣCoverage	Score 0	Score 68
IMMUNOPRECIPITATED SEQUENCES ONLY BY THE SGE INMMUNE SERA				
V5HMC9	Putative small ribonucleoprotein particle protein smg (Fragment)	16.22	0.00	54.37
A0A131XPM3	Putative 60 kDa heat shock protein mitochondrial (Fragment)	15.21	0.00	151.93
V5H3S3	Putative 60s ribosomal protein l23 (Fragment)	12.44	0.00	67.50
V5I095	Adenosylhomocysteinase (Fragment)	10.77	0.00	93.01
V5HG89	ATP synthase subunit beta (Fragment)	8.61	0.00	87.40
A0A0K8RQM9	Putative small nuclear ribonucleoprotein sm d3 (Fragment)	8.40	0.00	58.85
A0A0K8RC23	Putative 40s ribosomal protein s13	7.95	0.00	33.57
A0A131Y512	Putative ribosomal protein s16 (Fragment)	7.63	0.00	32.98
V5HWD5	**Putative metis5 protein**	**7.33**	**0.00**	**44.26**
A0A0K8RIJ1	Histone H2A	7.26	0.00	50.33
A0A0K8RP16	Dolichyl-diphosphooligosaccharide--protein glycosyltransferase subunit 1	6.84	0.00	115.81
A0A0K8RQ35	40S ribosomal protein S8 (Fragment)	6.77	0.00	40.95
A0A0K8RKT7	Putative glutathione s-transferase mu class *Rhipicephalus annulatus* glutathione s-transferase	5.38	0.00	39.95
A0A0K8RPW5	Putative metalloprotease (Fragment)	5.33	0.00	45.77
V5HRY6	Sodium/potassium-transporting ATPase subunit alpha (Fragment)	5.12	0.00	144.31
A0A0K8RL33	Superoxide dismutase [Cu-Zn]	4.57	0.00	35.85
A0A0K8RG01	Glyceraldehyde-3-phosphate dehydrogenase	4.49	0.00	51.70
A0A131XPA0	Putative eukaryotic translation initiation factor 3 subunit m (Fragment)	3.98	0.00	36.48
A0A0K8RHG9	Putative gamma tubulin	3.69	0.00	62.27
A0A0K8RMJ6	Putative ribosomal protein	3.60	0.00	37.81
V5HP83	Putative copi vesicle coat	3.49	0.00	61.57
A0A0K8RQF1	**Putative secreted protein (Fragment)**	**2.88**	**0.00**	**41.27**
A0A0K8R4C2	Dolichyl-diphosphooligosaccharide--protein glycosyltransferase 48 kDa subunit	2.52	0.00	37.19
A0A131XWG4	Putative vesicle coat complex copi beta' subunit	2.28	0.00	59.80
A0A0K8R8N9	Putative heat shock protein hsp 90-alpha isoform 1	1.50	0.00	37.81

Table 1.1. Immunoprecipitated proteins detected by LC/MS (Cont.).

Accession	Description	ΣCoverage	Score 0	Score 68
IMMUNOPRECIPITATED SEQUENCES THAT ARE SIGNIFICANTLY INCREASED IN THE SGE INMMUNE SERA RESPECT TO THE CONTROL				
A0A090XC63	Putative moesin/ezrin/radixin protein 1	14.45	81.17	206.20
V5HXA8	Putative 60s ribosomal protein l18	14.36	60.03	131.89
E3SS18	Translation elongation factor EF1-alpha (Fragment)	14.11	63.01	184.99
A0A0K8RCY6	Putative beta tubulin	7.86	40.59	127.53
V5GY25	Clathrin heavy chain	2.39	35.11	119.33

Accession	Description	ΣCoverage	Score 0	Score 68
IMMUNOPRECIPITATED SEQUENCES THAT ARE NOT SIGNIFICANTLY INCREASED IN THE SGE INMMUNE SERA RESPECT TO THE CONTROL				
V5H4T2	Putative glycinamide ribonucleotide synthetase gars/aminoimidazole ribonucleotide synthetase airs (Fragment)	20.90	41.20	71.91
A0A090XEK9	Putative myosin alkali light chain protein (Fragment)	17.02	41.67	44.63
V5I164	Putative tropomyosin (Fragment)	15.72	145.00	57.96
V5I150	Putative 60s ribosomal protein l5 (Fragment)	13.45	94.73	50.00
V5IF42	Putative myosin-2 essential light chain	12.64	40.41	0.00
V5IJC3	Putative 60s ribosomal protein l11 (Fragment)	12.07	128.84	79.57
A0A0K8RG40	40S ribosomal protein S4	11.07	74.40	81.92
V5I3C9	Putative myosin class v heavy chain (Fragment)	10.65	354.64	650.15
A0A0K8R4D7	Putative ubiquinol cytochrome c reductase subunit qcr2	8.79	105.77	115.65
A0A0K8RCY2	Putative metalloprotease	8.61	149.35	176.93
A0A0K8RCE8	Putative heat shock cognate 70 protein	8.33	60.97	115.44
A0A0K8RIU3	Putative heat shock 70 kDa protein 5	8.21	66.94	102.00
V5I135	Putative alpha crystallins	7.73	54.14	0.00
A0A131Y1S2	Putative microsomal triglyceride transfer protein	6.83	36.65	51.53
A0A131XNF3	Putative mitochondrial-processing peptidase subunit beta	6.05	105.08	87.93
V5HG43	Putative secreted stromal cell-derived factor 2 (Fragment)	5.11	34.15	0.00
A0A131XW65	Putative ribosomal protein (Fragment)	4.84	79.15	70.36
V5I085	Putative microsomal triglyceride transfer protein (Fragment)	3.42	36.01	58.33
A0A147BVX5	Putative secreted metalloprotease (Fragment)	3.24	34.45	0.00
A0A131XXE4	Putative zn-finger protein (Fragment)	0.78	37.74	0.00

Table 1.1. Immunoprecipitated proteins detected by LC/MS (Cont.).

Accession	Description	ΣCoverage	Score 0	Score 68
IMMUNOPRECIPITATED SEQUENCES ONLY BY THE ME ANTISERA				
V5H0K4	Putative biotinidase and vanin (Fragment)	32.21	0.00	161.39
A0A147BSS4	Putative biotinidase and vanin	16.74	0.00	206.82
V5HY31	Histone H4 (Fragment)	11.90	0.00	37.81
A0A131XRL8	Putative cathepsin l (Fragment)	5.53	0.00	72.31
A0A131XWI1	Putative salivary secreted cytotoxin (Fragment)	4.98	0.00	66.40
V5IFB6	Integrin beta (Fragment)	4.83	0.00	193.69
V5HWP4	Uncharacterized protein (Fragment)	4.44	0.00	48.01
V5I2L3	Putative adp/atp translocase (Fragment)	4.00	0.00	42.62
A0A0K8R8I3	Putative low-density lipoprotein receptor domain class a	3.40	0.00	80.81
A0A147BXB7	Putative cell adhesion molecule	3.35	0.00	70.59
V5HN24	Putative beta-n-acetylhexosaminidase (Fragment)	2.90	0.00	38.14
V5HEY6	Putative alpha-l-fucosidase	2.81	0.00	55.17
V5H7Z4	Putative alpha-macroglobulin	2.74	0.00	114.53
V5HBQ2	Putative prolylcarboxypeptidase angiotensinase c	2.59	0.00	40.01
A0A131XPM3	Putative 60 kDa heat shock protein mitochondrial (Fragment)	2.33	0.00	89.26
V5IJN2	Putative calcium-activated chloride channel protein 1 (Fragment)	2.33	0.00	39.96
A0A131XPI3	Putative aminopeptidase (Fragment)	2.02	0.00	34.48
A0A147BMG4	Putative antigen b membrane protein (Fragment)	1.86	0.00	34.22
A0A0K8RQE7	Alpha-mannosidase (Fragment)	1.64	0.00	62.70
V5GPX7	Putative alpha actinin	1.43	0.00	38.52
A0A131YAQ2	Putative conserved secreted protein (Fragment)	1.32	0.00	71.18
V5H492	Putative vitronectin receptor alpha subunit (Fragment)	1.20	0.00	43.73
A0A131XS30	Putative mam and ldl-receptor class a domain-containing protein 2 (Fragment)	0.31	0.00	40.27

Table 1.1. Immunoprecipitated proteins detected by LC/MS (Cont.).

Accession	Description	ΣCoverage	Score 0	Score 68
IMMUNOPRECIPITATED SEQUENCES THAT ARE NOT SIGNIFICANTLY INCREASED IN THE ME ANTISERA RESPECT TO THE CONTROL				
Q5D579	Actin (Fragment)	21.66	248.34	38.91
V5H4T2	Putative glycinamide ribonucleotide synthetase gars/aminoimidazole ribonucleotide synthetase airs (Fragment)	20.90	52.26	0.00
A0A131Y7G4	Putative secreted protein (Fragment)	14.20	58.35	84.84
A0A0K8RQA6	Putative ubiquitin/40s ribosomal protein s27a fusion (Fragment)	13.95	47.08	0.00
A0A090X8W5	Putative sulfotransferase	12.12	73.12	61.59
V5HHC0	Putative secreted protein	10.96	58.35	95.16
E3SS18	Translation elongation factor EF1-alpha (Fragment)	10.51	54.98	36.81
A0A0K8RCE8	Putative heat shock cognate 70 protein	10.00	171.54	0.00
V5HB74	Putative formyltetrahydrofolate dehydrogenase (Fragment)	9.80	181.55	90.92
A0A0K8RNA0	Putative nad-dependent malate dehydrogenase	8.24	73.48	0.00
A0A0K8RIU3	Putative heat shock 70 kDa protein 5	8.21	179.61	0.00
V5I135	Putative alpha crystallins	7.73	110.22	0.00
A0A131YAP7	Putative tropomyosin-2 isoform 4 mori tropomyosin isoform 4 (Fragment)	6.34	61.58	0.00
A0A0K8RK48	Putative ixodes 10 kDa peptide protein	5.17	43.68	44.01
A0A0K8RG01	Glyceraldehyde-3-phosphate dehydrogenase	4.49	39.91	0.00
A0A131XX88	Ribosomal protein L19 (Fragment)	4.37	44.69	0.00
V5I3C9	Putative myosin class v heavy chain (Fragment)	3.75	68.25	71.36
V5I4B8	Putative myosin class i heavy chain	3.46	178.22	52.04
A0A0K8RCB1	Putative enolase	2.77	38.63	0.00
A0A131XNF3	Putative mitochondrial-processing peptidase subunit beta	2.71	50.89	0.00
A0A131XQI6	Putative moesin/ezrin/radixin protein 1 (Fragment)	2.46	97.17	0.00
A0A131Y0J3	Putative aldehyde dehydrogenase (Fragment)	2.21	39.78	0.00
V5GY25	Clathrin heavy chain	1.02	47.55	0.00

For the selection of the new target antigens used to validate the immunoprecipitation assay, we first identified those specifically recognized by the hyperimmune sera. Then, we eliminated those proteins with housekeeping function, including ribosomal proteins, histones, etc. With the remaining list of proteins, we applied the following criteria in order to identify those of the highest interest:

- Proteins that were annotated as secreted or extracellularly exposed.
- Proteins with putative activities that could enhance our understanding of the relationship between the tick and the mammalian host.

When applying these criteria, we selected the proteins shown in Table 1.2 for furhter analysis.

UNIPROT ID	ORIGIN	DESCRIPTION
V5IFB6	Midgut	Integrin beta (Fragment)
A0A131YAQ2	Midgut	Putative conserved secreted protein
V5HWD5	Salivary Gland	Putative metis5 protein
A0A0K8RQF1	Salivary Gland	Putative secreted protein (Fragment)

Table 1.2. Identification of specific midgut and salivary gland extracts immunoprecipiated by the specific bovine antisera.

Following, there is a brief description of the four selected proteins, with the inclusion of some salient features identified by a preliminary *in silico* analysis.

V5IFB6: beta integrin. The analysis of the sequence of this protein (Fig. 1.22) revealed the presence of two EGF repeats (Fig. 1.23), related to integrin-like proteins. Integrins are transmembrane proteins with extracellular domains involved in processes such as cell motility, survival, proliferation and differentiation (Barczyk et al., 2010). According to SignalP 4.1, the protein does not contain a signal peptide. However, the online tool HMMTOP (http://www.enzim.hu/hmmtop/) identified a transmembrane domain in aminoacids 693-713, predicting an extracellular N-terminal domain and an intracellular C-terminus.

```
  1 SSCGECLRQP QCAWCTQQDF PRGLERCAPE KLLVDSGCSQ DAIENPQSKM IQETPLDKAG
 61 SDVQLQPGKV RLALRQGAPQ TFTVRYRQAD DYPVDLYYLM DLTHSMKDHR DKVAELADDM
121 VASMLNVTRN FRLGFGSFID KVVMPYVDTT PARLQNPCHD TQCAPPYGFH HQLPLTTNSS
181 LFTETVSSAA LSGNLDNAEG GFDAIMQAIV CKEKIGWNER SRKILLFATD SIFHAAGDGL
241 LGGIVRRNDE ECHLDQDGFY SESSDQDYPS LSQIVGVVQR SKINLIFAVP EGAYDVYRQL
301 SAFIDGSSVG KLVGDSSNIV HLVRDQYYKI RSEVVLKDNA PWFLRVNYSS NCLSGTGAKN
361 KQKTNACGGI RVGDEVEFQV SVELVNCPAD ASSHVFRISP VGVNEYVEVQ VEPICSCDCE
421 APQRTETNSS RCNGRGSSAC GVCSCDPNFY GKQCECLDTE LQLHKALCQA SNSSTELCSN
481 RGDCVCGECQ CYNPQGGGRV FGQWCQCDSF SCERDAESRV CGGPERGQCC GGECQCNSGW
541 GGSACDCSTD TSTCVAPGDP AGRMCGGHGD CVCGACRCRA DAGGRYSGPF CQDCAACVGR
601 CSEFRSCVQC TMFGSGEQSE KCRSECSKLN IVPVDKAEEA GPEERKCIFK DVDDCSFSFV
661 YYYDENNEPV IEAQKTKECG KEALTWYIVG GVVGGIVIFG LLAVCIGRFL LYLKDKLEYE
721 KFVKERKNAA WRLEMNPIFK EPVSEYRNPM YETGQPSTAG LSSGRS
```

Figure 1.22. Amino acid sequence corresponding to the *I. ricinus* protein annotated as V5IFB6. The peptides identified by LC/MS are highlighted in green. A putative transmembrane domain is highlighted in blue

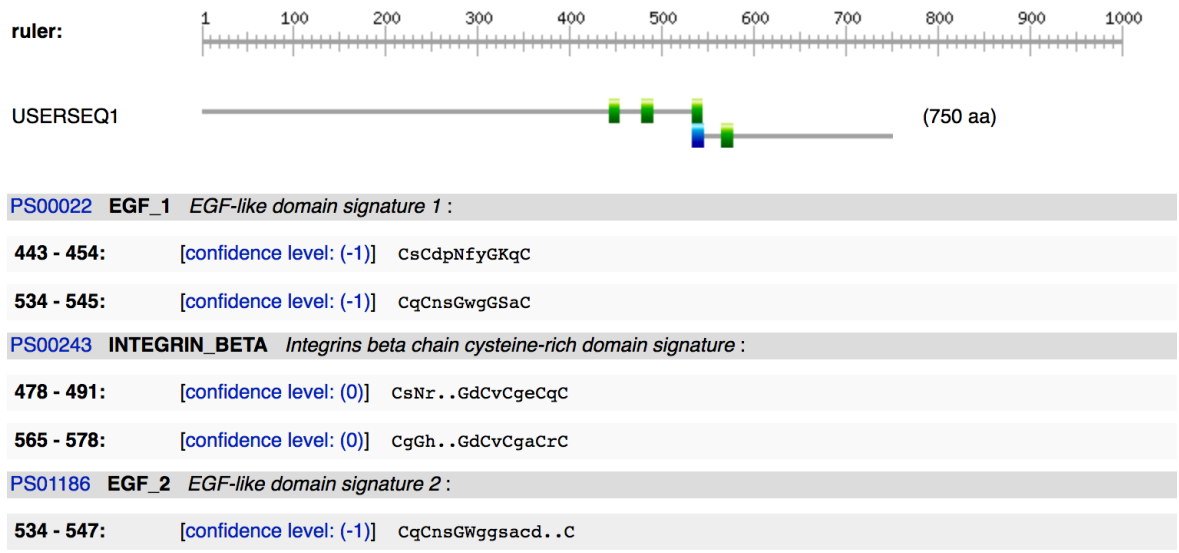

Figure 1.23. **Output of the ScanProsite webserver for the V5IFB6 sequence.** The specific domains and their location on the amino acid sequence are noted.

A0A131YAQ2: putative conserved secreted protein. This protein (Fig. 1.24) contains two PAN/Apple domains (Fig. 1.25), known to be involved in the inhibition of blood coagulation. According to SignalP 4.1, the protein contains a signal peptide ranging from residues 1 through 24.

```
  1 MRLTACLAAA VALTTLSVIE QSNGACDVRP KPGVKPKKYP DMLKVYENGY KLTAEINVEG
 61 EKSTLFFHEY YSFDFKQGLL ELTYRGITTN ILYLHHTEEI FVFDNRSCVT FPITSPPKLI
121 SPLLLRWSSL FTGNNTIFGP SVLFLSPALN PAVRMTFQGS DEEVRGIQTI KWATCLKNSD
181 DPYEVYFVDK KWNYGYGTGK TIPLRVRHGK VVTDIMRMQP YVGDPEQKLK IPMFVGCQRL
241 ARGFPKPPNF DNIPMEFHSA LAFSNPTVNG QYSYTSHLDI IRDPVNNIFS HIFAPWNTGS
301 GKLDQQLSVL PETQTIFDVT NGIQYLKVPH YFGYEPFGRG KCYVSSRKDF RPVVQLPDNT
361 TLSLLDTIAP SYETLKNANY LGIHVVRNAP VHVYEIVTTN VPVSGAVFSH AVITYCYLVE
421 WVYPTFTSQR NLPIRVSMRA YSTNKNLKIP YFWFTANIHD ISTAMEELND KMNVMDCYDE
481 NEASYTWFQM GFPYTDMYEE FLRYSPQIKS KFLATFLRTT SLSPMRVPRV LVDITENMIY
541 VTSLILERPL LETDYDRKKN FDLKDHQLKF GVVTLDECLK ICSSADYPDC KAVAYCGASC
601 YTSSLSSGGV DAGIVKSTDC TTYIKNDLSK KRKLPLTRDA IRKVETAVKE SKFTFTVEDS
661 TTFVVATLVA ESTDDSLGSL SMTFRGDDRF GTPHSHRRDG EELDGFKTYS LKSRLLADVD
721 GAVDLGSYPL NDCADICRDR PDCQFFSSCL VDSQCVISTI PAQTSKWIEM KLQCSTFAKS
781 VKDNFELFSG ISLDVGARKA VMTINDEECA RLCMVETGFD CKSFDYCGQA KDMH
```

Figure 1.24. Amino acid sequence corresponding to the *I. ricinus* protein annotated as V5IFB6. The peptide identified by LC/MS is highlighted in green. A putative signal peptide is highlighted in yellow.

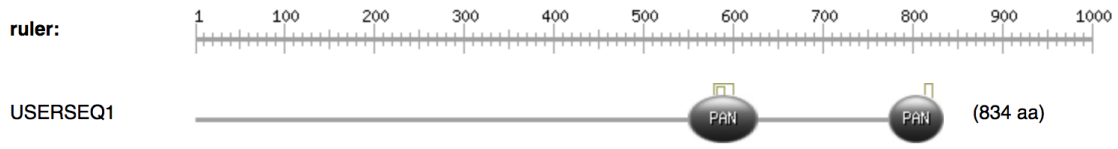

Figure 1.25. Output of the ScanProsite webserver corresponding to A0A131YAQ2.

V5HWD5: putative metis5 protein. This protein (Fig. 1.26) is a putative metalloprotease. Metalloproteases are protein hydrolytic enzymes whose catalytic mechanism involves a metal ion (Hamin Neto et al., 2016). They are also known to act as anticoagulants and show fibrinolytic activity (Stibániová & Kazimírová, 2013). According to SignalP 4.1, the sequence does not contain a signal peptide.

```
  1 MSSFAGVLTE DCFKVVSSQS YTFSKKPKPG TNWNLFPGKA WNKTFYCQKL HPQFLGVTGH
 61 DHESYSPRCK LLCCPKYHRT CFVNDMADGM GCGGDKVCMR HVCARPGGHP TAPPRTTTTP
121 STTTTKTTTT RRRWRWTGLN RHRRPATKLL
```

Figure 1.26. Amino acid sequence corresponding to the *I. ricinus* protein annotated as V5HWD5. The peptide identified by LC/MS is highlighted in green.

A0A0K8RQF1: putative secreted protein. A BLAST search of this protein (Fig. 1.27) revealed that it belongs to the Toll-like receptor family (Fig. 1.28). We argued that if indeed it is a secreted protein, it may function as a decoy receptor to prevent the activation of innate immune responses in mammalian cells. The protein also possesses a Leucine-rich repeat (LRR) motif at its C-terminus, which is characteristic of Toll like receptors (Fig. 1.27). However, the *in silico* analysis of the amino acid sequence predicted a transmembrane domain between amino acids 20 and 43, with an intracellular N-terminal domain and an extracellular C-terminus. On the other hand, SignalP 4.1 predicted a signal peptide spanning the first 40 amino acids.

```
  1 IMNRRRSGRV FPASAASAKM FSAFFFKLSL LLLVASIVLS SPVCYDQESS NKYRCMNFTS
 61 PDDFSEHVKP PILHQDLTFI VKNSRLSHLP TRAFAGVNVS VLEFDNVHLE PFTLQDENPF
121 AGLETTLRKV IFSEGSTVPE NWGLFANMLR LVTVRLSEIT NLNLTSGFNQ LPKSVRVITI
181 AFSTIGHVDE NWVSELENLE AVGIRHCDLL TXSRSMLPKP ALHLWRLDLY KNNLTSLPRD
241 FYR
```

Figure 1.27. Amino acid sequence corresponding to the *I. ricinus* protein annotated as A0A0K8RQF1. The peptide identified by LC/MS is highlighted in green. A putative signal peptide is highlighted in yellow. The LRR motif is shaded in grey.

TPA_inf: toll-like receptor 5 [Amblyomma variegatum]
Sequence ID: DAA34254.1 **Length:** 189 **Number of Matches:** 1

Range 1: 1 to 189 GenPept Graphics Next Match Previous Match

Score	Expect	Method	Identities	Positives	Gaps
154 bits(390)	2e-43	Composition-based stats.	98/189(52%)	133/189(70%)	2/189(1%)

```
Query  20   MFSAFFFKLSLLLLVASIVLSSPVCYD--QESSNKYRCMNFTSPDDFSEHVKPPILHQDL  77
            M+     + L + +      VL+ P C D  +      YRC NF+SPDDFS ++  P L  DL
Sbjct  1    MWGVLPYVLVVAIAATREVLAEPSCRDPSESDYEYYRCFNFSSPDDFSTYLVRPQLRSDL  60

Query  78   TFIVKNSRLSHLPTRAFAGVNVSVLEFDNVHLEPFTLQDENPFAGLETTLRKVIFSEGST  137
            TF++K+S+LSHLP RAF+ +N +VL+  NV LE F+L  ENPF GL+++LRK+I SEGST
Sbjct  61   TFVLKDSQLSHLPDRAFSQINATVLDLSNVQLETFSLPGENPFDGLQSSLRKIILSEGST  120

Query  138  VPENWGLFANMLRLVTVRLSEITNLNLTSGFNQLPKSVRVITIAFSTIGHVDENWVSELE  197
            +P +W +F++ +L TVR+SE  NL L   FN+LP+SV+VI IAFS I  VDE+WVS L+
Sbjct  121  IPTSWAVFSSLEQLKTVRISEAKNLVLARSFNELPQSVKVINIAFSNIASVDEDWVSGLQ  180

Query  198  NLEAVGIRH  206
            NLE VGIRH
Sbjct  181  NLEVVGIRH  189
```

Figure 1.28. A0A0K8RQF1 is a TLR family member. Output of the Basic Local Alignment Search Tool (BLAST) of the National Center for Biotechnology Information (NCBI) webserver for A0A0K8RQF1 sequence. The two sequences show a homology of 52%.

Initial validation of the immunoprecipitacion/proteomic identification of SGE and ME antigens. The four proteins identified as specifically recognized by bovine immune antisera were cloned into the pHIS-parallel2 expression vector for their subsequent purification. The validation of the immunoprecipitation was performed with the protein A0A0K8RQF1, which was produced and tested for the differential recognition of anti-SGE and day 0 antisera. A0A0K8RQF1 was cloned excluding the first 40 amino acids to avoid solubility problems. However, the protein remained in the insoluble cellular fraction after induction (Fig. 1.29A). Therefore, we proceeded to its extraction in the presence of urea and its refolding after solubilization (Fig. 1.29B). Then, we tested its differential recognition by the antisera by Western blotting. Figure 1.29C shows that the protein A0A0K8RQF1 is specifically recognized by hyperimmune anti-SGE but not the control cow sera. These data confirm that A0A0K8RQF1 is a candidate antigen that could participate in the protective immune response observed in SGE-immunized cows.

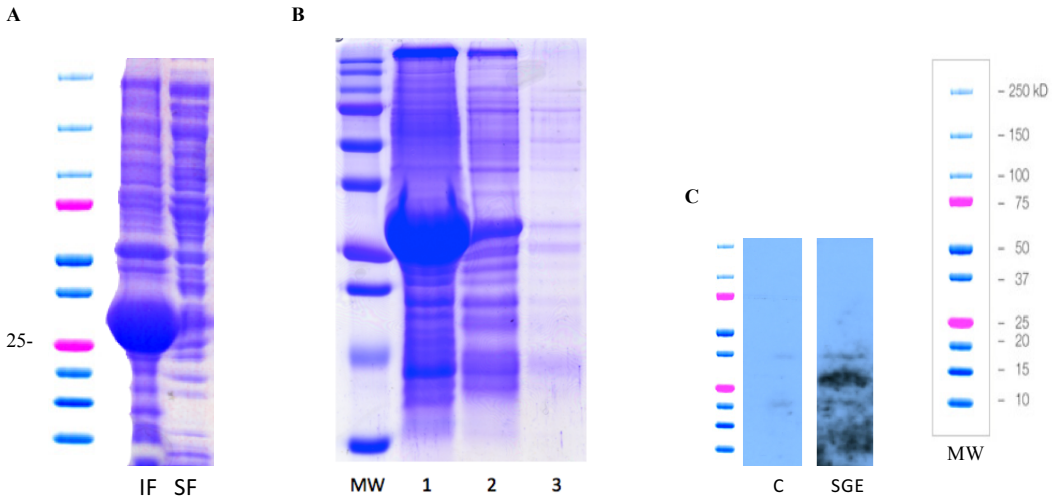

Figure 1.29. Validation of A0A0K8RQF1 as an antigen specifically recognized by immune anti-SGE sera. (A) Insoluble (IF) and soluble (SF) fractions obtained after induction and *E. coli* cell lysis. **(B)** Refolding of A0A0K8RQF1. 1: soluble protein in buffer containing 7 M urea. 2: intermediate refolding step in buffer containing 2 M urea. 3: refolded protein once the urea was completely removed. **(C)** Validation of the immunoprecipitation employed for the detection of new vaccine antigens. C: Control cow serum at day 0 (α-SGE d0). SGE: hyperimmune cow serum at day 68 (α-SGE d68).

1.4. DISCUSSION

The mouse is a widely used animal model to study infectious diseases and the development of vaccine candidates. Besides the determination of the use of these animals as an appropriate model for human or veterinary pathologies, welfare considerations need to be taken into account (Neuhaus, 2017). The test of adhesives approved for veterinary use is required in order to prevent unwanted and unnecessary distress to the animals (Gargili et al.; 2007). Therefore, we tested the use of tissue cement as adhesive to attach the tick capsules to the shaved skin of the mice, in order to follow regulations regarding animal welfare stablished by the Association for Assessment and Acreditation of Laboratory Care Animal International (AAALAC). Our experiments provide both an improved capsule design as well as evidence that tissue cement is able to provide strong bonding capabilities that are durable along the life of the experiment (at least 5 days). Our initial tests also resulted in an improved tick attachment protocol that minimizes animal discomfort while providing consistent and robust results.

The choice of an animal model is decisive in the development of human or veterinary vaccines. In this regard, the evaluation of the quantity and quality of the immune response against pathogens or parasites such as ticks is a critical step (Gerdts et al.; 2007). Previous results suggest that the utilization of the murine model is appropriate for vaccine assessment (Carpentier et al., 1996). Moreover, the use of small laboratory animals in vaccine evaluation has economic advantages (Lee et al., 2016), as well as other benefits including the availability of inbred, genetically defined strains, time and labor savings and easy handling (Lee et al., 2016; Gerds et al., 2007). The mouse model has been extensively used to study different aspects related to the relationship between ticks and mammalian hosts, including the design and test of vaccine candidates (Dai et al., 2010; de la Fuente et al., 2006; Schuijt et al., 2011; Dai et al., 2009). However, albeit one study claimed that Balb/c mice develop immunity after several rounds of tick infestation (Wikel et al., 1997), it is widely believed that mice do not develop tick immunity.

The immunization of mice with *I. scapularis* tHRF results in effects on tick feeding parameters (Dai et al., 2010) and we argued that this was an appropriate control to test whether its *I. ricinus* ortholog would induce the same effects against the

European tick. Our results, however, demonstrate that, regardless of the type of adjuvant used, mice are not able to mount a response that is able to significantly affect *I. ricinus* feeding, in spite of the almost complete homology between both orthologs. These results suggest that there are significant differences in the immune relationship stablished between mice and *I. scapularis* or *I. ricinus* ticks, which can result from the differential expression of tHRF or the participation of other antigens or immunomodulators with the host immune system. Further work will determine whether this is indeed the case. Mice are the natural tick hosts and the reservoir of the pathogens they transmit (Levine et al., 1985; Keesing et al. 2012; Hersh et al., 2012; Donoso-Mantke et al., 2011). Coevolutionary mechanisms have probably resulted in the mouse being unresponive to tick feeding, since they do not develop resistance to repeated infestations as other species do (Borsky et al., 1994) However, ticks can affect the murine immune response. For example, tick feeding results in the polarization of CD4 T cells toward a Th2 phenotype with a suppression of Th1 lymphocyte activity (Schoeler et al., 2000; Ferreira and Silva, 1999; Mejri et al., 2001), which seems to be advantageous for the survival of the ticks (Kaximírová & Iveta Štibrániová, 2013).

Passive immunization also results in effects on *I. scapularis* feeding parameters (Dai et al., 2010; Brossard et al., 1979; Askenase et al., 1982) indicating that antibody mediated responses can thwart tick feeding. The specific mechanisms by which tick-specific antibodies affect the feeding process are not defined but can include 1) the blockade of essential tick functions during feeding, as it seems to be the case for tHRF (since passive immunization mimics the effects after silencing of the gene) (Dai et al., 2010); 2) the perturbation of blood acquisition due to the formation of immune complexes; or 3) the activation of immune cells through the interaction of antibody-antigen complexes with specific receptors. The last mechanism would also be important when considering the protective effect of antibodies in passive transfer experiments using sera from species other than mice. Some crossreactivity has been demonstrated between human antibodies and murine immunoglobulin receptors (Ober et al., 2001) and our results show that passive immunization with cow sera exert some effects over tick feeding. However, our results show that mice are in general not a suitable model to test anti-tick vaccines, regardless of the mechanism(s) of action responsible for protection and that the blockade of essential activities exerted by salivary proteins may not be sufficient

to elicit a rejection response under our experimental conditions, as has been reported by others (Dincer et al., 2006).

As part of our implication in the ANTIDotE project (www.antidote-fp7.org), we aim to identify vaccine candidates that can foil tick feeding and the transmission of tick-borne pathogens. As part of this approach, we pursued an approach combining immunoprecipitation and proteomics tools using sera that had been generated by our collaborators in immunized cows that had shown protection against tick feeding. Using this approach, we identified tick antigens that are currently being tested as candidates for tick vaccines, of which we validated the differential recognition by the bovine sera of one of them. Of the identified differentially recognized tick proteins, we chose 2 present in the salivary gland and 2 from the midgut, based on their extracellular exposure (either because they are transmembrane or putatively secreted) or because they represented activities of interest. The identified metalloprotease, the integrin and the A0A131YAQ2 secreted protein are predicted to have activities related to the prevention of blood coagulation. On the other hand, the protein annotated as A0A0K8RQF1 is described as a secreted protein, and shows high homology with Toll-like receptors, including those present in several species of ticks. This is, therefore, likely a protein that could form part of the tick immune response belonging to one of the three identified innate immune pathways that are present in arthropods (Buchon et al., 2014; Smith et al. 2016; Liu et al., 2012; Narasimhan et al., 2014). In spite of being annotated as a secreted protein, an *in silico* analysis indicated the presence of an transmembrane domain, suggesting that it may act as a classic TLR. These results underscore the absence of a complete and accurate annotated genome and proteome for *I. ricinus* and advice that care must be taken assigning defined functions and cellular locations to the tick's proteins. Overall, we describe here the identification of a putative, validated, antigen that is recognized by immune sera that is protective against tick feeding in cows and that could provide the basis for a new vaccine formulation of veterinary and perhaps, human, use. Further work will determine the protective effect elicited by vaccination with this and other recognized antigens identified in this work and in the larger work performed by the ANTIDotE consortium.

CHAPTER 2

THE IMMUNOSUPPRESSIVE EFFECT OF THE TICK PROTEIN, SALP15, IS LONG-LASTING AND PERSISTS IN A MURINE MODEL OF HEMATOPOIETIC TRANSPLANT

2.1. INTRODUCTION

Salp15. The salivary protein of 15 kDa (Salp15) was identified from the salivary gland of *I. scapularis* ticks as one of several antigenic proteins recognized by tick-immune guinea pigs (Das et al., 2001). A 408-bp gene encoding a 14.7 kDa protein with a signal sequence of 21 amino acids was detected. *In silico* analysis of the amino acid sequence showed a weak homology with the active motif region of Inhibin A, a member of the TGFß superfamily (Anguita, 2002), suggesting that the protein may have immunomodulatory activity. Indeed, Salp15 inhibits the proliferation of CD4 T cells by repressing the production of the autocrine growth factor IL-2. Salp15 interferes T Cell Receptor (TCR) (Fig. 2.1; Fig. 2.3) signaling, since at lower concentrations of anti-CD3ε mAb or in the absence of co-stimulation (Fig. 2.2), the production of IL-2 was still markedly affected (Anguita et al., 2002). Confocal microscopy localized Salp15 attached to CD4 T cells, but not CD8 T cells. Further experiments showed that CD4 is the receptor for Salp15. Salp15 is able to impede the proper activation of the Src kinase Lck through the induction of a conformational change in CD4 that prevents the binding of Lck (Ashish et al., 2008). This results in the inhition of downstream signaling cascades, including Zap-70, the downstream effector enzyme PLCγ1, and other downstream early signaling intermediate components of T cell activation such as Vav1, Lat and CD3ε. Salp15 also affected negatively lipid raft organization, actin reorganization and TCR-triggered Ca^{+2} fluxes from intracellular stores during the activation of $CD4^{+}$ T cells. All these effects contribute to the diminished activation of regulatory elements that bind the proximal IL-2 promoter, including NF-kB and NF-AT and therefore, the inhibition of the expression of the *il-2* gene and the production of the cytokine (Garg et al., 2006; Juncadella et al., 2007).

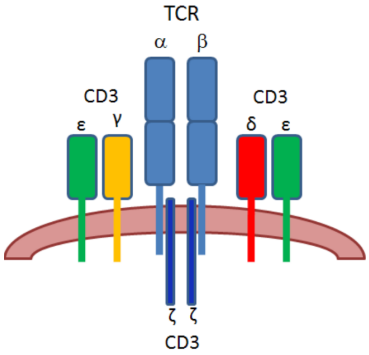

Figure 2.1. Basic composition of the T Cell Receptor (TCR).

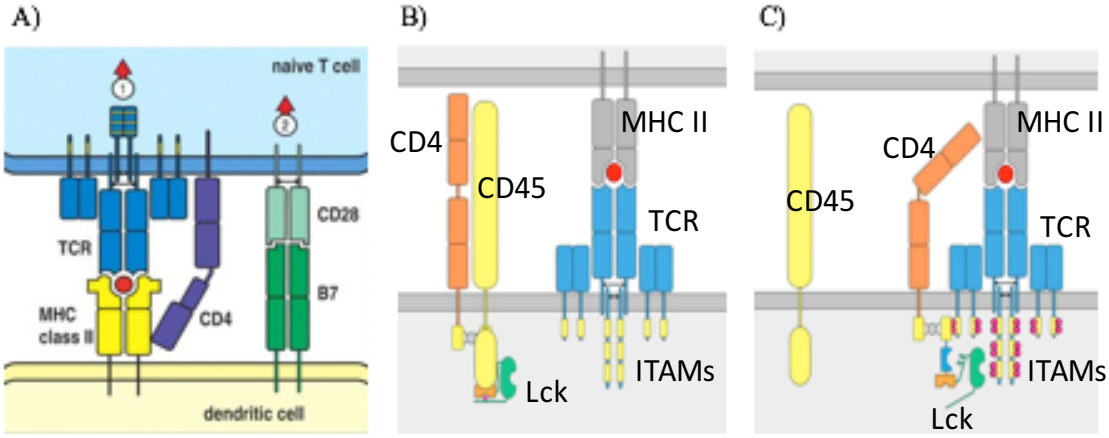

Figure 2.2. **Activation of CD4 T cells** The activation of CD4 T cells is mediated by two independent stimulations or signals: TCR stimulation and CD28 co-stimulation (A). When the TCR encounters with an antigen presented by an antigen presenting cell or APC, CD45 dephosphorylate Lck initiating its kinase activity (B). In turn, CD4 co-receptor initiates its aproximation to TCR to interact with MHC class II molecule bringing Lck into close proximity to phosphorilate ITAMs (immunoreceptor tyrosine-based activation motif) (C) and originate the signal cascade that will finish with the production of IL-2 via TCR signaling pathway (see Fig 2.3). Adapted from Janeway Immunobiology (7th edition), 2008.

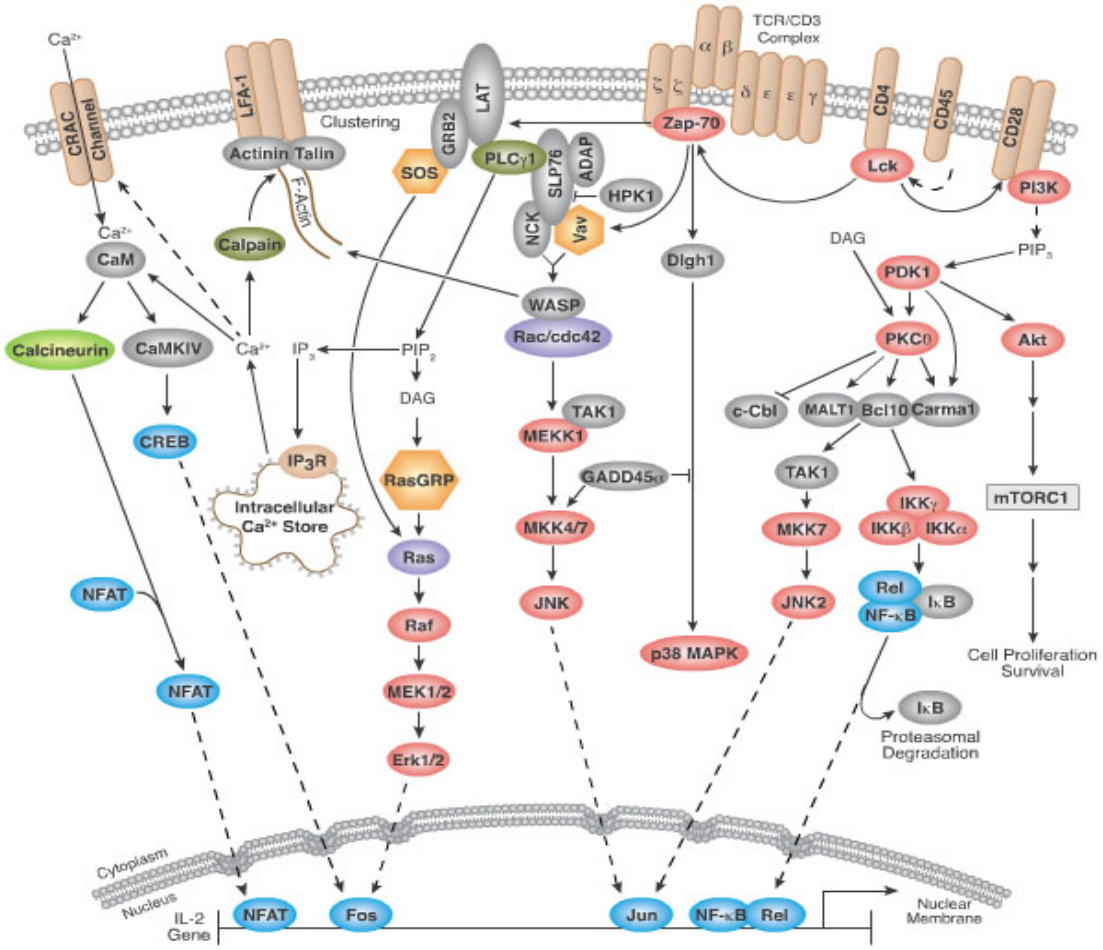

Figure 2.3. **TCR signaling pathway** Once ITAMs are phosphorylated on the cytosolic side of the TCR/CD3 by the tyrosine kinase Lck, the zeta-chain associated to the 70kDa tyrosine phosphoprotein kinase (Zap70) is recruited by ITAMs to the TCR/CD3 complex and is phosphorylated by Lck tyrosine kinase. This promotes the recruitment and phosphorylation of downstream intermediate components such as PLCy1, Vav, LAT, etc... The phosphorylation of PLCy1 results in the hydrolysis of PIP2 which act producing the second messengers DAG and IP3. DAG is necessary to promote the pathway that will finish with the production of the transcription factor NF-kB. IP3, in contrast, is the responsible of the release of Ca^{2+} from the ER, activating the entry of extracellular Ca^{2+} into cells via CRAC (Calcium Release-Activated Channels). In turn, calmodulin binds to the extracellular Ca2+ to mobilize calcineurin in order to promote the transcription of the autocrine growth factor IL-2 via the binding of NFAT to the promoter region of the gene *il-2* (Modified imagen from cell signaling technology).

Use of Salp15 as immunotherapy. The described effects of Salp15 in CD4 T cells made the saliva protein an interesting candidate as a therapeutic agent in pathologies mediated by these cells. Fisrt, Salp15 was tested in a mouse model of allergic asthma. Salp15 prevented the development of ovalbumin-induced asthma (Paveglio et. al., 2007), but once the disease was developed, the treatment with Salp15 was inefficient, suggesting that tick saliva protein does not affect memory or effector CD4+ T cells. Next, Salp15 was tested in experimental autoimmune encephalomyelitis (EAE), a mouse model for multiple sclerosis. However, treatment with the salivary protein resulted in increased pathology (Juncadella et al., 2010). Salp15 induced the differentiation of proinflammatory Th17 effector cells, suggesting that under strong TCR signals, Salp15 leads to a Th17 phenotype (Juncadella et al., 2009).

Graft versus host disease. The previous results suggested that the use of Salp15 as a therapy could be restricted to diseases in which the activation of CD4 T cells is predictable, such as transplants. A common complication associated with allogeneic hematopoietic stem cell transplantation (HSCT) is the appearance of Graft-versus-host disease (GvHD). In the early 1950s experimental evidence showed that the inoculation of bone marrow or fetal spleen cells into irradiated animals could rescue the hematopoietic system (Jacobson et al., 1950; Lorenz et al. 1951). Soon, irradiation followed by transplantation was proposed as an approach to treat hematopoietic malignancies, such as leukemia (Barnes & Loutit, 1956). The first successful human bone marrow autologous transplant was performed in 1959 (Thomas et al., 1959) in identical twins. Later, allogeneic transplantations were proposed as an alternative approach to treat hematopoietic malignancies. Nowadays, the number of allogeneic transplants worldwide reaches around 400.000 per year (Gratwohl et al., 2015). Unfortunately, allogeneic transplants can lead to secondary pathologies including Graft versus Host Disease (GvHD).

GvHD appears when donor T cells recognize as foreign the recipient antigens, including both human leukocyte (HLA) and minor histocompatibility antigens. GVHD appears in 50% of the transplants and causes death in 15% of the cases (Blazar et al., 2012). The induction of immunosuppression after HSCT can produce undesirable effects, even though it is usually effective. These include the inhibition of graft-versus-tumor effector cells (GvT) and the appearance of infections

and neoplasms (Blazar et al. 2012; Mikulska et al., 2009; Dykewicz et al., 2001; Akhtari et al., 2013; Friedman et al., 2013). The treatments used for the mitigation or elimination of this disease are ineffective and unspecific. In fact, pre-transplantation chemotherapy and radiotherapy treatments (conditioning) applied in these cases for the elimination of the cancer cells and the establishment of the transplanted cells can result in nonspecific inflammatory events, helping create the necessary conditions for the activation of donor T cells (Holler et al., 2004). After pre-transplantation conditioning, human GvHD is classically manifested first as acute GvHD (aGvHD), around 100 days after transplantation and comprise the activation of antigen presenting cells by the conditioning regimen, the activation of alloreactive T and tissue destruction by the activated T cells. Typically, a chronic phase (cGvHD) develops around 2-5 years after transplantation. cGvHD occurs in 50% of long-term survivors and is still the leading cause of death in HSCT patients (Schroeder & DiPersio, 2011; Boieri et al., 2016). The clinical manifestations of cGvHD are comparable to an autoimmune syndrome, characterized by systemic fibrosis, autoantibody production, chronic inflammation and immune complex deposition in different tissues. Interestingly, therapies that prevent aGvHD do not decrease in general the occurrence of cGvHD (Lee, 2010). These therapies include the use of immunosuppressive drugs such as folic acid and/or calcineurin inhibitors, as well as cytokine antagonists, including TNF, IL-6 or IL-2. Other approaches target chemokines or chemokines receptors as well as co-stimulatory molecules including CD28, CD80 and CD86, among others. Cell therapy has also broadly been used as GvHD treatment, particularly mesenchymal stem cells and regulatory T cells (Boieri et al. 2016). However, despite the advances performed through preclinical modeling of GvHD in mice, many questions remain. Basic research using murine models of GvHD can therefore enhance our understanding of human GvHD and help design novel therapeutic approaches (Schroeder & DiPersio, 2011).

Although several murine models of transplantation exist (Schroeder et al. 2008; Chu et al., 2008), none recapitulates exactly the pathology observed in human transplantation. The dose and type of the T cell subsets influences the severity of the disease, but also the conditioning regimen as well as genetic disparities in the antigens expressed in MHC molecules or minor histocompatibility antigens (miHAs) (Schroeder & DiPersio, 2011). The following modified tables (Schroeder & DiPersio; 2011) show the GvHD models that have been developed so far:

Donor strain	Recipient strain	Conditioning regimen	Genetics	Main T-cell type contributing to phenotype	Cell type and dose	Outcome	Reference example(s)
miHA mismatched							
B10.D2 ($H2^d$)	BALB/c ($H2^d$)	Sub-lethal 600-750 cGy or Fractionated 1000 cGy	miHA mismatches	CD4 (minor contribution by $CD8^+$)	1×10^7 BM cells and 1×10^8 whole splenocytes	Systemic disease	Korngold and Sprent, 1987; Eyrich et al., 2005
B10 ($H2^b$)	BALB.b ($H2^b$)	775 cGy	miHA mismatches	$CD4^+$ (with some contribution from $CD8^+$)	8×10^6 TCD BM cells and 10^7 unfractionated spleen cells or 1.4×10^6 $CD4^+$ or 6×10^5 $CD8^+$ T cells	Systemic disease; no cutaneous involvement	Kaplan et al., 2004
C57/Bl6 ($H2^b$)	BALB.b ($H2^b$)	850–1000 cGy	miHA mismatches	$CD4^+$	5×10^6 TCD BM cells and 2×10^6 T cells	Systemic disease	Berger et al., 1994; Zhang et al., 2005
DBA/2 ($H2^d$)	B10.D2 ($H2^d$)	820 cGy	miHA mismatches	$CD8^+$	4×10^6 TCD BM cells and 1×10^6 T cells, or purified $CD4^+$ or $CD8^+$ T cells	Minimal systemic disease with whole spleen cells but increased with purified $CD8^+$ T cells; up to 50% mortality at day 25	Korngold and Sprent, 1987
Xenotransplantation models							
Human PBMCs	NOD/SCID IL2rγ-null (NSG)	No XRT or 200-250 cGy	Mistmatched for MHC I, MHC II and miHAs	$CD4^+$	1×10^7 or $5\text{-}10\times10^6$	Death from GvHD in 30-50 days	Ito et al., 2009; King et al., 2009
Human PBMCs	BALB/cA-$RAG2^{-/-}$ $IL2r\gamma^{-/-}$	350 cGy	Mismatched for MHC I, MHC II and miHAs	$CD4^+$ and $CD8^+$	$5\text{-}30\times10^6$	Systemic disease	van Rijn et al., 2003
Human peripheral blood T cells: naive or CD3/CD28 bead expanded	NOD/SCID β2m-null	250-300 cGy	Mismatched for MHC I, MHC II and miHAs	–	1×10^7 human T cells RO injection	Systemic disease	Nervi et al., 2007

BM, bone marrow; cGy, centigray; RO, retro-orbital injection; TCD, T-cell depleted; XRT, radiation conditioning.

Donor strain	Recipient strain	Conditioning regimen	Genetics	Main T-cell type contributing to phenotype	Cell type and dose	Outcome	Reference example(s)
miHA mismatched							
B10.D2 ($H2^d$)	BALB/c ($H2^d$)	Sub-lethal 600-750 cGy or Fractionated 1000 cGy	miHA mismatches	CD4 (minor contribution by $CD8^+$)	1×10^7 BM cells and 1×10^8 whole splenocytes	Systemic disease	Korngold and Sprent, 1987; Eyrich et al., 2005
B10 ($H2^b$)	BALB.b ($H2^b$)	775 cGy	miHA mismatches	$CD4^+$ (with some contribution from $CD8^+$)	8×10^6 TCD BM cells and 10^7 unfractionated spleen cells or 1.4×10^6 $CD4^+$ or 6×10^5 $CD8^+$ T cells	Systemic disease; no cutaneous involvement	Kaplan et al., 2004
C57/Bl6 ($H2^b$)	BALB.b ($H2^b$)	850–1000 cGy	miHA mismatches	$CD4^+$	5×10^6 TCD BM cells and 2×10^6 T cells	Systemic disease	Berger et al., 1994; Zhang et al., 2005
DBA/2 ($H2^d$)	B10.D2 ($H2^d$)	820 cGy	miHA mismatches	$CD8^+$	4×10^6 TCD BM cells and 1×10^6 T cells, or purified $CD4^+$ or $CD8^+$ T cells	Minimal systemic disease with whole spleen cells but increased with purified $CD8^+$ T cells; up to 50% mortality at day 25	Korngold and Sprent, 1987
Xenotransplantation models							
Human PBMCs	NOD/SCID IL2rγ-null (NSG)	No XRT or 200-250 cGy	Mistmatched for MHC I, MHC II and miHAs	$CD4^+$	1×10^7 or $5\text{-}10\times10^6$	Death from GvHD in 30-50 days	Ito et al., 2009; King et al., 2009
Human PBMCs	BALB/cA-$RAG2^{-/-}$ $IL2r\gamma^{-/-}$	350 cGy	Mismatched for MHC I, MHC II and miHAs	$CD4^+$ and $CD8^+$	$5\text{-}30\times10^6$	Systemic disease	van Rijn et al., 2003
Human peripheral blood T cells: naive or CD3/CD28 bead expanded	NOD/SCID β2m-null	250-300 cGy	Mismatched for MHC I, MHC II and miHAs	–	1×10^7 human T cells RO injection	Systemic disease	Nervi et al., 2007

BM, bone marrow; cGy, centigray; RO, retro-orbital injection; TCD, T-cell depleted; XRT, radiation conditioning.

Donor strain	Recipient strain	Conditioning regimen	Genetics	Main T-cell type contributing to phenotype	Cells and dose	Outcome	Reference example(s)
Scleroderma (pro-fibrotic models)							
B10.D2 ($H2^d$)	BALB/c ($H2^d$)	700-900 cGy	miHA mismatched	$CD4^+$	TCD BM cells and 1×10^7 whole splenocytes or purified T cells	Scleroderma; progressive fibrosis of organs	Korngold and Sprent, 1978; Jaffee and Claman, 1983; Claman et al., 1985; Hamilton, 1987; Korngold and Sprent, 1987; McCormick et al., 1999; Levy et al., 2000; Kaplan et al., 2004; Zhou et al., 2007
LP/J ($H2^b$)	C57/Bl6 ($H2^b$)	900-1100 cGy	Mismatched for miHAs and MHC	ND	20-50$\times10^6$ spleen cells and 5×10^7 BM	Scleroderma occurring by day 28	Hamilton and Parkman, 1983; DeClerck et al., 1986
B10.D2 ($H2^d$)	BALB/c Rag2$^{-/-}$ ($H2^d$)	None	$H2^d$ matched but miHA mismatched	ND	Whole spleen cells (2-5$\times10^7$)	Scleroderma; progressive fibrosis of organs; autoantibodies	Ruzek et al., 2004
Autoantibody-mediated (lupus-like) models							
DBA/2 ($H2^d$)	B6D2F1 ($H2^{b/d}$)	No conditioning	Mismatched for MHC I, MHC II and miHAs	$CD4^+$	1-10$\times10^7$	Lupus Sjorgren's (Sialoadenitis); autoantibodies	Via et al., 1987; Fujiwara et al., 1991; De Wit et al., 1993; Via et al., 1996a; Slayback et al., 2000; Kim et al., 2006; Kim et al., 2008
BALB/c ($H2^d$)	(BALB/cxA)F1 ($H2^{d/a}$)	No conditioning	Mismatched for MHC I, MHC II and miHAs	$CD4^+$	8-12$\times10^7$ spleen cells	Polyarthritis, scleroderma, glomerulonephritis, Sjorgren's, sclorosing cholangitis	Pals et al., 1985; Vidal et al., 1996
C57/Bl6 ($H2^b$)	(B6xBALB/c)F1 ($H2^{b/d}$)	No conditioning	Mismatched for MHC I, MHC II and miHAs	$CD4^+$	6×10^7 whole spleen cells	Acute progressing to chronic GvHD	Tschetter et al., 2000
DBA/2 ($H2^d$)	BALB/c ($H2^d$)	650 cGy	miHA mismatches	–	5×10^7 whole spleen cells	Autoantibodies; skin scleroderma	Zhang et al., 2006
C57/Bl6 ($H2^b$)	(C57/Bl6 × B6.C-$H2^{bm1}$)F1 ($H2^b$ background with mutation at MHC I)	No conditioning	MHC I mismatched	$CD8^+$	5×10^7 spleen cells or 10^8 spleen (2/3) and lymph node (1/3) cells; 2 doses of cells on day 0 and 7	Glomerulonephritis; non-lethal in unirradiated mice; lethal in irradiated mice at 30-60 days	Rolink et al., 1983; Ito et al., 1992
C57/Bl6 ($H2^b$)	(C57/Bl6 × B6.C-$H2^{bm12}$)F1 ($H2^b$ background with mutation at MHC II)	None or 900 cGy	MHC II mismatched	$CD4^+$	No conditioning: 4-5$\times10^6$ spleen $CD4^+$ T cells, 2-3$\times10^6$ BM cells; 2 doses of cells on day 0 and 7 Conditioned: 4-5$\times10^6$ $CD4^+$ T cells and 1-2$\times10^6$ TCD BM cells	Systemic disease and death by 20-40 days	Rolink et al., 1983; Ito et al., 1992; Brown et al., 2002
Thymic dysfunction model							
Bl6-H2-Abl$^{-/-}$ ($H2^b$)	C3H/HeN ($H2^k$)	1300 cGy split in two fractions	Mismatched for MHC I, MHC II and miHAs	BM-derived $CD4^+$ and $CD8^+$	5×10^6 TCD BM cells	Epidermal atrophy, fat loss, follicular drop out and dermal thickening; bile duct loss and periportal fibrosis in liver; salivary gland fibrosis and atrophy; cytopenias	Sakoda et al., 2007

Abbreviations as for Table 1, plus: B6, C57/Bl6; B6D2F1, (C57/Bl6 x DBA/2)F1; ND, not determined.

Because Salp15 is able to inhibit early T cell signaling events, we hypothesized that the protein could preclude the activation of CD4 T cells and induce a long-term unresponsive or anergic state after the exposure to the salivary protein. We used a murine model in which a transplant from pure strains is injected into the F1 offspring, which does not require previous conditioning and results in mild episodes of acute GVHD followed by a period of chronic disease characterized by the production of autoantibodies (Tschetter et al., 2000). Our results show that Salp15 is able to change the transcriptional program of CD4 T cells during activation that nevertheless, fades over time and does not result in increased populations of anergic or regulatory T cells. However, the protein induces the upregulation of the ectoenzyme, CD73 on the surface of regulatory T cells, likely inducing increased production of the immunosuppressive molecule, adenosine. Overall, the activity of Salp15 is evident in a long-term transplantation murine model and prevents the deposition of immune complexes in the kidney, a hallmark of chronic GVHD.

2.2. METHODS

Protein purification and labeling. Salp15 and an inactive deletion mutant lacking the last 20 aminoacids (Salp15Δ11) (Juncadella et al., 2010) were purified from Drosophila S2 cells, as described (Anguita et al., 2002). Protein labeling was performed using the Alexa Fluor® 488 Protein Labeling Kit (Thermo Fisher Scientific, Eugene, OR), following the manufacturer's instructions.

Cell purification and activation. CD4 T cells were purified from the spleens of C57BL/6 mice by negative selection using a CD4 T cell isolation Kit (Miltenyi Biotec, Bergisch Gladbach, GE) according to the manufacturer's instructions. Purified CD4 T cells at the indicated concentrations were activated with 5 μg/ml of plate-bound anti-CD3ε and 1 μg/ml of soluble anti-CD28 (BD Biosciences, San Diego, CA) in the presence of Salp15 or Salp15ΔP11. Cells were incubated at 37ºC in TexMACS Medium (Miltenyi Biotec).

Flow cytometry. Blood was extracted from the saphenous vein in the presence of EDTA and depleted of erythrocytes by hypotonic lysis. Whole splenocytes were isolated from immunized or GvHD mice by mechanical disruption followed by lysis of erythrocytes. The cells (10^6/ml) were incubated with Fc Block (anti-CD16/CD32; BD BioSciences) and labelled with fluorochrome-labeled antibodies against CD4, CD8, B220, CD69, Ly6C, F4/80, GR-1, CD25, CD11b, CD44, CD73, FR4, NRP1, Foxp3, CD93, IgM, CD23 (Miltenyi Biotec). To detect Salp15 binding to CD4 T cells, splenic purified CD4 T cells were labeled with Salp15-Alexa Fluor^{488} or Salp15ΔP11-Alexa Fluor^{488}.

Graft versus host disease murine model. Splenocytes were extracted from 8-week old C57BL/6 (H-2^b) mice and 60 x 10^6/mouse were injected intraperitoneally into CB6F1 (H-$2^{b,d}$) mice (Envigo, Gannat, France). The mice were treated with 50 μg of Salp15 by intraperitoneal injection starting the day of cell transfer and every other day until day 10. Blood was extracted from day 10 to day 80 at 10-days intervals. Erythrocytes were removed by hypotonic lysis and the cells were analyzed by flow cytometry. At sacrifice, kidneys were processed for histochemical evaluation.

Renal deposited IgG detection, PAS and HE. Kidneys were fixed in 10% neutral buffered formalin, dehydrated, embedded in paraffin and cut into 5μm thick sections. For histopathology, sections were hydrated and stained with hematoxylin – eosin (HE) or periodic acid-Schiff (PAS) according to standard protocols. For immunohistochemical analysis, tissue sections were subjected to antigen retrieval using protease K for 20 minutes at 37 ºC. After blocking, sections were incubated with primary antibody overnight. The slides were then sequentially incubated with DAB chromogen for 5 min, counterstained with Mayer's hematoxylin and mounted for microscopy. Goat Anti-Mouse IgG-HRP Light chain specific (Jackson ImmunoResearch Laboratories) was used at 1/250 concentration as the primary antibody. Photographs were taken with an Axioimager A1 microscope and analyzed with Frida software (Gurel et al., 2008).

RNAseq. Purified CD4 T cells from three mice were activated independently with 5 μg/ml of plate-bound anti-CD3ε and 1 μg/ml of soluble anti-CD28 (BD Bioscience) in the presence of 25 μg/ml of Salp15 or Salp15ΔP11 (control). Cells were incubated at 37ºC in TexMACS Medium (Miltenyi Biotec) for 48 and 96h. RNA extraction was performed using the PureLink RNA Micro Scale Kit (Thermo Fisher Scientific) according to the manufacturer´s protocol. The quantity and quality of the RNAs were evaluated using the Qubit RNA Assay Kit (Invitrogen, Eugene, OR) and RNA Nano Chips in a 2100 Bioanalyzer (Agilent Technologies, Waldbronn, GE), respectively. Libraries for sequencing were prepared using the TruSeq RNA Sample Preparation Kit v2 (Illumina Inc, San Diego, CA) following the protocol provided by the manufacturer. Single-read, 50 nt sequencing of pooled libraries was carried out in a HiScanSQ platform (Illumina Inc.).

The quality control of the sequenced samples was performed with FASTQC software (www.bioinformatics.babraham.ac.uk/projects/fastq). Reads were mapped against the mouse (*mm10*) reference genome by using the program Tophat (Trapnell et al., 2009) to account for spliced junctions. The resulting BAM alignment files for the samples were the input for the Differential Expression (DE) analysis, carried out by DESeq2 (Love et al., 2014), to detect differentially expressed genes among the different conditions. GO enrichment was tested using the ClusterProfiler (Yu et al., 2012) Bioconductor package and the Panther Database (Thomas et al.,

2003). Transcriptomics data were also analyzed using QIAGEN´s Ingenuity Pathway Analysis (IPA, QIAGEN, Red Wood city, CA).

Real-time RT-PCR. RNA was reverse transcribed using M-MLV reverse transcriptase (Thermo Fisher Scientific) and random hexamers. Real-time PCR was then performed using SYBR Green PCR Master Mix (Quanta Biosciences, Beverly, MA) on a QuantStudio 6 real-time PCR System (Thermo Fisher Scientific). Fold induction of the genes was calculated using the $2^{-\Delta\Delta Ct}$ method relative to the reference, previously validated genes, *Rpl19* and *Actb*, as indicated. The primers used are listed below (Table 2.4):

Gene	Forward	Reverse	Purpose
IL2	TGTGCTCCTTGTCAACAGCG	TTTCAATTCTGTGGCCTGCTTG	RNAseq validation
Zfp750	CCCACCTTTGCTGCAGGT	GGGGGCCGTGGAATATAGTG	RNAseq validation
Klf2	GCCTTCGGTCTTTTCGAGGA	AGGCTTCTCACCTGTGTGTG	RNAseq validation
Serpine2	GATCCAAGCGAGGACGGG	GACCTGGATCCCTGTGTTGG	RNAseq validation
Cd44	ATCCTCGTCACGTCCAACAC	GCTTTCTGGGGTGCTCTTCT	RNAseq validation
Jchain	GACGACGAAGCGACCATTCT	GCTCTGGGTGGCAGTAACAA	RNAseq validation
Amy2a5	TTCGTTCTGCTGCTTTCCCT	CATTGGGTGGAGAGACCTGC	RNAseq validation
Cd7	ATGCCCAAGACGTACAACAG	CTCCTGCCGGTCTTCAAAGT	RNAseq validation
Art2a-ps	GGCTAACCCAGCAGGTGACT	GGCTTCTGTGGATGTTCCCA	RNAseq validation
Rpl19	GACCAAGGAAGCACGAAAGC	CAGGCCGCTATGTACAGACA	Reference, RNAseq validation
Actb	GACGATGCTCCCCGGGCTGTATTC	TCTCTTGCTCTGGGCCTCGTCACC	Reference, RNAseq validation

Table 2.4. Sequence of the Primers used for RNAseq validation by qRT-PCR.

Determination of adenosine levels. The levels of adenosine were determined in the culture supernatants of activated CD4 T cells using the fluorometric adenosine assay kit (Abnova, Walnut, CA) following the methods provided by the manufacturer.

Statistical analysis. Results are presented as means ± SE, unless otherwise stated. The differences in means between groups were tested using the Student´s T-test. Differences in antibody titers were assessed by a 2-way ANOVA. All calculations were made in GraphPad Prism, version 7. A p-value < 0.05 was considered statistically significant. All experiments were performed at least 3 times. *In vivo* experiments consisted of groups of 5 mice and were performed at least twice.

Ethics statement. All work involving animals was approved by the Institutional Animal Care and Use Committee (IACUC) at CIC bioGUNE and the competent

authority (Diputación de Bizkaia). CIC bioGUNE animal facility is accredited by AAALAC Intl. All experiments were performed in accordance with European and Spanish guidelines and regulations.

Data availability. The transcriptomic data are deposited under GEO accession number GSE98700.

2.3. RESULTS

The effect of Salp15 on activating CD4 T cells is long-lasting. In order to determine whether the effect of Salp15 on the activation of CD4 T cells is sustained, we activated purified splenic CD4 T cells in the presence of the salivary protein for 2 days, followed by their extensive washing and re-stimulation for 2 more days. The production of IL-2 was significantly reduced at both time points, including after 4 days of activation when Salp15 was no longer present (Fig. 2.4A). The longer-term effect of Salp15 could be due to its persistent binding to the surface of CD4 T cells. Thus, we determined the binding of Alexa Fluor^{488}-labeled Salp15 as well as the inactive control (Salp15Δ11) by flow cytometry. Although both Salp15 and Salp15Δ11 bound to purified CD4 T cells, the deletion of the C-terminal peptide, P11, resulted in decreased binding (Fig. 2.4B) in agreement with its reported lack of activity (Juncadella et al., 2010). Importantly, binding of Salp15 to CD4 T cells was detectable for up to 72h (Fig. 2.4B), indicating a persistent ability of this protein to remain attached to CD4.

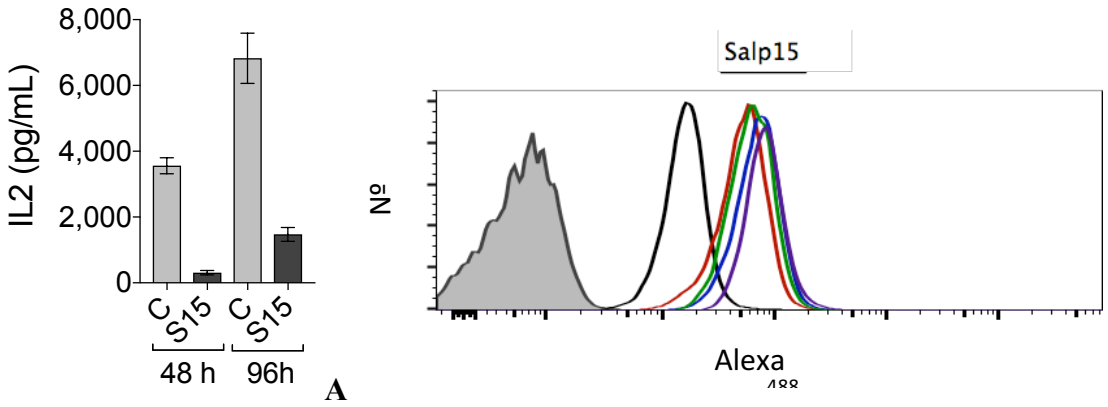

Figure 2.4. The effect of Salp15 on CD4 T cells is persistent. (A) IL-2 production by purified splenic CD4 T cells activated with anti-CD3/CD28 for 2 days in the presence of 50 μg/ml of Salp15, washed and re-stimulated under the same conditions for another 48 h in the absence of the immunosuppressive protein. The results represent the average ± SE of one experiment in triplicate and are representative of 3 performed. (B) Binding of Salp15 or the C-terminal deletion mutant, Salp15ΔP11 to purified CD4 T cells. The proteins were labeled with Alexa Fluor^{488} and tested for their binding for different time periods. The binding was assessed by flow cytometry. The shaded histogram represents unlabeled cells. The black histogram represents binding of Salp15ΔP11. Color histograms represent binding of Salp15 at different time points (12, 24, 48 and 72 h).

In order to assess whether Salp15 could also exert long-term effects *in vivo*, we followed an immunization regime against ovalbumin and the unrelated protein, keyhole limpet hemocyanin (KLH). Groups of mice were immunized with ovalbumin in aluminum hydroxide in the absence or presence of Salp15 (day 0). Seven days later, the mice were boosted with ovalbumin under the same conditions. At day 14, the mice in each group were subdivided and immunized with ovalbumin or KLH in the absence of Salp15. All the mice were sacrificed at day 21. Sera were then analyzed for the presence of ovalbumin- and KLH-specific IgG levels. As expected, ovalbumin-specific IgG levels were significantly lower in mice that had received Salp15 in the first 2 immunizations (Fig. 2.5). In order to establish whether the effect of Salp15 was circumscribed to ovalbumin, we also determined sera IgG levels against KLH. Mice that had not been immunized with this antigen did not show KLH-specific IgG in the sera. Notably, the levels of KLH-specific IgG were high in those mice receiving the antigen, and significantly lower in those that had received two previous doses of Salp15, but not at the time of immunization with KLH (Fig. 2.5). These data show that the effect of Salp15 lasts beyond the treatment and can affect the response to unrelated antigens, such as KLH.

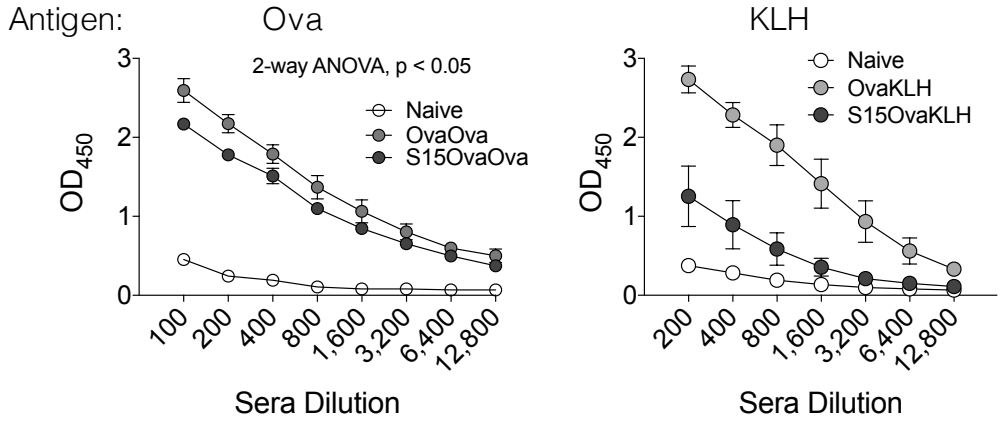

Figure 2.5. Salp15 affects antibody generation in a persistent manner. Antibody titers specific for ovalbumin (left panel) and KLH (right panel) in mice immunized with the antigens as described in Methods and treated with 50 μg of Salp15 (S15OvaOva or S15OvaKLH) or left untreated (OvaOva or OvaKLH). Non-immunized mice served as controls (Naive).

To further address the long-term effect associated with the treatment with Salp15, we utilized a murine model of GvHD resulting from the adoptive transfer of spleen cells from B6 into unconditioned CB6 F1 mice (Tschetter et al., 2000). In this model of transplantation, the proliferation of drafted cells can be monitored in the blood and results in two different phases of the disease: an acute phase in which the transplanted cells proliferate, followed by a chronic phase predominantly characterized by symptomatology similar to autoimmune disease, including the deposition of IgG immune complex in the kidney (Tschetter et al., 2000). CB6 F1 mice were transplanted 60 x 10^6 spleen cells and divided into two groups. One of the groups received intraperitoneal injections of Salp15 every other day for 10 days, while the control group received the same dose of Salp15ΔP11. Control animals showed a peak of parental cells at day 20 relative to the transplant, followed by a decline and another increase around 60 days post-transplant (Fig. 2.6). In contrast, the treatment with Salp15 during the first 10 days post transplantation resulted in a significantly reduced level of parental cells in the blood (Fig. 2.6). However, no effect was detected during the chronic phase of the disease.

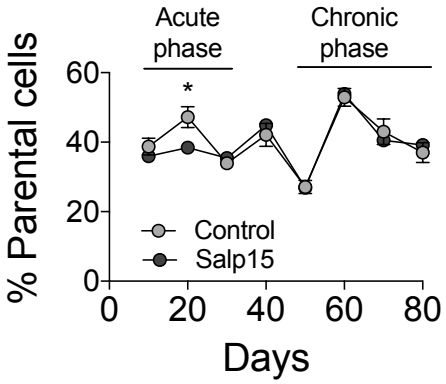

Figure 2.6. Long and short-term effect of Salp15 in a GvHD mouse model. Parental cell percentage during the acute and chronic phase of the disease under the treatment of Salp15 or its control, Salp15ΔP11. The acute phase comprises from the day 0 to day 30 and the chronic phase from day 30 to 80.

We also analyzed the potential effect of the treatment with Salp15 on the pathology associated with this model at day 80 after transplantation. CB6 F1 mice transplanted with B6 splenocytes showed some disorganization in the glomerular basement membrane and tubular brush border of the kidney upon transplantation that was not affected by the treatment with Salp15 (Fig. 2.7A). However, immune complex deposition that was readily detected in the control-treated mice was significantly

reduced in the animals that had been treated with Salp15 (Fig. 2.7A, B). Overall, our results show that Salp15 has short-term and long-term effects during the development of immune responses that specifically affect the expansion of CD4 T cells and the production of antibodies.

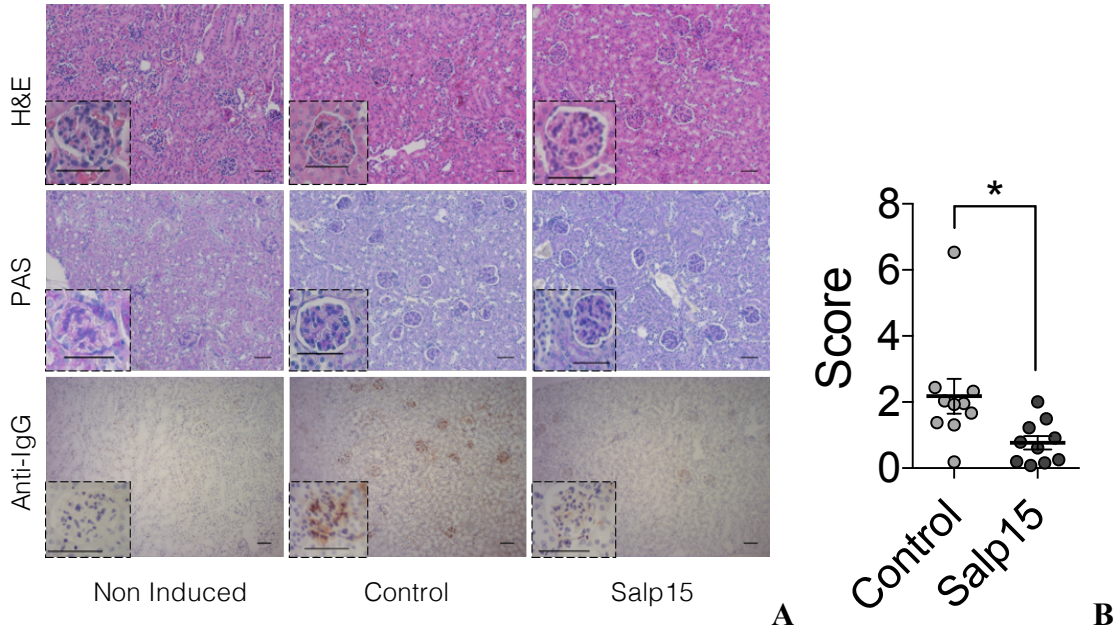

Figure 2.7. Long-term effect of Salp15 treatment of Immune complex deposition during GvDH. (A) Histological features of the kidneys of CB6F1 mice transplanted with B6 splenocytes after 80 days. Kidney sections were stained with H&E (top panels), periodic acid schiff (PAS) staining (middle panels) and anti-mouse IgG immune complex deposition (lower panels). The scale bars represent 50 μm. (B) Assessment of IgG immune complex deposition scores in the kidneys of the transplanted mice by analysis of 5 different micrographs with the FriDA software package and averaged per section. The experiments in vivo were performed with groups of 5 mice and performed at least twice.

Identification of transcriptional traits in activating CD4 T cells treated with Salp15. We then sought to determine the transcriptional signature of activated CD4 T cells for 48 and 96 hours with plate-bound anti-CD3 and soluble anti-CD28 in the presence of Salp15 or its control, Salp15ΔP11 (Fig. 2.8A). To allow the survival of the CD4 T cells throughout the activation process, a low dose of Salp15 (25 μg/ml) was used. This dose reduced the activation of CD4 T cells (Fig. 2.8A) without significant cell death at 4 days post-activation (data not shown). Principal component analysis (PCA) showed a distinct pattern of gene expression in control activated cells over the analyzed period of time (Fig. 2.8B). The presence of Salp15 resulted in variations in

the PCA at 2 days of activation, while the differences faded when the transcriptome was analyzed after 4 days of activation (Fig. 2.8B).

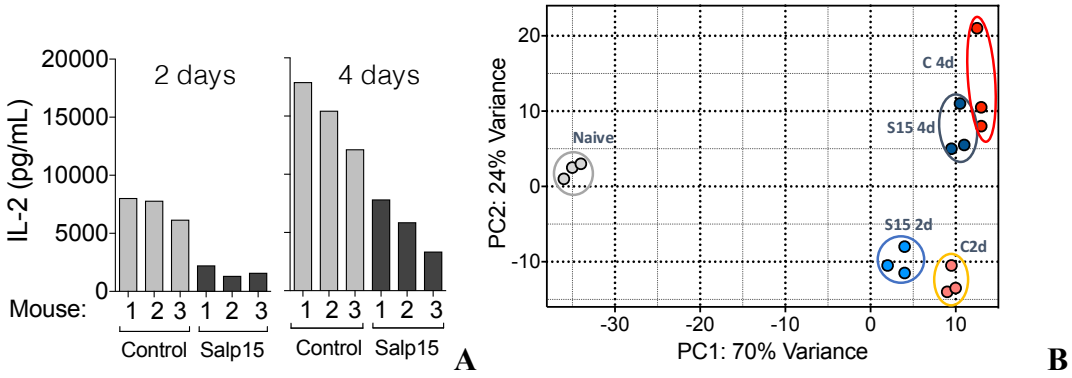

Figure 2.8. Transcriptional traits of CD4 T cells activated in the presence of Salp15. (A) IL-2 production by CD4 T cells used for the transcriptomic analysis. Each bar represents one of the 3 mice used. The amount of Salp15 used was 25 µg/ml. Control cells were treated with Salp15ΔP11 (Control). (B) Principal component analysis showing the grouping of the different assay conditions according to their transcriptome. Non-activated cells (Naive, grey); Salp15ΔP11-treated at 2 days (C 2d, orange) or 4 days of activation (C 4d, red); Salp15-treated at 2 days (S15 2d, light blue) or 4 days (S15 4d, dark blue).

These differences were also noticeable when the 1,000 most regulated genes were analyzed, with maximal differences between Salp15-treated and control activated CD4 T cells at 2 days and more discrete differences when analyzed at 4 days of activation (Fig. 2.9A). The activation of CD4 T cells under control conditions revealed 2382 genes upregulated and 2848 genes downregulated at 2 days of activation (Fig. 2.8B), while 1882 genes were upregulated and 1841 genes downregulated after 4 days of activation, using a cut-off value of 1 $\log_2$fold change and an adjusted p-value < 0.05 (Fig. 2.8B). Of these genes, 1245 were upregulated at both 2d and 4d of activation, 1601 were downregulated at both time points and 40 were regulated in opposite directions (Fig. 2.8D). Using the same cut-off values, we found 154 genes upregulated as a consequence of the presence of Salp15 during activation at 2d while only 1 gene was downregulated (Fig. 2.8C). Notably, the number of genes regulated at 4d of activation in the presence of Salp15 was dramatically reduced to 5 genes upregulated and just 1 (*Il10)* downregulated (Fig. 2.8E). Selected transcriptional changes were validated as shown in Fig. 2.10.

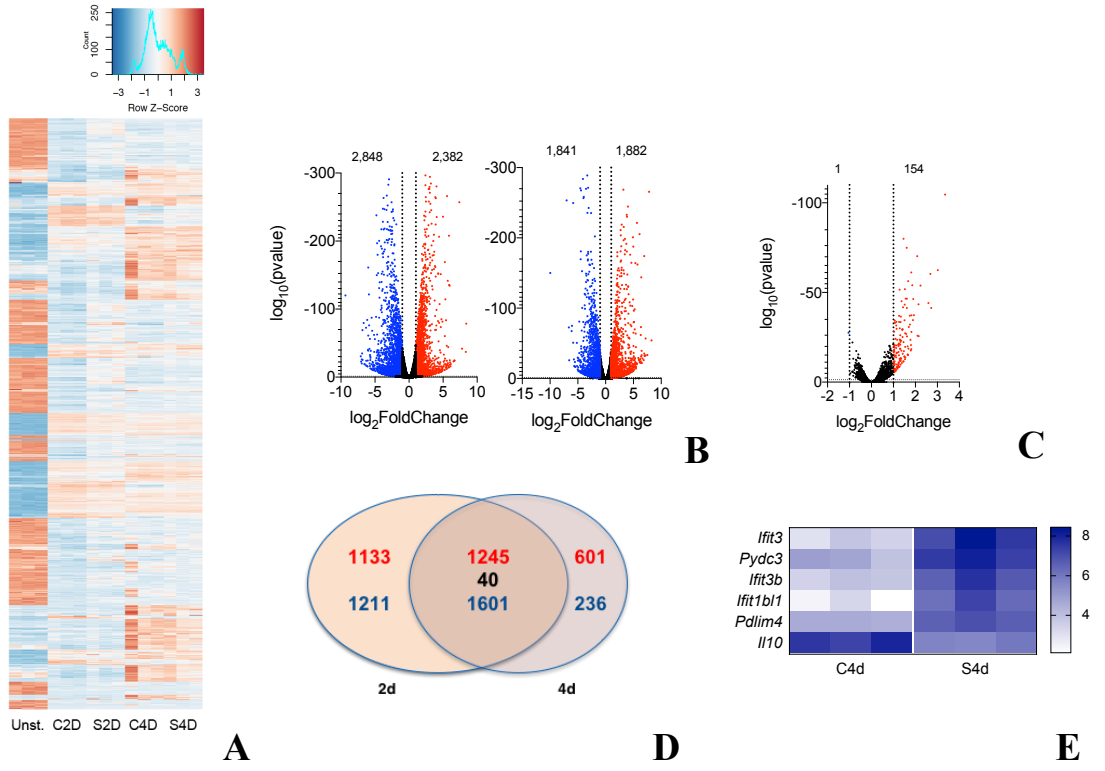

Figure 2.9. Transcriptional changes induced by Salp15 on activating CD4 T cells. (A) Heatmap corresponding to the 1,000 most regulated genes over the conditions analyzed by RNAseq. **(B)** Volcano plots showing the genes upregulated (red) or downregulated (blue) by activation with anti-CD3ε and CD28 at 2 (left) and 4 days (right) of stimulation. **(C)** Volcano plot showing the number of genes differentially regulated during the activation of CD4 T cells in the presence of Salp15 or Salp15ΔP11 (control) after 2 days of stimulation **(D)** Venn diagram showing the number of genes regulated at both 2 and 4 days of activation in the absence of Salp15. **(E)** Heatmap of the genes regulated in the presence of Salp15 at 4 days of activation.

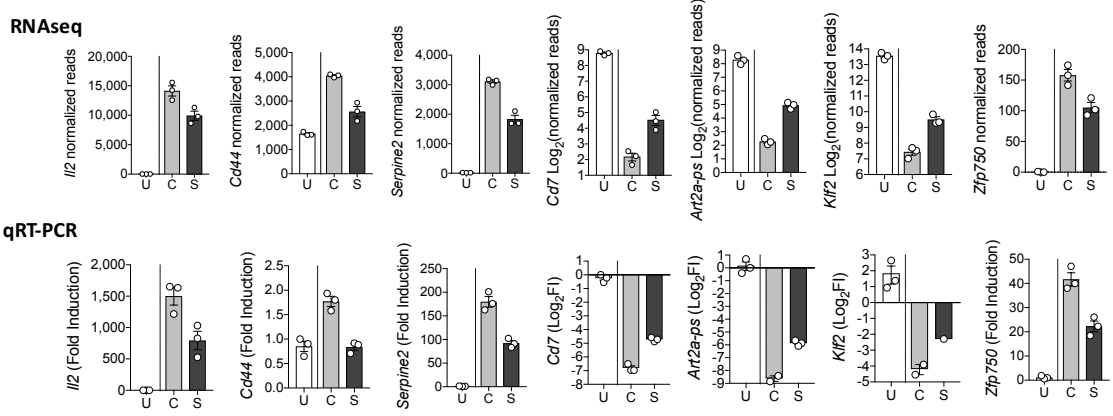

Figure 2.10. (previous page) Validation of the RNAseq on selected genes. Normalized reads (top) and fold induction changes by qRT-PCR (bottom) of a group of selected genes differentially regulated in CD4 T cells activated with anti-CD3/CD28 for 2 days in the presence of Salp15 (S) or Salp15ΔP11 (C). U: Non-stimulated CD4 T cells.

Salp15 affects CD4 T cell genes early during the activation process. The activation of CD4 T cells produced the expected profile, involving genes such as *Il2*, *Cd44* or *IL2ra* (Fig. 2.11A). Gene ontology analysis of Biological Processes (GOBP) revealed that the most over-represented groups included genes related to leukocyte cell-cell adhesion and aggregation or T cell activation, among other immune-related processes (Fig. 2.11B). As expected, the presence of Salp15 induced a reduction of *Il2* gene expression and the production of IL-2 at 2 days of activation (Fig. 2.11A, C, D; see also Fig. 2.8A). Furthermore, the activation marker CD44 was significantly reduced both at the gene expression level (Fig. 2.11A, E, F), by surface analysis of the protein by flow cytometry in *in vitro* activated CD4 T cells (Fig. 2.11G), and *in vivo* in the spleens of ovalbumin-immunized mice at day 7 post-immunization (Fig. 2.11H). Although the effect of Salp15 on *Il2ra* expression was not evident at this concentration (25 μg/ml, Fig. 2.11J), the analysis of CD25 on the surface of 2-day activated CD4 T cells revealed decreased levels of the protein in the presence of this dose of Salp15 (Fig. 2.11K).

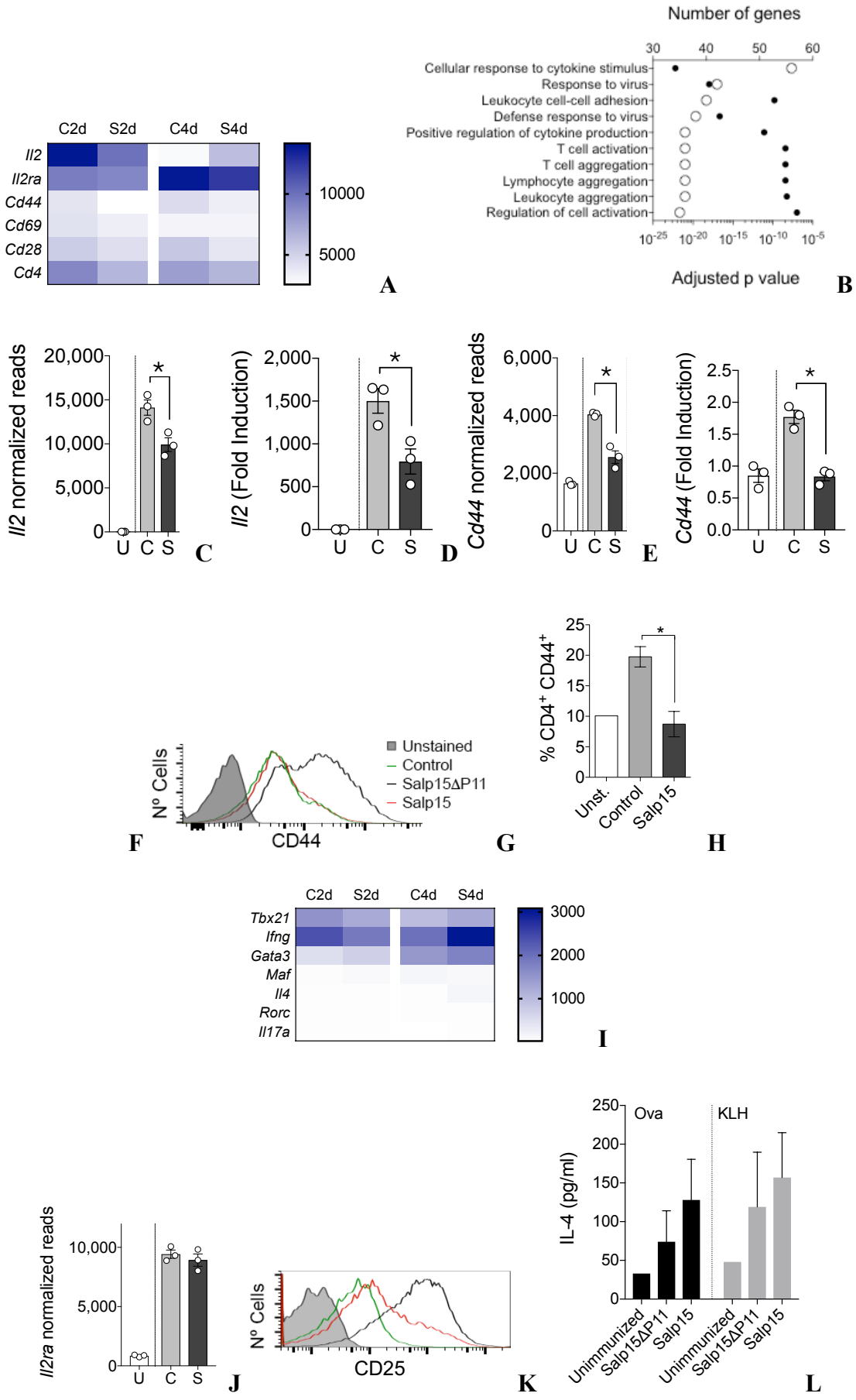
C2d
S2d
C4d
S4d
Il2
Il2ra
Cd44
Cd69
Cd28
Cd4
10000
5000
A
Number of genes
30
40
50
60
Cellular response to cytokine stimulus
Response to virus
Leukocyte cell-cell adhesion
Defense response to virus
Positive regulation of cytokine production
T cell activation
T cell aggregation
Lymphocyte aggregation
Leukocyte aggregation
Regulation of cell activation
10-25
10-20
10-15
10-10
10-5
Adjusted p value
B
Il2 normalized reads
20,000
15,000
10,000
5,000
0
U C S
C
Il2 (Fold Induction)
2,000
1,500
1,000
500
0
U C S
D
Cd44 normalized reads
6,000
4,000
2,000
0
U C S
E
Cd44 (Fold Induction)
2.5
2.0
1.5
1.0
0.5
0.0
U C S
F
Nº Cells
Unstained
Control
Salp15ΔP11
Salp15
CD44
G
% CD4+ CD44+
25
20
15
10
5
0
Unst.
Control
Salp15
H
C2d
S2d
C4d
S4d
Tbx21
Ifng
Gata3
Maf
Il4
Rorc
Il17a
3000
2000
1000
I
Il2ra normalized reads
10,000
5,000
0
U C S
J
Nº Cells
CD25
K
IL-4 (pg/ml)
250
200
150
100
50
0
Ova
KLH
Unimmunized
Salp15ΔP11
Salp15
Unimmunized
Salp15ΔP11
Salp15
L

Figure 2.11. (previous page) Salp15 affects CD4 T cell genes early during the activation process. (A) Heatmap of the activation markers of CD4 T cells regulated in the presence of Salp15 at 2 and 4 days of activation. **(B)** Biological processes significantly regulated by the treatment of Salp15. **(C)** Normalized reads and **(D)** fold induction of il2 gene by qRT-PCR in activated CD4 T cells. **(E)** Normalized reads and **(F)** fold induction of cd44 gene by qRT-PCR in activated CD4 T cells. **(G)** Flow cytometry showing the expression of CD44 in activated CD4 T cells under the treatment with Sap15 or its control, Salp15ΔP11. The grey histogram represents the unstained control. **(H)** Percentage of $CD4^{+}CD44^{+}$ in vivo in the spleens of ovalbumin immunized mice at day 7 post-immunization under the treatment with Sap15 or its control, Salp15ΔP11 **(I)** Heatmap representing the genes associated with CD4 T cell differentiation according to the transcriptomic analysis in the presence of Salp15 (S) or Salp15ΔP11 (C) at 2 and 4 days of activation. **(J)** Normalized reads of cd44 gene by qRT-PCR **(K)** Flow cytometry showing the expression of CD25 in activated CD4 T cells under the treatment with Sap15 or its control, Salp15ΔP11. The grey histogram represents the unstained control. **(L)** Ovalbumin/KLH-immunized mice (see Materials an Methods) were sacrificed at day 21 and whole splenocytes (3×10^6/ml) were re-stimulated with ovalbumin (Ova) or KLH. The re-stimulation supernatants were analyzed for IFN-γ and IL-4 by capture ELISA. The levels of IFN-γ were below the detection limit. No differences were observed between Salp15- or Salp15ΔP11 (control)-treated, immunized mice ($p > 0.05$, 2-way ANOVA). The data represent 10 mice in each group immunized with ovalbumin and 5 per group with KLH and are representative of 2 independent experiments.

Salp15 induces the expression of 5'-ectonucleotidase (CD73) in regulatory T cells. The repressed activation of CD4 T cells in the presence of Salp15 could result in the induction of anergy. We therefore analyzed the expression levels of genes associated with this phenomenon in CD4 T cells, including *Satb1*, *Cd7*, *Rap1a*, *Itch*, *Rnf128*, *Dtx1*, *Izumo1r*, *Cblb, Dgka* (Lechner et al., 2001), *Nr4a1* or *Pdcd1* (Kalekar et al., 2016). Salp15 induced small and inconsistent changes in these genes (Fig. 2.12A, Table 2.2), suggesting that this protein does not induce anergy in CD4 T cells. In order to confirm these results, we analyzed by flow cytometry markers of anergy in CD4 T cells that were activated *in vitro* in the presence of Salp15. The percentage of $CD4^{+}FoxP3^{-}CD44^{high}CD73^{high}FR4^{high}$ (Kalekar et al., 2016) cells increased upon CD4 T cell activation but remained as low as in naive cells in the presence of Salp15 (Fig. 2.12B). Furthermore, the analysis of anergic CD4 T cells in mice either immunized with ovalbumin (Table 2.3) or induced GvHD (Table 2.4) showed no effect on this population as a consequence of the treatment with Salp15. Similarly, the treatment with Salp15 did not result in the generation of a significant anergic B cell population or increased the pool of monocytic myeloid suppressor cells (Table 2.3). These data confirm that Salp15 act as an immunosuppressor on CD4 T cells that depends on its

interaction with CD4 and that does not induce a long-term anergic state in T or B cells, nor the generation of myeloid suppressor cells.

Gene	S2D vs. C2D		S4D vs. C4D	
	Log $_2$ FI	Adj. p-value	Log $_2$ FI	Adj. p-value
CD4 T cell differentiation				
Tbx21	-0,310	0,004	0,305	0,011
Ifng	-0,292	0,014	0,496	0,003
Gata3	0,418	0,002	0,191	0,461
Maf	0,561	0,008	-0,191	0,575
Il4	0,602	0,012	0,903	5,44E-07
Rorc	0,321	0,254	0,282	0,342
Il17a	0,018	0,959	0,084	0,813
Anergy				
Satb1	0,304	0,012	0,002	0,997
Cd7	0,750	0,001	0,166	NA
Rap1a	0,030	0,894	-0,223	0,116
Itch	0,087	0,613	-0,065	0,816
Rnf128	-0,077	0,858	-0,321	0,186
Dtx1	-0,039	0,908	0,047	0,921
Izumo1r	-0,090	0,573	-0,251	0,094
Cblb	-0,403	8,40E-06	-0,656	3,74E-07
Dgka	0,282	0,001	-0,215	0,114
Regulatory T cells				
Foxp3	0,815	7,85E-09	-0,352	0,095
Ctla4	0,109	0,535	-0,691	1,19E-07
Nrp1	0,048	0,859	0,015	0,975
Pdcd1	-0,568	3,90E-11	0,144	0,612
Lag3	-0,721	1,81E-11	-0,540	5,44E-07
Havcr2	-0,166	0,668	-0,177	0,620
Lrrc32	0,527	0,044	-0,268	0,345
Tgfb1	-0,148	0,197	-0,164	0,473
Ikzf2	0,438	0,117	-0,558	0,00027
Il7r	***1,504***	***6,21E-15***	-0,040	0,914
Entpd1	0,402	0,163	-0,004	0,995
Type 1 Regulatory T cells				
Il10	-0,236	0,492	***-1,069***	***4,01E-10***
Eomes	0,136	0,477	-0,193	0,351
Il2rb	0,171	0,367	-0,069	0,808
Itga4	0,536	0,027	-0,260	0,178
Itgb7	-0,578	1,78E-06	0,047	0,878
Ly6c1	0,200	0,233	-0,190	0,511
Tigit	-0,387	0,001	-0,500	0,001

Table 2.2. Differential expression of genes associated with CD4 T cell differentiation, anergy and regulatory T cells.

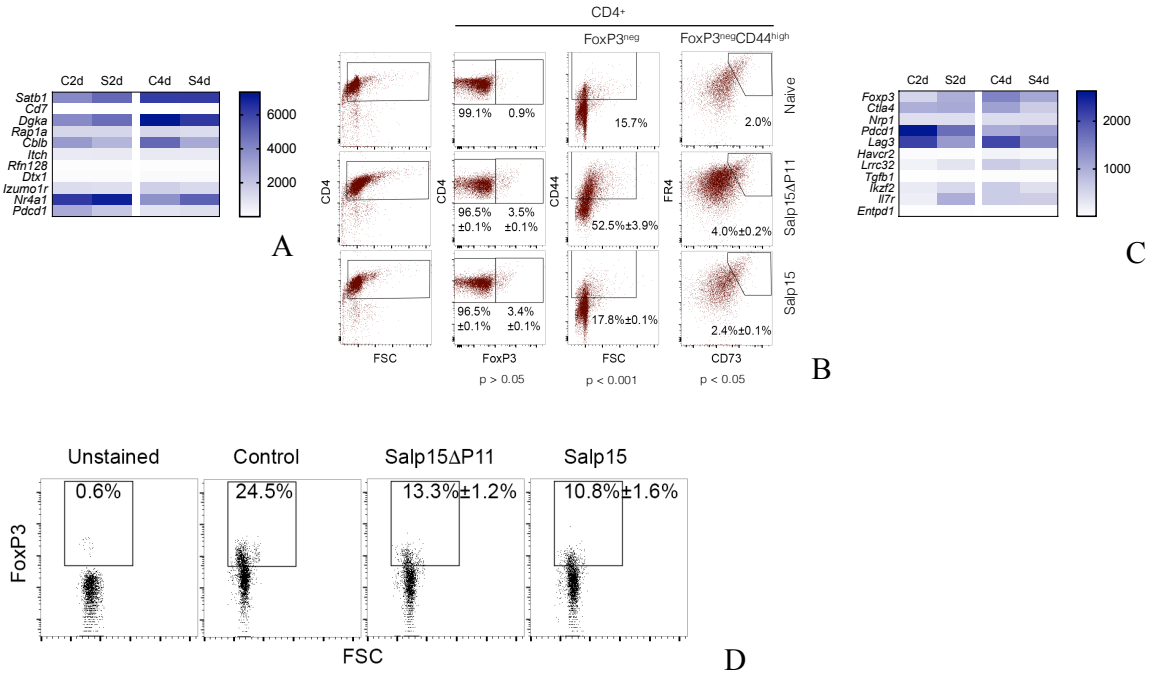

Figure 2.12. Salp15 does not induce genes associated with either anergy nor regulatory T cells. (A) Heatmap of the genes associated with anergy in activated CD4 T cells in the presence of Salp15 at 2 and 4 days of activation. **(B)** Percentage of $FoxP3^{+}CD44^{+}FR4^{+}$ in activated CD4 T cells in the presence of Salp15 at 2 days of in vitro activation. **(C)** Heatmap of the specific markers of regulatory T cells in activated CD4 T cells in the presence of Salp15 at 2 and 4 days of activation. **(D)** Percentage of regulatory T cells in mice immunized with ovalbumin in the presence of Salp15.

The transcriptomic data also helped us elucidate whether activated CD4 T cells in the presence of Salp15 acquired specific markers of regulatory T cells, such as *Foxp3, Ctla4, Nrp1, Pdcd1, Lag3, Havcr2, Lrrc32, Tgfb1, Ikzf2, Il7r* or *Entpd1* (Chaudhary et al., 2014; Elkord et al., 2015). No major differences were found between controls and CD4 T cells activated in the presence of Salp15 (Fig. 2.12C, Table 2.2). Moreover, the analysis of FoxP3-positive cells after 4 days of activation *in vitro* did not show changes in the percentage of Tregs associated with the presence of Salp15 (Fig. 2.12B). The effect of Salp15 on the pool of Tregs *in vivo* was also negligible in mice that had been immunized with ovalbumin (Fig. 2.12D). Furthermore, the analysis of FoxP3-positive CD4 T cells in the peripheral blood of CB6 F1 mice transplanted with B6 splenocytes did not show differences associated with the treatment with Salp15 throughout the life of the experiment (Table 2.4). Similar results were found when we analyzed the expression of Nrp1 on CD4 T cells,

another marker of regulatory T cells (Table 2.3) (Bruder et al., 2004). The analysis of type 1 regulatory T (Tr1) cells markers, including *Il10*, *Eomes*, *Il2rb*, *Itga4*, *Itgb7*, *Ly6c1* or *Tigit* (Zhang et al., 2017), showed that Salp15 does not induce the generation of these cells, although *Il10* expression levels were significantly reduced in the presence of the salivary protein at 4 days of activation (Table 2.2). These results demonstrate that the treatment with Salp15 does not result in the generation of a population of regulatory T cells that could account for long-term immunomodulatory effects.

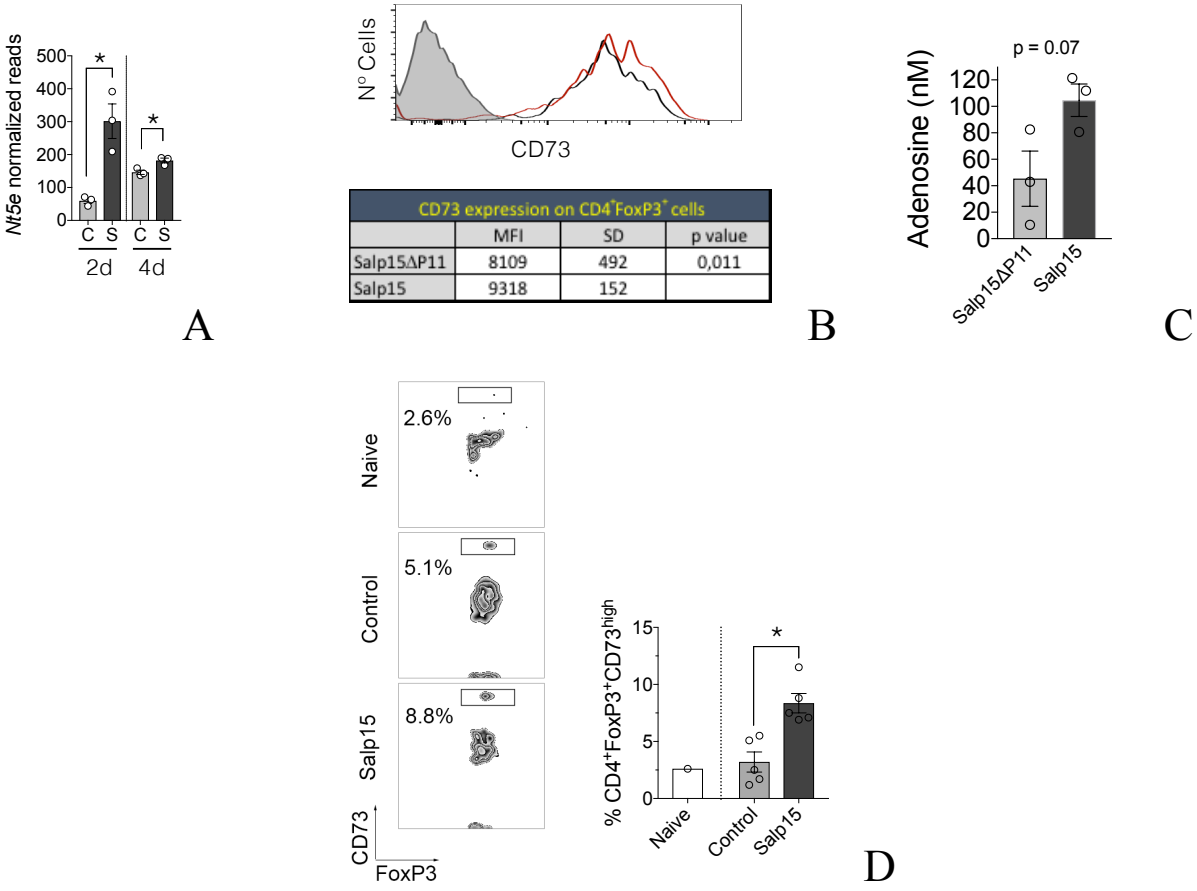

Figure 2.13. Salp15 does not induce genes associated with either anergy nor regulatory T cells. (A) Normalized reads of *cd44* gene by qRT-PCR in CD4 T cells in the presence of Salp15 at 2 and 4 days of activation. **(B)** Flow cytometry showing the expression of CD25 in activated CD4 T in vitro cells under the treatment with Sap15 or its control, Salp15ΔP11. The grey histogram represents the unstained control. **(C)** Levels of adenosine of three different mice. In vitro activated CD4 T cells under the treatment with Sap15 or its control, Salp15ΔP11. (D) Percentage of the population $CD4^{+}FoxP3^{+}CD73^{high}$ at day 50 post-transplant under the treatment with Sap15 or its control, Salp15ΔP11

We then addressed whether the treatment with Salp15 would impact the activity rather than the size of the Treg population. The ectoenzyme CD73 is expressed by Tregs and mediates the production of adenosine, an immunosuppressive molecule on T cells (Ehrentraut et al., 2013; Wang et al., 2013; Whitehill et al., 2016). We observed that expression levels of *Nt5e* (which encodes CD73) were increased upon the treatment of CD4 T cells with Salp15 (Fig. 2.13A). Therefore, we determined the expression levels of CD73 on the surface of FoxP3-positive cells. We found that the activation of CD4 T cells *in vitro* in the presence of Salp15 resulted in a significant increase in the surface expression of CD73 (Fig. 2.13B). Furthermore, the levels of adenosine increased upon the treatment of activating CD4 T cells with Salp15 (Fig. 2.13C). Importantly, we observed an increase in a population of $CD4^{+}FoxP3^{+}CD73^{high}$ in the blood of mice that have been induced GvHD at day 50 post-transplant (Fig. 2.13D). Overall, our results show that Salp15 is able to induce long-term effects on activating CD4 T cells that involve, at least in part, the increased expression and activity of CD73 on regulatory T cells.

Blood B cell populations	**Control**	**ΔO**		**SO**	
		Average	*SD*	*Average*	*SD*
B cells ($B220^{+}$)	45,10	43,50	1,87	40,07	4,43
$B220^{+}CD69^{+}$	28,50	12,41	4,15	11,50	4,76
Anergic B cells ($B220^{+}CD93^{+}IgM^{+}CD23^{+}$)	3,85	2,28	0,40	1,80	0,76
Mature B cells ($B220^{+}CD93^{-}CD23^{+}$)	27,87	28,77	0,56	27,80	1,50
Spleen populations	**Control**	**ΔOO**		**SOO**	
		Average	*SD*	*Average*	*SD*
$CD4^{+}$	11,60	11,02	2,31	10,77	2,08
$CD8^{+}$	7,84	6,10	0,98	6,38	0,87
$CD4^{+}CD25^{+}$	12,90	8,47	1,33	5,60	2,34
$CD4^{+}CD44^{+}$	28,10	7,48	2,43	7,55	4,21
Anergic T cells ($CD4^{+}CD44^{high}CD73^{high}FR4^{high}$)	3,60	0,92	0,35	0,86	0,39
Tregs ($CD4^{+}NRP1^{+}$)	2,02	1,54	0,20	1,46	0,16
Macrophages ($F4/80^{+}GR\text{-}1^{-}$)	2,15	2,08	0,09	2,44	1,30
Neutrophils ($F4/80^{-}GR\text{-}1^{+}$)	1,30	1,52	0,21	2,73	0,71
Monocytic myeloid suppressor cells ($CD11b^{high}GR\text{-}1^{high}Ly6C^{+}$)	1,01	0,56	0,24	0,82	0,36
Inflammatory macrophages ($F4/80^{+}GR\text{-}1^{int}Ly6C^{high}$)	1,97	2,42	0,38	2,52	0,64

Table 2.3. Cell populations in blood and spleen of mice immunized with ovalbumin (O) and treated with Salp15 (S) or the control protein (D). All comparisons between Control vs. Salp15, $p > 0.05$ n = 5 mice per group. The gating strategies are shown in Fig. 2.14.

Blood B cell populations	Day 20		Day 30		Day 40		Day 60		Day 80	
	Control	*Salp15*	*Control*	*Salp15*	*Control*	*Salp15*	*Control*	*Salp15*	*Control*	*Salp15*
CD4+ T cells	26.1 ± 0.7	26.5 ± 0.5	33.5 ± 1.6	30.0 ± 1.2	34.9 ± 2.2	38.4 ± 2.7	30.9 ± 1.6	28.5 ± 1.8	21.0 ± 1.8	25.2 ± 2.7
CD8+ T cells	12.8 ± 1.2	13.8 ± 0.4	17.6 ± 1.0	18.0 ± 0.9	18.5 ± 1.1	17.4 ± 0.8	15.6 ± 0.8	16.2 ± 0.4	15.9 ± 1.4	18.4 ± 1.6
Tregs (CD4+FoxP3+)	7.1 ± 0.4	6.2 ± 0.3	7.3 ± 0.3	7.1 ± 0.2	4.7 ± 0.4	3.9 ± 0.7	6.8 ± 0.4	7.2 ± 0.5	7.7 ± 0.6	7.7 ± 1.2
Anergic T cells ($CD4^{+}CD44^{high}CD73^{high}FR4^{high}$)	6.2 ± 1.8	3.9 ± 0.9	20.0 ± 2.7	16.5 ± 1.9	13.4 ± 1.1	12.3 ± 1.1	4.4 ± 0.9	5.4 ± 0.5	7.0 ± 1.4	5.9 ± 1.0

Table 2.4. Cell populations (average ± SD) in blood upon B6 splenocyte transplant into CB6 F*1*. All comparisons between Control vs. Salp15, $p > 0.05$ n = 5 mice per group.

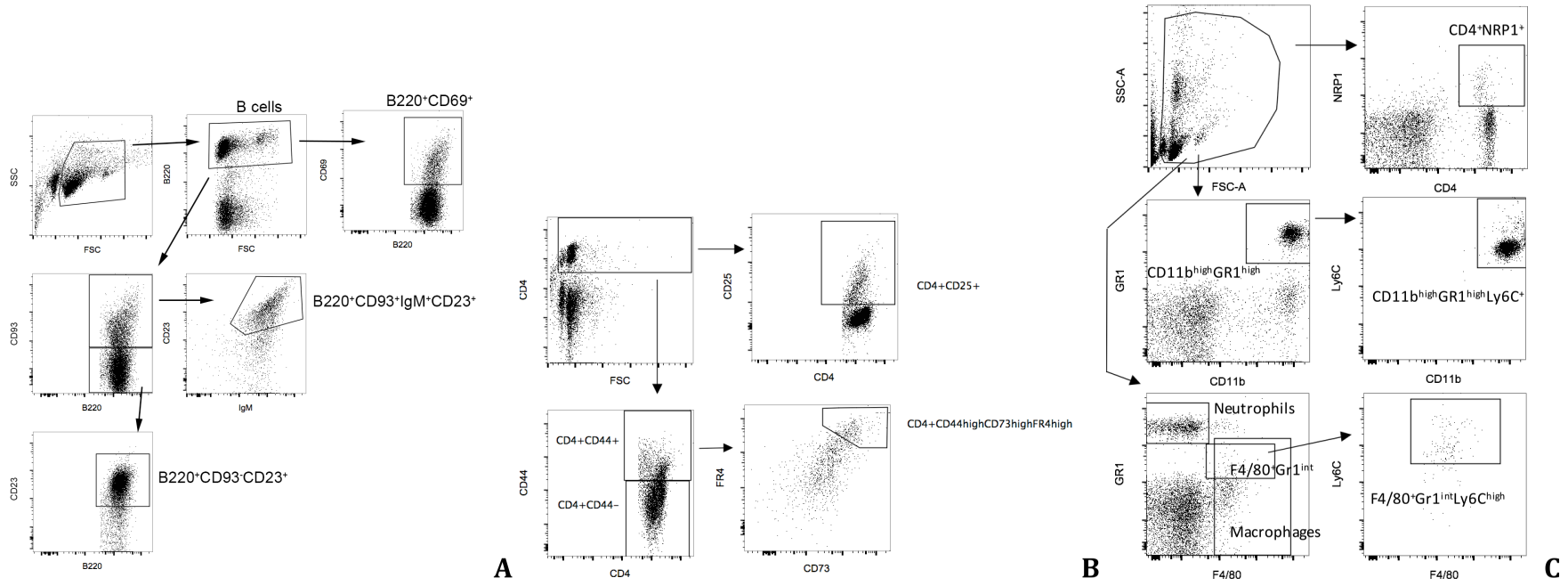

Fig. 2.14. Gating strategy to identify the populations in ovalbumin-immunized mice. (A) B cell populations in the blood. (B) CD25 (top right blot), CD44 (bottom left blot) and anergic CD4 T cells (bottom right blot) in the spleen. (C) CD4+NRP1+ (Tregs; top right blot) and myeloid populations in the spleen.

2.4. DISCUSSION

The tick salivary protein Salp15 inhibits early CD4 T cell signaling events and, in consequence, their activation. The activity of Salp15 on CD4 T cells is well-characterized (Anguita et al., 2002; Garg et al., 2006; Kalekar et al., 2016). Both *in vitro* and *in vivo*, this protein is able to prevent a full activation program on these immune cells (Juncadella and Anguita, 2009). The fate of CD4 T cells affected by the activity of Salp15 is not known. They could become permanently unable to respond to antigen or, alternatively, revert to a state in which they are amenable to become activated when antigen is present again. Here, we show that the presence of Salp15 during the activation of CD4 T cells results in long-term effects that affect their encounter with new antigens. Using transcriptomics, two models of CD4 T cell activation *in vivo* and the polyclonal activation of these cells *in vitro*, we show that whereas Salp15 does not affect the generation of anergic CD4 T cells or Tregs, it induces the increased expression of the ectoenzyme, CD73, in $Foxp3^+$ regulatory T cells. This effect results in an elevated production of adenosine, a known immunomosuppressive molecule produced by Tregs (Ohta and Sitkovsky, 2001; Sitkovsky et al., 2004).

Treatment with Tregs has been proposed as an appropriate therapy for GvHD and other immune disorders (Fessler et al., 2013; Trzonkowski et al., 2013). In fact, several biological agents, including CTLA4 fusion proteins or anti-TNF antibodies (Fessler et al., 2013), have the ability to either induce an increase in number or the activity of Tregs. Treg function involves CD73 activity and other mechanisms of action (Kalekar and Mueller, 2017; Rueda et al., 2016). Indeed, the importance of CD73 activity has been studied in a murine model of GvDH, demonstrating that the ectonuclease helps control the disease (Wang et al., 2013). The conversion of 5´-AMP to adenosine mediated by CD73 in Tregs has been broadly described (Yegutkin, 2008). The anti-inflammatory effect of adenosine present in the pericellular microenvironment results in the suppression of proliferation of effector CD4 T cells and the reduction of cytokine production (Kobie et al., 2006). Indeed, we found that the levels of this molecule were increased in *in vitro* assays of CD4 T cell activation in the presence of Salp15. The capacity of Salp15 to increase *Nt5e* transcription and the

upregulation of CD73 on the surface of FoxP3$^+$ T cells can therefore help explain the long-lasting effects elicited by Salp15. Future studies will determine whether the absence of CD73 on Tregs can indeed suppress the long-term immunomodulatory effect exerted by the salivary protein.

Our results show that the binding of Salp15 to CD4 persists along the activation period *in vitro*. However, the changes induced by Salp15 at the transcriptional level fade over time. Furthermore, Salp15 does not affect CD4 T cell differentiation in the absence of polarizing cytokines, including the induction of Th1, Th2, Th17 or Treg gene markers (Fig. 2.10I). We cannot exclude that under polarizing conditions, Salp15 may affect CD4 T cell differentiation. In fact, in the presence of IL-6, the inhibition of IL-2 production during CD4 T cell activation can lead to their differentiation towards a Th17 phenotype (Juncadella et al., 2010). Nevertheless, the restimulation of splenocytes of ovalbumin and KLH immunized mice resulted in similar levels of IL-4, while IFNγ was not detected in the restimulation supernatants (2.10L), arguing against an effect of Salp15 on Th1 or Th2 differentiation under these conditions. Our analysis also show that Salp15 does not seem to exert a direct effect on other cellular types, including the generation of anergic B cells or myeloid-derived suppressor cells (MDSCs). Nevertheless, in both *in vivo* models, the treatment with Salp15 results in an indirect effect on the ability of B cells to produce antigen-specific antibodies, as we have previously demonstrated (Anguita et al., 2002).

In summary, we show that the tick salivary immunosuppressor Salp15 is able to induce the sustained repression of CD4 T cell activation that involves the direct effect on these immune cells during the activation period and the increased expression of CD73 on regulatory T cells. These data support the notion that Salp15 is able to maintain its immunomodulatory action through the induction of increased Treg activity, leading to long-term effects in two *in vivo* models, including a pre-clinically relevant murine model of graft versus host disease.

CONCLUSSIONS

CONCLUSSIONS

1. We evaluated the use of the murine model for the development of tick vaccines by stablishing first a tick feeding system. We improved both the design of the tick capsules and the use of veterinary grade adhesives to obtain repetitive and reliable tick feeding parameters.

2. Our results showed small and inconsistent protective effects on tick feeding parameters (attachment, weight at detachment, molting efficiency) when using active and passive immunization regimes against both isolated antigens and whole tick or tissue extracts, as well as human sera from forestry workers with responses to ticks.

3. The use of larger animals models that better replicate immune responses associated with tick rejection are required to test vaccine candidates.

4. We identified new putative protective antigens by immunoprecipitation of hyperimmune cow sera that had been shown to be protective against tick feeding.

5. We cloned and initially characterized four proteins specifically recognized by bovine immune sera. An integrin, a metalloprotease and a secreted putative protein containing APPLE domains may function as antihemostatic factors.

6. The protein annotated as A0A0K8RQF1 is homologous to Toll-like receptors and could play a role in one of the three tick immune patways present in arthropods. This protein is specifically recognized by anti-salivary gland immune sera and could serve as the basis for a potential anti-tick vaccine.

7. Treatment with the salivary protein, Salp15, during the course of hematopoietic transplantation has short and long-term effects during acute and chronic graft versus host disease.

8. Salp15 induces transcriptional changes in activating CD4 T cells that fade over time and are related to genes associated with activation.

9. The long-term effects exerted by Salp15 are not related to increased populations of anergic or regulatory T cells. However, regulatory CD4 T cells show the specific upregulation of the ectoenzyme, CD73, in response to Salp15 treatment, and the augmented production of adenosine.

BIBLIOGRAPHY

BIBLIOGRAPHY

Akhtari, M., V. R. Bhatt, P. K. Tandra, J. Krishnamurthy, H. Horstman, A. Dreessen, P. X. Chen and J. O. Armitage (2013). Therapy-related myeloid neoplasms after autologous hematopoietic stem cell transplantation in lymphoma patients. Cancer Biol Ther 14: 1077-1088.

Alberdi, P., N. Ayllón, A. Cabezas-Cruz, L. Bell-Sakyi, E. Zweygarth, S. Stuen and J. de la Fuente (2015). Infection of *Ixodes* spp. tick cells with different *Anaplasma phagocytophilum* isolates induces the inhibition of apoptotic cell death. Ticks Tick Borne Dis 6: 758-767.

Anguita, J., N. Ramamoorthi, J. W. Hovius, S. Das, V. Thomas, R. Persinski, D. Conze, P. W. Askenase, M. Rincón, F. S. Kantor and E. Fikrig (2002). Salp15, an *Ixodes scapularis* salivary protein, inhibits CD4(+) T cell activation. Immunity 16: 849-859.

Aristotle (343 BC). Historia Animalium

Arthur D. R. (1965). Feeding in ectoparasitic *Acari* with special reference to ticks. Adv. Parasitol. 3: 249

Ash, A., A. Elliot, S. Godfrey, H. Burmej, M. Y. Abdad, A. Northover, A. Wayne, K. Morris, P. Clode, A. Lymbery and R. C. Thompson (2017). Morphological and molecular description of *Ixodes woyliei* n. sp. (*Ixodidae*) with consideration for co-extinction with its critically endangered marsupial host. Parasit Vectors 10: 70.

Ashish, I. J. Juncadella, R. Garg, C. D. Boone, J. Anguita and J. K. Krueger (2008). Conformational rearrangement within the soluble domains of the CD4 receptor is ligand-specific. J Biol Chem 283: 2761-2772.

Askenase, P. W., B. G. Bagnall and M. J. Worms (1982). Cutaneous basophil-associated resistance to ectoparasites (ticks). I. Transfer with immune serum or immune cells. Immunology 45: 501-511.

Assadian, O. and G. Stanek (2002). Theobald Smith--the discoverer of ticks as vectors of disease. Wien Klin Wochenschr 114: 479-481.

Ayllón, N., V. Naranjo, O. Hajdušek, M. Villar, R. C. Galindo, K. M. Kocan, P. Alberdi, R. Šíma, A. Cabezas-Cruz, C. Rückert, L. Bell-Sakyi, M. Kazimírová, S. Havlíková, B. Klempa, P. Kopáček and J. de la Fuente (2015). Nuclease Tudor-SN is involved in tick dsrna-mediated RNA interference and feeding but not in defense against flaviviral or *Anaplasma phagocytophilum* rickettsial infection. PLoS One 10: e0133038.

Bakken, J. S. and J. S. Dumler (2015). Human granulocytic anaplasmosis. Infect Dis Clin North Am 29: 341-355.

Barnes, D. W., M. J. Corp, J. F. Loutit and F. E. Neal (1956). Treatment of murine leukaemia with X rays and homologous bone marrow; preliminary communication. Br Med J 2: 626-627.

Bensaci, M., D. Bhattacharya, R. Clark and L. T. Hu (2012). Oral vaccination with vaccinia virus expressing the tick antigen subolesin inhibits tick feeding and transmission of *Borrelia burgdorferi*. Vaccine 30: 6040-6046.

Bishop, R., A. Musoke, S. Morzaria, M. Gardner and V. Nene (2004). *Theileria*: intracellular protozoan parasites of wild and domestic ruminants transmitted by ixodid ticks. Parasitology 129 Suppl: S271-283.

Blazar, B. R., W. J. Murphy and M. Abedi (2012). Advances in graft-versus-host disease biology and therapy. Nat Rev Immunol 12: 443-458.

Bock, R., L. Jackson, A. de Vos and W. Jorgensen (2004). Babesiosis of cattle. Parasitology 129 Suppl: S247-269.

Bogovic, P. and F. Strle (2015). Tick-borne encephalitis: A review of epidemiology, clinical characteristics, and management. World J Clin Cases 3: 430-441.

Boieri, M., P. Shah, R. Dressel and M. Inngjerdingen (2016). The Role of Animal Models in the Study of Hematopoietic Stem Cell Transplantation and GvHD: A Historical Overview. Front Immunol 7: 333.

Borský, I., J. Hermánek, J. Uhlír and F. Dusbábek (1994). Humoral and cellular immune response of BALB/c mice to repeated infestations with *Ixodes ricinus* nymphs. Int J Parasitol 24: 127-132.

Bowman, A. S. and J. R. Sauer (2004). Tick salivary glands: function, physiology and future. Parasitology 129 Suppl: S67-81.

Brossard, M. and P. Girardin (1979). Passive transfer of resistance in rabbits infested with adult *Ixodes ricinus* L: humoral factors influence feeding and egg laying. Experientia 35: 1395-1397.

Bruder, D., M. Probst-Kepper, A. M. Westendorf, R. Geffers, S. Beissert, K. Loser, H. von Boehmer, J. Buer and W. Hansen (2004). Neuropilin-1: a surface marker of regulatory T cells. Eur J Immunol 34: 623-630.

Buchon, N., N. Silverman and S. Cherry (2014). Immunity in *Drosophila melanogaster*--from microbial recognition to whole-organism physiology." Nat Rev Immunol 14: 796-810.

Burke, G., S. K. Wikel, A. Spielman, S. R. Telford, K. McKay, P. J. Krause and T.-b. I. S. Group (2005). Hypersensitivity to ticks and Lyme disease risk. Emerg Infect Dis 11: 36-41.

Cerar, T., F. Strle, D. Stupica, E. Ruzic-Sabljic, G. McHugh, A. C. Steere and K. Strle (2016). Differences in genotype, clinical features, and inflammatory potential of *Borrelia burgdorferi sensu stricto* strains from Europe and the United States. Emerg Infect Dis 22: 818-827.

Chaudhary, B., M. Abd Al Samid, B. K. al-Ramadi and E. Elkord (2014). Phenotypic alterations, clinical impact and therapeutic potential of regulatory T cells in cancer. Expert Opin Biol Ther 14: 931-945.

Chmelar, J., J. M. Anderson, J. Mu, R. C. Jochim, J. G. Valenzuela and J. Kopecký (2008). Insight into the sialome of the castor bean tick, *Ixodes ricinus*. BMC Genomics 9: 233.

Chmelar, J., E. Calvo, J. H. Pedra, I. M. Francischetti and M. Kotsyfakis (2012). Tick salivary secretion as a source of antihemostatics. J Proteomics 75: 3842-3854.

Chmelař, J., J. Kotál, S. Karim, P. Kopacek, I. M. Francischetti, J. H. Pedra and M. Kotsyfakis (2016). Sialomes and mialomes: A systems-Biology view of tick tissues and tick-host interactions. Trends Parasitol 32: 242-254.

Chu, Y. W. and R. E. Gress (2008). Murine models of chronic graft-versus-host disease: insights and unresolved issues. Biol Blood Marrow Transplant 14: 365-378.

Cotté, V., L. Sabatier, G. Schnell, A. Carmi-Leroy, J. C. Rousselle, F. Arsène-Ploetze, L. Malandrin, N. Sertour, A. Namane, E. Ferquel and V. Choumet (2014). Differential expression of *Ixodes ricinus* salivary gland proteins in the presence of the *Borrelia burgdorferi sensu lato* complex. J Proteomics 96: 29-43.

Coumou, J., A. Wagemakers, J. J. Trentelman, A. M. Nijhof and J. W. Hovius (2014). Vaccination against Bm86 homologues in rabbits does not impair *Ixodes ricinus* feeding or oviposition. PLoS One 10: e0123495.

Cramaro, W. J., O. E. Hunewald, L. Bell-Sakyi and C. P. Muller (2017). Genome scaffolding and annotation for the pathogen vector *Ixodes ricinus* by ultra-long single molecule sequencing. Parasit Vectors 10: 71.

Cramaro, W. J., D. Revets, O. E. Hunewald, R. Sinner, A. L. Reye and C. P. Muller (2015). Integration of *Ixodes ricinus* genome sequencing with transcriptome and proteome annotation of the naïve midgut. BMC Genomics 16: 871.

Dai, J., S. Narasimhan, L. Zhang, L. Liu, P. Wang and E. Fikrig (2010). Tick histamine release factor is critical for *Ixodes scapularis* engorgement and transmission of the lyme disease agent. PLoS Pathog 6: e1001205.

Dai, J., P. Wang, S. Adusumilli, C. J. Booth, S. Narasimhan, J. Anguita and E. Fikrig (2009). Antibodies against a tick protein, Salp15, protect mice from the Lyme disease agent. Cell Host Microbe 6: 482-492.

Das, S., G. Banerjee, K. DePonte, N. Marcantonio, F. S. Kantor and E. Fikrig (2001). Salp25D, an *Ixodes scapularis* antioxidant, is 1 of 14 immunodominant antigens in engorged tick salivary glands. J Infect Dis 184: 1056-1064.

de la Fuente, J., C. Almazán, E. F. Blouin, V. Naranjo and K. M. Kocan (2006). Reduction of tick infections with *Anaplasma marginale* and *A. phagocytophilum* by targeting the tick protective antigen subolesin. Parasitol Res 100: 85-91.

de la Fuente, J., P. Kopáček, A. Lew-Tabor and C. Maritz-Olivier (2016). Strategies for new and improved vaccines against ticks and tick-borne diseases. Parasite Immunol 38: 754-769.

de la Fuente, J., J. A. Moreno-Cid, M. Canales, M. Villar, J. M. de la Lastra, K. M. Kocan, R. C. Galindo, C. Almazán and E. F. Blouin (2011). Targeting arthropod subolesin/akirin for the development of a universal vaccine for control of vector infestations and pathogen transmission. Vet Parasitol 181: 17-22.

de Silva, A. M., S. R. Telford, L. R. Brunet, S. W. Barthold and E. Fikrig (1996). *Borrelia burgdorferi* OspA is an arthropod-specific transmission-blocking Lyme disease vaccine. J Exp Med 183: 271-275.

Dincer, Z., S. Jones and R. Haworth (2006). Preclinical safety assessment of a DNA vaccine using particle-mediated epidermal delivery in domestic pig, minipig and mouse. Exp Toxicol Pathol 57: 351-357.

Domingos, A., S. Antunes, L. Borges and V. E. Rosário (2013). Approaches towards tick and tick-borne diseases control. Rev Soc Bras Med Trop 46: 265-269.

Donoso Mantke, O., C. Escadafal, M. Niedrig, M. Pfeffer and C. Working Group For Tick-Borne Encephalitis Virus (2011). Tick-borne encephalitis in Europe, 2007 to 2009. Euro Surveill 16.

Dykewicz, C. A., C. n. f. D. C. a. P. National Center for Infectious Diseases, I. D. S. o. America and A. S. f. B. a. M. Transplantation (2001). Guidelines for preventing opportunistic infections among hematopoietic stem cell transplant recipients: focus on community respiratory virus infections. Biol Blood Marrow Transplant 7 Suppl: 19S-22S.

Ehrentraut, H., E. T. Clambey, E. N. McNamee, K. S. Brodsky, S. F. Ehrentraut, J. M. Poth, A. K. Riegel, J. A. Westrich, S. P. Colgan and H. K. Eltzschig (2013). $CD73^{+}$ regulatory T cells contribute to adenosine-mediated resolution of acute lung injury. FASEB J 27: 2207-2219.

Elkord, E., M. Abd Al Samid and B. Chaudhary (2015). Helios, and not FoxP3, is the marker of activated Tregs expressing GARP/LAP. Oncotarget 6: 20026-20036.

Estrada-Peña, A. (2015). Ticks as vectors: taxonomy, biology and ecology. Rev Sci Tech 34: 53-65.

Ferreira, B. R. and J. S. Silva (1999). Successive tick infestations selectively promote a T-helper 2 cytokine profile in mice. Immunology 96: 434-439.

Garg, R., I. J. Juncadella, N. Ramamoorthi, Ashish, S. K. Ananthanarayanan, V. Thomas, M. Rincón, J. K. Krueger, E. Fikrig, C. M. Yengo and J. Anguita (2006). Cutting edge: CD4 is the receptor for the tick saliva immunosuppressor, Salp15. J Immunol 177: 6579-6583.

Gargili, A., S. Thangamani and D. Bente (2013). Influence of laboratory animal hosts on the life cycle of *Hyalomma marginatum* and implications for an *in vivo* transmission model for Crimean-Congo hemorrhagic fever virus. Front Cell Infect Microbiol 3: 39.

Gerdts, V., S. Littel-van den Hurk, P. J. Griebel and L. A. Babiuk (2007). Use of animal models in the development of human vaccines. Future Microbiol 2: 667-675.

Gortazar, C., I. Diez-Delgado, J. A. Barasona, J. Vicente, J. De La Fuente and M. Boadella (2014). The Wild Side of Disease Control at the Wildlife-Livestock-Human Interface: A Review. Front Vet Sci 1: 27.

Gratwohl, A., M. C. Pasquini, M. Aljurf, Y. Atsuta, H. Baldomero, L. Foeken, M. Gratwohl, L. F. Bouzas, D. Confer, K. Frauendorfer, E. Gluckman, H. Greinix, M. Horowitz, M. Iida, J. Lipton, A. Madrigal, M. Mohty, L. Noel, N. Novitzky, J. Nunez, M. Oudshoorn, J. Passweg, J. van Rood, J. Szer, K. Blume, F. R. Appelbaum, Y. Kodera, D. Niederwieser and W. N. f. B. a. M. T. (WBMT) (2015). One million haemopoietic stem-cell transplants: a retrospective observational study. Lancet Haematol 2: e91-100.

Gulia-Nuss, M., A. B. Nuss, J. M. Meyer, D. E. Sonenshine, R. M. Roe, R. M. Waterhouse, D. B. Sattelle, J. de la Fuente, J. M. Ribeiro, K. Megy, J. Thimmapuram, J. R. Miller, B. P. Walenz, S. Koren, J. B. Hostetler, M. Thiagarajan, V. S. Joardar, L. I. Hannick, S. Bidwell, M. P. Hammond, S. Young, Q. Zeng, J. L. Abrudan, F. C. Almeida, N. Ayllón, K. Bhide, B. W. Bissinger, E. Bonzon-Kulichenko, S. D. Buckingham, D. R. Caffrey, M. J. Caimano, V. Croset, T. Driscoll, D. Gilbert, J. J. Gillespie, G. I. Giraldo-Calderón, J. M. Grabowski, D. Jiang, S. M. Khalil, D. Kim, K. M. Kocan, J. Koči, R. J. Kuhn, T. J. Kurtti, K. Lees, E. G. Lang, R. C. Kennedy, H. Kwon, R. Perera, Y. Qi, J. D. Radolf, J. M. Sakamoto, A. Sánchez-Gracia, M. S. Severo, N. Silverman, L. Šimo, M. Tojo, C. Tornador, J. P. Van Zee, J. Vázquez, F. G. Vieira, M. Villar, A. R. Wespiser, Y. Yang, J. Zhu, P. Arensburger, P. V. Pietrantonio, S. C. Barker, R. Shao, E. M. Zdobnov, F. Hauser, C. J. Grimmelikhuijzen, Y. Park, J. Rozas, R. Benton, J. H. Pedra, D. R. Nelson, M. F. Unger, J. M. Tubio, Z. Tu, H. M. Robertson, M. Shumway, G. Sutton, J. R. Wortman, D. Lawson, S. K. Wikel, V. M. Nene, C. M. Fraser, F. H. Collins, B. Birren, K. E. Nelson, E. Caler and C. A. Hill (2016). Genomic insights into the *Ixodes scapularis* tick vector of Lyme disease. Nat Commun 7: 10507.

Gurel, B., T. Iwata, C. M. Koh, R. B. Jenkins, F. Lan, C. Van Dang, J. L. Hicks, J. Morgan, T. C. Cornish, S. Sutcliffe, W. B. Isaacs, J. Luo and A. M. De Marzo (2008). Nuclear MYC protein overexpression is an early alteration in human prostate carcinogenesis. Mod Pathol 21: 1156-1167.

Hajdusek, O., D. Sojka, P. Kopacek, V. Buresova, Z. Franta, I. Sauman, J. Winzerling and L. Grubhoffer (2009). Knockdown of proteins involved in iron metabolism limits tick reproduction and development. Proc Natl Acad Sci U S A 106: 1033-1038.

Hamin Neto, Y. A., L. C. de Oliveira, J. R. de Oliveira, M. A. Juliano, L. Juliano, E. C. Arantes and H. Cabral (2016). Analysis of the specificity and biochemical characterization of metalloproteases isolated from *Eupenicillium javanicum* using fluorescence resonance energy transfer peptides. Front Microbiol 7: 2141.

Hersh, M. H., M. Tibbetts, M. Strauss, R. S. Ostfeld and F. Keesing (2012). Reservoir competence of wildlife host species for *Babesia microti*. Emerg Infect Dis 18: 1951-1957.

Holler, E., G. Rogler, H. Herfarth, J. Brenmoehl, P. J. Wild, J. Hahn, G. Eissner, J. Schölmerich and R. Andreesen (2004). Both donor and recipient NOD2/CARD15 mutations associate with transplant-related mortality and GvHD following allogeneic stem cell transplantation. Blood 104: 889-894.

Homer, M. J., I. Aguilar-Delfin, S. R. Telford, P. J. Krause and D. H. Persing (2000). Babesiosis. Clin Microbiol Rev 13: 451-469.

Hovius, J. W., M. A. de Jong, J. den Dunnen, M. Litjens, E. Fikrig, T. van der Poll, S. I. Gringhuis and T. B. Geijtenbeek (2008). Salp15 binding to DC-SIGN inhibits cytokine expression by impairing both nucleosome remodeling and mRNA stabilization. PLoS Pathog 4: e31.

Hovius, J. W., M. A. de Jong, J. den Dunnen, M. Litjens, E. Fikrig, T. van der Poll, S. I. Gringhuis and T. B. Geijtenbeek (2008). Salp15 binding to DC-SIGN

inhibits cytokine expression by impairing both nucleosome remodeling and mRNA stabilization. PLoS Pathog 4: e31.

Hovius, J. W., M. Levi and E. Fikrig (2008). Salivating for knowledge: potential pharmacological agents in tick saliva. PLoS Med 5: e43.

Imamura, S., I. da Silva Vaz Junior, M. Sugino, K. Ohashi and M. Onuma (2005). A serine protease inhibitor (serpin) from *Haemaphysalis longicornis* as an anti-tick vaccine. Vaccine 23: 1301-1311.

Imamura, S., S. Konnai, I. a. S. Vaz, S. Yamada, C. Nakajima, Y. Ito, T. Tajima, J. Yasuda, M. Simuunza, M. Onuma and K. Ohashi (2008). Effects of anti-tick cocktail vaccine against *Rhipicephalus appendiculatus*. Jpn J Vet Res 56: 85-98.

Imamura, S., B. Namangala, T. Tajima, M. E. Tembo, J. Yasuda, K. Ohashi and M. Onuma (2006). Two serine protease inhibitors (serpins) that induce a bovine protective immune response against *Rhipicephalus appendiculatus* ticks. Vaccine 24: 2230-2237.

Jacobson, L. O., E. L. Simmons and W. F. Bethard (1950). Studies on hematopoietic recovery from radiation injury. J Clin Invest 29: 825.

Juncadella, I. J. and J. Anguita (2009). The immunosuppresive tick salivary protein, Salp15. Adv Exp Med Biol 666: 121-131.

Juncadella, I. J., T. C. Bates, R. Suleiman, A. Monteagudo-Mera, C. M. Olson, N. Navasa, E. R. Olivera, B. A. Osborne and J. Anguita (2010). The tick saliva immunosuppressor, Salp15, contributes to Th17-induced pathology during Experimental Autoimmune Encephalomyelitis. Biochem Biophys Res Commun 402: 105-109.

Kalekar, L. A. and D. L. Mueller (2017). Relationship between CD4 Regulatory T Cells and Anergy In Vivo. J Immunol 198: 2527-2533.

Kalekar, L. A., S. E. Schmiel, S. L. Nandiwada, W. Y. Lam, L. O. Barsness, N. Zhang, G. L. Stritesky, D. Malhotra, K. E. Pauken, J. L. Linehan, M. G.

O'Sullivan, B. T. Fife, K. A. Hogquist, M. K. Jenkins and D. L. Mueller (2016). $CD4^+$ T cell anergy prevents autoimmunity and generates regulatory T cell precursors. Nat Immunol 17: 304-314.

Kazimírová, M. and I. Štibrániová (2013). Tick salivary compounds: their role in modulation of host defences and pathogen transmission. Front Cell Infect Microbiol 3: 43.

Keesing, F., M. H. Hersh, M. Tibbetts, D. J. McHenry, S. Duerr, J. Brunner, M. Killilea, K. LoGiudice, K. A. Schmidt and R. S. Ostfeld (2012). Reservoir competence of vertebrate hosts for *Anaplasma phagoc*ytophilum. Emerg Infect Dis 18: 2013-2016.

Kobie, J. J., P. R. Shah, L. Yang, J. A. Rebhahn, D. J. Fowell and T. R. Mosmann (2006). T regulatory and primed uncommitted CD4 T cells express CD73, which suppresses effector CD4 T cells by converting 5'-adenosine monophosphate to adenosine. J Immunol 177: 6780-6786.

Kocan, K. M., J. de la Fuente, E. F. Blouin, J. F. Coetzee and S. A. Ewing (2010). The natural history of *Anaplasma marginale*. Vet Parasitol 167: 95-107.

Kotsyfakis, M., A. Schwarz, J. Erhart and J. M. Ribeiro (2015). Tissue- and time-dependent transcription in *Ixodes ricinus* salivary glands and midguts when blood feeding on the vertebrate host. Sci Rep 5: 9103.

Labuda, M., L. D. Jones, T. Williams and P. A. Nuttall (1993). Enhancement of tick-borne encephalitis virus transmission by tick salivary gland extracts. Med Vet Entomol 7: 193-196.

Labuda, M., A. R. Trimnell, M. Licková, M. Kazimírová, G. M. Davies, O. Lissina, R. S. Hails and P. A. Nuttall (2006). An antivector vaccine protects against a lethal vector-borne pathogen. PLoS Pathog 2: e27.

Lechner, O., J. Lauber, A. Franzke, A. Sarukhan, H. von Boehmer and J. Buer (2001). Fingerprints of anergic T cells. Curr Biol 11: 587-595.

Lee, S. J. (2010). Have we made progress in the management of chronic graft-vs-host disease? Best Pract Res Clin Haematol 23: 529-535.

Lee, S. Y., M. K. Ko, K. N. Lee, J. H. Choi, S. H. You, H. M. Pyo, M. H. Lee, B. Kim, J. S. Lee and J. H. Park (2016). Application of mouse model for effective evaluation of foot-and-mouth disease vaccine. Vaccine 34: 3731-3737.

Levine, J. F., M. L. Wilson and A. Spielman (1985). Mice as reservoirs of the Lyme disease spirochete. Am J Trop Med Hyg 34: 355-360.

Liu, L., J. Dai, Y. O. Zhao, S. Narasimhan, Y. Yang, L. Zhang and E. Fikrig (2012). *Ixodes scapularis* JAK-STAT pathway regulates tick antimicrobial peptides, thereby controlling the agent of human granulocytic anaplasmosis. J Infect Dis 206: 1233-1241.

Lorenz, E., D. Uphoff, T. R. Reid and E. Shelton (1951). Modification of irradiation injury in mice and guinea pigs by bone marrow injections. J Natl Cancer Inst 12: 197-201.

Love, M. I., W. Huber and S. Anders (2014). Moderated estimation of fold change and dispersion for RNA-seq data with DESeq2. Genome Biol 15: 550.

Mansfield, K. L., N. Johnson, L. P. Phipps, J. R. Stephenson, A. R. Fooks and T. Solomon (2009). Tick-borne encephalitis virus - a review of an emerging zoonosis. J Gen Virol 90: 1781-1794.

Manzano-Román, R., V. Díaz-Martín, M. González-González, S. Matarraz, A. F. Álvarez-Prado, J. LaBaer, A. Orfao, R. Pérez-Sánchez and M. Fuentes (2012). Self-assembled protein arrays from an *Ornithodoros moubata* salivary gland expression library. J Proteome Res 11: 5972-5982.

Medlock, J. M., K. M. Hansford, A. Bormane, M. Derdakova, A. Estrada-Peña, J. C. George, I. Golovljova, T. G. Jaenson, J. K. Jensen, P. M. Jensen, M. Kazimirova, J. A. Oteo, A. Papa, K. Pfister, O. Plantard, S. E. Randolph, A. Rizzoli, M. M. Santos-Silva, H. Sprong, L. Vial, G. Hendrickx, H. Zeller and W. Van Bortel (2013). Driving forces for changes in

geographical distribution of *Ixodes ricinus* ticks in Europe. Parasit Vectors 6: 1.

Mejri, N., N. Franscini, B. Rutti and M. Brossard (2001). Th2 polarization of the immune response of BALB/c mice to *Ixodes ricinus* instars, importance of several antigens in activation of specific Th2 subpopulations. Parasite Immunol 23: 61-69.

Merino, O., C. Almazán, M. Canales, M. Villar, J. A. Moreno-Cid, R. C. Galindo and J. de la Fuente (2011). Targeting the tick protective antigen subolesin reduces vector infestations and pathogen infection by *Anaplasma marginale* and *Babesia bigemina*. Vaccine 29: 8575-8579.

Merino, O., S. Antunes, J. Mosqueda, J. A. Moreno-Cid, J. M. Pérez de la Lastra, R. Rosario-Cruz, S. Rodríguez, A. Domingos and J. de la Fuente (2013). Vaccination with proteins involved in tick-pathogen interactions reduces vector infestations and pathogen infection. Vaccine 31: 5889-5896.

Mikulska, M., A. M. Raiola, B. Bruno, E. Furfaro, M. T. Van Lint, S. Bregante, A. Ibatici, V. Del Bono, A. Bacigalupo and C. Viscoli (2009). Risk factors for invasive aspergillosis and related mortality in recipients of allogeneic SCT from alternative donors: an analysis of 306 patients. Bone Marrow Transplant 44: 361-370.

Moreno-Cid, J. A., J. M. Pérez de la Lastra, M. Villar, M. Jiménez, R. Pinal, A. Estrada-Peña, R. Molina, J. Lucientes, C. Gortázar, J. de la Fuente and S. A. V. S. Group (2013). Control of multiple arthropod vector infestations with subolesin/akirin vaccines. Vaccine 31: 1187-1196.

Mulenga, A., C. Sugimoto, G. Ingram, K. Ohashi and O. Misao (2001). Characterization of two cDNAs encoding serine proteinases from the hard tick *Haemaphysalis longicornis*. Insect Biochem Mol Biol 31: 817-825.

Murphy, K., Travers, P., Walport, M., & Janeway, C. (2008). *Janeway's immunobiology*. 7th Edition. New York: Garland Science

Narasimhan, S., K. Deponte, N. Marcantonio, X. Liang, T. E. Royce, K. F. Nelson, C. J. Booth, B. Koski, J. F. Anderson, F. Kantor and E. Fikrig (2007). Immunity against *Ixodes scapularis* salivary proteins expressed within 24 hours of attachment thwarts tick feeding and impairs *Borreli*a transmission. PLoS One 2: e451.

Narasimhan, S., N. Rajeevan, L. Liu, Y. O. Zhao, J. Heisig, J. Pan, R. Eppler-Epstein, K. Deponte, D. Fish and E. Fikrig (2014). Gut microbiota of the tick vector *Ixodes scapularis* modulate colonization of the Lyme disease spirochete. Cell Host Microbe 15: 58-71.

Narasimhan, S., B. Sukumaran, U. Bozdogan, V. Thomas, X. Liang, K. DePonte, N. Marcantonio, R. A. Koski, J. F. Anderson, F. Kantor and E. Fikrig (2007). A tick antioxidant facilitates the Lyme disease agent's successful migration from the mammalian host to the arthropod vector. Cell Host Microbe 2: 7-18.

Nestel, F. P., K. S. Price, T. A. Seemayer and W. S. Lapp (1992). Macrophage priming and lipopolysaccharide-triggered release of tumor necrosis factor alpha during graft-versus-host disease. J Exp Med 175: 405-413.

Neuhaus, C. P. (2017). "Ethical issues when modelling brain disorders in non-human primates." J Med Ethics Published Online First: 11 August 2017.

Ober, R. J., C. G. Radu, V. Ghetie and E. S. Ward (2001). Differences in promiscuity for antibody-FcRn interactions across species: implications for therapeutic antibodies. Int Immunol 13: 1551-1559.

Ohta, A. and M. Sitkovsky (2001). Role of G-protein-coupled adenosine receptors in downregulation of inflammation and protection from tissue damage. Nature 414: 916-920.

Pal, U., X. Li, T. Wang, R. R. Montgomery, N. Ramamoorthi, A. M. Desilva, F. Bao, X. Yang, M. Pypaert, D. Pradhan, F. S. Kantor, S. Telford, J. F. Anderson and E. Fikrig (2004). TROSPA, an *Ixodes scapu*laris receptor for *Borrelia burgdorferi*. Cell 119: 457-468.

Paveglio, S. A., J. Allard, J. Mayette, L. A. Whittaker, I. Juncadella, J. Anguita and M. E. Poynter (2007). The tick salivary protein, Salp15, inhibits the development of experimental asthma. J Immunol 178: 7064-7071.

Piesman, J. and L. Gern (2004). Lyme borreliosis in Europe and North America. Parasitology 129 Suppl: S191-220.

Ramamoorthi, N., S. Narasimhan, U. Pal, F. Bao, X. F. Yang, D. Fish, J. Anguita, M. V. Norgard, F. S. Kantor, J. F. Anderson, R. A. Koski and E. Fikrig (2005). The Lyme disease agent exploits a tick protein to infect the mammalian host. Nature 436: 573-577.

Rizzoli, A., C. Silaghi, A. Obiegala, I. Rudolf, Z. Hubálek, G. Földvári, O. Plantard, M. Vayssier-Taussat, S. Bonnet, E. Spitalská and M. Kazimírová (2014). *Ixodes r*icinus and its transmitted pathogens in urban and peri-urban areas in Europe: new hazards and relevance for public health. Front Public Health 2: 251.

Rueda, C. M., C. M. Jackson and C. A. Chougnet (2016). Regulatory T-Cell-Mediated Suppression of Conventional T-Cells and Dendritic Cells by Different cAMP Intracellular Pathways. Front Immunol 7: 216.

Schetters, T., R. Bishop, M. Crampton, P. Kopáček, A. Lew-Tabor, C. Maritz-Olivier, R. Miller, J. Mosqueda, J. Patarroyo, M. Rodriguez-Valle, G. A. Scoles and J. de la Fuente (2016). Cattle tick vaccine researchers join forces in CATVAC. Parasit Vectors 9: 105.

Schroeder, M. A. and J. F. DiPersio (2011). Mouse models of graft-versus-host disease: advances and limitations. Dis Model Mech 4: 318-333.

Schoeler, G. B., S. A. Manweiler, D. K. Bergman and S. K. Wikel (2000). Influence of repeated infestations with pathogen-free *Ixodes scapularis* (*Acari*: *Ixodidae*) on *in vitro* lymphocyte proliferation responses of C3H/HeN mice. J Med Entomol 37: 885-892.

Schuijt, T. J., J. Coumou, S. Narasimhan, J. Dai, K. Deponte, D. Wouters, M. Brouwer, A. Oei, J. J. Roelofs, A. P. van Dam, T. van der Poll, C. Van't

Veer, J. W. Hovius and E. Fikrig (2011). A tick mannose-binding lectin inhibitor interferes with the vertebrate complement cascade to enhance transmission of the lyme disease agent. Cell Host Microbe 10: 136-146.

Schuijt, T. J., J. W. Hovius, N. D. van Burgel, N. Ramamoorthi, E. Fikrig and A. P. van Dam (2008). The tick salivary protein Salp15 inhibits the killing of serum-sensitive *Borrelia burgdorferi sensu lato* isolates. Infect Immun 76: 2888-2894.

Schuijt, T. J., S. Narasimhan, S. Daffre, K. DePonte, J. W. Hovius, C. Van't Veer, T. van der Poll, K. Bakhtiari, J. C. Meijers, E. T. Boder, A. P. van Dam and E. Fikrig (2011). Identification and characterization of *Ixodes scapularis* antigens that elicit tick immunity using yeast surface display. PLoS One 6: e15926.

Sitkovsky, M. V., D. Lukashev, S. Apasov, H. Kojima, M. Koshiba, C. Caldwell, A. Ohta and M. Thiel (2004). Physiological control of immune response and inflammatory tissue damage by hypoxia-inducible factors and adenosine A2A receptors. Annu Rev Immunol 22: 657-682.

Šmit, R. and M. J. Postma (2016). Vaccines for tick-borne diseases and cost-effectiveness of vaccination: a public health challenge to reduce the diseases' burden. Expert Rev Vaccines 15: 5-7.

Smith, A. A., N. Navasa, X. Yang, C. N. Wilder, O. Buyuktanir, A. Marques, J. Anguita and U. Pal (2016). Cross-Species interferon signaling boosts microbicidal activity within the tick vector. Cell Host Microbe 20: 91-98.

Smith, R. P., R. T. Schoen, D. W. Rahn, V. K. Sikand, J. Nowakowski, D. L. Parenti, M. S. Holman, D. H. Persing and A. C. Steere (2002). Clinical characteristics and treatment outcome of early Lyme disease in patients with microbiologically confirmed erythema migrans. Ann Intern Med 136: 421-428.

Sonenshine DE, Roe RM (2014). Biology of ticks. 2nd. Oxford University Press; New York.

Sonenshine DE, Roe RM (2013) Biology of Ticks. Volume 1. Oxford: Oxford University Press. 540p.

Sprong, H., J. Trentelman, I. Seemann, L. Grubhoffer, R. O. Rego, O. Hajdušek, P. Kopáček, R. Šíma, A. M. Nijhof, J. Anguita, P. Winter, B. Rotter, S. Havlíková, B. Klempa, T. P. Schetters and J. W. Hovius (2014). ANTIDotE: anti-tick vaccines to prevent tick-borne diseases in Europe. Parasit Vectors 7: 77.

Steere, A. C. (2001). Lyme disease. N Engl J Med 345: 115-125.

Steere, A. C., N. H. Bartenhagen, J. E. Craft, G. J. Hutchinson, J. H. Newman, D. W. Rahn, L. H. Sigal, P. N. Spieler, K. S. Stenn and S. E. Malawista (1983). The early clinical manifestations of Lyme disease. Ann Intern Med 99: 76-82.

Thomas, E. D., H. L. Lochte, J. H. Cannon, O. D. Sahler and J. W. Ferrebee (1959). Supralethal whole body irradiation and isologous marrow transplantation in man. J Clin Invest 38: 1709-1716.

Thomas, P. D., M. J. Campbell, A. Kejariwal, H. Mi, B. Karlak, R. Daverman, K. Diemer, A. Muruganujan and A. Narechania (2003). PANTHER: a library of protein families and subfamilies indexed by function. Genome Res 13: 2129-2141.

Trager, W. 1939 Acquired immunity to ticks. J. Parasitol. 25: 57-81.

Trapnell, C., L. Pachter and S. L. Salzberg (2009). TopHat: discovering splice junctions with RNA-Seq. Bioinformatics 25: 1105-1111.

Trimnell, A. R., G. M. Davies, O. Lissina, R. S. Hails and P. A. Nuttall (2005). A cross-reactive tick cement antigen is a candidate broad-spectrum tick vaccine. Vaccine 23: 4329-4341.

Trimnell, A. R., R. S. Hails and P. A. Nuttall (2002). Dual action ectoparasite vaccine targeting 'exposed' and 'concealed' antigens. Vaccine 20: 3560-3568.

Trzonkowski, P., A. Dukat-Mazurek, M. Bieniaszewska, N. Marek-Trzonkowska, A. Dobyszuk, J. Juścińska, M. Dutka, J. Myśliwska and A. Hellmann (2013). Treatment of graft-versus-host disease with naturally occurring T regulatory cells. BioDrugs 27: 605-614.

Tschetter, J. R., E. Mozes and G. M. Shearer (2000). Progression from acute to chronic disease in a murine parent-into-F1 model of graft-versus-host disease. J Immunol 165: 5987-5994.

Tschetter, J. R., E. Mozes and G. M. Shearer (2000). Progression from acute to chronic disease in a murine parent-into-F1 model of graft-versus-host disease. J Immunol 165: 5987-5994.

Uspensky, I. (2014). "Tick pests and vectors (Acari: *Ixodoidea*) in European towns: Introduction, persistence and management. Ticks Tick Borne Dis 5: 41-47.

Valenzuela, J. G. (2004). Exploring tick saliva: from biochemistry to 'sialomes' and functional genomics. Parasitology 129 Suppl: S83-94.

van Duijvendijk, G., C. Coipan, A. Wagemakers, M. Fonville, J. Ersöz, A. Oei, G. Földvári, J. Hovius, W. Takken and H. Sprong (2016). Larvae of *Ixodes ricinus* transmit *Borrelia afzelii* and *B. miyamotoi* to vertebrate hosts. Parasit Vectors 9: 97.

Villar, M., A. Marina and J. de la Fuente (2017). Applying proteomics to tick vaccine development: where are we? Expert Rev Proteomics 14: 211-221.

Wagemakers, A., J. Coumou, T. J. Schuijt, A. Oei, A. M. Nijhof, C. van 't Veer, T. van der Poll, A. D. Bins and J. W. Hovius (2016). An *Ixodes ricinus* tick salivary lectin pathway inhibitor protects *Borrelia burgdorferi sensu lato* from human complement. Vector Borne Zoonotic Dis 16: 223-228.

Wang, L., J. Fan, S. Chen, Y. Zhang, T. J. Curiel and B. Zhang (2013). Graft-versus-host disease is enhanced by selective CD73 blockade in mice. PLoS One 8: e58397.

Whelen, A. C. and S. K. Wikel (1993). Acquired resistance of guinea pigs to *Dermacentor andersoni* mediated by humoral factors. J Parasitol 79: 908-912.

Whitehill, G. D., S. Amarnath, P. Muranski, K. Keyvanfar, M. Battiwalla, A. J. Barrett and D. Chinnassamy (2016). Adenosine Selectively Depletes Alloreactive T Cells to Prevent GVHD While Conserving Immunity to Viruses and Leukemia. Mol Ther 24: 1655-1664.

Wikel, S. K., R. N. Ramachandra, D. K. Bergman, T. R. Burkot and J. Piesman (1997). Infestation with pathogen-free nymphs of the tick *Ixodes scapularis* induces host resistance to transmission of *Borrelia burgdorferi* by ticks. Infect Immun 65: 335-338.

Yegutkin, G. G. (2008). Nucleotide- and nucleoside-converting ectoenzymes: important modulators of purinergic signalling cascade. Biochim Biophys Acta 1783: 673-694.

Zhang, P., J. S. Lee, K. H. Gartlan, I. S. Schuster, I. Comerford, A. Varelias, M. A. Ullah, S. Vuckovic, M. Koyama, R. D. Kuns, K. R. Locke, K. J. Beckett, S. D. Olver, L. D. Samson, M. Montes de Oca, F. de Labastida Rivera, A. D. Clouston, G. T. Belz, B. R. Blazar, K. P. MacDonald, S. R. McColl, R. Thomas, C. R. Engwerda, M. A. Degli-Esposti, A. Kallies, S. K. Tey and G. R. Hill (2017). Eomesodermin promotes the development of type 1 regulatory T (TR1) cells. Sci Immunol 2: eaah7152.

Zivkovic, Z., A. Torina, R. Mitra, A. Alongi, S. Scimeca, K. M. Kocan, R. C. Galindo, C. Almazán, E. F. Blouin, M. Villar, A. M. Nijhof, R. Mani, G. La Barbera, S. Caracappa, F. Jongejan and J. de la Fuente (2010). Subolesin expression in response to pathogen infection in ticks. BMC Immunol 11: 7.

PUBLICATIONS AUTHORED DURING THE THESIS

PUBLICATIONS AUTHORED DURING THE THESIS

1. **Tomás-Cortázar, J**., I. Martín-Ruiz, D. Barriales, M. Pascual-Itoiz, V. G. de Juan, A. Caro-Maldonado, N. Merino, A. Marina, F. J. Blanco, J. M. Flores, J. D. Sutherland, R. Barrio, A. Rojas, M. L. Martínez-Chantar, A. Carracedo, C. Simó, V. García-Cañas, L. Abecia, J. L. Lavín, A. M. Aransay, H. Rodríguez and J. Anguita (2017). The immunosuppressive effect of the tick protein, Salp15, is long-lasting and persists in a murine model of hematopoietic transplant. **Scientific Reports** 7: 10740.
2. **Tomás-Cortázar, J***., L. Plaza-Vinuesa*, B. de las Rivas, J. L. Lavín , D. Barriales , L. Abecia , J.M. Mancheño , A.M. Aransay , R. Muñoz , J. Anguita, H. Rodríguez (2017). Identification of a highly active tannase enzyme from the oral pathogen *Fusobacterium nucleatum subsp polymorphum.* **Under Review**.
3. Carreras-González, A., N. Navasa, I. Martin-Ruiz, J.L. Lavín, M. Azkargorta, E. Atondo, D. Barriales, N. Macías-Cámara, M.A. Pascual-Itoiz, L. Sampedro, **J. Tomás-Cortázar**, A. Peña-Cearra, R. Prados-Rosales, L. Abecia, F. Elortza, A.M. Aransay, H. Rodríguez and Juan Anguita (2017). A multi-omic analysis reveals the regulatory role of CD180 during the response of macrophages to *Borrelia burgdorferi*. **Under Review**.
4. Zabala-Letona, A., A. Arruabarrena-Aristorena, N. Martín-Martín, S. Fernandez-Ruiz, J. D. Sutherland, M. Clasquin, **J. Tomás-Cortázar**, J. Jimenez, I. Torres, P. Quang, P. Ximenez-Embun, R. Bago, A. Ugalde-Olano, A. Loizaga-Iriarte, I. Lacasa-Viscasillas, M. Unda, V. Torrano, D. Cabrera, S. M. van Liempd, Y. Cendon, E. Castro, S. Murray, A. Revandkar, A. Alimonti, Y. Zhang, A. Barnett, G. Lein, D. Pirman, A. R. Cortazar, L. Arreal, L. Prudkin, I. Astobiza, L. Valcarcel-Jimenez, P. Zuñiga-GarcÌa, I. Fernandez-Dominguez, M. Piva, A. Caro-Maldonado, P. S·nchez-Mosquera, M. Castillo-MartÌn, V. Serra, N. Beraza, A. Gentilella, G. Thomas, M. Azkargorta, F. Elortza, R. Farr‡s, D. Olmos, A. Efeyan, J. Anguita, J. Muñoz, J. M. Falcón-Pérez, R. Barrio, T. Macarulla, J. M. Mato, M. L. Martinez-Chantar, C. Cordon-Cardo, A. M. Aransay, K. Marks, J. Baselga, J. Tabernero, P. Nuciforo, B. D. Manning, K. Marjon and A. Carracedo

(2017). mTORC1-dependent AMD1 regulation sustains polyamine metabolism in prostate cancer. **Nature** 547: 109-113.

5. Prados-Rosales, R., L. Carreño, T. Cheng, C. Blanc, B. Weinrick, A. Malek, T. L. Lowary, A. Baena, M. Joe, Y. Bai, R. Kalscheuer, A. Batista-Gonzalez, N. A. Saavedra, L. Sampedro, **J. Tomás**, J. Anguita, S. C. Hung, A. Tripathi, J. Xu, A. Glatman-Freedman, W. R. Jacobs, J. Chan, S. A. Porcelli, J. M. Achkar and A. Casadevall (2017). Enhanced control of Mycobacterium tuberculosis extrapulmonary dissemination in mice by an arabinomannan-protein conjugate vaccine. **PLoS Pathogens** 13: e1006250.
6. Champagne, D. P., K. M. Hatle, K. A. Fortner, A. D'Alessandro, T. M. Thornton, R. Yang, D. Torralba, **J. Tomás-Cortázar**, Y. W. Jun, K. H. Ahn, K. C. Hansen, L. Haynes, J. Anguita and M. Rincon (2016). Fine-Tuning of CD8(+) T Cell Mitochondrial Metabolism by the Respiratory Chain Repressor MCJ Dictates Protection to Influenza Virus. **Immunity** 44: 1299-1311.
7. Navasa, N., I. Martin-Ruiz, E. Atondo, J. D. Sutherland, M. Angel Pascual-Itoiz, A. Carreras-González, H. Izadi, **J. Tomás-Cortázar**, F. Ayaz, N. Martin-Martin, I. M. Torres, R. Barrio, A. Carracedo, E. R. Olivera, M. Rincón and J. Anguita (2015). Ikaros mediates the DNA methylation-independent silencing of MCJ/DNAJC15 gene expression in macrophages. **Scientific Reports** 5: 14692.

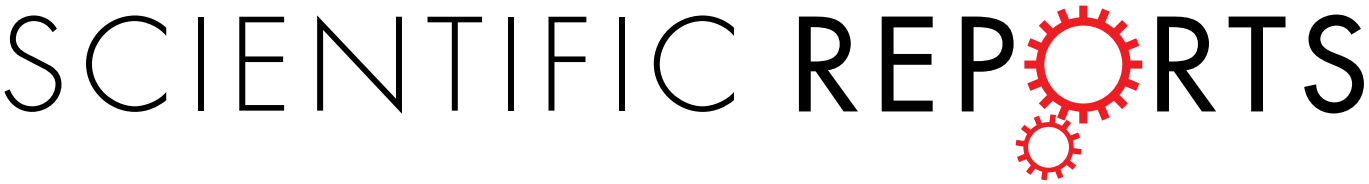

OPEN

The immunosuppressive effect of the tick protein, Salp15, is long-lasting and persists in a murine model of hematopoietic transplant

Received: 22 May 2017
Accepted: 23 August 2017
Published online: 06 September 2017

Julen Tomás-Cortázar[1], Itziar Martín-Ruiz[1], Diego Barriales[1], Miguel Ángel Pascual-Itoiz[1], Virginia Gutiérrez de Juan[1], Alfredo Caro-Maldonado[1], Nekane Merino[1], Alberto Marina[1], Francisco J. Blanco[1,2], Juana María Flores[3], James D. Sutherland[1], Rosa Barrio[1], Adriana Rojas[1], María Luz Martínez-Chantar[1,4], Arkaitz Carracedo[1,2,5,6], Carolina Simó[7], Virginia García-Cañas[7], Leticia Abecia[1], José Luis Lavín[1], Ana M. Aransay[1,4], Héctor Rodríguez[1] & Juan Anguita[1,2]

Salp15, a salivary protein of *Ixodes* ticks, inhibits the activation of naïve CD4 T cells. Treatment with Salp15 results in the inhibition of early signaling events and the production of the autocrine growth factor, interleukin-2. The fate of the CD4 T cells activated in the presence of Salp15 or its long-term effects are, however, unknown. We now show that Salp15 binding to CD4 is persistent and induces a long-lasting immunomodulatory effect. The activity of Salp15 results in sustained diminished cross-antigenic antibody production even after interruption of the treatment with the protein. Transcriptionally, the salivary protein provokes an acute effect that includes known activation markers, such as *Il2* or *Cd44*, and that fades over time. The long-term effects exerted by Salp15 do not involve the induction of either anergy traits nor increased populations of regulatory T cells. Similarly, the treatment with Salp15 does not result in B cell anergy or the generation of myeloid suppressor cells. However, Salp15 induces the increased expression of the ectoenzyme, CD73, in regulatory T cells and increased production of adenosine. Our study provides a profound characterization of the immunomodulatory activity of Salp15 and suggests that its long-term effects are due to the specific regulation of CD73.

Tick saliva is composed of a cocktail of pharmacologically active biomolecules that modulate among other host responses, the activation of CD4 T cells[1–5]. One of the best-studied components of tick saliva is the protein Salp15 from *Ixodes scapularis*. This protein inhibits the activation of naïve CD4 T cells, blocking early T cell signaling pathways, and thereby, the production of the autocrine growth factor IL-2[6–10]. Salp15 specifically binds to the first domain (D1) of the CD4 co-receptor causing a conformational change that impedes its interaction with the Src kinase, Lck and its activation[11]. Due to the specificity of Salp15 for CD4 and its capacity to inhibit the activation of CD4 T cells, the use of this tick saliva protein has been suggested for the treatment of immune diseases. In addition, our group has demonstrated the ability of Salp15 to inhibit the development of CD4 T cell-mediated immune responses *in vivo* upon challenge with different antigens[7,10,12]. Moreover, Salp15 prevents the development of experimental asthma in a mouse model[7]. However, whether the inhibition of CD4 T cells by Salp15 has long-term effects on future encounters with specific or unrelated antigens is currently unknown.

[1]CIC bioGUNE, 48160, Derio, Bizkaia, Spain. [2]Ikerbasque, Basque Foundation for Science, 48013, Bilbao, Bizkaia, Spain. [3]Department of Animal Medicine and Surgery, School of Veterinary Medicine, Complutense University of Madrid, 28040, Madrid, Spain. [4]Centro de Investigación Biomédica en Red de enfermedades hepáticas y digestivas (CIBERehd), Instituto de Salud Carlos III, 28029, Madrid, Spain. [5]Centro de Investigación Biomédica en Red en cáncer (CIBERonc), Instituto de Salud Carlos III, 28029, Madrid, Spain. [6]Department of Biochemistry and Molecular Biology, University of the Basque Country, 48940, Leioa, Bizkaia, Spain. [7]Molecular Nutrition and Metabolism, Institute of Food Science Research (CIAL, CSIC), 28049, Madrid, Spain. Correspondence and requests for materials should be addressed to J.A. (email: janguita@cicbiogune.es)

A common complication associated with allogeneic hematopoietic stem cell transplantation (HSCT) is the appearance of Graft-versus-host disease (GvHD). GvHD appears when donor T cells recognize as foreign the recipient antigens, including both human leukocyte (HLA) and minor histocompatibility antigens. Allogeneic HSCTs are used both in treatments of malignant disease and in ordinary transplants. GvHD appears in 50% of the transplants and causes death in 15% of the cases[13]. Despite its effectiveness, the induction of immunosuppression after HSCT can produce undesirable effects. These include the inhibition of graft-versus-tumor effector cells (GvT) and the appearance of infections and neoplasms[13–17]. Other treatments used for the mitigation or elimination of this disease are ineffective and unspecific. In fact, pre-transplantation chemotherapy and radiotherapy treatments (conditioning) applied in these cases for the elimination of the cancer cells and the establishment of the transplanted cells can result in nonspecific inflammatory events, helping create the necessary conditions for the activation of donor T cells[18]. Although several murine models of transplantation exist[19,20], none recapitulates in full the pathology observed in human transplantation. The transplant model of pure strains into F1 offspring does not require previous conditioning and results in mild episodes of acute GvHD followed by a period of chronic disease characterized by the production of autoantibodies[21].

Because Salp15 is able to inhibit early T cell signaling events, we hypothesized that the protein could preclude the activation of CD4 T cells and induce a long-term unresponsive or anergic after the exposure to the salivary protein. Our results show that Salp15 is able to change the transcriptional program of CD4 T cells during activation that nevertheless fades over time and does not result in increased populations of anergic or regulatory T cells. However, the protein induces the upregulation of the ectoenzyme, CD73 on the surface of Tregs, inducing increased production of the immunosuppressive molecule adenosine. Overall, the activity of Salp15 is evident in a long-term transplantation murine model and prevents the deposition of immune complexes in the kidney, a hallmark of murine chronic GvHD[21].

Results

The effect of Salp15 on activating CD4 T cells is long-lasting. In order to determine whether the effect of Salp15 on the activation of CD4 T cells is sustained, we activated purified splenic CD4 T cells in the presence of the salivary protein for 2 days, followed by their extensive washing and re-stimulation for 2 more days. The production of IL-2 was significantly reduced at both time points, including after 4 days of activation when Salp15 was no longer present (Fig. 1A). The longer-term effect of Salp15 could be due to its persistent binding to the surface of CD4 T cells. Thus, we determined the binding of Alexa Fluor^{488}-labeled Salp15 as well as the inactive control (Salp15ΔP11) by flow cytometry. Although both Salp15 and Salp15ΔP11 bound to purified CD4 T cells, the deletion of the C-terminal peptide, P11, resulted in decreased binding (Fig. 1B) in agreement with its reported lack of activity[22]. Importantly, binding of Salp15 to CD4 T cells was detectable for up to 72 h (Fig. 1B), indicating a persistent ability of this protein to remain attached to CD4.

In order to assess whether Salp15 could also exert long-term effects *in vivo*, we performed an immunization regime against ovalbumin and the unrelated protein, keyhole limpet hemocyanin (KLH). Groups of mice were immunized with ovalbumin in aluminum hydroxide in the absence or presence of Salp15 (day 0). Seven days later, the mice were boosted with ovalbumin under the same conditions. At day 14, the mice in each group were subdivided and immunized with ovalbumin or KLH in the absence of Salp15. All the mice were sacrificed at day 21. Sera were then analyzed for the presence of ovalbumin- and KLH-specific IgG levels. As expected, ovalbumin-specific IgG levels were significantly lower in mice that had received Salp15 in the first 2 immunizations (Fig. 1C). In order to establish whether the effect of Salp15 was circumscribed to ovalbumin, we also determined sera IgG levels against KLH. Mice that had not been immunized with this antigen did not show KLH-specific IgG in the sera. Notably, the levels of KLH-specific IgG were high in those mice receiving the antigen, and significantly lower in those that had received two previous doses of Salp15, but not at the time of immunization with KLH (Fig. 1C). These data show that the effect of Salp15 lasts beyond the treatment and can affect the response to unrelated antigens, such as KLH.

To further address the long-term effect associated with the treatment with Salp15, we utilized a murine model of GvHD resulting from the adoptive transfer of spleen cells from B6 into unconditioned CB6 F1 mice[21]. In this model of transplantation, the proliferation of drafted cells can be monitored in the blood and results in two different phases of the disease: an acute phase in which the transplanted cells proliferate, followed by a chronic phase predominantly characterized by symptomatology similar to autoimmune disease, including the deposition of IgG immune complex in the kidney[21]. CB6 F1 mice were transplanted 60×10^6 spleen cells and divided into two groups. One of the groups received intraperitoneal injections of Salp15 every other day for 10 days, while the control group received the same dose of Salp15ΔP11. Control animals showed a peak of parental cells at day 20 relative to the transplant, followed by a decline and another increase around 60 days post-transplant (Fig. 1D). In contrast, the treatment with Salp15 during the first 10 days post transplantation resulted in a significantly reduced level of parental cells in the blood (Fig. 1D). However, no effect was detected during the chronic phase of the disease. We also analyzed the potential effect of the treatment with Salp15 on the pathology associated with this model at day 80 after transplantation of the parental splenocytes. CB6 F1 mice transplanted with B6 splenocytes showed some disorganization in the glomerular basement membrane and tubular brush border of the kidney upon transplantation that was not affected by the treatment (Fig. 1E). However, immune complex deposition that was readily detected in the control-treated mice was significantly reduced in the animals that had been treated with Salp15 (Fig. 1E,F). Overall, our results show that Salp15 has short-term and long-term effects during the development of immune responses that specifically affect the expansion of CD4 T cells and the production of antibodies.

Identification of transcriptional traits in activating CD4 T cells treated with Salp15. We then sought to determine the transcriptional signature of activated CD4 T cells for 48 and 96 hours with plate-bound

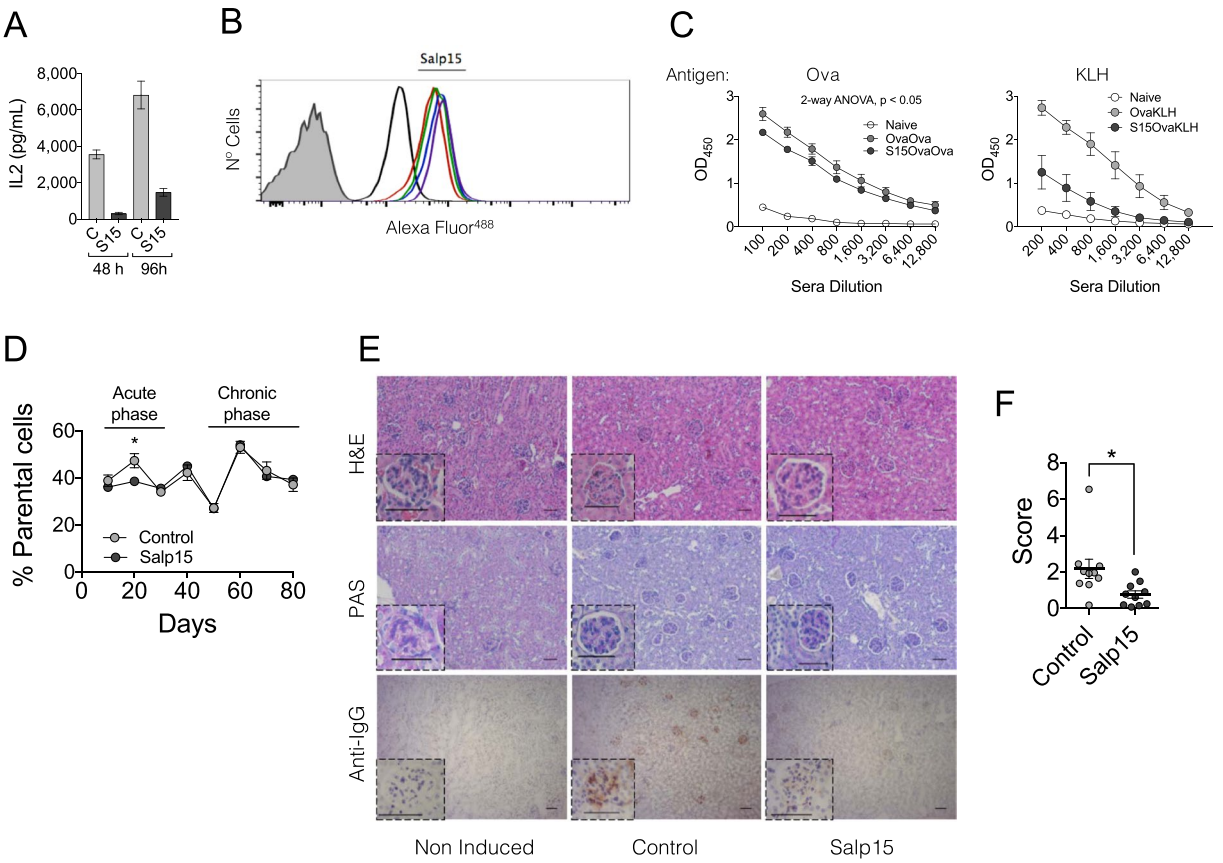

Figure 1. The effect of Salp15 on CD4 T cells is long-lasting. (**A**) IL-2 production by purified splenic CD4 T cells activated with anti-CD3/CD28 for 2 days in the presence of 50 μg/ml of Salp15, washed and re-stimulated under the same conditions for another 48 h in the absence of the immunosuppressive protein. The results represent the average ± SE of one experiment in triplicate and are representative of 3 performed. (**B**) Binding of Salp15 or the C-terminal deletion mutant, Salp15ΔP11 to purified CD4 T cells. The proteins were labeled with Alexa Fluor^{488} and tested for their binding for different time periods. The binding was assessed by flow cytometry. The shaded histogram represents unlabeled cells. The black histogram represents binding of Salp15ΔP11. Color histograms represent binding of Salp15 at different time points (12, 24, 48 and 72 h). (**C**) Antibody titers specific for ovalbumin (left panel) and KLH (right panel) in mice immunized with the antigens as described in Methods and treated with 50 μg of Salp15 (S15OvaOva or S15OvaKLH) or left untreated (OvaOva or OvaKLH). Non-immunized mice served as controls (Naive) (**D**) Percentage of parental (H2^{b}) cells in the blood of transplanted CB6F1 mice (H2^{b,d}) over a period of 80 days. The mice were either treated with 50 μg of Salp15 or Salp15ΔP11 (Control) (**E**) Histological features of the kidneys of CB6F1 mice transplanted with B6 splenocytes after 80 days. Kidney sections were stained with H&E (top panels), periodic acid schiff (PAS) staining (middle panels) and anti-mouse IgG immune complex deposition (lower panels). The scale bars represent 50 μm. (**F**) Assessment of IgG immune complex deposition scores in the kidneys of the transplanted mice by analysis of 5 different micrographs with the FriDA software package and averaged per section. The experiments *in vivo* were performed with groups of 5 mice and performed at least twice.

anti-CD3 and soluble anti-CD28 in the presence of Salp15 or its control, Salp15ΔP11 (Fig. 2A). To allow the survival of the CD4 T cells throughout the activation process, a low dose of Salp15 (25 μg/ml) was used. This dose reduced the activation of CD4 T cells (Fig. 2A) without significant cell death at 4 days post-activation (data not shown). Principal component analysis (PCA) showed a distinct pattern of gene expression in control activated cells over the analyzed period of time (Fig. 2B). The presence of Salp15 resulted in variations in the PCA at 2 days of activation, while the differences faded when the transcriptome was analyzed after 4 days of activation (Fig. 2B). These differences were also noticeable when the 1000 most regulated genes were analyzed, with maximal differences between Salp15-treated and control activated CD4 T cells at 2 days and more discrete differences when analyzed at 4 days of activation (Fig. 2C). The activation of CD4 T cells under control conditions revealed 2382 genes upregulated and 2848 genes downregulated at 2 days of activation (Fig. 2D), while 1882 genes were upregulated and 1841 genes downregulated after 4 days of activation, using a cut-off value of 1 $\log_2$fold change and an adjusted p-value < 0.05 (Fig. 2D). Of these genes, 1245 were upregulated at both 2d and 4d of activation, 1601 were downregulated at both time points and 40 were regulated in opposite directions (Fig. 2E). Using the same cut-off values, we found 154 genes upregulated as a consequence of the presence of Salp15 during activation at 2d while only 1 gene was downregulated (Fig. 2F). Notably, the number of genes regulated at 4d of activation in

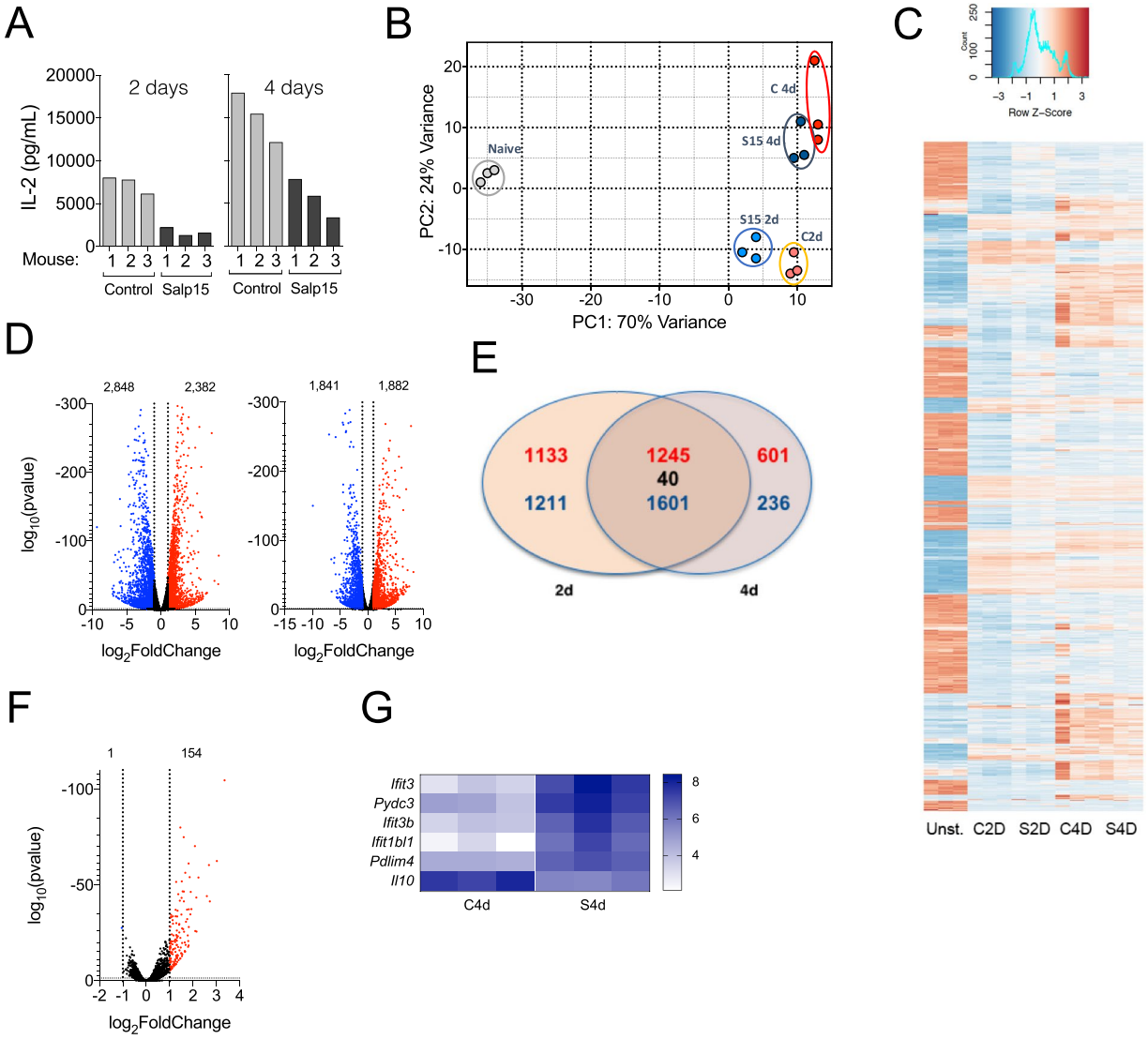

Figure 2. Transcriptional traits of CD4 T cells activated in the presence of Salp15. (**A**) IL-2 production by CD4 T cells used for the transcriptomic analysis. Each bar represents one of the 3 mice used. The amount of Salp15 used was 25 μg/ml. Control cells were treated with Salp15ΔP11 (Control). (**B**) Principal component analysis showing the grouping of the different assay conditions according to their transcriptome. Non-activated cells (Naive, grey); Salp15ΔP11-treated at 2 days (C 2d, orange) or 4 days of activation (C 4d, red); Salp15-treated at 2 days (S15 2d, light blue) or 4 days (S15 4d, dark blue). (**C**) Heatmap corresponding to the 1000 most regulated genes over the conditions analyzed by RNAseq. (**D**) Volcano plots showing the genes upregulated (red) or downregulated (blue) by activation with anti-CD3 and CD-28 at 2 (left) and 4 days (right) of stimulation. (**E**) Venn diagram showing the number of genes regulated at both 2 and 4 days of activation in the absence of Salp15. (**F**) Volcano plot showing the number of genes differentially regulated during the activation of CD4 T cells in the presence of Salp15 or Salp15ΔP11 (control) after 2 days of stimulation. (**G**) Heatmap of the genes regulated in the presence of Salp15 at 4 days of activation.

the presence of Salp15 was dramatically reduced to 5 genes upregulated and just 1 (*Il10)* downregulated (Fig. 2G). Selected transcriptional changes were validated as shown in Supplementary Fig. 1.

Salp15 affects CD4 T cell genes early during the activation process. The activation of CD4 T cells produced the expected profile, involving genes such as *Il2*, *Cd44* or *IL2ra* (Fig. 3A). Gene ontology analysis of Biological Processes (GOBP) revealed that the most over-represented groups included genes related to leukocyte cell-cell adhesion and aggregation or T cell activation, among other immune-related processes (Supplementary Fig. 2). As expected, the presence of Salp15 induced a reduction of *Il2* gene expression and the production of IL-2 at 2 days of activation (Fig. 3A,B,C; see also Fig. 2A). Furthermore, the activation marker CD44 was significantly reduced both at the gene expression level (Fig. 3A,D,E), by surface analysis of the protein by flow cytometry in *in vitro* activated CD4 T cells (Fig. 3F), and *in vivo* in the spleens of ovalbumin-immunized mice at day 7

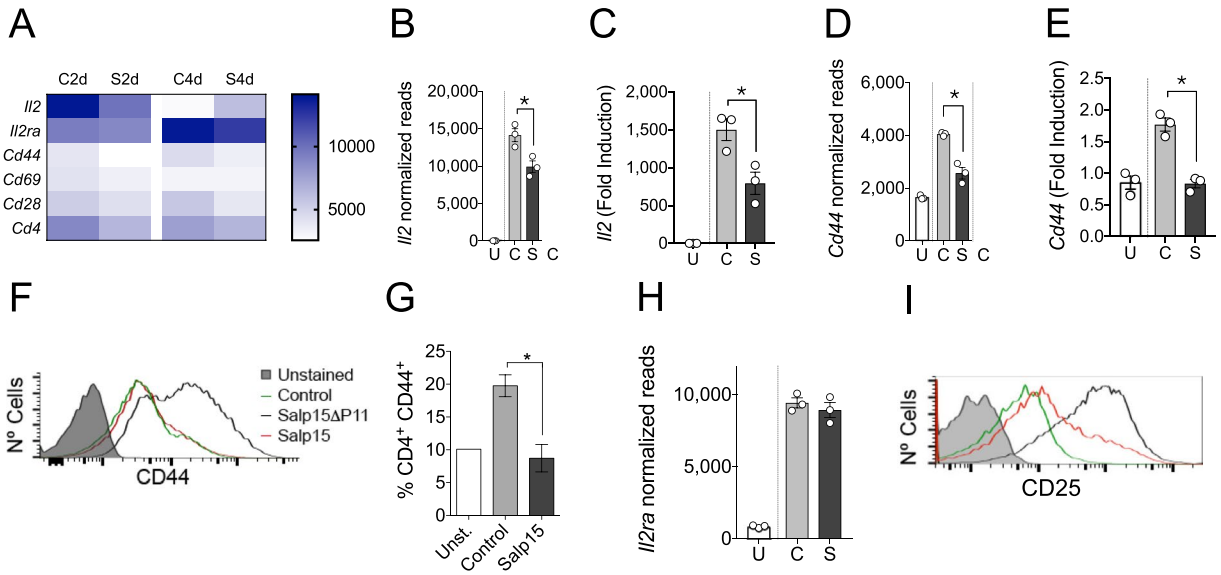

Figure 3. Salp15 affects the activation of CD4 T cells. (**A**) Heatmap of genes involved in the activation of CD4 T cells at 2 and 4 days of stimulation with anti-CD3/CD28 in the absence or presence of Salp15. (**B**) Normalized reads corresponding to the *Il2* gene at 2 days of activation in the presence of Salp15 (S) or Salp15ΔP11 (**C**). U- Unstimulated cells. (**C**) Transcriptional levels of *Il2* at 2 days of activation in the presence of Salp15 (S) or Salp15ΔP11 (**C**) of Salp15 determined by qRT-PCR. Normalized reads of *Cd44* (**D**) and transcriptional levels by qRT-PCR (**E**) in CD4 T cells at 2 days of activation, as before. (**F**) Surface CD44 levels on CD4 T cells activated for 2 days in the presence of Salp15 or Salp15ΔP11. Control: Unstimulated cells. The grey histogram represents an unstained control. (**G**) Percentage of CD4 T cells expressing CD44 in the spleen of mice immunized with ovalbumin and treated with Salp15 compared to control treated, immunized mice (Control) and non immunized mice (Unst.). (**H**) Normalized reads of *Il2ra* in CD4 T cells at 2 days of activation, as before. (**F**) Surface CD25 levels on CD4 T cells activated for 2 days in the presence of Salp15 or Salp15ΔP11. The color legend is as indicated in (**F**). All the experiments were performed with 25 μg/ml of Salp15 or Salp15ΔP11 (control).

post-immunization (Fig. 3G). Although, the effect of Salp15 on *Il2ra* expression was not evident at this concentration (25 μg/ml, Fig. 3H), the analysis of CD25 on the surface of 2-day activated CD4 T cells revealed decreased levels of the protein in the presence of this dose of Salp15 (Fig. 3I).

Salp15 induces the expression of 5′-ectonucleotidase (CD73) in regulatory T cells. The repressed activation of CD4 T cells in the presence of Salp15 could result in the induction of anergy. We therefore analyzed the expression levels of genes associated with this phenomenon in CD4 T cells, including *Satb1*, *Cd7*, *Rap1a*, *Itch*, *Rnf128*, *Dtx1*, *Izumo1r*, *Cblb, Dgka*[23], *Nr4a1* or *Pdcd1*[24]. Salp15 induced small and inconsistent changes in these genes (Fig. 4A, Table 1), suggesting that this protein does not induce anergy in CD4 T cells. In order to confirm these results, we analyzed by flow cytometry markers of anergy in CD4 T cells that were activated *in vitro* in the presence of Salp15. The percentage of $CD4^{+}FoxP3^{-}CD44^{high}CD73^{high}FR4^{high}$[24] cells increased upon CD4 T cell activation but remained as low as in naive cells in the presence of Salp15 (Fig. 4B). Furthermore, the analysis of anergic CD4 T cells in mice either immunized with ovalbumin (Table 2) or induced GvHD (Table 3) showed no effect on this population as a consequence of the treatment with Salp15. Similarly, the treatment with Salp15 did not result in the generation of a significant anergic B cell population or increased the pool of monocytic myeloid suppressor cells (Table 2). These data confirm that Salp15 act as an immunosuppressor on CD4 T cells that depends on its interaction with CD4 and that does not induce a long-term anergic state in T or B cells, nor the generation of myeloid suppressor cells.

The transcriptomic data also helped us elucidate whether activated CD4 T cells in the presence of Salp15 acquired specific markers of regulatory T cells, such as *Foxp3, Ctla4, Nrp1, Pdcd1, Lag3, Havcr2, Lrrc32, Tgfb1, Ikzf2, Il7r* or *Entpd1*[25,26]. No major differences were found between controls and CD4 T cells activated in the presence of Salp15 (Fig. 4C, Table 1). Moreover, the analysis of FoxP3-positive cells after 4 days of activation *in vitro* did not show changes in the percentage of Tregs associated with the presence of Salp15 (Fig. 4B). The effect of Salp15 on the pool of Tregs *in vivo* was also negligible in mice that had been immunized with ovalbumin (Fig. 4D). Furthermore, the analysis of FoxP3-positive CD4 T cells in the peripheral blood of CB6 F1 mice transplanted with B6 splenocytes did not show differences associated with the treatment with Salp15 throughout the life of the experiment (Table 3). Similar results were found when we analyzed the expression of Nrp1 on CD4 T cells, another marker of regulatory T cells[27] (Table 2). The analysis of type 1 regulatory T (Tr1) cells markers, including *Il10*, *Eomes*, *Il2rb*, *Itga4*, *Itgb7*, *Ly6c1* or *Tigit*[28], showed that Salp15 does not induce the generation of these cells, although *Il10* expression levels were significantly reduced in the presence of the salivary protein at 4 days of activation (Table 1). These results demonstrate that the treatment with Salp15 does not result in the generation of a population of regulatory T cells that could account for long-term immunomodulatory effects.

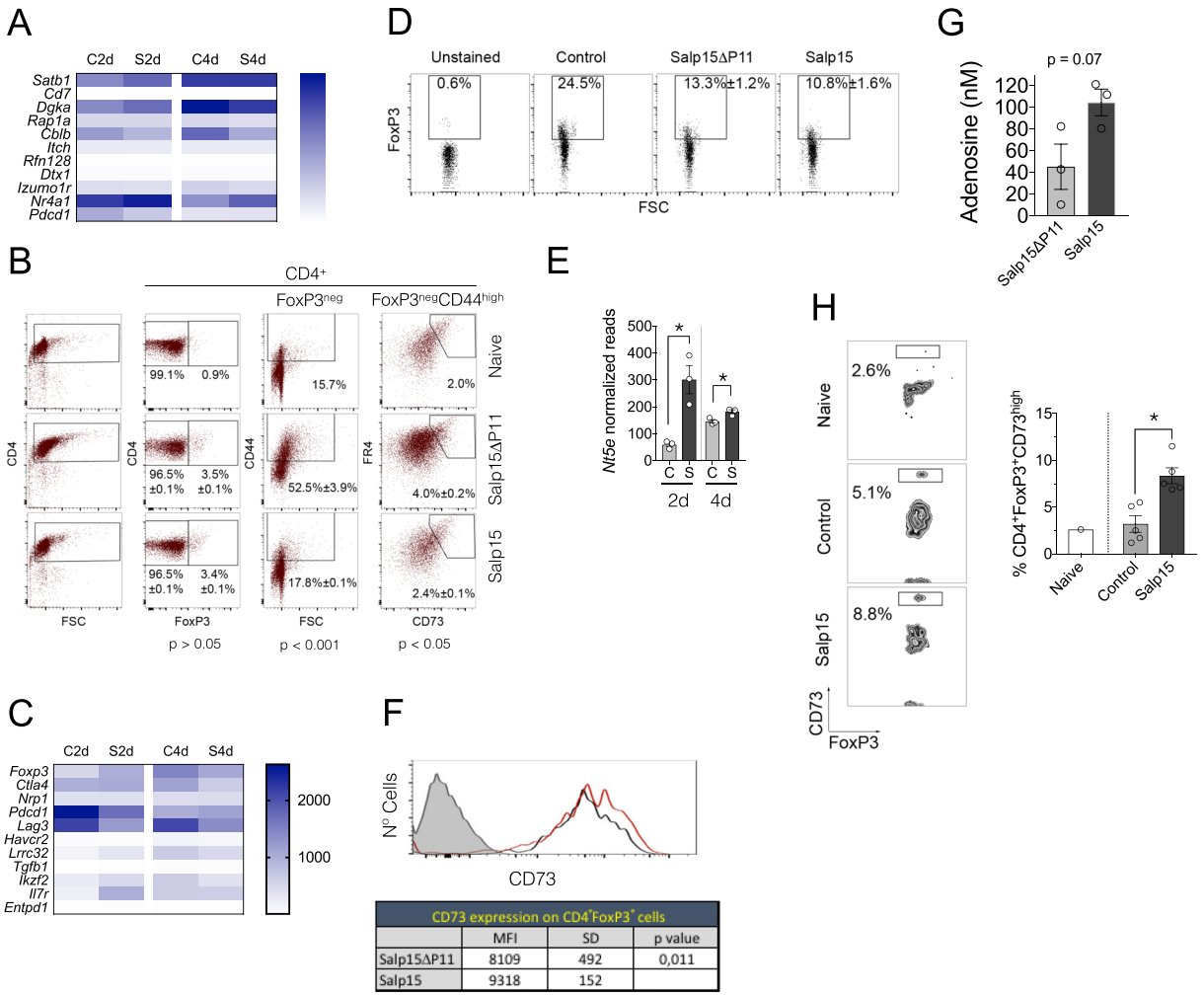

Figure 4. Salp15 does not induce increased anergic or Treg numbers but augments the levels of CD73 in FoxP3$^+$ cells. (**A**) Heatmap representing genes associated with anergy in CD4 T cells according to the RNAseq analysis in the presence of Salp15 (S) or Salp15ΔP11 (**C**) at 2 and 4 days of activation. (**B**) Percentage of FoxP3$^+$ and anergic CD4 T cells upon their exposure to 25 μg/ml of Salp15 or Salp15ΔP11 for 2 days. The average ± SE of triplicates is indicated. The p values (Student´s t test) correspond to the comparison between the Salp15ΔP11 and Salp15 groups. The data presented is representative of 2 independent experiments with similar results. (**C**) Heatmap corresponding to genes associated with regulatory T cells according to the RNAseq analysis in the presence of Salp15 (S) or Salp15ΔP11 (**C**) at 2 and 4 days of activation. (**D**) Percentage of FoxP3-positive CD4 T cells upon exposure to 25 μg/ml of Salp15 or Salp15ΔP11 *in vitro* for 2 days during activation. The values correspond to the average ± SE of 5 mice per group. No significant differences were detected between the Salp15ΔP11 and Salp15 groups. The data is representative of 2 independent experiments. (**E**) Normalized reads corresponding to the expression levels of *Nt5e* at 2 and 4 days of activation *in vitro* in the presence of Salp15 (S) or Salp15ΔP11 (**C**). (**F**) Surface expression levels of CD73 on CD4$^+$FoxP3$^+$ T cells (top) activated for 2 days in the presence of 25 μg/ml of Salp15 (red histogram) or Salp15ΔP11 (black histogram). The shaded histogram represents an unstained control. The table shows the average mean fluorescence intensity (MFI) ± standard deviation (SD) of 5 mice per group. Differences of the means were analyzed by the Student´s T-test. (**G**) Average adenosine levels in the supernatants of CD4 T cells activated in the presence of 25 μg/ml of Salp15 or Salp15ΔP11 for 2 days. The results represent 3 independent mice. (**H**) Increased percentage of CD4$^+$FoxP3$^+$CD73^{high} cells in the blood of CB6F1 mice transplanted with B6 splenocytes at day 50 post induction. The histogram on the right represents the average ± SE of 5 control (Salp15ΔP11) and 5 Salp15-treated mice. *$p < 0.05$.

We then addressed whether the treatment with Salp15 would impact the activity rather than the size of the Treg population. The ectoenzyme CD73 is expressed by Tregs and mediates the production of adenosine, an immunosuppressive molecule on T cells[29–31]. We observed that expression levels of *Nt5e* (which encodes CD73) were increased upon the treatment of CD4 T cells with Salp15 (Fig. 4E). Therefore, we determined the expression levels of CD73 on the surface of FoxP3-positive cells. We found that the activation of CD4 T cells *in vitro* in the presence of Salp15 resulted in a significant increase in the surface expression of CD73 (Fig. 4F). Furthermore, the levels of adenosine increased upon the treatment of activating CD4 T cells with Salp15 (Fig. 4G). Importantly,

Gene	S2D vs. C2D		S4D vs. C4D	
	Log_2FI	Adj. p-value	Log_2FI	Adj. p-value
Anergy				
Satb1	0,304	0,012	0,002	0,997
Cd7	0,750	0,001	0,166	NA
Rap1a	0,030	0,894	−0,223	0,116
Itch	0,087	0,613	−0,065	0,816
Rnf128	−0,077	0,858	−0,321	0,186
Dtx1	−0,039	0,908	0,047	0,921
Izumo1r	−0,090	0,573	−0,251	0,094
Cblb	−0,403	8,40E-06	−0,656	3,74E-07
Dgka	0,282	0,001	−0,215	0,114
Nr4a1	0,148	0,189	0,426	1,1E-04
Pdcd1	−0,568	3,9E-11	−0,144	0,612
Regulatory T cells				
Foxp3	0,815	7,85E-09	−0,352	0,095
Ctla4	0,109	0,535	−0,691	1,19E-07
Nrp1	0,048	0,859	0,015	0,975
Pdcd1	−0,568	3,90E-11	0,144	0,612
Lag3	−0,721	1,81E-11	−0,540	5,44E-07
Havcr2	−0,166	0,668	−0,177	0,620
Lrrc32	0,527	0,044	−0,268	0,345
Tgfb1	−0,148	0,197	−0,164	0,473
Ikzf2	0,438	0,117	−0,558	0,00027
Il7r	***1,504***	***6,21E-15***	−0,040	0,914
Entpd1	0,402	0,163	−0,004	0,995
Type 1 Regulatory T cells				
Il10	−0,236	0,492	***−1,069***	***4,01E-10***
Eomes	0,136	0,477	−0,193	0,351
Il2rb	0,171	0,367	−0,069	0,808
Itga4	0,536	0,027	−0,260	0,178
Itgb7	−0,578	1,78E-06	0,047	0,878
Ly6c1	0,200	0,233	−0,190	0,511
Tigit	−0,387	0,001	−0,500	0,001

Table 1. Differential expression of genes associated with CD4 T cell anergy and regulatory T cells.

we observed an increase in a population of $CD4^+FoxP3^+CD73^{high}$ in the blood of mice that have been induced GvHD at day 50 post transplant (Fig. 4H). Overall, our results show that Salp15 is able to induce long-term effects on activating CD4 T cells that involve, at least in part, the increased expression and activity of CD73 on regulatory T cells.

Discussion

The tick salivary protein Salp15 inhibits early CD4 T cell signaling events and, in consequence, their activation. The activity of Salp15 on CD4 T cells is well-characterized[9,10,24]. Both *in vitro* and *in vivo*, this protein is able to prevent a full activation program on these immune cells[6]. The fate of CD4 T cells affected by the activity of Salp15 is not known. They could become permanently unable to respond to antigen or, alternatively, revert to a state in which they are amenable to become activated when antigen is present again. Here, we show that the presence of Salp15 during the activation of CD4 T cells results in long-term effects that affect their encounter with new antigens. Using transcriptomics, two models of CD4 T cell activation *in vivo* and the polyclonal activation of these cells *in vitro*, we show that whereas Salp15 does not affect the generation of anergic CD4 T cells or Tregs, it induces the increased expression of the ectoenzyme, CD73, in $Foxp3^+$ regulatory T cells. This effect results in an elevated production of adenosine, a known immunomosuppressive molecule produced by Tregs[32,33].

Treatment with Tregs has been proposed as an appropriate therapy for GvHD and other immune disorders[34,35]. In fact, several biological agents, including CTLA4 fusion proteins or anti-TNF antibodies[34], have the ability to either induce an increase in number or the activity of Tregs. Treg function involves CD73 activity and other mechanisms of action[36,37]. Indeed, the importance of CD73 activity has been studied in a murine model of GvDH, demonstrating that the ectonuclease helps control the disease[30]. The conversion of 5′-AMP to adenosine mediated by CD73 in Tregs has been broadly described[38]. The anti-inflammatory effect of adenosine present in the pericellular microenvironment results in the suppression of proliferation of effector CD4 T cells and the reduction of cytokine production[39]. Indeed, we found that the levels of this molecule were increased in *in vitro* assays of CD4 T cell activation in the presence of Salp15. The capacity of Salp15 to increase *Nt5e* transcription

Blood B cell populations*	Control	ΔO		SO	
		Average	*SD*	*Average*	*SD*
B cells ($B220^+$)	45,10	43,50	1,87	40,07	4,43
$B220^+CD69^+$	28,50	12,41	4,15	11,50	4,76
Anergic B cells ($B220^+CD93^+IgM^+CD23^+$)	3,85	2,28	0,40	1,80	0,76
Mature B cells ($B220^+CD93^-CD23^+$)	27,87	28,77	0,56	27,80	1,50
Spleen populations*	**Control**	**ΔOO**		**SOO**	
		Average	*SD*	*Average*	*SD*
$CD4^+$	11,60	11,02	2,31	10,77	2,08
$CD8^+$	7,84	6,10	0,98	6,38	0,87
$CD4^+CD25^+$	12,90	8,47	1,33	5,60	2,34
$CD4^+CD44^+$	28,10	7,48	2,43	7,55	4,21
Anergic T cells ($CD4^+CD44^{high}CD73^{high}FR4^{high}$)	3,60	0,92	0,35	0,86	0,39
Tregs ($CD4^+NRP1^+$)	2,02	1,54	0,20	1,46	0,16
Macrophages ($F4/80^+GR\text{-}1^-$)	2,15	2,08	0,09	2,44	1,30
Neutrophils ($F4/80^-GR\text{-}1^+$)	1,30	1,52	0,21	2,73	0,71
Monocytic myeloid suppressor cells ($CD11b^{high}GR\text{-}1^{high}Ly6C^+$)	1,01	0,56	0,24	0,82	0,36
Inflammatory macrophages ($F4/80^+GR\text{-}1^{int}Ly6C^{high}$)	1,97	2,42	0,38	2,52	0,64
		n = 5		n = 5	

Table 2. Cell populations in blood and spleen of mice immunized with ovalbumin (O) and treated with Salp15 (S) or the control protein (Δ). All comparisons between ΔO vs. SO, $p > 0.05$. *The gating strategies are shown in Supplementary Fig. 3.

and the upregulation of CD73 on the surface of $FoxP3^+$ T cells can therefore help explain the long-lasting effects elicited by Salp15. Future studies will determine whether the absence of CD73 on Tregs can indeed suppress the long-term immunomodulatory effect exerted by the salivary protein.

Our results show that the binding of Salp15 to CD4 persists along the activation period *in vitro*. However, the changes induced by Salp15 at the transcriptional level fade over time. Furthermore, Salp15 does not affect CD4 T cell differentiation in the absence of polarizing cytokines, including the induction of Th1, Th2, Th17 or Treg gene markers (Suppl. Fig. 4A). We cannot exclude that under polarizing conditions, Salp15 may affect CD4 T cell differentiation. In fact, in the presence of IL-6, the inhibition of IL-2 production during CD4 T cell activation can lead to their differentiation towards a Th17 phenotype[22]. Nevertheless, the restimulation of splenocytes of ovalbumin and KLH immunized mice resulted in similar levels of IL-4, while IFNγ was not detected in the restimulation supernatants (Suppl. Fig. 4B), arguing against an effect of Salp15 on Th1 or Th2 differentiation under these conditions. Our analysis also show that Salp15 does not seem to exert a direct effect on other cellular types, including the generation of anergic B cells or myeloid-derived suppressor cells (MDSCs). Nevertheless, in both *in vivo* models, the treatment with Salp15 results in an indirect effect on the ability of B cells to produce antigen-specific antibodies, as we have previously demonstrated[10].

In summary, we show that the tick salivary immunosuppressor Salp15 is able to induce the sustained repression of CD4 T cell activation that involves the direct effect on these immune cells during the activation period and the increased expression of CD73 on regulatory T cells. These data support the notion that Salp15 is able to maintain its immunomodulatory action through the induction of increased Treg activity, leading to long-term effects in two *in vivo* models, including a pre-clinically relevant murine model of graft versus host disease.

Methods

Protein purification and labeling. Salp15 and an inactive deletion mutant lacking the last 20 aminoacids (Salp15ΔP11) were purified from Drosophila S2 cells, as described[10]. Protein labeling was performed using the Alexa Fluor® 488 Protein Labeling Kit (Thermo Fisher Scientific, Eugene, OR), following the manufacturer's instructions.

Cell purification and activation. CD4 T cells were purified from the spleens of C57BL/6 mice by negative selection using a CD4 T cell isolation Kit (Miltenyi Biotec, Bergisch Gladbach, GE) according to the manufacturer's instructions. Purified CD4 T cells at the indicated concentrations were activated with 5 μg/ml of plate-bound anti-CD3ε and 1 μg/ml of soluble anti-CD28 (BD Biosciences, San Diego, CA) in the presence of the indicated concentration of Salp15 or Salp15ΔP11. Cells were incubated at 37 °C in TexMACS Medium (Miltenyi Biotec).

Flow cytometry. Blood was extracted from the saphenous vein in the presence of EDTA and depleted of erythrocytes by hypotonic lysis. Whole splenocytes were isolated from immunized or GvHD mice by mechanical disruption followed by lysis of erythrocytes. The cells (10^6/ml) were incubated with Fc Block (anti-CD16/CD32; BD BioSciences) and labelled with fluorochrome-labeled antibodies against CD4, CD8, B220, CD69, Ly6C, F4/80, GR-1, CD25, CD11b, CD44, CD73, FR4, NRP1, Foxp3, CD93, IgM, CD23 (Miltenyi Biotec). To

Blood cell populations	Day 20		Day 30		Day 40		Day 60		Day 80	
	Control	*Salp15*	*Control*	*Salp15*	*Control*	*Salp15*	*Control*	*Salp15*	*Control*	*Salp15*
$CD4^+$ T cells	26.1 ± 0.7	26.5 ± 0.5	33.5 ± 1.6	30.0 ± 1.2	34.9 ± 2.2	38.4 ± 2.7	30.9 ± 1.6	28.5 ± 1.8	21.0 ± 1.8	25.2 ± 2.7
$CD8^+$ T cells	12.8 ± 1.2	13.8 ± 0.4	17.6 ± 1.0	18.0 ± 0.9	18.5 ± 1.1	17.4 ± 0.8	15.6 ± 0.8	16.2 ± 0.4	15.9 ± 1.4	18.4 ± 1.6
Tregs ($CD4^+FoxP3^+$)	7.1 ± 0.4	6.2 ± 0.3	7.3 ± 0.3	7.1 ± 0.2	4.7 ± 0.4	3.9 ± 0.7	6.8 ± 0.4	7.2 ± 0.5	7.7 ± 0.6	7.7 ± 1.2
Anergic T cells ($CD4^+CD44^{high}CD73^{high}FR4^{high}$)	6.2 ± 1.8	3.9 ± 0.9	20.0 ± 2.7	16.5 ± 1.9	13.4 ± 1.1	12.3 ± 1.1	4.4 ± 0.9	5.4 ± 0.5	7.0 ± 1.4	5.9 ± 1.0

Table 3. Cell populations (average ± SD) in blood upon B6 splenocyte transplant into CB6 F1 mice. All comparisons between Control vs. Salp15, $p > 0.05$. $n = 5$ mice per group.

detect Salp15 binding to CD4 T cells, splenic purified CD4 T cells were labeled with Salp15-Alexa $Fluor^{488}$ or Salp15ΔP11-Alexa $Fluor^{488}$.

Immunizations. Groups of C57Bl/6 mice were immunized subcutaneously with 50 μg of ovalbumin in aluminum hydroxide (50% Hydrogel, Invivogene. Tolouse, France) containing 50 mg of Salp15 or PBS (conbtrol). The mice were boosted under the same conditions 7 days later. At day 14, each group of mice was subdivided into 2 groups and immunized with either 50 μg of ovalbumin or keyhole lympet hemocyanin (KLH). The mice were sacrificed 7 days later and the spleens and sera were analyzed for cellular composition and antigen-specific immunoglobulin titers, respectively.

Graft versus host disease murine model. Splenocytes were extracted from 8-week old C57BL/6 ($H\text{-}2^b$) mice and 60×10^6/mouse were injected intraperitoneally into CB6F1 ($H\text{-}2^{b,d}$) mice (Envigo, Gannat, France). The mice were treated with 50 μg of Salp15 by intraperitoneal injection starting the day of cell transfer and every other day until day 10. Blood was extracted from day 10 to day 80 at 10-days intervals. Erythrocytes were removed by hypotonic lysis and the cells were analyzed by flow cytometry. At sacrifice, kidneys were processed for histochemical evaluation.

Renal deposited IgG detection, PAS and HE. Kidneys were fixed in 10% neutral buffered formalin, dehydrated, embedded in paraffin and cut into 5 μm thick sections. For histopathology, sections were hydrated and stained with hematoxylin – eosin (HE) or periodic acid-Schiff (PAS) according to standard protocols. For immunohistochemical analysis, tissue sections were subjected to antigen retrieval using protease K for 20 min at 37 °C. After blocking, sections were incubated with primary antibody overnight. The slides were then sequentially incubated with DAB chromogen for 5 min, counterstained with Mayer's hematoxylin and mounted for microscopy. Goat Anti-Mouse IgG-HRP Light chain specific (Jackson ImmunoResearch Laboratories) was used at 1/250 concentration as the primary antibody. Photographs were taken with an Axioimager A1 microscope and analyzed with Frida software[40].

RNAseq. Purified CD4 T cells from three mice were activated independently with 5 μg/ml of plate-bound anti-CD3 and 1 μg/ml of soluble anti-CD28 (BD Bioscience) in the presence of 25 μg/ml of Salp15 or Salp15ΔP11 (control). Cells were incubated at 37 °C in TexMACS Medium (Miltenyi Biotec) for 48 and 96 h. RNA extraction was performed using the PureLink RNA Micro Scale Kit (Thermo Fisher Scientific) according to the manufacturer's protocol. The quantity and quality of the RNAs were evaluated using the Qubit RNA Assay Kit (Invitrogen, Eugene, OR) and RNA Nano Chips in a 2100 Bioanalyzer (Agilent Technologies, Waldbronn, GE), respectively. Libraries for sequencing were prepared using the TruSeq RNA Sample Preparation Kit v2 (Illumina Inc, San Diego, CA) following the protocol provided by the manufacturer. Single-read, 50 nt sequencing of pooled libraries was carried out in a HiScanSQ platform (Illumina Inc.).

The quality control of the sequenced samples was performed with FASTQC software (www.bioinformatics.babraham.ac.uk/projects/fastq). Reads were mapped against the mouse (*mm10*) reference genome by using the program Tophat[41] to account for spliced junctions. The resulting BAM alignment files for the samples were the input for the Differential Expression (DE) analysis, carried out by DESeq. 2[42], to detect differentially expressed genes among the different conditions. GO enrichment was tested using the ClusterProfiler[43] Bioconductor package and the Panther Database[44]. Transcriptomics data were also analyzed using QIAGEN's Ingenuity Pathway Analysis (IPA, QIAGEN, Red Wood city, CA).

Real-time RT-PCR. RNA was reverse transcribed using M-MLV reverse transcriptase (Thermo Fisher Scientific) and random hexamers. Real-time PCR was then performed using SYBR Green PCR Master Mix (Quanta Biosciences, Beverly, MA) on a QuantStudio 6 real-time PCR System (Thermo Fisher Scientific). Fold induction of the genes was calculated using the $2^{-\Delta\Delta Ct}$ method relative to the reference, previously validated genes, *Rpl19* and *Actb*, as indicated. The primers used are listed in Table 4.

Determination of adenosine levels. The levels of adenosine were determined in the culture supernatants of activated CD4 T cells using the fluorometric adenosine assay kit (Abnova, Walnut, CA) following the methods provided by the manufacturer.

Statistical analysis. Results are presented as means ± SE, unless otherwise stated. The differences in means between groups were tested using the Student's T-test. Differences in antibody titers were assessed by a 2-way ANOVA. All calculations were made in GraphPad Prism, version 7. A p-value < 0.05 was considered statistically

Gene	Forward	Reverse	Purpose
IL2	TGTGCTCCTTGTCAACAGCG	TTTCAATTCTGTGGCCTGCTTG	RNAseq validation
Zfp750	CCCACCTTTGCTGCAGGT	GGGGGCCGTGGAATATAGTG	RNAseq validation
Klf2	GCCTTCGGTCTTTTCGAGGA	AGGCTTCTCACCTGTGTGTG	RNAseq validation
Serpine2	GATCCAAGCGAGGACGGG	GACCTGGATCCCTGTGTTGG	RNAseq validation
Cd44	ATCCTCGTCACGTCCAACAC	GCTTTCTGGGGTGCTCTTCT	RNaseq validation
Jchain	GACGACGAAGCGACCATTCT	GCTCTGGGTGGCAGTAACAA	RNAseq validation
Amy2a5	TTCGTTCTGCTGCTTTCCCT	CATTGGGTGGAGAGACCTGC	RNAseq validation
Cd7	ATGCCCAAGACGTACAACAG	CTCCTGCCGGTCTTCAAAGT	RNAseq validation
Art2a-ps	GGCTAACCCAGCAGGTGACT	GGCTTCTGTGGATGTTCCCA	RNAseq validation
Rpl19	GACCAAGGAAGCACGAAAGC	CAGGCCGCTATGTACAGACA	Reference, RNAseq validation
Actb	GACGATGCTCCCCGGGCTGTATTC	TCTCTTGCTCTGGGCCTCGTCACC	Reference, RNAseq validation

Table 4. Sequence of the Primers used for RNAseq validation by qRT-PCR.

significant. All experiments were performed at least 3 times. *In vivo* experiments consisted of groups of 5 mice and were performed at least twice.

Ethics statement. All work involving animals was approved by the Institutional Animal Care and Use Committee (IACUC) at CIC bioGUNE and the competent authority (Diputación de Bizkaia). CIC bioGUNE animal facility is accredited by AAALAC Intl. All experiments were performed in accordance with European and Spanish guidelines and regulations.

Data availability. The transcriptomic data are deposited under GEO accession number GSE98700.

References

1. Kotal, J. *et al*. Modulation of host immunity by tick saliva. *J Proteomics* **128**, 58–68 (2015).
2. Kern, A. *et al*. Tick saliva represses innate immunity and cutaneous inflammation in a murine model of Lyme disease. *Vector Borne Zoonotic Dis* **11**, 1343–1350 (2011).
3. Oliveira, C. J. *et al*. Deconstructing tick saliva: non-protein molecules with potent immunomodulatory properties. *J Biol Chem* **286**, 10960–10969 (2011).
4. Francischetti, I. M., Sa-Nunes, A., Mans, B. J., Santos, I. M. & Ribeiro, J. M. The role of saliva in tick feeding. *Front Biosci (Landmark Ed)* **14**, 2051–2088 (2009).
5. Hovius, J. W., Levi, M. & Fikrig, E. Salivating for knowledge: potential pharmacological agents in tick saliva. *PLoS Med* **5**, e43 (2008).
6. Juncadella, I. & Anguita, J. The Immunosuppresive Tick Salivary Protein, Salp15. *Pathogen-Derived Immunomodulatory Molecules* **666**, 121–131 (2009).
7. Paveglio, S. *et al*. The tick salivary protein, Salp15, inhibits the development of experimental asthma. *Journal of Immunology* **178**, 7064–7071 (2007).
8. Juncadella, I., Garg, R., Ananthnarayanan, S., Yengo, C. & Anguita, J. T-cell signaling pathways inhibited by the tick saliva immunosuppressor, Salp15. *Fems Immunology and Medical Microbiology* **49**, 433–438 (2007).
9. Garg, R. *et al*. Cutting edge: CD4 is the receptor for the tick saliva immunosuppressor, Salp15. *Journal of Immunology* **177**, 6579–6583 (2006).
10. Anguita, J. *et al*. Salp15, an Ixodes scapularis salivary protein, inhibits CD4(+) T cell activation. *Immunity* **16**, 849–859 (2002).
11. Ashish *et al*. Conformational rearrangement within the soluble domains of the CD4 receptor is ligand-specific. *Journal of Biological Chemistry* **283**, 2761–2772 (2008).
12. Motameni, A. *et al*. Delivery of the immunosuppressive antigen salp15 to antigen-presenting cells by Salmonella enterica serovar typhimurium aroA mutants. *Infection and Immunity* **72**, 3638–3642 (2004).
13. Blazar, B. R., Murphy, W. J. & Abedi, M. Advances in graft-versus-host disease biology and therapy. *Nat Rev Immunol* **12**, 443–458 (2012).
14. Mikulska, M. *et al*. Blood stream infections in allogeneic hematopoietic stem cell transplant recipients: reemergence of Gram-negative rods and increasing antibiotic resistance. *Biol Blood Marrow Transplant* **15**, 47–53 (2009).
15. Dykewicz, C. A. *et al*. Summary of the Guidelines for Preventing Opportunistic Infections among Hematopoietic Stem Cell Transplant Recipients. *Clin Infect Dis* **33**, 139–144 (2001).
16. Akhtari, M. *et al*. Therapy-related myeloid neoplasms after autologous hematopoietic stem cell transplantation in lymphoma patients. *Cancer Biol Ther* **14**, 1077–1088 (2013).
17. Friedman, D. L., Leisenring, W., Schwartz, J. L. & Deeg, H. J. Second malignant neoplasms following hematopoietic stem cell transplantation. *Int J Hematol* **79**, 229–234 (2004).
18. Holler, E. *et al*. Inflammatory reactions induced by pretransplant conditioning–an alternative target for modulation of acute GvHD and complications following allogeneic bone marrow transplantation? *Leuk Lymphoma* **25**, 217–224 (1997).
19. Schroeder, M. A. & DiPersio, J. F. Mouse models of graft-versus-host disease: advances and limitations. *Dis Model Mech* **4**, 318–333 (2011).
20. Chu, Y. W. & Gress, R. E. Murine models of chronic graft-versus-host disease: insights and unresolved issues. *Biol Blood Marrow Transplant* **14**, 365–378 (2008).
21. Tschetter, J. R., Mozes, E. & Shearer, G. M. Progression from acute to chronic disease in a murine parent-into-F1 model of graft-versus-host disease. *J Immunol* **165**, 5987–5994 (2000).
22. Juncadella, I. *et al*. The tick saliva immunosuppressor, Salp15, contributes to Th17-induced pathology during Experimental Autoimmune Encephalomyelitis. *Biochemical and Biophysical Research Communications* **402**, 105–109 (2010).
23. Lechner, O. *et al*. Fingerprints of anergic T cells. *Curr Biol* **11**, 587–595 (2001).
24. Kalekar, L. A. *et al*. CD4(+) T cell anergy prevents autoimmunity and generates regulatory T cell precursors. *Nat Immunol* **17**, 304–314 (2016).

25. Chaudhary, B. A. A., Samid, M., Al-Ramadi, B. K. & Elkord, E. Phenotypic alterations, clinical impact and therapeutic potential of regulatory T cells in cancer. *Expert Opin Biol Ther* **14**, 931–945 (2014).
26. Elkord, E., Abd Al Samid, M. & Chaudhary, B. Helios, and not FoxP3, is the marker of activated Tregs expressing GARP/LAP. *Oncotarget* **6**, 20026–20036 (2015).
27. Bruder, D. *et al*. Neuropilin-1: a surface marker of regulatory T cells. *Eur J Immunol* **34**, 623–630 (2004).
28. Zhang, P. *et al*. Eomesodermin promotes the development of type 1 regulatory T (TR1) cells. *Science Immunology* **2** (2017).
29. Whitehill, G. D. *et al*. Adenosine Selectively Depletes Alloreactive T Cells to Prevent GVHD While Conserving Immunity to Viruses and Leukemia. *Mol Ther* **24**, 1655–1664 (2016).
30. Wang, L. *et al*. Graft-versus-host disease is enhanced by selective CD73 blockade in mice. *PLoS One* **8**, e58397 (2013).
31. Ehrentraut, H. *et al*. CD73+ regulatory T cells contribute to adenosine-mediated resolution of acute lung injury. *FASEB J* **27**, 2207–2219 (2013).
32. Ohta, A. & Sitkovsky, M. Role of G-protein-coupled adenosine receptors in downregulation of inflammation and protection from tissue damage. *Nature* **414**, 916–920 (2001).
33. Sitkovsky, M. V. *et al*. Physiological control of immune response and inflammatory tissue damage by hypoxia-inducible factors and adenosine A2A receptors. *Annu Rev Immunol* **22**, 657–682 (2004).
34. Fessler, J., Felber, A., Duftner, C. & Dejaco, C. Therapeutic potential of regulatory T cells in autoimmune disorders. *BioDrugs* **27**, 281–291 (2013).
35. Trzonkowski, P. *et al*. Treatment of graft-versus-host disease with naturally occurring T regulatory cells. *BioDrugs* **27**, 605–614 (2013).
36. Kalekar, L. A. & Mueller, D. L. Relationship between CD4 Regulatory T Cells and Anergy *In Vivo*. *The Journal of Immunology* **198**, 2527–2533 (2017).
37. Rueda, C. M., Jackson, C. M. & Chougnet, C. A. Regulatory T-Cell-Mediated Suppression of Conventional T-Cells and Dendritic Cells by Different cAMP Intracellular Pathways. *Front Immunol* **7**, 216 (2016).
38. Yegutkin, G. G. Nucleotide- and nucleoside-converting ectoenzymes: Important modulators of purinergic signalling cascade. *Biochim Biophys Acta* **1783**, 673–694 (2008).
39. Kobie, J. J. *et al*. T regulatory and primed uncommitted CD4 T cells express CD73, which suppresses effector CD4 T cells by converting 5′-adenosine monophosphate to adenosine. *J Immunol* **177**, 6780–6786 (2006).
40. Gurel, B. *et al*. Nuclear MYC protein overexpression is an early alteration in human prostate carcinogenesis. *Mod Pathol* **21**, 1156–1167 (2008).
41. Trapnell, C., Pachter, L. & Salzberg, S. L. TopHat: discovering splice junctions with RNA-Seq. *Bioinformatics* **25**, 1105–1111 (2009).
42. Love, M. I., Huber, W. & Anders, S. Moderated estimation of fold change and dispersion for RNA-seq data with DESeq. 2. *Genome Biol* **15**, 550 (2014).
43. Yu, G., Wang, L. G., Han, Y. & He, Q. Y. clusterProfiler: an R package for comparing biological themes among gene clusters. *OMICS* **16**, 284–287 (2012).
44. Thomas, P. D. *et al*. PANTHER: a library of protein families and subfamilies indexed by function. *Genome Res* **13**, 2129–2141 (2003).

Acknowledgements

Supported by grants from the Department of Education of the Basque Government (PI2013-49 to JA and PI2012-42 to RB). JA is funded by the European Union (Grant Agreement number 602272). AMA and JLL's work was supported by the Basque Department of Industry, Tourism and Trade (Etortek and Elkartek Programs), the Innovation Technology Department of Bizkaia and the CIBERehd Network. The work of AC is supported by a Ramón y Cajal award, the Basque Department of Industry, Tourism and Trade (Etortek), ISCIII (PI13/00031), FERO VIII Fellowship, the BBVA foundation, MINECO (SAF2016-79381-R) and the European Research Council Starting Grant (336343). CIBERonc was co-funded with FEDER funds. AC-M was funded by a Juan de la Cierva program award and the European Union MSCA program (CIG 660191). RB was funded by MINECO grants BFU2011-25986 and BFU2014-52282-P and the Consolider Program (BFU2014-57703-REDC). FJB was funded by a MINECO grant (CTQ2014-56966-R). D.B. is funded by a MINECO FPI fellowship. We thank the MINECO for the Severo Ochoa Excellence accreditation (SEV-2016-0644).

Author Contributions

Performed the experiments: J.T.C., I.M.M., D.B., M.A.P.I., V.G.J., A.C.M., N.M., A.M., J.M.F., C.S., V.G.C., J.A. Analyzed the data: J.T.C., J.L.L., A.M.A., H.R., J.A. Provided reagents: F.J.B., J.D.S., R.B., A.R., M.L.M.C. Wrote the manuscript: J.T.C., A.C., L.A., H.R., J.A., J.A. designed the study and provided supervision.

Additional Information

Supplementary information accompanies this paper at doi:10.1038/s41598-017-11354-2

Competing Interests: The authors declare that they have no competing interests.

Publisher's note: Springer Nature remains neutral with regard to jurisdictional claims in published maps and institutional affiliations.

LETTER

doi:10.1038/nature22964

mTORC1-dependent AMD1 regulation sustains polyamine metabolism in prostate cancer

Amaia Zabala-Letona[1,2]*, Amaia Arruabarrena-Aristorena[1]*, Natalia Martín-Martín[1,2], Sonia Fernandez-Ruiz[1,2], James D. Sutherland[1], Michelle Clasquin[3], Julen Tomas-Cortazar[1], Jose Jimenez[4], Ines Torres[5], Phong Quang[3], Pilar Ximenez-Embun[6], Ruzica Bago[7], Aitziber Ugalde-Olano[8], Ana Loizaga-Iriarte[9], Isabel Lacasa-Viscasillas[9], Miguel Unda[9], Verónica Torrano[1,2], Diana Cabrera[1], Sebastiaan M. van Liempd[1], Ylenia Cendon[6,10], Elena Castro[6], Stuart Murray[3], Ajinkya Revandkar[11,12], Andrea Alimonti[11,12], Yinan Zhang[13], Amelia Barnett[3], Gina Lein[3], David Pirman[3], Ana R. Cortazar[1], Leire Arreal[1], Ludmila Prudkin[4], Ianire Astobiza[1], Lorea Valcarcel-Jimenez[1], Patricia Zuñiga-García[1], Itziar Fernandez-Dominguez[1], Marco Piva[1], Alfredo Caro-Maldonado[1], Pilar Sánchez-Mosquera[1], Mireia Castillo-Martín[14,15], Violeta Serra[4], Naiara Beraza[1]†, Antonio Gentilella[16,17], George Thomas[16], Mikel Azkargorta[1,18], Felix Elortza[1,18,19], Rosa Farràs[20], David Olmos[6,21], Alejo Efeyan[6], Juan Anguita[1,22], Javier Muñoz[6,18], Juan M. Falcón-Pérez[1,19,22], Rosa Barrio[1], Teresa Macarulla[2,4], Jose M. Mato[1,19], Maria L. Martinez-Chantar[1,19], Carlos Cordon-Cardo[14], Ana M. Aransay[1,19], Kevin Marks[3], José Baselga[23], Josep Tabernero[2,4], Paolo Nuciforo[4], Brendan D. Manning[13], Katya Marjon[3] & Arkaitz Carracedo[1,2,22,24]

Activation of the PTEN–PI3K–mTORC1 pathway consolidates metabolic programs that sustain cancer cell growth and proliferation[1,2]. Here we show that mechanistic target of rapamycin complex 1 (mTORC1) regulates polyamine dynamics, a metabolic route that is essential for oncogenicity. By using integrative metabolomics in a mouse model[3] and human biopsies[4] of prostate cancer, we identify alterations in tumours affecting the production of decarboxylated *S*-adenosylmethionine (dcSAM) and polyamine synthesis. Mechanistically, this metabolic rewiring stems from mTORC1-dependent regulation of *S*-adenosylmethionine decarboxylase 1 (AMD1) stability. This novel molecular regulation is validated in mouse and human cancer specimens. AMD1 is upregulated in human prostate cancer with activated mTORC1. Conversely, samples from a clinical trial with the mTORC1 inhibitor everolimus[5] exhibit a predominant decrease in AMD1 immunoreactivity that is associated with a decrease in proliferation, in line with the requirement of dcSAM production for oncogenicity. These findings provide fundamental information about the complex regulatory landscape controlled by mTORC1 to integrate and translate growth signals into an oncogenic metabolic program.

Alterations in the phosphoinositide 3-kinase (PI3K) pathway have been reported in a high percentage of human cancers[6,7]. We sought to identify metabolic requirements of prostate cancer taking advantage of a faithful genetically engineered mouse model of this disease driven by loss of *Pten*[3], a negative regulator of the PI3K pathway that is frequently downregulated in this tumour type[6,8]. First, we performed high-throughput quadrupole time-of-flight mass spectrometry (q-TOF-MS) to examine metabolic alterations at two time points (3 and 6 months, onset of prostate intraepithelial neoplasia (PIN) and invasive prostate carcinoma, respectively) (Extended Data Fig. 1a, b) in two different prostate lobes (Extended Data Fig. 1c). From 7,722 ions, we assigned metabolite identification (Human Metabolome Database score ≥ 40) to 632 (Supplementary Table 1). We did not observe significant influence of the prostate lobe or the time point of analysis, and after precluding significant alterations in candidate metabolic pathways, we focused on metabolites consistently and significantly altered in all conditions (Extended Data Fig. 1d, e and Supplementary Table 2). We identified 72 unique metabolites (73 assigned ions) fulfilling the criteria (Fig. 1a and Supplementary Table 1). Pathway enrichment analysis in this set did not show significantly altered pathways including a considerable number of metabolites (Supplementary Table 3). Strikingly, representation in waterfall plot revealed an increase in polyamine-synthesis-related metabolites in $Pten^{pc-/-}$ mice (Fig. 1b). These results were validated in this genetically engineered mouse model and human prostate cancer tissues by quantitative liquid chromatography (LC)/MS (Extended Data Fig. 1f, g and Supplementary Table 4).

To determine how metabolic rewiring affects polyamine dynamics, we set up ^{13}C-labelling metabolic analysis to trace the fate of L-methionine-derived carbons *in vivo* (Extended Data Fig. 2a). Next, we injected [U-$^{13}C_5$]L-methionine intravenously in $Pten^{pc+/+}$ and $Pten^{pc-/-}$ mice (Extended Data Fig. 2b). Prostate tissue analysis revealed an elevation in ^{13}C-labelled decarboxylated *S*-adenosylmethionine (dcSAM), together with increased synthesis and fractional labelling of polyamines (Fig. 1c, Extended Data Fig. 2c, d and Supplementary Table 5). Importantly, the increase of SAM decarboxylation (elevated dcSAM/SAM ratio) in both mouse and human pathological tissues strongly suggested that the enzyme that catalyses this reaction (*S*-adenosylmethionine decarboxylase 1, AMD1) is potentially responsible for the metabolic changes observed in prostate cancer (Fig. 1d–f).

To address the contribution of dcSAM production to cell oncogenicity in prostate cancer, we ectopically expressed AMD1 in cell lines from

[1]CIC bioGUNE, Bizkaia Technology Park, 801 Building, 48160 Derio, Spain. [2]CIBERONC, Instituto de Salud Carlos III, C/ Monforte de Lemos 3-5, Pabellón 11, Planta 0, 28029 Madrid, Spain. [3]AGIOS Pharmaceuticals, Cambridge, Massachusetts, 02139, USA. [4]Vall d'Hebron Institute of Oncology (VHIO), Universidad Autónoma de Barcelona, 08035 Barcelona, Spain. [5]Department of Pathology, Valld'Hebron Hospital, Universitat Autónoma de Barcelona, 08035 Barcelona, Spain. [6]Spanish National Cancer Research Centre (CNIO), 28029 Madrid, Spain. [7]MRC Protein Phosphorylation and Ubiquitylation Unit, College of Life Sciences, University of Dundee, Dow Street, Dundee DD1 5EH, UK. [8]Department of Pathology, Basurto University Hospital, 48013 Bilbao, Spain. [9]Department of Urology, Basurto University Hospital, 48013 Bilbao, Spain. [10]School of Medicine, Universidad Autónoma de Madrid, 28049 Madrid, Spain. [11]Institute of Oncology Research (IOR) and Oncology Institute of Southern Switzerland (IOSI), Bellinzona CH 6500, Switzerland. [12]Faculty of Biology and Medicine, University of Lausanne (UNIL), Lausanne CH 1011, Switzerland. [13]Department of Genetics and Complex Diseases, Harvard School of Public Health, Boston, Massachusetts 02115, USA. [14]Department of Pathology, Icahn School of Medicine at Mount Sinai, New York 10029-5674, USA. [15]Department of Pathology, Fundação Champalimaud, 1400-038 Lisboa, Portugal. [16]Laboratory of Metabolism and Cancer, Catalan Institute of Oncology, ICO, Bellvitge Biomedical Research Institute, IDIBELL, 08908 Barcelona, Spain. [17]Department of Biochemistry and Physiology, Faculty of Pharmacy, Universitat de Barcelona, 08028 Barcelona, Catalunya, Spain. [18]Carlos III Networked Proteomics Platform (ProteoRed-ISCIII), Instituto de Salud Carlos III, C/ Monforte de Lemos 3-5, Pabellón 11, Planta 0, 28029 Madrid, Spain. [19]Centro de Investigación Biomédica en Red de Enfermedades Hepáticas y Digestivas (CIBERehd), Instituto de Salud Carlos III, C/ Monforte de Lemos 3-5, Pabellón 11, Planta 0, 28029 Madrid, Spain. [20]Centro de Investigación Príncipe Felipe, Eduardo Primo Yúfera 3, 46012 Valencia, Spain. [21]CNIO-IBIMA Genitourinary Cancer Unit, Medical Oncology Department, Hospitales Universitarios Virgen de la Victoria y Regional de Málaga, 29010 Málaga, Spain. [22]Ikerbasque, Basque foundation for science, 48011 Bilbao, Spain. [23]Human Oncology & Pathogenesis Program, Memorial Sloan-Kettering Cancer Center, New York 10065, USA. [24]Biochemistry and Molecular Biology Department, University of the Basque Country (UPV/EHU), 48940 Bilbao, Spain. †Present address: Gut Health and Food Safety Programme, Institute of Food Research, Norwich Research Park, Norwich NR4 7UA, UK.
*These authors contributed equally to this work.

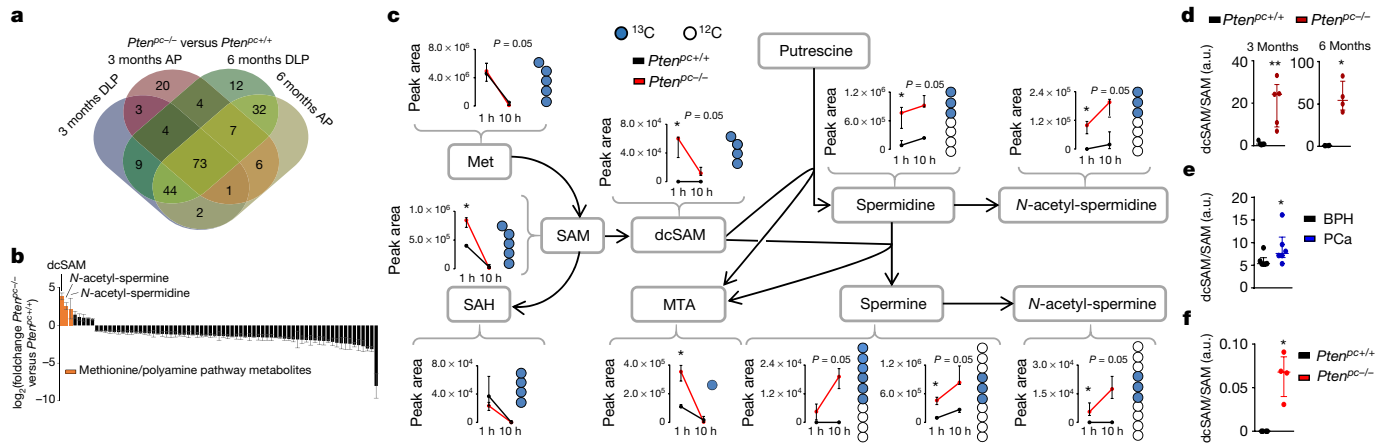

Figure 1 | Integrative metabolomics in prostate cancer reveals a rewiring from methionine metabolism towards polyamine synthesis. **a**, **b**, Venn diagram (anterior prostate (AP) and dorsolateral prostate (DLP)) (**a**) and waterfall plot (**b**) of altered metabolites from q-TOF-MS metabolomic analysis performed in *Pten*$^{pc-/-}$ and *Pten*$^{pc+/+}$ (6 months *Pten*$^{pc+/+}$anterior prostate, $n = 4$ mice; remainder of conditions, $n = 5$ mice) mouse prostate samples at the indicated age. Values in **b** represent the average of the $\log_2$(fold change) with the s.e.m. of the two lobes and two time points (3 and 6 months of age) per metabolite. **c**, Incorporation of carbon-13 (13C) from intravenously injected [U-$^{13}C_5$]L-methionine (100 mg kg^{-1}) into the indicated metabolites at 3 months of age (anterior prostate). Peak area refers to natural abundance-corrected values ($n = 4$ mice at 1 h; $n = 3$ mice at 10 h). Median ± interquartile range. Blue dots: ^{13}C; white dots: ^{12}C; 1 h/10 h: prostate samples extracted after 1-h/10-h pulse with [U-$^{13}C_5$]L-methionine. SAH, *S*-adenosylhomocysteine; Met, methionine. **d**, dcSAM/SAM ratios from Extended Data Fig. 1f ($n = 4$ as indicated by dots); a.u., arbitrary units. **e**, dcSAM/SAM ratio from Extended Data Fig. 1g ($n = 6$ as indicated by dots). BPH, benign prostate hyperplasia; PCa, prostate cancer. **f**, dcSAM/SAM ratio from Fig. 1c at 1 h ($n = 4$ as indicated by dots). *$P < 0.05$; **$P < 0.01$. One-tailed (**c**–**f**) Mann–Whitney *U*-test was used for data analysis.

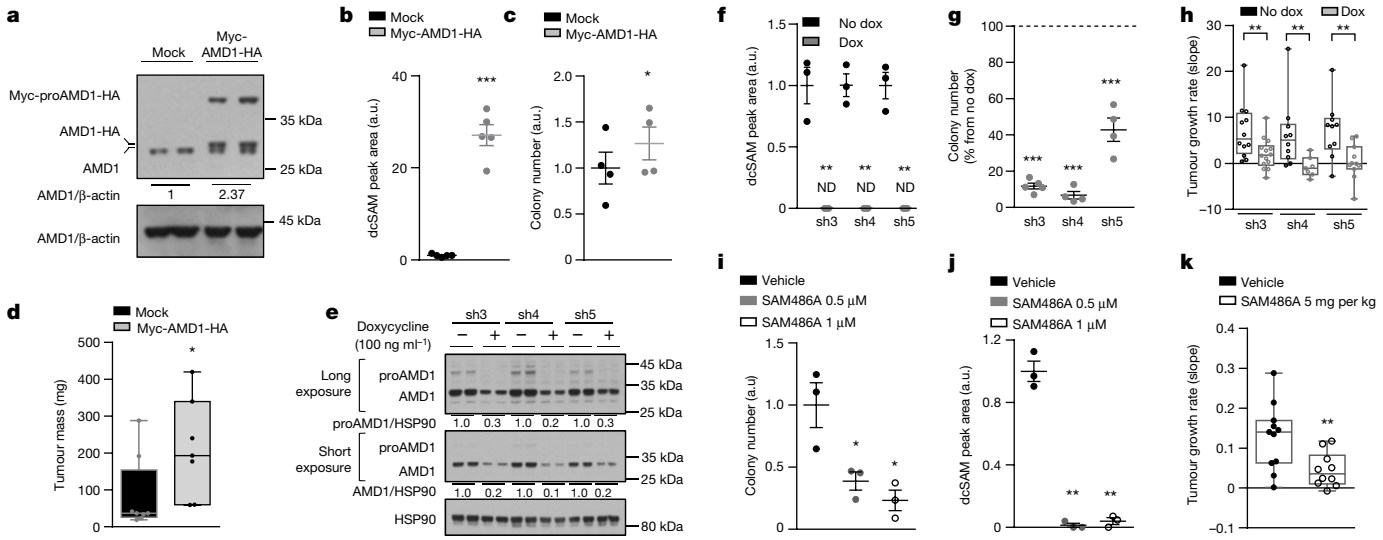

Figure 2 | Genetic and pharmacological AMD1 modulation affects prostate cancer oncogenicity. **a**–**c**, Impact of ectopic Myc-AMD1–HA expression (**a**, representative of three independent experiments) on dcSAM abundance (**b**, $n = 5$ independent experiments) and anchorage-independent growth (**c**, $n = 4$ independent experiments) in DU145 cells *in vitro*. Mock, empty vector. Myc-AMD1–HA, Myc and haemagglutinin (HA)-tagged AMD1 ectopic expression. Mean ± s.e.m. **d**, Impact of ectopic Myc-AMD1–HA expression on tumour mass in DU145 xenografts grown for 43 days (mock, $n = 8$ tumours; Myc-AMD1–HA, $n = 7$ tumours). Box-and-whisker plot. **e**–**g**, Effect of doxycycline (dox)-inducible (100 ng ml^{-1}; a minimum of 72 h) AMD1 silencing (sh3–sh5) on AMD1 protein expression (**e**, representative of three independent experiments), dcSAM abundance (**f**, $n = 3$ independent experiments), and anchorage-independent growth (**g**, $n = 4$ independent experiments) in DU145 cells. Dashed line in **g** indicates relative cell number of non-induced cells. No dox, without doxycycline treatment; Dox, doxycycline-induced (100 ng ml^{-1}) condition; sh, short hairpin RNA. Mean ± s.e.m. **h**, Impact of inducible AMD1 silencing on tumour growth rate of established DU145 xenografts (tumour numbers: sh3 no dox, $n = 12$; sh3 dox, $n = 14$; sh4 no dox, $n = 10$; sh4 dox, $n = 7$; sh5 no dox, $n = 10$; sh5 dox, $n = 11$). Growth rate was inferred from the linear regression calculated for the progressive change in tumour volume of each individual tumour during the period depicted in Extended Data Fig. 3q–s. Box-and-whisker plot. **i**, **j**, Effect of pharmacological AMD1 inhibition with SAM486A on anchorage-independent growth (**i**, $n = 3$ independent experiments) and dcSAM abundance (**j**, $n = 3$ independent experiments) in DU145 cells. Mean ± s.e.m. **k**, Impact of SAM486A treatment for 14 days (5 mg per kg (body weight) per day, 5 days per week) on tumour growth rate of established DU145 xenografts (vehicle, $n = 11$ tumours; SAM4856A, $n = 10$ tumours). Growth rate was inferred from the linear regression calculated for the progressive change in tumour volume of each individual tumour during the period depicted in Extended Data Fig. 4i. Box-and-whisker plot. *$P < 0.05$; **$P < 0.01$; ***$P < 0.001$. One-tailed Student's *t*-test was used for cell line data analysis (**b**, **c**, **f**, **g**, **i**, **j**) and one-tailed Mann–Whitney *U*-test for xenografts (**d**, **h**, **k**).

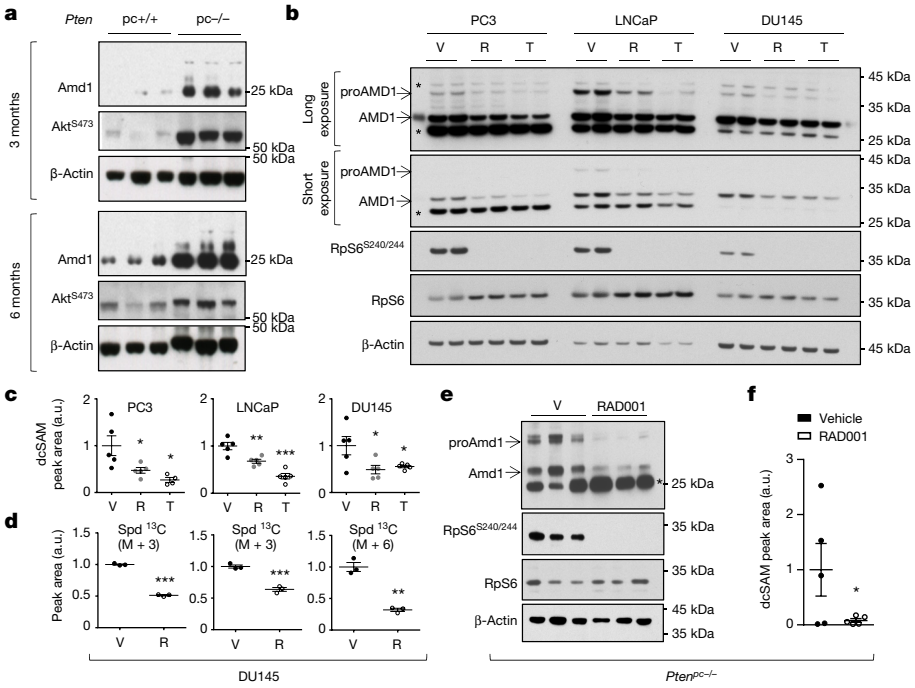

Figure 3 | mTORC1 regulates AMD1 expression, dcSAM production, and polyamine dynamics. a, Amd1 protein abundance in $Pten^{pc-/-}$ and $Pten^{pc+/+}$ prostate tissue from mice of the indicated age ($n = 3$ mice). AKT^{S473} is shown as control of PI3K pathway over-activation. 3 months, 3-month-old mouse prostate analysis; 6 months, 6-month-old prostate analysis. **b**, Representative western blot (out of three) depicting the changes in expression of the indicated proteins upon 24 h treatment of PC3, DU145, and LNCaP cells with vehicle (V, dimethylsulfoxide (DMSO)), rapamycin (R, 20 nM), and Torin-1 (T, 250 nM for PC3 and DU145, 125 nM for LNCaP). **c**, dcSAM abundance in PC3, LNCaP, and DU145 ($n = 4$ or 5 independent experiments as indicated by dots), upon 24 h treatment with vehicle (DMSO), rapamycin (20 nM), and Torin-1 (250 nM for PC3 and DU145, 125 nM for LNCaP). Mean ± s.e.m. **d**, Incorporation of carbon-13 (13C) from [U-$^{13}C_5$]L-methionine (2 h pulse) into the indicated metabolites after 30 h treatment with vehicle (DMSO) or rapamycin (20 nM) in DU145 cells ($n = 3$ independent experiments). $Spd^{13}C$ (M + 3): spermidine labelled in three carbons; $Spm^{13}C$ (M + 3): spermine labelled in three carbons; $Spm^{13}C$ (M + 6): spermine labelled in six carbons. Mean ± s.e.m. **e**, **f**, Effect of 4-week RAD001 treatment on mTORC1 activity ($RpS6^{S240/244}$) and Amd1 protein expression (**e**, $n = 3$ mice), and dcSAM abundance (**f**, $n = 5$ mice), in prostate tissue extracts from $Pten^{pc-/-}$ mice. Data in **f** are mean ± s.e.m. $^*P < 0.05$; $^{**}P < 0.01$; $^{***}P < 0.001$. Asterisks in western blots indicate non-specific bands; arrows indicate specific bands. One-tailed Student's *t*-test (**c**, **d**, **f**) was used.

this tumour type. AMD1 is produced as a pro-enzyme (proAMD1), which is subject to self-cleavage and heterotetramerization, resulting in the active enzyme[9]. After validation of a polyclonal antibody for the detection of proAMD1 and AMD1 (Extended Data Fig. 3a, b), we generated prostate cancer cells over-expressing AMD1, which resulted in increased dcSAM abundance (Fig. 2a, b). Interestingly, this perturbation increased foci formation, anchorage-independent growth, and *in vivo* tumour growth (Fig. 2c, d and Extended Data Fig. 3c–f).

If AMD1 activity is essential for prostate cancer cell function, targeting this enzyme would represent an attractive therapeutic strategy. To test this notion, we generated and validated three AMD1-targeting doxycycline-inducible and two constitutive short hairpin RNAs (shRNAs) (Fig. 2e and Extended Data Fig. 3g–j), which resulted in a profound reduction in dcSAM levels, the inhibition of two-imensional and anchorage-independent growth, and tumour growth *in vivo* (Fig. 2f–h and Extended Data Fig. 3k–t). We excluded doxycycline-dependent (Extended Data Fig. 3u, v) and off-target effects of the shRNA (by ectopic expression of shRNA-resistant wild type and non-processable (S229A[10]) AMD1 mutants) (Extended Data Fig. 4a–c). Of note, we did not observe a contribution of *MTAP*[11–14] or 5′-methylthioadenosine (MTA, a product of dcSAM metabolism to produce polyamines) to the effect of AMD1 inhibition (Extended Data Fig. 4d–f).

A pharmacological inhibitor of AMD1, SAM486A, has been designed and evaluated in pre-clinical and clinical settings[15–18]. Pharmacological AMD1 inhibition recapitulated the biological consequences of genetic silencing, in the absence of overt toxicity *in vivo* (Fig. 2i–k, Extended Data Fig. 4g–k and Supplementary Table 6). Our results collectively demonstrate that AMD1 activity is required for prostate cancer oncogenicity.

We next sought to elucidate the mechanism underlying the production of dcSAM. Interestingly, AMD1 protein levels were increased in prostate tissue from $Pten^{pc-/-}$ mice in the absence of transcriptional modulation, consistent with messenger RNA (mRNA) analysis in human prostate cancer data sets (Fig. 3a and Extended Data Fig. 5a–c). To ascertain whether this phenotype was a direct consequence of the loss of *PTEN*, we analysed *PTEN*-deficient prostate cancer cells (LNCaP). Re-expression of yellow fluorescent protein (YFP)–$PTEN^{WT}$, but not catalytically inactive YFP–$PTEN^{C124S}$, in these cells resulted in the reduction in AMD1 protein levels (Extended Data Fig. 5d)[19]. Further dissection of the PI3K–mTORC1 pathway revealed that only mTORC1 blockers among various signalling inhibitors decreased proAMD1 and AMD1 protein abundance (without consistent effects on mRNA expression; Fig. 3b and Extended Data Fig. 5e–h). The regulation of this enzyme by mTORC1 was validated upon genetic modulation of positive and negative regulators of the complex, RAPTOR and TSC2, respectively (Extended Data Fig. 5e, i, j). Importantly, mTORC1 inhibitor-elicited AMD1 down-regulation was accompanied by a decrease in dcSAM production and polyamine synthesis (Fig. 3c, d). Of interest, spermidine supplementation in rapamycin-treated PC3 cells (*PTEN*-deficient) elicited a significant (albeit small) increase in cell number (Extended Data Fig. 6a).

To ascertain the requirement of mTORC1 activation for dcSAM accumulation *in vivo*, we treated $Pten^{pc-/-}$ mice with the rapamycin-derivative RAD001 and found that Amd1 and dcSAM abundance was reduced in line with the inhibition of mTORC1 in prostate tissue (Fig. 3e, f and Extended Data Fig. 6b, c). Of note, a second genetically engineered mouse model of prostate cancer based on the expression of the *TRAMP* transgene[20], which presented low

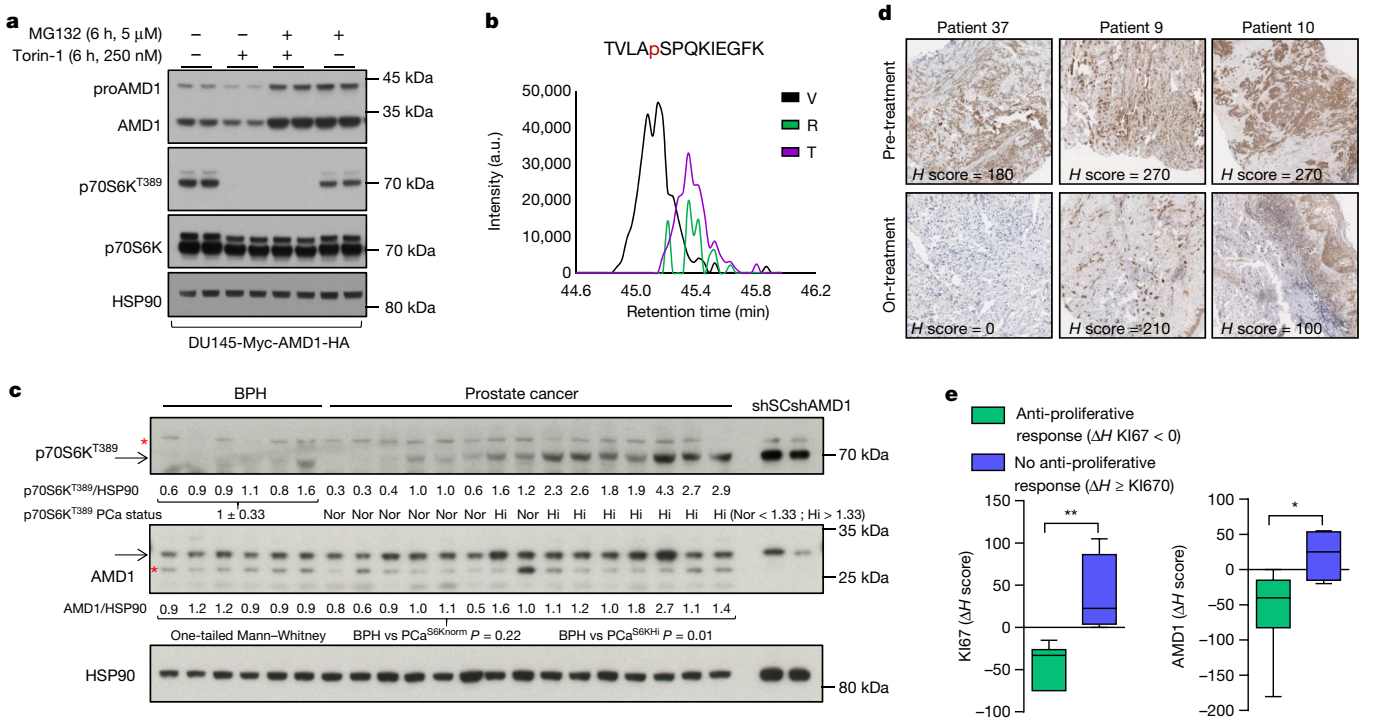

Figure 4 | mTORC1 regulates AMD1 stability and this molecular regulation is recapitulated *in vivo*. **a**, Representative western blot (out of three) of DU145 cells expressing Myc-AMD1–HA treated with vehicle or Torin-1 (250 nM, 6 h) in the presence or absence of MG132 (5 μM, 6 h). **b**, Extracted ion chromatogram of the TVLA**S**PQKIEGFK phosphorylated proAMD1 peptide upon 6 h treatment with vehicle (V, DMSO), rapamycin (R, 20 nM), and Torin-1 (T, 250 nM) in DU145 cells. **c**, Western blot analysis (individual tissue specimens are presented) of AMD1 and p70S6K^{T389} in prostate tissue samples of BPH and prostate cancer. Densitometry values of AMD1 and p70S6K^{T389}are provided below the scans (corrected by HSP90 immunoreactivity). p70S6K^{T389} prostate cancer status was defined as normal (Nor; PCa$^{S6K\ Nor}$) when the densitometry values of the prostate cancer sample were lower than (mean ± s.d.) of the BPH specimens, and high (Hi, PCa$^{S6K\ Hi}$) when greater. The statistical analysis related to differential AMD1 immunoreactivity was done by analysing PCa$^{S6K\ Nor}$ ($n = 7$) and PCa$^{S6K\ Hi}$ ($n = 8$) versus the BPH specimens ($n = 6$) separately. **d**, Representative AMD1 immunoreactivity images of three specimens from patients before (Pre-treatment) or after (On treatment) therapy with everolimus ($n = 14$ specimen pairs). **e**, Box-and-whisker plot of the immunoreactivity of KI67 and AMD1 in cancer patients with (ΔH score for KI67 < 0) or without (ΔH score for KI67 ≥ 0) anti-proliferative tumour response upon treatment with everolimus. *$P < 0.05$; **$P < 0.01$. Arrows indicate specific immunoreactive bands. Red asterisk in western blot indicates non-specific band. Mann–Whitney *U*-test (**c**, **e**).

mTORC1 activation, did not exhibit an increase in Amd1 or dcSAM abundance, in support of our postulated mTORC1–AMD1 regulation (Extended Data Fig. 6d, e and Supplementary Table 7).

Mechanistically, we excluded the contribution of ornithine decarboxylase 1 (ref. 21) (ODC1; Extended Data Fig. 7a–e) and canonical mTORC1 downstream effectors and pathways[1,22,23], including translation initiation, p70S6K, 4EBP, and macro-autophagy (since DU145 cells lack functional ATG5 (ref. 24) but retain the mTORC1-dependent regulation of AMD1) (Extended Data Fig. 7f–i). Interestingly, we found that mTORC1 inhibition-dependent decrease in AMD1 (wild type and S229A) protein levels was rescued by the proteasome inhibitor MG132 (Fig. 4a and Extended Data Fig. 8a, b). To elucidate the molecular link between mTORC1 activity and proAMD1 stability, we performed a phosphoproteomic analysis on ectopic proAMD1/AMD1 and identified a single phosphorylated residue (S298) on the pro-enzyme and enzyme (TVLApSPQKIEGFK) (Extended Data Fig. 8c) that was compatible with a consensus mTORC1 site[25]. Importantly, treatment for 6 h with rapamycin or Torin-1 reduced the phosphorylation of S298 in the pro-enzyme (and the ratio phospho-proAMD1/total proAMD1) but not the enzyme, leading us to hypothesize that S298 phosphorylation could be controlled by mTORC1 and promote proAMD1 stability (Fig. 4b and Extended Data Fig. 8d–f). We evaluated the stability of proAMD1 after treatment for 2 h with Torin-1 (before the detection of any effect on pro-enzyme abundance) and found reduced half-life upon mTORC1 inhibition (Extended Data Fig. 8g–k). To establish the contribution of S298 phosphorylation in the regulation of proAMD1 stability, we inactivated this phosphorylation site (S298A). As predicted, non-phosphorylated proAMD1^{S298A} exhibited decreased half-life, and this parameter was augmented upon inhibition of the proteasome (Extended Data Fig. 9a–c). These results support the notion that mTORC1 activity promotes proAMD1 stability, at least in part, through the regulation of its phosphorylation in S298, hence allowing enzyme processing and activity. *In vitro* mTORC1 kinase assay with glutathione *S*-transferase (GST)–proAMD1^{S229A} did not show significant activity towards proAMD1 phosphorylation in these conditions, suggesting either that mTORC1 does not directly phosphorylate S298, or that additional cellular conditions (for example, biochemical conditions, adaptor or intermediary proteins, subcellular compartments) are required for mTORC1 to phosphorylate proAMD1 (Extended Data Fig. 9d). It is worth noting that our data do not rule out additional mechanisms downstream of mTORC1 regulating proteasome-mediated protein degradation[23,26]. To extend this mechanistic link to human prostate cancer, we extracted protein from well-diagnosed benign prostate hyperplasia (BPH) and prostate cancer specimens[4] (Supplementary Table 4). The results revealed that AMD1 was selectively more abundant in prostate cancer specimens exhibiting high mTORC1 activity, and that the phosphorylation of p70S6K significantly correlated with the levels of AMD1 (correlation coefficient $R = 0.81$; Fig. 4c and Extended Data Fig. 9e).

mTORC1 inhibitors are currently used to treat certain tumours (despite the unpredicted inefficacy in many others)[27], and previous work by us has contributed to defining the pharmaco-dynamic properties of everolimus in individuals with advanced cancers of different

origin[5,28,29]. Strikingly, we observed a predominant decrease (64% of cases) in AMD1 immunoreactivity in 14 biopsies obtained from patients treated with this drug relative to a biopsy of the same lesion before treatment (Fig. 4d, Extended Data Fig. 9f and Supplementary Table 8). When we stratified patients on the basis of the anti-proliferative response achieved after everolimus therapy (responders: differential KI67 H score, $\Delta H < 0$, $n = 6$ specimen pairs; non-responders: differential KI67 H score, $\Delta H \geq 0$, $n = 4$ specimen pairs; where $\Delta H = (H$ score on therapy) – (H score pre-therapy)), we found that only AMD1 (among all targets analysed) presented significantly decreased immunoreactivity in responders (Fig. 4e and Extended Data Fig. 9g).

Polyamine production is a hallmark of highly proliferating cells[30], but their regulation by oncogenic signals remains largely unknown. Our results demonstrate that increased polyamine synthesis is associated with oncogenic signalling in prostate cancer. The regulation of AMD1 production and dcSAM synthesis downstream of mTORC1 described herein provides a mechanistic explanation for the control of this metabolic program (Extended Data Fig. 9h). AMD1 is an unprecedented metabolic target of this protein complex and supports its role in cancer cell proliferation. Importantly, the control of dcSAM and polyamine synthesis is relevant beyond the cancer scenario, and suggests that physiological and developmental processes that require active cell proliferation might be tightly associated with the regulation of AMD1 and polyamine synthesis downstream of mTORC1.

Online Content Methods, along with any additional Extended Data display items and Source Data, are available in the online version of the paper; references unique to these sections appear only in the online paper.

Received 12 September 2016; accepted 4 May 2017.
Published online 28 June 2017.

1. Efeyan, A., Comb, W. C. & Sabatini, D. M. Nutrient-sensing mechanisms and pathways. *Nature* **517,** 302–310 (2015).
2. Ben-Sahra, I. & Manning, B. D. mTORC1 signaling and the metabolic control of cell growth. *Curr. Opin. Cell Biol.* **12,** 72–82 (2017).
3. Chen, Z. *et al.* Crucial role of p53-dependent cellular senescence in suppression of Pten-deficient tumorigenesis. *Nature* **436,** 725–730 (2005).
4. Ugalde-Olano, A. *et al.* Methodological aspects of the molecular and histological study of prostate cancer: focus on PTEN. *Methods* **77-78,** 25–30 (2015).
5. Tabernero, J. *et al.* Dose- and schedule-dependent inhibition of the mammalian target of rapamycin pathway with everolimus: a phase I tumor pharmacodynamic study in patients with advanced solid tumors. *J. Clin. Oncol.* **26,** 1603–1610 (2008).
6. Carracedo, A. & Pandolfi, P. P. The PTEN-PI3K pathway: of feedbacks and cross-talks. *Oncogene* **27,** 5527–5541 (2008).
7. Engelman, J. A., Luo, J. & Cantley, L. C. The evolution of phosphatidylinositol 3-kinases as regulators of growth and metabolism. *Nat. Rev. Genet.* **7,** 606–619 (2006).
8. Song, M. S., Salmena, L. & Pandolfi, P. P. The functions and regulation of the PTEN tumour suppressor. *Nat. Rev. Mol. Cell Biol.* **13,** 283–296 (2012).
9. Pegg, A. E. *S*-Adenosylmethionine decarboxylase. *Essays Biochem.* **46,** 25–45 (2009).
10. Xiong, H. & Pegg, A. E. Mechanistic studies of the processing of human *S*-adenosylmethionine decarboxylase proenzyme. Isolation of an ester intermediate. *J. Biol. Chem.* **274,** 35059–35066 (1999).
11. Kryukov, G. V. *et al.* MTAP deletion confers enhanced dependency on the PRMT5 arginine methyltransferase in cancer cells. *Science* **351,** 1214–1218 (2016).
12. Marjon, K. *et al.* MTAP deletions in cancer create vulnerability to targeting of the MAT2A/PRMT5/RIOK1 axis. *Cell Reports* **15,** 574–587 (2016).
13. Mavrakis, K. J. *et al.* Disordered methionine metabolism in MTAP/CDKN2A-deleted cancers leads to dependence on PRMT5. *Science* **351,** 1208–1213 (2016).
14. Shlomi, T., Fan, J., Tang, B., Kruger, W. D. & Rabinowitz, J. D. Quantitation of cellular metabolic fluxes of methionine. *Anal. Chem.* **86,** 1583–1591 (2014).
15. Eskens, F. A. *et al.*; European Organization for Research and Treatment of Cancer Early Clinical Studies Group. Phase I and pharmacological study of weekly administration of the polyamine synthesis inhibitor SAM 486A (CGP 48 664) in patients with solid tumors. *Clin. Cancer Res.* **6,** 1736–1743 (2000).
16. Paridaens, R. *et al.* A phase I study of a new polyamine biosynthesis inhibitor, SAM486A, in cancer patients with solid tumours. *Br. J. Cancer* **83,** 594–601 (2000).
17. Regenass, U. *et al.* CGP 48664, a new *S*-adenosylmethionine decarboxylase inhibitor with broad spectrum antiproliferative and antitumor activity. *Cancer Res.* **54,** 3210–3217 (1994).
18. Siu, L. L. *et al.* A phase I and pharmacokinetic study of SAM486A, a novel polyamine biosynthesis inhibitor, administered on a daily-times-five every-three-week schedule in patients with advanced solid malignancies. *Clin. Cancer Res.* **8,** 2157–2166 (2002).
19. Serra, H. *et al.* PTEN mediates Notch-dependent stalk cell arrest in angiogenesis. *Nat. Commun.* **6,** 7935 (2015).
20. Greenberg, N. M. *et al.* Prostate cancer in a transgenic mouse. *Proc. Natl Acad. Sci. USA* **92,** 3439–3443 (1995).
21. Origanti, S. *et al.* Ornithine decarboxylase mRNA is stabilized in an mTORC1-dependent manner in Ras-transformed cells. *Biochem. J.* **442,** 199–207 (2012).
22. Bale, S. & Ealick, S. E. Structural biology of *S*-adenosylmethionine decarboxylase. *Amino Acids* **38,** 451–460 (2010).
23. Zhang, Y. *et al.* Coordinated regulation of protein synthesis and degradation by mTORC1. *Nature* **513,** 440–443 (2014).
24. Ouyang, D. Y. *et al.* Autophagy is differentially induced in prostate cancer LNCaP, DU145 and PC-3 cells via distinct splicing profiles of ATG5. *Autophagy* **9,** 20–32 (2013).
25. Hsu, P. P. *et al.* The mTOR-regulated phosphoproteome reveals a mechanism of mTORC1-mediated inhibition of growth factor signaling. *Science* **332,** 1317–1322 (2011).
26. Zhao, J., Zhai, B., Gygi, S. P. & Goldberg, A. L. mTOR inhibition activates overall protein degradation by the ubiquitin proteasome system as well as by autophagy. *Proc. Natl Acad. Sci. USA* **112,** 15790–15797 (2015).
27. Huang, Z. *et al.* Clinical efficacy of mTOR inhibitors in solid tumors: a systematic review. *Future Oncol.* **11,** 1687–1699 (2015).
28. O'Reilly, K. E. *et al.* mTOR inhibition induces upstream receptor tyrosine kinase signaling and activates Akt. *Cancer Res.* **66,** 1500–1508 (2006).
29. Carracedo, A. *et al.* Inhibition of mTORC1 leads to MAPK pathway activation through a PI3K-dependent feedback loop in human cancer. *J. Clin. Invest.* **118,** 3065–3074 (2008).
30. Gerner, E. W. & Meyskens, F. L., Jr. Polyamines and cancer: old molecules, new understanding. *Nat. Rev. Cancer* **4,** 781–792 (2004).

Supplementary Information is available in the online version of the paper.

Acknowledgements We thank N. Sonenberg for providing 4EBP1- and 4EBP2-targeting shRNAs, D. Alessi for discussions and technical advice, A.M. Cuervo and E. Arias-Perez for technical advice, the Basque biobank for research (BIOEF) for critical support with human specimens and Novartis for providing SAM486A. Funding: Ramón y Cajal award (to A.C., A.E., J.M., D.O.), Juan de la Cierva (to E.C., A.C.-M.), BFU grant (to R.B.: BFU2014-52282-P and BFU2011-25986), SAF grant (to A.C.: SAF2016-79381-R, FEDER/EU; M.L.M.-C.: SAF2014-54658-R; to J.M.F.-P.: SAF2015-66312; to J.M.M: SAF 2014-52097R; to A.E.: SAF2015-67538-R; to J.A.: SAF2015-65327R; to G.T.: SAF2011-24967) from the Spanish Ministry of Economy, Industry and Competitiveness (MINECO); European Union (to A.C.: ERC-StG-336343, PoC754627; to A.C.-M.: CIG 660191; to J.A.: 602272; to A.E.: ERC-2014-STG-638891); Basque Government Department of Health (to V.T.: 2016111109; to J.M.F.-P: 2015111149), Department of Education (to A.C.: PI2012/03 and IKERTALDE I.T.1106-16; to R.B.: PI2012/42; to M.L.M.-C.: 2013) and PhD grants (to A.A.-A. and L.V.-J.); AECC (to V.T.: 2016 JP Bizkaia; to N.M.-M.: 2011 JP Bizkaia; to M.L.M.-C.); ISCIII (to A.C.: PI10/01484, PI13/00031; to J.M.: Proteored PR.B.2 and grant PT13/0001; to R.F.: PI15/209; to V.S.: PI13/01714, CP14/00228); Ramón Areces foundation (to J.M.F.-P.); Basque Department of Industry, Tourism and Trade (Etortek) (to A.C.); FERO Foundation (to A.C., V.S.); Fundación Vasca de Innovación e Investigación Sanitarias, BIOEF (to V.T.: BIO15/CA/052); BBVA Foundation (to A.C.; P.N. team); National Institutes of Health (to C.C.-C. and M.C.: P01CA087497; to J.M.M.: R01AT001576); Fundación CRIS contra el Cáncer (to D.O. team); 2014 Stewart Rahr Young Investigator Award from the Prostate Cancer Foundation (to D.O.); FPU predoctoral fellowship (to Y.C.: 15/05126); Catalan Agency AGAUR (to V.S.: 2014 SGR 1331); Medical Research Council (to R. Bago, D. Alessi laboratory: grant number MC_UU_12016/2). The activity of CIBERONC was co-funded with FEDER funds.

Author Contributions *In vitro* studies: A.Z.-L. and A.A.-A. with support from N.M.-M., S.F.-R., and L.A. *In vivo* studies: A.Z.-L., A.A.-A. and N.M.-M. with support for tail vein from N.B. Genotyping: P.S.-M. Metabolomics analysis: M.Clas., P.Q., S.M., A.B., G.L., and D.P., K. Marks and K. Marjon at AGIOS and D.C., S.M.V.L., and J.M.F.-P. at CIC bioGUNE. Everolimus trial samples and staining: V.S., J.J., L.P., P.N., I.T., J.T., T.M., and J.B. Human prostate specimens: A.U.-O., A.L.-I., I.L.-V., and M.U. Histochemical analysis in mice: S.F.-R., A. Rev., and A. Alim. Generation of molecular AMD1 tools: J.D.S. and R.B. Immune cell analysis and GST–AMD1 purification: J.T.-C., I.F.-D., and J.A. Phosphoproteomics: P.X.-E., A.E., and J.M. Kinase assay: R. Bago. TRAMP mice material: statistical supervision and bioinformatics, A.R.-C.; polysome profiling, A.G. and G.T. Genetically engineered mouse model pathology: M.C.-M. and C.C.-C. Technical support and discussions: B.D.M., J.M.M., M.L.M.-C., M.A., F.E., I.A., A.M.A., V.T., L.V.-J., P.Z.-G., M.P., A.C.-M., R.F., and Y.Z. K. Marjon directed the metabolomics strategy, analysed the results, and contributed to discussions and manuscript preparation and revision. A.C. directed the project, supervised data analysis, and wrote the manuscript.

Author Information Reprints and permissions information is available at www.nature.com/reprints. The authors declare no competing financial interests. Readers are welcome to comment on the online version of the paper. Publisher's note: Springer Nature remains neutral with regard to jurisdictional claims in published maps and institutional affiliations. Correspondence and requests for materials should be addressed to A.C. (acarracedo@cicbiogune.es).

METHODS

Patient samples. All prostate specimens were obtained upon informed consent and with evaluation and approval from the corresponding ethics committee (Comité de Ética en Investigación Clínica (CEIC) codes OHEUN11-12 and OHEUN14-14)[4]. Clinico-pathological information is included as Supplementary Table 4. The details of the clinical trial with everolimus are described in ref. 5 and in Supplementary Table 8.

Animals. All mouse experiments were performed following the ethical guidelines established by the Biosafety and Animal Welfare Committee at CIC bioGUNE, Derio, Spain (under protocol P-CBG-CBBA-0715). The procedures used followed the recommendations from the Association for Assessment and Accreditation of Laboratory Animal Care International (AAALAC). Xenograft experiments were performed as previously described (maximum total tumour volume per mouse 1.5 cm^3)[31], injecting 4×10^6 (AMD1 silencing) or 4×10^6 (AMD1 ectopic expression) cells with Matrigel (BD Biosciences) per condition in two flanks per mouse. Doxycycline was administered *in vivo* in the food pellets (Research diets, D12100402). Genetically engineered mouse model experiments were performed in a mixed background as reported[32]. The *Pten*^{lox} conditional knockout allele has been described elsewhere[3]. Prostate epithelium-specific deletion was effected by the Pb-Cre4 (ref. 3). Mice were fasted for 6 h before tissue harvest (9:00–15:00) to prevent metabolic alterations due to immediate food intake. The TRAMP mice strain was originally obtained from The Jackson Laboratory repository. Animals were maintained at the Animal Facility (awarded with AAALAC accreditation) of the Spanish National Cancer Research Centre (CNIO) in accordance with the guidelines stated in the International Guiding Principles for Biomedical Research Involving Animals, developed by the Council for International Organizations of Medical Sciences. All animal experiments were approved by the Competent Authority of the Comunidad de Madrid. The generation and characterization of TRAMP mice have been previously described[20]. At CNIO, TRAMP mice originally provided in FVB/NJ genetic background were backcrossed to a C57BL/6 background by successive mating of (T/+) male-mice to (+/+) C57BL/6 female-mice and then maintained in a C57BL/6 background.

To address the potential undesirable effects of systemic AMD1 inhibition, we administered SAM486A intraperitoneally (5 mg per kg (body weight) per day, 5 days per week) for 17 days in immunocompetent C57BL/6 mice. We measured body and organ weight, blood biochemistry, haematocrit, and white blood cell count (information provided in Supplementary Table 6). Terminal blood harvest was performed intracardially after CO_2inhalation-based euthanasia. For non-terminal harvest, a facial vein blood sample was obtained by puncture with a sterile 4 mm lancet (MEDIpoint, USA). For plasma preparation, blood was deposited in tubes with dipotassium EDTA (Microtainer, Becton Dickinson, Franklin, New Jersey, USA) (for haematocrit and FACS analysis) or heparinized tubes (10 µl, 1 U µl^{-1}) (for plasma metabolomics). For haematocrit analysis, blood samples were analysed using an Abacus Junior Vet analyser (Diatron, Hungary) according to the manufacturer's guidelines. For blood biochemistry, a Selectra Junior Spinlab 100 analyser (Vital Scientific, Dieren, The Netherlands) was used. A calibrated control was run before each use and was within established ranges before analysing samples. For white blood cell analysis, the spleen of SAM486A or saline-treated mice was grinded by using a syringe plunger and passing the cells through a 70 µm cell strainer; cellular composition was evaluated by flow cytometry, using the following antibodies: CD4, CD8, B220, Ly6C, F4/80, GR-1, CD25, CD11b, CD44, CD73, FR4, Nrp-1 (Miltenyi Biotec).

Purification and activation of mouse splenic CD4$^+$ T cells. To address the toxicity of SAM486A, we purified CD4 T cells from the spleen of C57BL/6 mice by negative selection using a CD4 purification kit following the manufacturer's instructions (Miltenyi Biotec, Auburn, California, USA). Five hundred thousand CD4 T cells were activated in TexMACS Medium (Miltenyi Biotec) with plate-bound anti-CD3 (5 µg ml^{-1}) and soluble anti-CD28 (1 µg ml^{-1}) in the presence of vehicle or SAM486A (1 µM) for 16 and 96 h and assessed for interleukin(IL)-2 production by capture enzyme-linked immunosorbent assay (ELISA) (R&D Systems, MAB702). To analyse the effect of SAM486A on T-cell proliferation, purified CD4 T cells were recovered 4 days after activation and treatment and counted in a haemocytometer chamber.

Immunization with ovalbumin. To address the effect of SAM486A on immune cell proliferation *in vivo*, we administered SAM486A intraperitoneally (5 mg per kg (body weight) per day, 5 days per week) for 17 days in immunocompetent C57BL/6 mice, and then immunized them subcutaneously with 50 µg ovalbumin in complete Freund's adjuvant and kept on treatment. After 2 weeks, the mice were analysed for ovalbumin-specific serum immunoglobulin-G(IgG) andimmunoglobulin-M(IgM) levels by ELISA[33].

Reagents. Cell lines were purchased from Leibniz-Institut Deutsche Sammlung von Mikroorganismen und Zellkulturen (DSMZ) and tested negative for mycoplasma. An authentication certificate was provided by DSMZ for cell lines. Rapamycin (prepared in DMSO, final concentration 20 nM), Torin-1 (prepared in DMSO, final concentration 125–250 nM), dimethylfluoromithine (DFMO, prepared in water, final concentration 50 µM), PF-4708671 (PF47, prepared in DMSO, final concentration 10 µM), hydroxychloroquine (HCQ, prepared in water, final concentration 30 ng ml^{-1}), MG132 (5 µM, prepared in DMSO), PD0325901 (100 nM, prepared in DMSO), SB203580 (5 µM, prepared in DMSO), SP600125 (10 µM, prepared in DMSO), spermidine (0.5–1 µM, prepared in water), 5′-deoxy-5′-(methylthio)adenosine (MTA, final concentration 25 µM), and cycloheximide (CHX, prepared in ethanol, final concentration 5 µg ml^{-1}) were purchased from LC Laboratories (rapamycin, PD0325901), Sigma (CHX, PF47, HCQ, spermidine, MTA), Calbiochem (SB203580), and Tocris (Torin-1, DFMO, SP600125). RAD001 was purchased from Selleckchem and administered 6 days per week by oral gavage (prepared in 1.5% NMP/98.5% PEG) at 10 mg per kg (body weight). SAM486A was provided by Novartis and prepared in water (*in vitro*) or saline solution (*in vivo*, 5 mg per kg (body weight) per day intraperitoneally Monday–Friday). [U-$^{13}C_5$] L-methionine was purchased from Cambridge Isotope Laboratories and administered intravenously at a final concentration of 100 mg kg^{-1}*in vivo* and at 30 µg ml^{-1}*in vitro* (with dialysed FBS). Doxycycline was purchased from Sigma and used at 500 ng ml^{-1} for overexpression of *YFP–PTEN*, 100 ng ml^{-1} for silencing of *AMD1*, and 250 ng ml^{-1} for silencing of *RAPTOR* and *TSC2*. shRNAs against AMD1 were purchased from Sigma (TRCN0000078462: sh3; TRCN0000078460: sh4, TRCN0000078461: sh5) and the control shRNA sequence included (CCGGC AACAAGATGAAGAGCACCAACTCGAGTTGGTGCTCTTCATCTTGTTG)[34]. shRNAs against *4EBP1* and *4EBP2* were provided by N. Sonenberg[35]. Sub-cloning of shRNA AMD1 into pLKO-Tet-On vector was done by introducing AgeI and EcoRI in the 5′ end of top and bottom shRNA oligonucleotides respectively (TET-pLKO puro was a gift from D. Wiederschain[36], Addgene plasmid 21915). *Myc-AMD1–HA*-expressing vector was generated starting from the open reading frame obtained from PlasmID Harvard (https://plasmid.med.harvard.edu/PLASMID/Home.xhtml) and cloned into a modified retroviral pLNCX vector harbouring BglII–SalI sites (cloned with BamHI–SalI). RNA interference (RNAi)-resistant versions of AMD1 were generated using overlap extension PCR and cloned into a lentiviral backbone derived from vector pLenti-Cas9-blast (Cas9 removed; lentiCas9-Blast was a gift from F. Zhang, Addgene 52962; ref. 37) using a HiFi Assembly Kit (NEB). The resulting vectors expressed *AMD1–HA-2A-blast* (wild type or S229A) with the *AMD1–HA* portion being excisable using BshT1–BamH1. The target of AMD1 shRNA3 (5′-gtctccaagagacgtttcatt-3′) was changed to an RNAi-resistant version (5′-gtGAGcaaACGTAGAttTatCtt-3′). Cloning details are available upon request. All clones were sequence-validated. Site-directed mutagenesis for generation of *AMD1*^{S229A} and *AMD1*^{S298A} was performed using an Agilent QuikChange II Site-Directed Mutagenesis Kit. *YFP–PTEN*-expressing lentiviral constructs were described in ref. 19.

Cellular and molecular assays. Cell number quantification was done with crystal violet[29]. Doxycycline-mediated inducible shRNA expression was performed by treating cell cultures for 72–96 h with the antibiotic (100–250 ng ml^{-1}) and then seeding for cellular or molecular assays in the presence of doxycycline. Western blot was performed as previously described[38] and run in Nupage gradient precast gels (Life Technologies) in MOPS or MES buffer (depending on the proteins analysed; note that the migration pattern of molecular mass markers varies in these two buffers). Anti-AMD1 was from Proteintech (11052-1-AP). Anti-RpS6$^{S240/244}$, anti-RpS6, anti-p70S6K^{T389}, anti-p70S6K, anti-LC3B, anti-HSP90, anti-PTEN, anti-AKT^{S473}, anti-AKT, anti-4EBP1, and anti-RAPTOR antibodies were from Cell Signalling Technologies. Anti-β-actin antibody was from Sigma and anti-TSC2 from Thermo Scientific (MA5-15004). Densitometry-based quantification was performed using ImageJ software. For half-life assays, DU145 cells stably expressing the indicated constructs were challenged with CHX (5 µg ml^{-1}) and protein was extracted at the indicated time points (cells were treated with vehicle (DMSO), MG132 (5 µM), or Torin-1 (250 nM) 120 min before CHX challenges when indicated). Anchorage-independent growth assays were performed as previously described[39], seeding 3000 (PC3) or 5000 (DU145) cells per well. RNA was extracted using a NucleoSpin RNA isolation kit from Macherey-Nagel (740955.240C). One microgram of total RNA was used for complementary DNA (cDNA) synthesis using qScript cDNA Supermix from Quanta (95048). Quantitative PCR (qPCR) was performed as previously described[38]. Applied Biosystems TaqMan probes were as follows: *Amd1*/*AMD1* (Mm04207265, Hs00750876s1), *β-ACTIN*/*β-Actin* (Hs99999903_m1/Mm00607939_s1), and *GAPDH*/*Gapdh* (Hs02758991_g1/Mm99999915_g1). Universal Probe Library (UPL, Roche) probes were as follows: *AMD1* (probe 72, primer F: CAGACCTCCTATGATGACCTGA; primer R: TCAGGTCACGAATTCCACTCT), *Odc1* (probe 80, primer F: GCTAAGTCG ACCTTGTGAGGA; primer R: AGCTGCTCATGGTTCTCGAT), *ODC1* (probe 34, primer F: AAAACATGGGCGCTTACACT; primer R: TGGAATTGC TGCATGAGTTG), and *Mtap* (probe 12, primer F: CCATGGCAACCGACT ATGAT; primer R: AAACCCCATCCACTGACACT). Foci assays were performed seeding 500 cells per well (six-well plate) and staining and counting them by crystal

violet after 10 days. Lentiviral and retroviral transductions were performed as previously described[34,38].

Kinase assay. Human AMD1 variants (carboxy-terminal HA tag, non-processing mutant S229A; S298 (wild type) or S298A; details available upon request) were prepared by overlapping PCR and cloned as BamH1–Not1 into pGEX-6P-1 (GE Healthcare). Sequence-confirmed clones were induced with 1 mM IPTG (isopropyl-β-D-thiogalactoside) for 16 h at 20 °C in C41 (DE3) pLysS (Lucigen). GST fusion proteins were purified first by glutathione affinity chromatography (eluted in 40 mM reduced glutathione; 25 mM HEPES pH 8; 50 mM KCl; 0.1% BME buffer) and then separated by gel filtration chromatography. Proteins were concentrated by ultrafiltration (Vivaspin 5K MWCO cut-off; Sartorius) and used for kinase assays.

Endogenous mTORC1 complex was immunoprecipitated from HEK293 cells using anti-Raptor antibody (S682B, fourth bleed, https://mrcppureagents.dundee.ac.uk/) coupled to Protein G Sepharose beads (Amersham). The cells were stimulated with IGF (50 ng ml^{-1}) for 20 min before lysis in mTORC1 lysis buffer (40 mM HEPES pH 7.4, 120 mMNaCl, 1 mM EDTA, 0.3% (w/v), CHAPS, 10 mM Na-pyrophosphate, 10 mM Na-glycerophosphate, 1 mM Na-orthovanadate, protease inhibitor cocktail (Roche)). The immunoprecipitate was washed twice with mTORC1 lysis buffer, containing 0.5 M NaCl, twice with mTORC1 lysis buffer, and twice with mTORC1 kinase assay buffer (25 mM HEPES pH 7.4, 50 mMKCl). The substrates were added to immunoprecipitate in kinase assay buffer (15 μl) before adding the 10 μl of the ATP mixture (10 mM $MnCl_2$, 100 μM ATP, 1 μCi [γ-^{32}P]ATP in kinase buffer). The reaction was performed in a thermomixer at 30 °C for 30 min and was terminated by adding the 4× sample buffer (NuPAGE LDS sample buffer, Life Technologies). The reaction mixture was loaded on gel. Dried gel was exposed to X-ray films (Amersham). One microlitre of reaction mixture was loaded on gel for immunoblot analysis. GST–S6K^{D236A} (DU32609, https://mrcppureagents.dundee.ac.uk/) was purified from HEK293 cells pre-treated with 0.1 μM AZD-8055. The protein was purified using GST–Sepharose beads (Amersham) according to the manufacturer's instructions. Anti-Raptor (S682B, fourth bleed, https://mrcppureagents.dundee.ac.uk/), anti-phospho-S6K1 T389 (9205, Cell Signaling Technology), anti-GST (S902A, third bleed, https://mrcppureagents.dundee.ac.uk/).

Immunohistochemical analysis. Histochemical analysis by haematoxylin and eosin, anti-RpS6$^{S235/6}$, anti-Akt^{S473} (Cell Signaling Technology), and Pten (51-2400) immunostaining was performed as previously described[40,41]. Immunohistochemical analysis of AMD1 (Proteintech, dilution 1/100) was performed using DAKO EnVision FLEX High pH (DAKO). The scoring system was based on the quantification of the percentage of cells' negative, low (1+), medium (2+), or high (3+) immunoreactivity. Subsequently, the *H* score was calculated as follows: $H = (\text{percentage of cells } 1+) + (2 \times (\text{percentage of cells } 2+)] + [3 \times (\text{percentage of cells } 3+))$. Differential *H* score was calculated as $\Delta H = H_{\text{on treatment}} - H_{\text{pre-treatment}}$.

Metabolomic analysis. For *in vitro* metabolomic analysis, growing cells were washed with ammonium carbonate pH 7.4 and snap-frozen in liquid nitrogen. Metabolites were extracted from cells or tissues with cold 80/20 (v/v) methanol/water. Samples were then dried and stored at −80 °C until MS analysis. High-throughput time-of-flight analysis was conducted using flow injection analysis as previously described[42]. In short, samples were re-suspended and injected on an Agilent 1100 coupled with an Agilent 6520 QToF mass spectrometer with an electrospray ionization source. The mobile phase consisted of 60/40 methanol/water with 0.1% formic acid and was used to deliver 2 μl of each sample to the MS, flowing at 150 μl min^{-1}. Data were collected in positive mode with 4 GHz HiRes resolving power with internal lock masses. Data processing was conducted with Matlab R2010b. Relative cell number or protein amount was used for normalization.

Quantitative LC/MS was conducted as previously described[43]. A ThermoAccela 1250 pump delivered a gradient of 0.025% heptafluorobutyric acid, 0.1% formic acid in water and acetonitrile at 400 μl min^{-1}. The stationary phase was an Atlantis T3, 3 μm, 2.1 mm × 150 mm column. A QExactive mass spectrometer was used at 70,000 resolving power to acquire data in full-scan mode. Data analysis was conducted in MAVEN[44] and Spotfire. Peak areas derived from stable isotope labelling experiments were corrected for naturally occurring isotope abundance.

For plasma [^{13}C]methionine analysis, blood samples from mice were extracted at the indicated times, transferred at room temperature to heparinized collection tubes, and centrifuged at 13,000 r.p.m. and 4 °C for 10 min. Plasma was transferred to fresh tubes and processed for ultra-high-performance LC coupled to mass spectrometry (UPLC–MS) analysis. Briefly, to 40 μl aliquots of mouse plasma, 40 μl of water/0.15% formic acid was added. Subsequently, proteins were precipitated by addition of 120 μl of acetonitrile. To optimize extraction, after addition of acetonitrile, the samples were sonicated for 10 min at 4 °C and agitated at 1,400 r.p.m. for 30 min at 4 °C. Next, the samples were centrifuged at 14,000 r.p.m. for 30 min at 4 °C. The supernatant was transferred to a fresh vial and measured with a UPLC system (Acquity, Waters, Manchester, UK) coupled to a time-of-flight mass spectrometer (SYNAPT G2, Waters). A 2.1 mm × 100 mm, 1.7 μm BEH AMIDE column (Waters), thermostated at 40 °C was used for the assay. Solvent A (aqueous phase) consisted of 99.5% water, 0.5% formic acid, and 20 mM ammonium formate, while solvent B (organic phase) consisted of 29.5% water, 70% MeCN, 0.5% formic acid, and 1 mM ammonium formate. To obtain a good separation of the analytes, the following gradient was used: from 5% A to 50% A in 2.4 min in curved gradient (number 8, as defined by Waters), from 50% A to 99.9% A in 0.2 min constant at 99.9% A for 1.2 min, back to 5% A in 0.2 min. The flow rate was 0.250 ml min^{-1} and the injection volume was 2 μl. All samples were injected randomly and analytes were measured in enhanced duty cycle mode, optimized for the mass of the analyte in question. Methionine and [$^{13}C_5$]L-methionine were measured in scan function 1 (enhanced duty cycle at 152), SAH and $^{13}C_4$-SAH were measured in scan function 2 (enhanced duty cycle at 387), and SAM and $^{13}C_5$-SAM were measured in scan function 3 (enhanced duty cycle at 402). Extracted ion traces were obtained for methionine ($m/z = 150.0589$), [$^{13}C_5$]L-methionine ($m/z = 155.0756$), SAH ($m/z = 385.1294$), [$^{13}C_4$]SAH ($m/z = 389.1428$), SAM ($m/z = 399.145$), and [$^{13}C_5$]SAM ($m/z = 404.1618$) in a 20 mDa window and subsequently smoothed (two points, two iterations) and integrated with QuanLynx software (Waters). For quantitation, stock solutions of 10 mM in water for each of the analytes were prepared. Stock solutions were pooled and diluted to obtain a mixture including all analytes. The mixture was further diluted in water to obtain the concentrations as used in the calibration curve. The calibration range for all analytes included the following concentrations: 100, 50, 25, 10, 5, 2.5, 1, 0.5, 0.25, 0.1, 0.05, and 0.025 μM.

Targeted metabolomics. Levels of dcSAM in cell cultures and tissues were analysed by UPLC–MS. Briefly, extraction and homogenization were done in methanol/acetic acid (80/20% v/v). Speed-vacuum-dried metabolites were solubilized in 100 μl of a mixture of water/acetonitrile (40/60% v/v) and injected onto the UPLC–MS system (Acquity and SYNAPT G2, Waters). The extracted ion traces were obtained for dcSAM (retention time = 3.0minutes, m/z 355.16). Corrected signals were normalized to relative cell number.

Polysome profiling. Distribution of mRNAs across sucrose gradients was performed as described earlier[45], except for minor modifications.

Phosphoproteomic analysis of AMD1. DU145 cells stably expressing Myc-AMD1–HA were plated in two or three 150 mm plates per condition to ensure a final density no higher than 50–60% and sufficient protein amounts to immunoprecipitate ectopic AMD1 (using agarose HA-beads, Sigma, according to the manufacturer's instructions). Cells were treated for 6 h with rapamycin (20 nM) and Torin-1 (250 nM) before immunoprecipitation. Protein eluates from the immunoprecipitated samples were separated by SDS–PAGE. The bands corresponding to AMD1 and the pro-enzyme were visualized using Sypro-Ruby (Invitrogen), excised, and in-gel digested with trypsin. The resulting peptides were analysed by LC–MS/MS using an LTQ Orbitrap Velos mass spectrometer (Thermo Scientific). Raw files were searched against a Uniprot *Homo sapiens* database (20,187 sequences) using Sequest-HT as the search engine through the Proteome Discoverer 1.4 (Thermo Scientific) software. Peptide identifications were filtered by Percolator at a false discovery rate of 1% using the target-decoy strategy. Label-free quantification was performed with MaxQuant, and extracted ion chromatograms for AMD1 phosphopeptides were manually validated in Xcalibur 2.2 (Thermo).

Bioinformatic analysis. All the data sets used for the data mining analysis[46–49] were downloaded from the Gene Expression Omnibus, and subjected to background correction, $\log_2$ transformation, and quartile normalization. In the case of using a pre-processed data set, this normalization was reviewed and corrected if required.

Statistical analysis. No statistics were applied to determine sample size. The experiments were not randomized. The investigators were not blinded to allocation during experiments and outcome assessment. Data analysed by parametric tests are represented by the mean ± s.e.m. of pooled experiments; for non-parametric tests, the median with interquartile range is depicted, unless otherwise stated. Values of *n* represent the number of independent experiments performed or the number of individual mice or patient specimens. For each independent *in vitro* experiment, at least three technical replicates were used and a minimum number of three experiments were performed to ensure adequate statistical power. Analysis of variance was used for multi-component comparisons and Student's *t*-test for two-component comparisons. In the *in vitro* experiments, normal distribution was confirmed or assumed (for $n < 5$). Two-tailed statistical analysis was applied for experimental design without predicted result, and one-tailed analysis for validation or hypothesis-driven experiments. The confidence level used for all the statistical analyses was 0.95 ($\alpha = 0.05$).

Data availability. The authors declare that data supporting the findings of this study are available within the paper and its supplementary information files. Source data for unprocessed scans and Fig. 2d and Extended Data Figs 3d, q–s and 4i are provided with the paper.

31. Song, M. S. *et al.* Nuclear PTEN regulates the APC-CDH1 tumor-suppressive complex in a phosphatase-independent manner. *Cell* **144,** 187–199 (2011).
32. Chen, Z. *et al.* Differential p53-independent outcomes of p19(Arf) loss in oncogenesis. *Sci. Signal.* **2,** ra44 (2009).
33. Motameni, A. R. *et al.* Delivery of the immunosuppressive antigen Salp15 to antigen-presenting cells by *Salmonella enterica* serovar Typhimurium *aroA* mutants. *Infect. Immun.* **72,** 3638–3642 (2004).
34. Torrano, V. *et al.* The metabolic co-regulator PGC1α suppresses prostate cancer metastasis. *Nat. Cell Biol.* **18,** 645–656 (2016).
35. Dowling, R. J. *et al.* mTORC1-mediated cell proliferation, but not cell growth, controlled by the 4E-BPs. *Science* **328,** 1172–1176 (2010).
36. Wiederschain, D. *et al.* Single-vector inducible lentiviral RNAi system for oncology target validation. *Cell Cycle* **8,** 498–504 (2009).
37. Sanjana, N. E., Shalem, O. & Zhang, F. Improved vectors and genome-wide libraries for CRISPR screening. *Nat. Methods* **11,** 783–784 (2014).
38. Carracedo, A. *et al.* A metabolic prosurvival role for PML in breast cancer. *J. Clin. Investigation* **122,** 3088–3100 (2012).
39. Salazar, M. *et al.* Loss of Tribbles pseudokinase-3 promotes Akt-driven tumorigenesis via FOXO inactivation. *Cell Death Differ.* **22,** 131–144 (2015).
40. Alimonti, A. *et al.* A novel type of cellular senescence that can be enhanced in mouse models and human tumor xenografts to suppress prostate tumorigenesis. *J. Clin. Invest.* **120,** 681–693 (2010).
41. Revandkar, A. *et al.* Inhibition of Notch pathway arrests PTEN-deficient advanced prostate cancer by triggering p27-driven cellular senescence. *Nat. Commun.* **7,** 13719 (2016).
42. Fuhrer, T., Heer, D., Begemann, B. & Zamboni, N. High-throughput, accurate mass metabolome profiling of cellular extracts by flow injection–time-of-flight mass spectrometry. *Anal. Chem.* **83,** 7074–7080 (2011).
43. Jha, A. K. *et al.* Network integration of parallel metabolic and transcriptional data reveals metabolic modules that regulate macrophage polarization. *Immunity* **42,** 419–430 (2015).
44. Melamud, E., Vastag, L. & Rabinowitz, J. D. Metabolomic analysis and visualization engine for LC-MS data. *Anal. Chem.* **82,** 9818–9826 (2010).
45. Fumagalli, S., Ivanenkov, V. V., Teng, T. & Thomas, G. Suprainduction of p53 by disruption of 40S and 60S ribosome biogenesis leads to the activation of a novel G2/M checkpoint. *Genes Dev.* **26,** 1028–1040 (2012).
46. Grasso, C. S. *et al.* The mutational landscape of lethal castration-resistant prostate cancer. *Nature* **487,** 239–243 (2012).
47. Lapointe, J. *et al.* Gene expression profiling identifies clinically relevant subtypes of prostate cancer. *Proc. Natl Acad. Sci. USA* **101,** 811–816 (2004).
48. Taylor, B. S. *et al.* Integrative genomic profiling of human prostate cancer. *Cancer Cell* **18,** 11–22 (2010).
49. Tomlins, S. A. *et al.* Integrative molecular concept modeling of prostate cancer progression. *Nat. Genet.* **39,** 41–51 (2007).

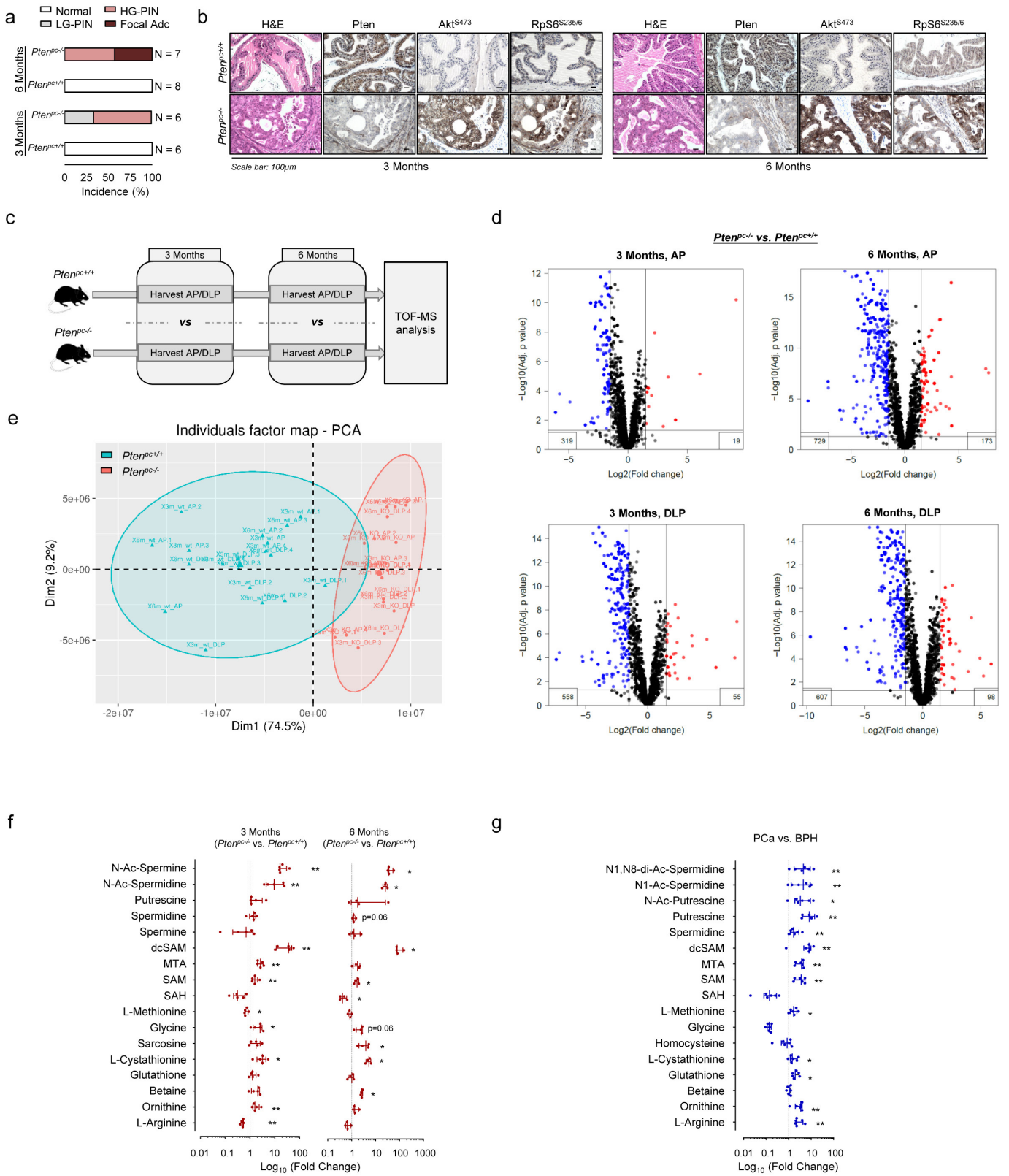

Extended Data Figure 1 | See next page for caption.

Extended Data Figure 1 | Metabolomics characterization of mouse and human prostate cancer. a, Incidence of pathological alterations observed in $Pten^{pc+/+}$ and $Pten^{pc-/-}$ mice. Number of mice as indicated. LG-PIN, low-grade prostatic intraepithelial neoplasia; HG-PIN: high-grade prostatic intraepithelial neoplasia; Focal Adc, focal adenocarcinoma. **b**, Representative immunohistochemical images of prostate tissue stained with haematoxylin and eosin (H&E), Pten, Akt^{S473}, and $RpS6^{S235/6}$ from mice at 3 and 6 months of age (representative of three mice per condition). **c**, Experimental design of the TOF-MS metabolomics analysis. AP, anterior prostate; DLP, dorsolateral prostate. **d**, **e**, Volcano plot (**d**) and principal component analysis (PCA, **e**) from altered metabolites in TOF-MS metabolomic analysis performed in $Pten^{pc-/-}$ and $Pten^{pc+/+}$ mouse prostate samples at the indicated age (6 months $Pten^{pc+/+}$anterior prostate, $n = 4$ mice; remainder of conditions, $n = 5$ mice). Grey dots: not significantly altered; red dots: significantly increased in $Pten^{pc-/-}$ prostate extracts; blue dots: significantly decreased in $Pten^{pc-/-}$ prostate extracts. **f**, LC/MS analysis of methionine cycle and polyamine pathway metabolites from $Pten^{pc-/-}$ versus $Pten^{pc+/+}$ mouse prostate samples at the indicated age (anterior prostate 3 months, $n = 5$ mice; 6 months, $n = 4$ mice). Median ± interquartile range. **g**, LC/MS analysis of methionine cycle and polyamine pathway metabolites from prostate cancer versus BPH human specimens (six prostate specimens per condition). Median ± interquartile range. $*P < 0.05$; $**P < 0.01$; $***P < 0.001$. One-tailed Mann–Whitney *U*-test (**f**, **g**) was used for data analysis.

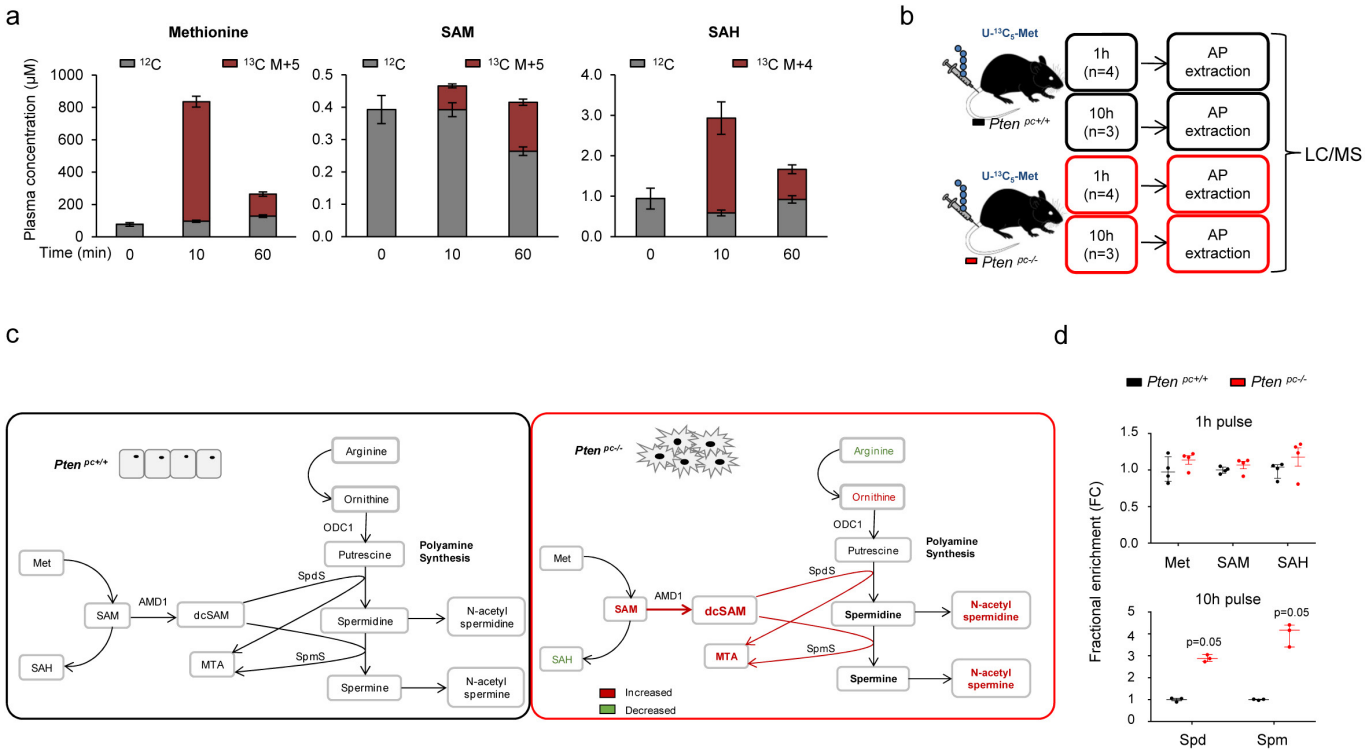

Extended Data Figure 2 | Metabolic tracing of [^{13}C]L-methionine in *Pten*-prostate specific knockout mice. a, Plasma LC/MS analysis of the indicated metabolite concentration after intravenous injection of [U-$^{13}C_5$] L-methionine (100 mg kg^{-1}) in C57BL/6 mice at 3 months of age (time 0 min, $n = 7$ mice; time 10 min/60 min, $n = 6$ mice). The unlabelled (M + 0, ^{12}C) and major labelled (^{13}C, M + 4 or M + 5) metabolite concentration is presented in the histogram. Error bars, s.e.m. **b**, Experimental design of the [U-$^{13}C_5$]L-methionine (100 mg kg^{-1}) *in vivo*. U-$^{13}C_5$-Met, L-methionine labelled with ^{13}C in five carbons;1 h, prostate samples extracted after 1 h pulse with [U-$^{13}C_5$]L-methionine; 10 h, prostate samples extracted after 10 h pulse with [U-$^{13}C_5$]L-methionine; **c**, Summary schematic of the alterations observed in the metabolomic analysis in *Pten*$^{pc-/-}$ versus *Pten*$^{pc+/+}$. Spm, spermine; spd, spermidine; ODC1, ornithine decarboxylase 1; SpdS, spermidine synthase; SpmS, spermine synthase. **d**, Fractional labelling of the indicated metabolites from Fig. 1c. Median ± interquartile range (1 h (top), $n = 4$; 10 h (bottom), $n = 3$). FC, fold change. One-tailed Mann–Whitney *U*-test (**d**) was used for data analysis.

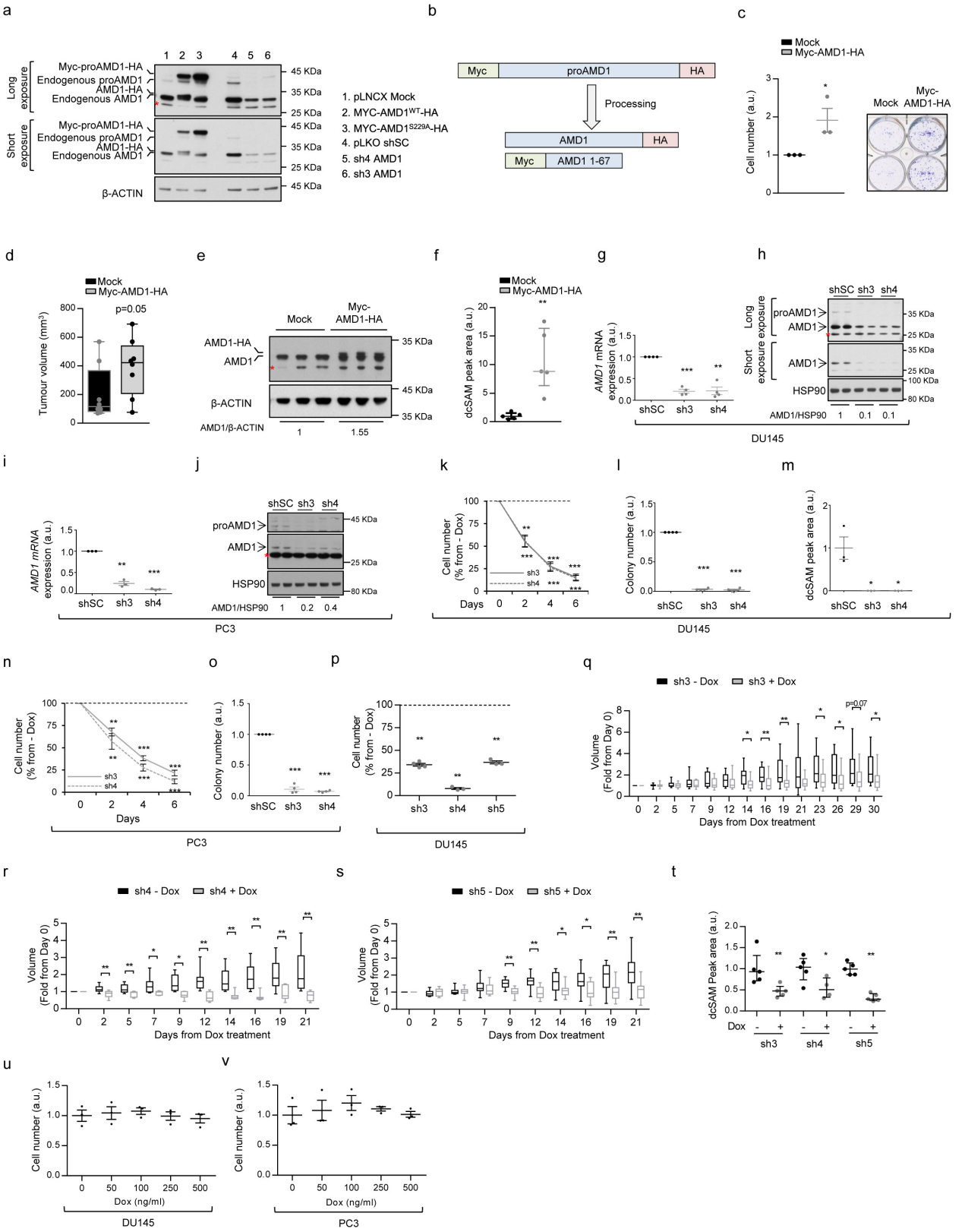

Extended Data Figure 3 | See next page for caption.

Extended Data Figure 3 | Genetic modulation of AMD1 in prostate cancer cells. a, Technical setup of anti-AMD1 antibody using the indicated constructs or shRNAs in DU145 cells. AMD1^{S229A} mutant lacks processing ability and is expressed exclusively as a pro-enzyme (representative western blot out of three independent experiments). **b**, Schematic representation of tagged ectopic AMD1 processing. **c**, Impact of ectopic Myc-AMD1–HA expression on foci number in DU145 cells *in vitro* ($n = 3$ independent experiments). **d**–**f**, Impact of ectopic Myc-AMD1–HA expression on tumour volume (**d**, $n = 8$ tumours per condition), AMD1 protein levels (**e**, $n = 3$ tumours per condition), and dcSAM abundance (**f**, $n = 5$ tumours per condition) in DU145 xenografts grown for 43 days. Data in **d** are represented as box-and-whisker plot. **f**, Dot plot with the median and the interquartile range. **g**–**o**, Effect of constitutive silencing of AMD1 (**g**, **i**, mRNA levels; **h**–**j**, protein expression) on cell number (**k**, **n**), anchorage-independent growth (**l**, **o**), and dcSAM abundance (**m**) with two different hairpins in DU145 (**g**, **h**, **k**, **l**, **m**) and PC3 (**i**, **j**, **n**, **o**) cells ($n = 3$ or 4 independent experiments as indicated by dots). shSC, scramble short hairpin; sh3 and sh4, two different short-hairpins targeting AMD1. Mean ± s.e.m. **p**, Effect of doxycycline-inducible (100 ng ml^{-1}) AMD1 silencing on cell number in DU145 cells (sh3, $n = 4$; sh4 and sh5, $n = 3$ independent experiments as indicated by dots). **q**–**s**, Impact of AMD1-inducible silencing in tumour volume from DU145 xenografts (tumours analysed: sh3 no doxycycline, $n = 12$; sh3 doxycycline, $n = 14$; sh4 no doxycycline, $n = 10$; sh4 doxycycline, $n = 7$; sh5 no doxycycline, $n = 10$; sh5 doxycycline, $n = 11$). Box-and-whisker plot. **t**, Impact of AMD1-inducible silencing in dcSAM abundance in DU145 xenografts from **q** to **s** ($n = 5$ tumours). Median ± interquartile range. **u**, **v**, Dose-dependent effect of doxycycline on cell number in DU145 (**u**) and PC3 (**v**) cells (cell number measured at day 6) ($n = 3$ independent experiments as indicated by dots). *$P < 0.05$; **$P < 0.01$; ***$P < 0.001$. Error bars, mean ± s.e.m. Red asterisk in western blots indicates non-specific band. Dashed lines indicate cell numbers in scramble short-hairpin-transduced cells. One-tailed *t*-test (**c**, **g**, **i**, **k**–**p**, **u**, **v**), and one-tailed Mann–Whitney *U*-test (**d**, **f**, **q**–**t**).

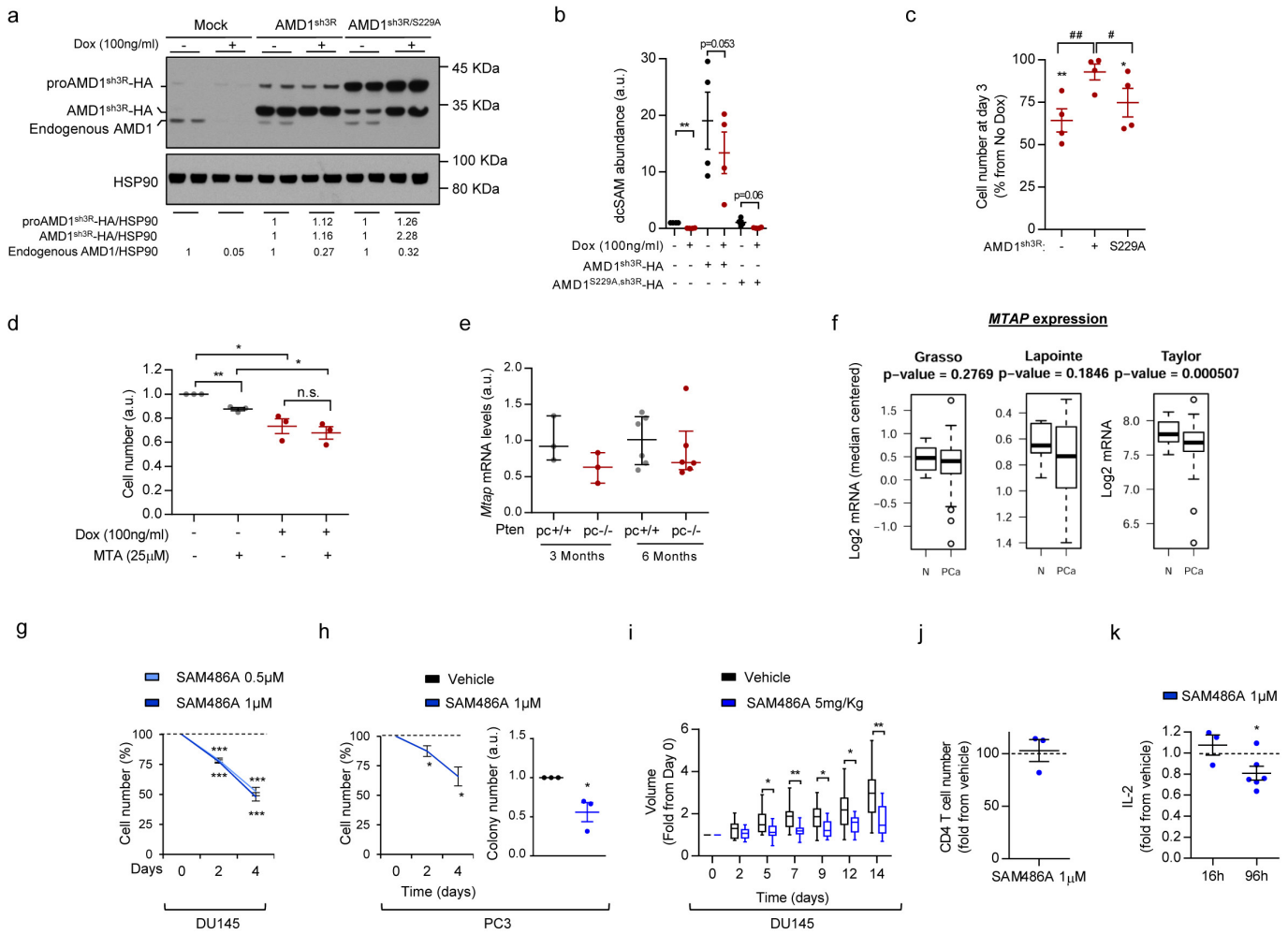

Extended Data Figure 4 | Genetic and pharmacological manipulation of AMD1 in prostate cancer cells. a–c, DU145 cells carrying doxycycline-inducible shRNA against AMD1 (sh3) were transduced with empty (Mock), sh3-resistant wild type (AMD1^{sh3R}), or processing-deficient (AMD1$^{sh3R/S229A}$) AMD1 constructs. AMD1 protein (**a**, representative experiment out of four), dcSAM abundance (**b**), and cell number expression (**c**) in the aforementioned cells ($n = 4$ independent experiments as indicated by dots). Asterisks indicate significant differences compared with the corresponding DU145 cells in the absence of doxycycline, and hash symbol indicates significant differences in the indicated comparison. Mean ± s.e.m. **d**, Effect of MTA (25 μM) on AMD1 silencing (sh3)-elicited anti-proliferative activity. MTA was administered at day 0 and cells were analysed at day 3 ($n = 3$ independent experiments as indicated by dots). **e**, *Mtap* gene expression levels in *Pten*$^{pc+/+}$ and *Pten*$^{pc-/-}$ mice at the indicated time points (see Extended Data Fig. 1a) (3 months, $n = 3$ mice; 6 months, $n = 6$ mice). Median ± interquartile range. **f**, *MTAP* gene expression analysis in publicly available data sets (see Methods; N, normal; number of patients analysed: ref. 48, normal $n = 29$, prostate cancer $n = 150$; ref. 46, normal $n = 12$, prostate cancer $n = 76$; ref. 47, normal, $n = 9$, prostate cancer, $n = 17$). **g**, **h**, Effect of pharmacological AMD1 inhibition with SAM486A on cell number (**g** and left **h**; DU145, $n = 5$; PC3, $n = 4$ independent experiments as indicated by dots), and anchorage-independent growth (right **h**, $n = 3$ independent experiments as indicated by dots) in PC3 or DU145 cells as indicated. Mean ± s.e.m. **i**, Effect of pharmacological AMD1 inhibition with SAM486A in established DU145 xenograft tumour volume (vehicle, $n = 11$ tumours; SAM486A, $n = 10$ tumours). Box-and-whisker plot. **j**, **k**, Effect of pharmacological AMD1 inhibition with SAM486A in activated T CD4 cell number (96 h (**j**), $n = 3$ independent experiments as indicated by dots) or IL-2 production (**k**, $n = 3$–6 independent experiments as indicated by dots). */$^{\#}P < 0.05$; **/$^{\#\#}P < 0.01$; ***$P < 0.001$. Dashed line indicates cell number (**g**, **h** left) or IL-2 abundance (**j**, **k**) in vehicle-treated cells. Student's *t*-test (**b**–**d**, **f**–**h**, **j**, **k**) and one-tailed Mann–Whitney test (**e**, **i**).

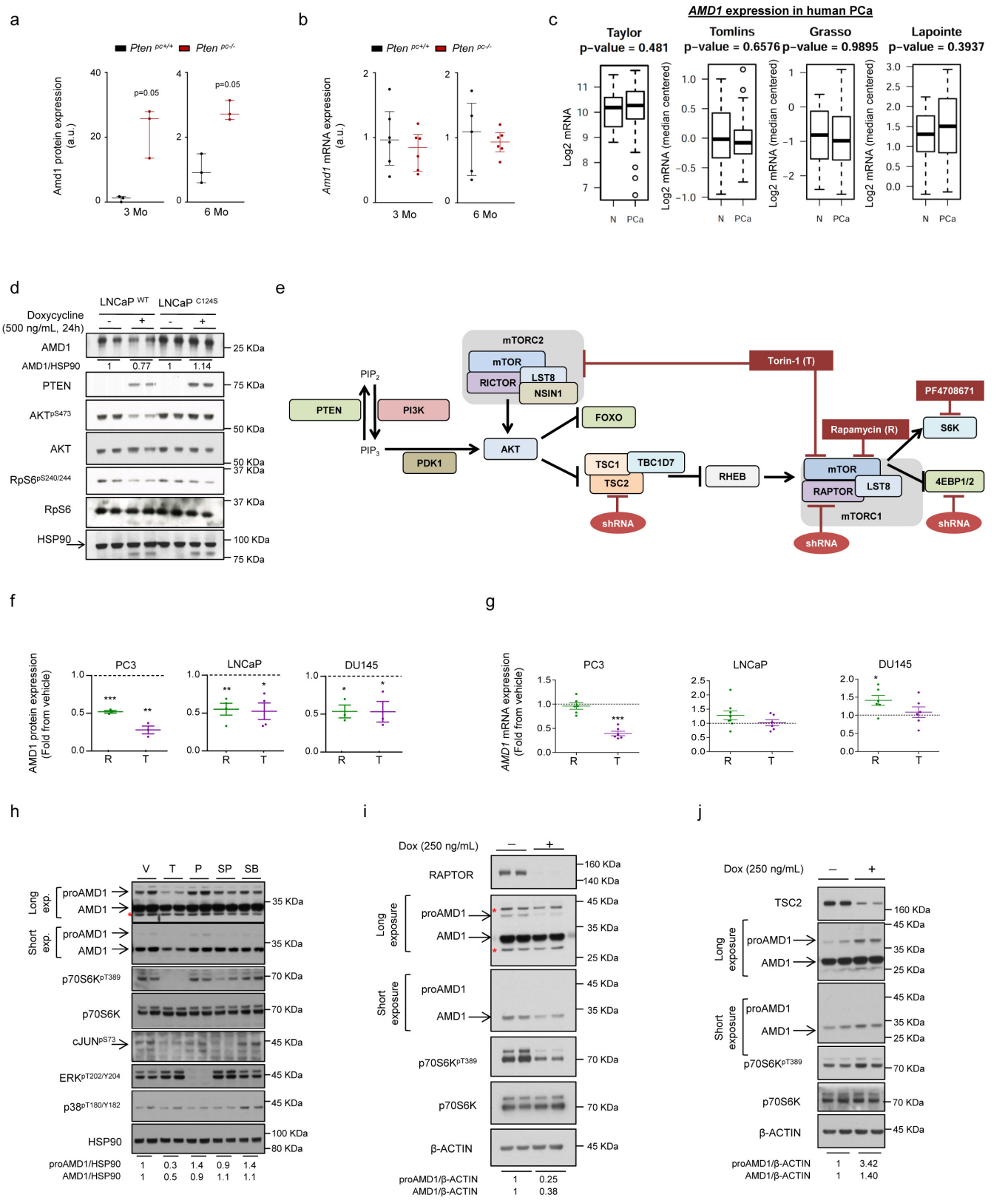

Extended Data Figure 5 | See next page for caption.

Extended Data Figure 5 | PTEN–PI3K–mTORC1-dependent regulation of AMD1 in prostate cancer. a, **b**, Amd1 protein quantification from Fig. 3a (a, $n = 3$ mice) and mRNA expression (**b**, $n = 5$ or 6 mice as indicated by dots) in $Pten^{pc-/-}$ and $Pten^{pc+/+}$ mice of the indicated age. Median ± interquartile range. **c**, *AMD1* gene expression analysis in publicly available data sets (see Methods; number of patients analysed: ref. 48, normal $n = 29$, prostate cancer $n = 150$; ref. 46, normal $n = 12$, prostate cancer $n = 76$; ref. 47, normal $n = 9$, prostate cancer $n = 17$). **d**, Representative western blot showing the expression of the indicated proteins upon doxycycline-inducible expression (24 h) of YFP–$PTEN^{WT}$ or catalytically inactive YFP–$PTEN^{C124S}$ in *PTEN*-deficient LNCaP prostate cancer cells ($n = 3$ independent experiments). **e**, Schematic representation of the PI3K signalling pathway and the pharmacological/genetic tools used in this study. **f**, ProAMD1 and AMD1 protein quantification from Fig. 3b (sample number as indicated by dots). **g**, *AMD1* gene expression upon treatment (24 h) with vehicle (V, DMSO), rapamycin (R, 20nM) and Torin-1 (T, 250 nM for PC3 and DU145, 125 nM for LNCaP) (LNCaP, $n = 8$ for Torin-1 and $n = 6$ for rapamycin; PC3 and DU145, $n = 6$ independent experiments as indicated by dots). Mean ± s.e.m. **h**, Representative western blot analysis of AMD1 levels upon 24-h treatment of DU145 cells with vehicle, Torin-1 (mTORC1/2 inhibitor; 250 nM), PD032901 (ERK-MAPK inhibitor, PD; 100 nM), SP600125 (JNK-SAPK inhibitor, SP; 10 μM), and SB203580 (p38-MAPK inhibitor, SB; 5 μM) ($n = 3$ independent experiments). **i**, Impact of inducible *RAPTOR* silencing in DU145 cells on proAMD1 protein levels (doxycycline-induced, 250 ng ml^{-1}) (representative experiment out of $n = 6$). **j**, Impact of inducible *TSC2* silencing in DU145 cells on proAMD1 protein levels (doxycycline-induced, 250 ng ml^{-1}) (representative experiment out of $n = 6$). $^{*}P < 0.05$; $^{**}P < 0.01$; $^{***}P < 0.001$. Red asterisk in western blots indicates non-specific band. Arrows indicate specific immunoreactive bands. Student's *t*-test (**c**, **f**, **g**) and Mann–Whitney test (**a**, **b**).

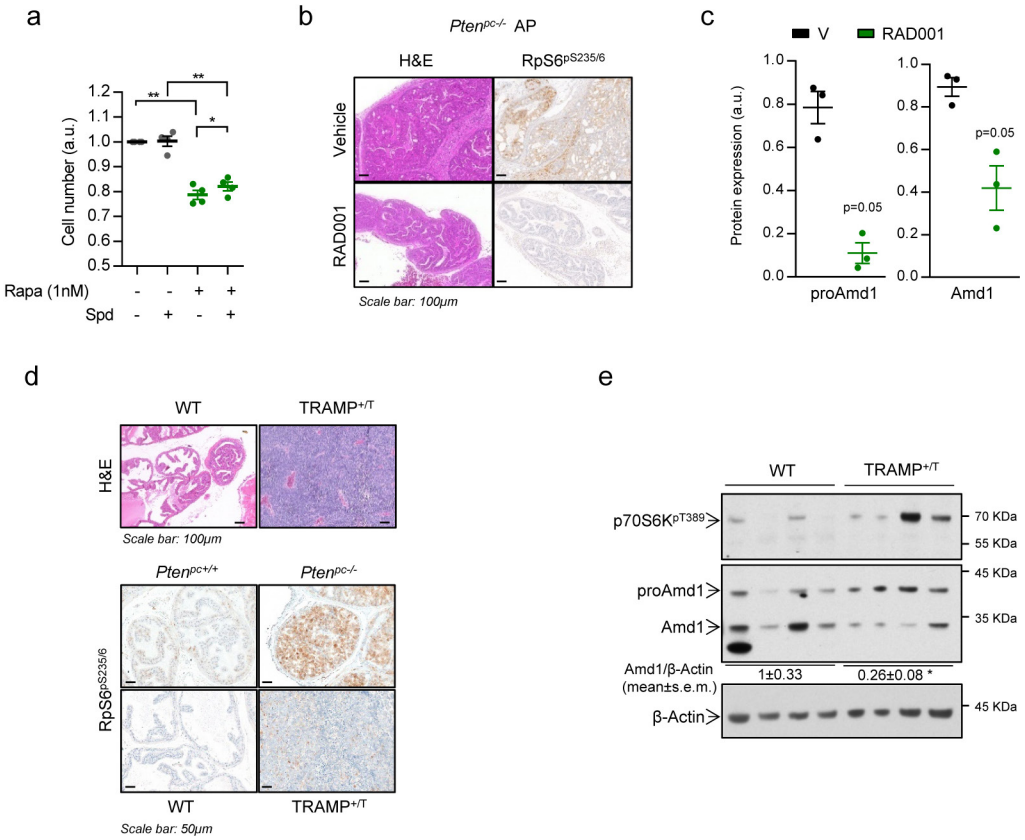

Extended Data Figure 6 | mTORC1-dependent AMD1 regulation *in vivo*. **a**, Effect of spermidine (Spd, 0.75 μM) on PC3 cell number upon rapamycin treatment (1 nM, outcome measured 72 h after treatment). Drugs were administered at day 0 and only spermidine was additionally administered at day 1 ($n = 4$ independent experiments as indicated by dots). **b**, Effect of RAD001 treatment on prostate pathological features and mTORC1 activity (haematoxylin and eosin and $RpS6^{S235/6}$ staining by immunohistochemistry) ($n = 3$ mice). **c**, ProAmd1 and Amd1 protein abundance quantification from Fig. 3e (left; number of mice as indicated by dots). **d**, Representative immunohistochemical images of prostate tissue from wild-type or TRAMP mice (+/T, 28–32 weeks old) stained with haematoxylin and eosin (top) and $RpS6^{S235/6}$ (bottom, $Pten^{pc+/+}$ and $Pten^{pc-/-}$ prostate tissues are presented as a comparison of the RpS6 phosphorylation levels) ($n = 3$ mice). **e**, Evaluation of AMD1 expression by western blot in prostate tissues from wild-type or TRAMP mice (+/T, 28–32 weeks old) ($n = 4$ mice). $^*P < 0.05$; $^{**}P < 0.01$. Error bars, mean ± s.e.m. Arrows indicate specific immunoreactive bands. Student's *t*-test (**a**) and Mann–Whitney test (**c**, **e**).

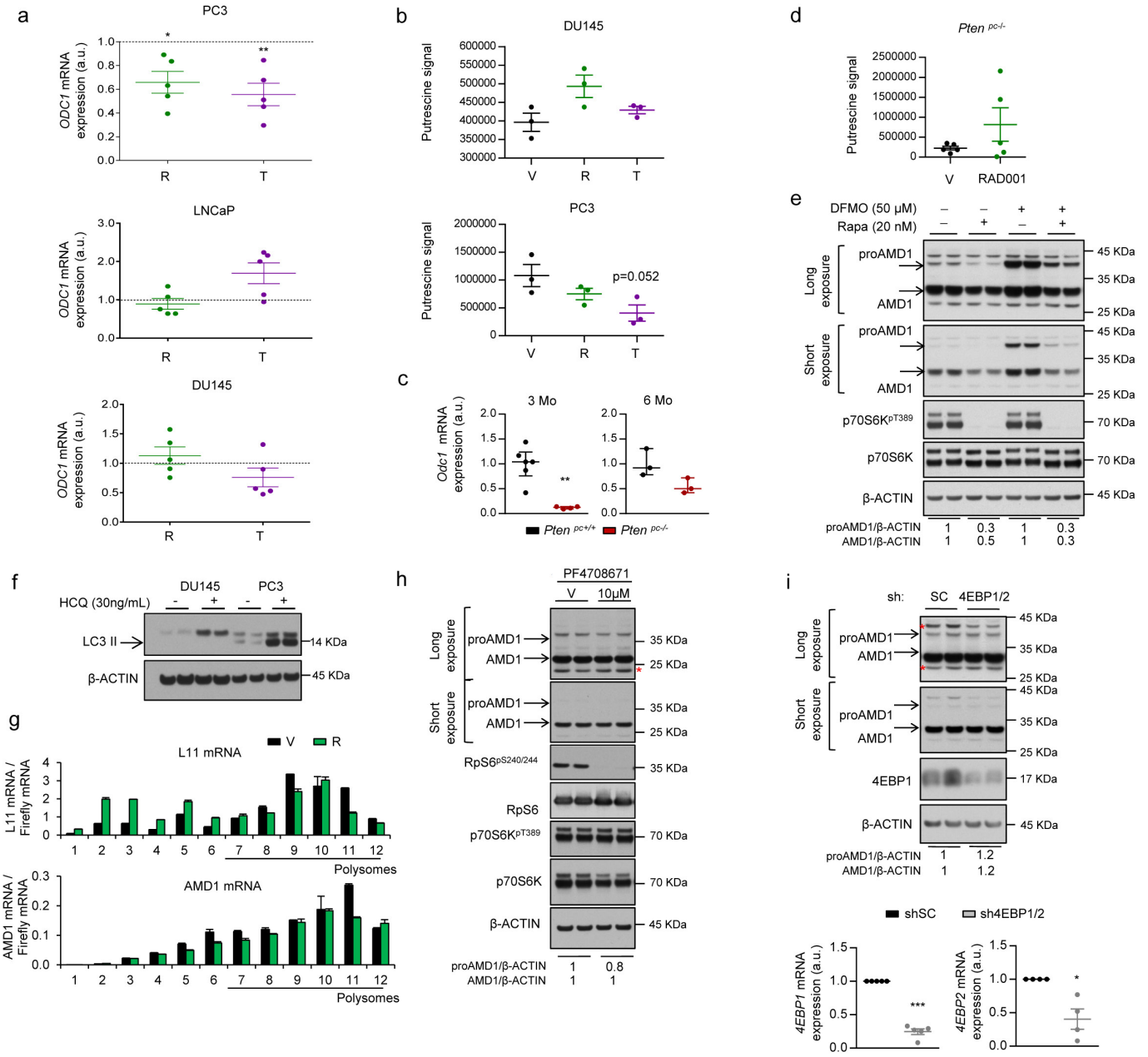

Extended Data Figure 7 | Contribution of mTORC1 effector pathways and targets on the regulation of AMD1. a, *ODC1* gene expression upon treatment (24 h) of vehicle (DMSO), rapamycin (20 nM) and Torin-1 (250 nM for PC3 and DU145, 125 nM for LNCaP) in PC3, LNCaP, and DU145 cells ($n = 5$ independent experiments as indicated by dots). Mean ± s.e.m. **b**, Putrescine abundance upon treatment (24 h) of vehicle (DMSO), rapamycin (20 nM), and Torin-1 (250 nM) in DU145 and PC3 cells ($n = 3$ independent experiments as indicated by dots). Mean ± s.e.m. **c**, *Odc1* gene expression in 3- and 6-month-old $Pten^{pc+/+}$ and $Pten^{pc-/-}$ mice ($n = 3$–6 as indicated by dots). Median ± interquartile range. **d**, Putrescine abundance in 12-week-old $Pten^{pc-/-}$ mice upon treatment with vehicle or RAD001 (10 mg per kg (body weight), 6 days per week) for 4 weeks ($n = 5$ mice). Mean ± s.e.m. **e**, Representative western blot ($n = 3$ independent experiments) depicting the changes in expression of the indicated proteins upon 24 h treatment of DU145 cells with rapamycin (20 nM) and/or DFMO (an inhibitor of ODC1, 50 μM) with the corresponding vehicles. **f**, Representative western blot showing LC3 lipidation in HCQ-treated (6 h) DU145 and PC3 cells, as a readout of macro-autophagy ($n = 3$ independent experiments). Arrow indicates LC3-II. **g**, For the analysis of translation initiation, polysome profiling analysis of AMD1 and L11 as positive control in DU145 cells treated with vehicle or rapamycin (20 nM, 8 h) is shown. Error bars, s.d. from technical replicates. **h**, Effect of pharmacological p70S6K inhibition with PF4708671 (10 μM) on AMD1 protein expression in DU145 cells (representative experiment out of five). **i**, Effect of 4EBP1/2 silencing on proAMD1 and AMD1 protein expression (upper panels) (representative experiment out of three). Lower panels show 4EBP1 ($n = 5$ independent experiments) and 4EBP2 ($n = 4$ independent experiments) gene expression in shRNA-transduced DU145 cells. $*P < 0.05$; $**P < 0.01$; $***P < 0.001$. Red asterisks in western blots indicate non-specific band. Arrows indicate specific immunoreactive bands. Student's *t*-test (**a**, **b**, **d**, **i**) and Mann–Whitney *U*-test (**c**).

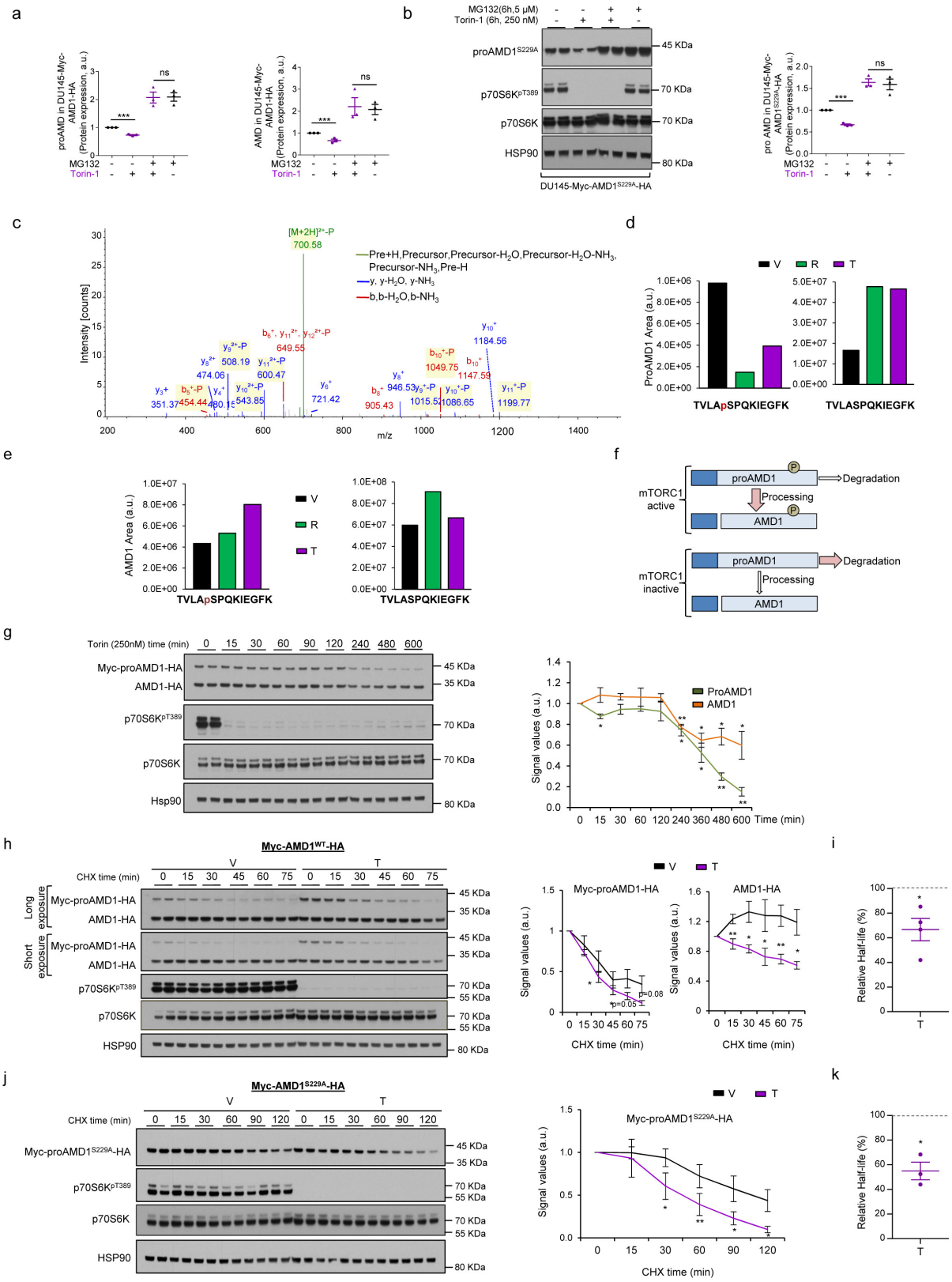

Extended Data Figure 8 | See next page for caption.

Extended Data Figure 8 | Regulation of proAMD1 stability by mTORC1. a, ProAmd1 (left) and Amd1 (right) protein abundance quantification from Fig. 4a ($n = 3$ independent experiments as indicated by dots). Error bars, mean ± s.e.m. **b**, Representative western blot of DU145 cells expressing Ser-229-Ala (S229A) mutant Myc-AMD1–HA treated with vehicle or Torin-1 (250 nM, 6 h) in the presence or absence of MG132 (5 μM, 6 h) ($n = 3$ independent experiments). Quantification is provided in the right panel. **c**, Representative MS/MS spectrum of the TVLASPQKIEGFK peptide in proAMD1 and AMD1, in which phosphorylation was unambiguously assigned to the S298 residue. **d**, Calculated areas under the curves from extracted ion chromatogram in Fig. 4b of the TVLASPQKIEGFK peptide for phosphorylated (highlighted in red in the sequence, left) and total (right) proAMD1. **e**, Calculated areas under the curves from extracted ion chromatogram of the TVLASPQKIEGFK peptide for phosphorylated (highlighted in brown in the sequence, left) and total (right) AMD1. **f**, Schematic representation of the working hypothesis of proAMD1 regulation by mTORC1-dependent phosphorylation. **g**, Effect of Torin (250 nM) on proAMD1 and AMD1 protein at different time points in Myc-AMD1–HA-expressing DU145 cells (representative western blot out of three independent experiments; right, densitometric quantification). Error bars, s.e.m. **h**, **i**, Representative western blot depicting the stability of ectopic proAMD1 and AMD1 in DU145 cells challenged with vehicle or Torin-1 (250 nM, 2 h) upon CHX treatment (densitometry of proAMD1 and AMD1 levels is represented in right panels (**h**) and half-life reduction in proAMD1 (**i**) ($n = 4$ independent experiments). **j**, **k**, Representative western blot depicting the stability of S229A mutant Myc-AMD1-HA construct in DU145 cells challenged with vehicle or Torin-1 (250 nM, 2 h) upon CHX treatment (densitometry of proAMD1 is represented in the right panel (**j**) and half-life reduction in proAMD1 (**k**) ($n = 3$ independent experiments). Mean ± s.e.m. NS, not significant. $^{*}P < 0.05$; $^{**}P < 0.01$; $^{***}P < 0.001$. Student's *t*-test.

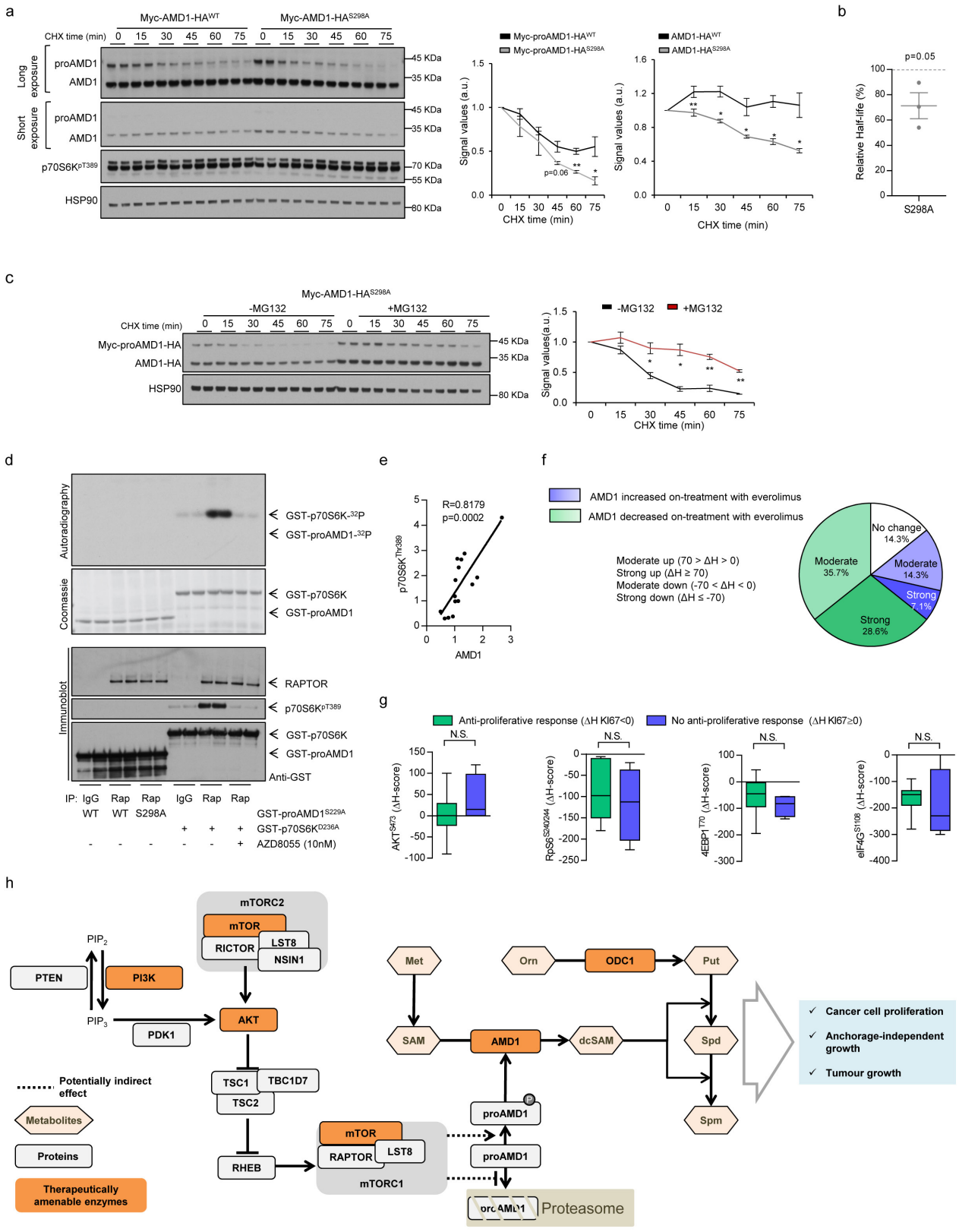

Extended Data Figure 9 | See next page for caption.

Extended Data Figure 9 | Contribution of proAMD1 phosphorylation downstream mTORC1 to the stability of the enzyme. a, **b**, Representative western blot depicting the stability of wild type and S298A phospho-mutant Myc-AMD1-HA constructs in DU145 cells upon cycloheximide treatment (densitometry of proAMD1 and AMD1 is represented in right panels (**a**) and half-life reduction in proAMD1 (**b**) ($n = 3$ independent experiments). Mean ± s.e.m. **c**, Representative western blot depicting the stability of S298A phospho-mutant Myc-AMD1-HA construct in DU145 cells challenged with vehicle (V) or MG132 (5 μM) upon CHX treatment (densitometry of proAMD1 is represented in right panel, $n = 3$ independent experiments). Mean ± s.e.m. **d**, mTORC1 kinase activity (by means of RAPTOR immunoprecipitation from HEK293 cells) on GST–proAMD1^{S229A} or GST–proAMD1$^{S229A/S298A}$, using bacteria-purified proteins. GST–p70S6K is presented as positive control. AZD8055 is used as control of mTORC1 inhibition. **e**, Correlation analysis between p70S6K^{pT389} and AMD1 densitometry values in prostate cancer specimens from Fig. 4c ($n = 15$ patient specimens). **f**, Quantification of AMD1 immunoreactivity in response to everolimus in tumour biopsies, on the basis of the ΔH score ($n = 14$ specimen pairs). **g**, Box-and-whisker plot of the immunoreactivity of mTOR downstream effectors (AKT^{S473}, RpS6$^{pS240/244}$, 4EBP1/2^{pT70}, eIF4G^{pS1108}) in cancer patients with (ΔH score for KI67 < 0; $n = 6$ specimen pairs) or without (ΔH score for KI67 ≥ 0; $n = 4$ specimen pairs) anti-proliferative tumour response upon treatment with everolimus. **h**, Schematic representation of the main findings of this study. Orn, ornithine; Put, putrescine; Spm, spermine; ODC1, ornithine decarboxylase 1; PIP_2, phosphatidyl inositol bisphosphate; PIP_3, phosphatidyl inositol triphosphate; $^*P < 0.05$; $^{**}P < 0.01$; NS, not significant. Arrows indicate specific immunoreactive/autoradiographic bands. One-tailed Student's *t*-test (**a**–**c**), two-tailed Mann–Whitney test (**g**), and Spearman's correlation analysis (**e**).

Immunity
Article

Fine-Tuning of CD8$^+$ T Cell Mitochondrial Metabolism by the Respiratory Chain Repressor MCJ Dictates Protection to Influenza Virus

Devin P. Champagne,[1] Ketki M. Hatle,[1] Karen A. Fortner,[1] Angelo D'Alessandro,[2] Tina M. Thornton,[1] Rui Yang,[1] Daniel Torralba,[1] Julen Tomás-Cortázar,[3] Yong Woong Jun,[4] Kyo Han Ahn,[4] Kirk C. Hansen,[2] Laura Haynes,[5] Juan Anguita,[3,6] and Mercedes Rincon[1,*]
[1]Program in Immunobiology, Department of Medicine, University of Vermont, Burlington, Vermont, 05405 USA
[2]Department of Biochemistry and Molecular Genetics, University of Colorado Denver, Aurora, CO 80045, USA
[3]Center for Cooperative Research in Biosciences (CIC bioGUNE), Derio 48160 Bizkaia, Spain
[4]Department of Chemistry, Center for Electro-Photo Behaviors in Advanced Molecular Systems, Pohang University of Science and Technology (POSTECH), Nam-Gu, Pohang, 790-784 Gyeongbuk, Republic of Korea
[5]Center on Aging and Department of Immunology, University of Connecticut Health Center, Farmington, CT 06030 USA
[6]Ikerbasque, Basque Foundation for Science, Bilbao, Bizkaia, Spain
*Correspondence: mrincon@uvm.edu
http://dx.doi.org/10.1016/j.immuni.2016.02.018

SUMMARY

Mitochondrial respiration is regulated in CD8$^+$ T cells during the transition from naive to effector and memory cells, but mechanisms controlling this process have not been defined. Here we show that MCJ (methylation-controlled J protein) acted as an endogenous break for mitochondrial respiration in CD8$^+$ T cells by interfering with the formation of electron transport chain respiratory supercomplexes. Metabolic profiling revealed enhanced mitochondrial metabolism in MCJ-deficient CD8$^+$ T cells. Increased oxidative phosphorylation and subcellular ATP accumulation caused by MCJ deficiency selectively increased the secretion, but not expression, of interferon-γ. MCJ also adapted effector CD8$^+$ T cell metabolism during the contraction phase. Consequently, memory CD8$^+$ T cells lacking MCJ provided superior protection against influenza virus infection. Thus, MCJ offers a mechanism for fine-tuning CD8$^+$ T cell mitochondrial metabolism as an alternative to modulating mitochondrial mass, an energetically expensive process. MCJ could be a therapeutic target to enhance CD8$^+$ T cell responses.

INTRODUCTION

Metabolism is emerging as a major factor that regulates the function and differentiation of immune cells and influences the course of an immune response (Pearce et al., 2013; van der Windt and Pearce, 2012; Wang and Green, 2012). Naive, effector, and memory T cell subsets have distinct metabolic profiles to provide the energy and bioenergetic precursors required for cell growth and expansion. Naive cells use glucose and free fatty acids (FFA) as sources of ATP through mitochondrial oxidative phosphorylation (OXPHOS) (van der Windt et al., 2012; Wang et al., 2011). After activation, CD8$^+$ T cells undergo a metabolic reprograming and switch to glycolysis as a source of ATP. Effector T cells can also use glutamine to generate ATP through glutaminolysis, which can further fuel OXPHOS (Carr et al., 2010; Wang et al., 2011). Proliferation of effector CD8$^+$ T cells appears to be more dependent on glucose than effector CD4$^+$ T cells (Frauwirth et al., 2002; Macintyre et al., 2011). In contrast, production of some cytokines by effector CD8$^+$ T cells is not affected by a strong inhibition of glycolysis (Cham et al., 2008), and cytotoxic activity can occur in the absence of glucose (MacDonald and Koch, 1977).

Effector CD8$^+$ T cells further reprogram metabolism during memory cell generation in response to antigen and cytokine withdrawal. Memory CD8$^+$ T cells primarily use FFA oxidation in mitochondria as the main energy pathway (Araki et al., 2009; Pearce et al., 2009; van der Windt et al., 2012). Additionally, memory CD8$^+$ T cells manifest a greater increase in both OXPHOS and aerobic glycolysis following activation compared with naive cells, and the induction of glycolysis is dependent on mitochondrial ATP (van der Windt et al., 2013). Importantly, intervention of metabolism with metformin (AMPK activator) or rapamycin (mTOR inhibitor) to promote FFA oxidation enhances the generation of memory CD8$^+$ T cells and protection against viral infection (Araki et al., 2009; Pearce et al., 2009). A recent study revealed that memory CD8$^+$ T cells have developed their own intrinsic pathways to mobilize fatty acids for oxidation (Pearce et al., 2009). Considering this highly dynamic metabolic reprogramming, CD8$^+$ T cells likely utilize specific checkpoints to regulate these transitions and their effector functions. However, while a number of studies have addressed the effect of different metabolic substrates that fuel the mitochondrial electron transport chain (ETC), little is known about endogenous mechanisms that control mitochondrial respiration and, thereby, the immune response.

Methylation-controlled J protein (MCJ), a protein encoded by the *Dnajc15* gene, is a member of the DnaJ family of chaperones. MCJ is a small protein with features that distinguish it from other DnaJ family members. While most DnaJ family members are soluble proteins, MCJ contains a transmembrane domain and has a

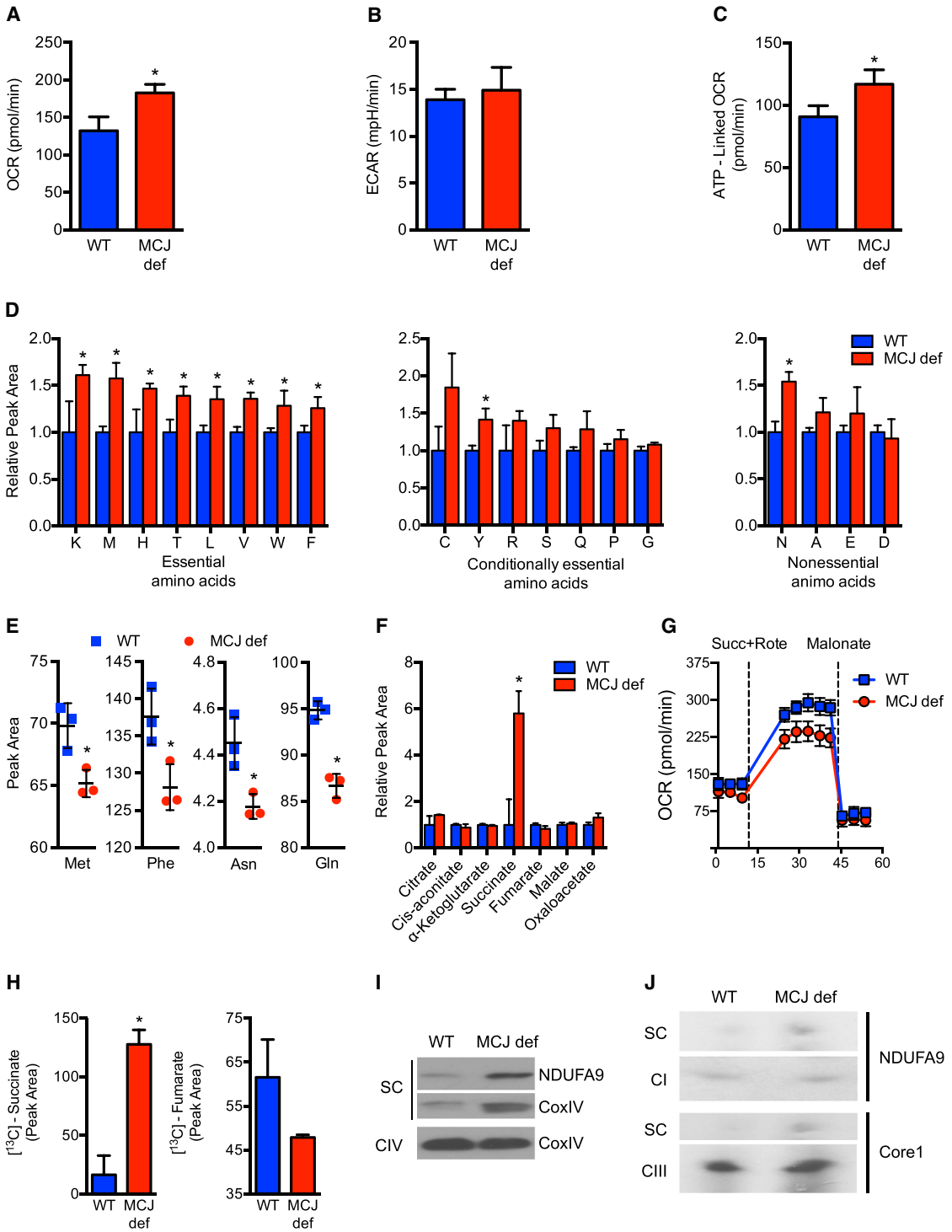

Figure 1. MCJ Restrains Mitochondrial Respiration in Naive CD8$^+$ T Cells

WT (blue) and MCJ-deficient CD8$^+$ T cells (MCJ def, red).

(A) Baseline OCR, (B) ECAR, and (C) OCR linked to mitochondrial ATP production (baseline OCR minus OCR in the presence of oligomycin) of freshly isolated cells as determined by MitoStress (A and C) or Glycolysis Stress assays (B).

(D and F) Metabolic profiles of cells were determined by UPLC-MS analysis. Relative amounts of (D) amino acids and (F) TCA cycle metabolites.

(E) Equal numbers of cells were incubated in culture medium for 16 hr, and metabolic profiles of the culture supernatants were determined.

(G) Complex II activity was determined by examining OCR at baseline and in the response to succinate with rotenone (Succ+Rote) and malonate.

(H) Cells were cultured with ^{13}C- and ^{15}N-labeled amino acids, and metabolic flux was determined by UPLC-MS analysis. ^{13}C-succinate and ^{13}C-fumarate peak areas shown.

(legend continued on next page)

unique N-terminal domain that shares no significant sequence similarity with any other known protein. MCJ was first reported in ovarian cancer cells as a gene negatively regulated by methylation (Shridhar et al., 2001; Strathdee et al., 2004). Loss of MCJ is associated with chemoresistance of human breast and ovarian cancer cell lines (Hatle et al., 2007; Shridhar et al., 2001; Strathdee et al., 2005). We recently showed that MCJ is abundantly expressed primarily in tissues with a highly active mitochondrial metabolism, including heart and liver (Hatle et al., 2013). Within the immune system, MCJ is highly expressed in $CD8^+$ T cells, but not in $CD4^+$ T and B cells (Hatle et al., 2013), and less in macrophages (Navasa et al., 2015a). Importantly, MCJ localizes to the inner membrane of mitochondria (Hatle et al., 2013; Schusdziarra et al., 2013) and acts as a negative regulator of the ETC. MCJ deficiency in vivo results in increased complex I activity and mitochondrial membrane potential (MMP) without affecting mitochondrial mass (Hatle et al., 2013). Endogenous MCJ in primary tissues associates with complex I and acts as a natural inhibitor, making MCJ one of the first described endogenous negative regulators of complex I. The activity of complex I is enhanced by assembly in "respirasomes," which are mitochondrial ETC supercomplexes containing complexes I, III, and IV (Acín-Pérez et al., 2008). Supercomplexes facilitate efficient transfer of electrons to enhance complex I activity and minimize electron "leak" that results in ROS production (Moreno-Lastres et al., 2012). We have shown that MCJ interferes with the formation of these supercomplexes in heart (Hatle et al., 2013), a mechanism to inhibit complex I activity and MMP.

Although MCJ is abundantly present in $CD8^+$ T cells, its role in regulating mitochondrial metabolism and function of these cells is unknown. Here, we show that MCJ acts a negative regulator of mitochondrial respiration in $CD8^+$ T cells. MCJ deficiency did not affect proliferation of naive $CD8^+$ T cells upon activation, nor activation marker or cytokine gene expression. However, increased OXPHOS in MCJ-deficient $CD8^+$ T cells enhanced the secretion of cytokines and sustained the metabolic state of effector $CD8^+$ T cells during the contraction phase. MCJ-deficient memory $CD8^+$ T cells had greater protective capacity against influenza virus infection. Therefore, MCJ is emerging as an important negative regulator of mitochondrial activity of $CD8^+$ T cells.

RESULTS

Loss of MCJ Promotes Respiratory Supercomplexes and Mitochondrial Metabolism in Naive $CD8^+$ T Cells

To investigate the role of MCJ in $CD8^+$ T cell development and function, we used MCJ-deficient mice previously described to have no obvious phenotypic alterations under physiological conditions (Hatle et al., 2013). Although $CD8^+$ T cells freshly isolated from MCJ-deficient mice display higher mitochondrial membrane potential (MMP) (Figure S1A), there was no difference in the percentage (Figure S1B) or number (data not shown) of $CD8^+$ or $CD4^+$ T cells in the spleen and lymph nodes (LN) of WT and MCJ-deficient mice. No difference in the expression of activation markers such as CD44 was observed (Figure S1C). The percentage (Figure S1B) and number (data not shown) of single-positive, double-positive (DP), or double-negative (DN) populations in the thymus were also comparable. Thus, MCJ deficiency does not affect the development of $CD8^+$ and $CD4^+$ T cells in the thymus or homeostasis in the periphery.

MMP is the driver for oxidative phosphorylation (OXPHOS), generation of ATP, and oxygen consumption. To investigate the impact that increased MMP in MCJ-deficient $CD8^+$ T cells has on mitochondrial respiration, we examined the oxygen consumption rate (OCR) in freshly isolated $CD8^+$ T cells using the Seahorse MitoStress assay. Correlating with the increased MMP, OCR was also elevated in MCJ-deficient $CD8^+$ T cells compared with WT $CD8^+$ T cells (Figure 1A). In contrast, the extracellular acidification rate (ECAR), a parameter for glycolysis, was not affected in MCJ-deficient $CD8^+$ T cells (Figure 1B). Mitochondrial ATP production, determined by subtracting the OCR in the presence of oligomycin (Complex V/ATP Synthase inhibitor) from the OCR at baseline, was also higher in MCJ-deficient $CD8^+$ T cells (Figure 1C). Thus, MCJ is a negative regulator of mitochondrial respiration in $CD8^+$ T cells.

To identify the impact of MCJ on the overall metabolism of naive $CD8^+$ T cells, we performed nonbiased high-throughput metabolic profiling. Metabolome analysis of $CD8^+$ T cells freshly isolated from WT and MCJ-deficient mice showed a large number of metabolic intermediates from different pathways equally present in both (Table S1). However, there was a significant increase in the amounts of several amino acids in MCJ-deficient $CD8^+$ T cells (Figure 1D). Most of the amino acids that were significantly elevated belonged to the essential amino acid group (Figure 1D). In contrast, only tyrosine in the conditionally essential amino acid group and asparagine in the non-essential group were significantly increased (Figure 1D).

The preferential accumulation of amino acids that need to be imported suggested a greater amino acid transport occurred in the absence of MCJ. Since amino acid transport is highly dependent on ATP, increased mitochondrial OXPHOS due to MCJ deficiency could be responsible for this transport. To investigate this, we incubated freshly isolated $CD8^+$ T cells in culture medium. After 16 hr, the metabolic profile of the culture supernatants was analyzed to determine the amino acid consumption. The amounts of amino acids were significantly reduced in the culture supernatant of MCJ-deficient $CD8^+$ T cells (Figure 1E). In addition, metabolic flux analyses with ^{13}C and ^{15}N labeled amino acids showed increased uptake of extracellular [^{13}C, ^{15}N]-glutamine (Figure S1D). Thus, the increased mitochondrial respiration resulting from MCJ deficiency in naive $CD8^+$ T cells in vivo promotes amino acid uptake.

The other metabolite significantly increased in MCJ-deficient $CD8^+$ T cells was succinate (Table S1 and Figure 1F), which is oxidized to fumarate by succinate dehydrogenase (ETC complex II) in the TCA cycle. However, the amounts of fumarate and

(I and J) Mitochondrial extracts were resolved by BNE. (I) Bands corresponding to supercomplexes (SC) or monomeric complex IV were excised, resolved by SDS-PAGE, and examined by Western blot analysis for NDUFA9 (complex I) and CoxIV (complex IV).

(J) Proteins separated by BNE were examined by Western blot analysis for NDUFA9 and Core1 (complex III). Bands corresponding to supercomplexes (SC) and monomeric complexes I (CI) and III (CIII) regions of the Western blot shown. *$p < 0.05$ by unpaired t test. Avg ± SD ($n \geq 3$) shown. Results are representative of 2–3 experiments. See also Figure S1 and Table S1.

the other components of the TCA cycle were not different (Figure 1F). These results suggested that elevated succinate in MCJ-deficient CD8$^+$ T cells was the result of impaired complex II activity. Indeed, reduced complex II activity was found in freshly isolated MCJ-deficient CD8$^+$ T cells as measured by OCR in response to succinate using a Seahorse Extracellular Flux analyzer (Figure 1G). In addition, metabolic flux analyses of freshly isolated CD8$^+$ T cells incubated with ^{13}C- and ^{15}N-labeled amino acids revealed an increase in newly synthesized succinate, but not fumarate (the product of complex II), in MCJ-deficient CD8$^+$ T cells (Figure 1H). Thus, complex II appears to be uncoupled from the rest of the ETC in MCJ-deficient CD8$^+$ T cells.

We have shown that the absence of MCJ in heart favors the accumulation of mitochondrial respiratory supercomplexes (Hatle et al., 2013), composed of complexes I, III, and IV but not complex II. To investigate whether supercomplexes were increased in naive MCJ-deficient CD8$^+$ T cells, we generated mitochondrial extracts with digitonin to preserve supercomplexes and resolved them by blue native electrophoresis (BNE) as previously described (Yang et al., 2015). The supercomplex region was excised, resolved by SDS-PAGE, and analyzed by Western blot for subunits of complexes I (NDUFA9) and IV (CoxIV). The amounts of supercomplexes were higher in MCJ-deficient CD8$^+$ T cells (Figure 1I). Monomeric complex IV analyzed as a control and was not different (Figure 1I). To further support the accumulation of supercomplexes in MCJ-deficient CD8$^+$ T cells, we resolved mitochondrial extracts by BNE, followed by immunoblot analysis for subunits of complexes I (NDUFA9) and III (Core1). Increased NDUFA9 amounts were present in the supercomplex region in MCJ-deficient CD8$^+$ T cells, while the amounts of NDUFA9 in the monomeric complex I region were comparable between MCJ-deficient and WT cells (Figure 1J). Similar results were obtained for Core1 (Figure 1J). Thus, loss of MCJ promotes the formation of respiratory supercomplexes in naive CD8$^+$ T cells. Uncoupling complex III from complex II could compromise complex II activity and cause the observed accumulation of succinate. Together, these results indicate that the function of MCJ in naive CD8$^+$ T cells is to restrict mitochondrial metabolism, and a deficiency in MCJ alters normal mitochondrial metabolism.

MCJ Deficiency Does Not Affect Proliferation, but Enhances the Secretion of Cytokines in Activated CD8$^+$ T Cells

We investigated whether the enhanced mitochondrial metabolism found in MCJ-deficient CD8$^+$ T cells could alter proliferation. Freshly isolated CD8$^+$ T cells were stained with CFSE and activated with anti-CD3 and anti-CD28 antibodies (Abs), and proliferation was analyzed by flow cytometry. No differences were observed in the frequency of proliferating cells or number of cell divisions (Figure 2A), the survival of cells after 2 days of activation (Figure 2B), or expression of the cell surface activation markers CD69 and CD25 (Figure 2C). In contrast, greater IFN-γ (Figure 2D) and IL-2 (Figure 2E) production was detected in activated MCJ-deficient CD8$^+$ T cells as determined by ELISA. Thus, loss of MCJ does not interfere with activation or expansion of CD8$^+$ T cells, but results in a greater production of cytokines.

Production of cytokines by CD8$^+$ T cells upon activation is primarily regulated at the level of gene expression either by transcription or mRNA stability. However, analysis of cytokine mRNA by quantitative RT-PCR showed no difference in the amounts of IFN-γ and IL-2 mRNA between activated MCJ-deficient and WT CD8$^+$ T cells (Figure 2F). Thus, MCJ had no effect on cytokine gene expression in CD8$^+$ T cells. A recent study reported that aerobic glycolysis promotes IFN-γ production at the translational level in effector CD4$^+$ T cells (Chang et al., 2013). However, intracellular staining analysis for IFN-γ showed no difference between WT and MCJ-deficient CD8$^+$ T cells (Figure 2G). Similarly, there was no difference in IL-2 intracellular staining (Figure 2G). Thus, the increased amounts of cytokines in MCJ-deficient CD8$^+$ T cell supernatants were not due to increased gene or protein expression.

Secretion of cytokines is another mechanism that regulates the overall amount of cytokines being produced, although little is known about the pathways involved. To investigate whether the increased IFN-γ in the supernatants of MCJ-deficient CD8$^+$ T cells was caused by enhanced secretion, we activated CD8$^+$ T cells with anti-CD3 and anti-CD28 Abs for 2 days, washed, and equal numbers of cells were incubated in medium alone without any additional stimuli for different periods of time. IFN-γ in the supernatants from MCJ-deficient CD8$^+$ T cells after 2 hr was higher than WT CD8$^+$ T cells (Figure 2H). IFN-γ in MCJ-deficient CD8$^+$ T cell supernatants continued increasing for at least 4 hr and then remained constant, while the amount secreted by WT CD8$^+$ T cells did not increase (Figure 2H). Treatment with cycloheximide (CHX), an inhibitor of protein synthesis, did not affect the IFN-γ produced during this period (Figure S2A), although CHX prevented new protein synthesis triggered by the activation of naive CD8$^+$ T cells (Figure S2B). These results further support the conclusion that increased protein translation was most likely not the primary cause of enhanced IFN-γ production by MCJ-deficient CD8$^+$ T cells. IL-2 and GM-CSF were also elevated in the supernatant of MCJ-deficient CD8$^+$ T cells after 4 hr (Figure S2C), indicating that the effect of MCJ on secretion is not restricted to IFN-γ. To further confirm the enhanced capacity of secretion by MCJ-deficient CD8$^+$ T cells, we performed ELISpot assays for IFN-γ. The number of spots with a larger area (high IFN-γ producers) was increased in MCJ-deficient CD8$^+$ T cells (Figure 2I). Enhanced secretion should result in lower accumulation of intracellular IFN-γ if no additional synthesis takes place. Intracellular staining for IFN-γ after activated cells were washed and incubated in medium alone showed lower IFN-γ in MCJ-deficient CD8$^+$ T cells after 1 hr (Figure S2D). Together these results indicate that MCJ deficiency augments cytokine production primarily by promoting the cytokine secretion capacity of effector CD8$^+$ T cells.

Localized Mitochondrial Production of ATP in the Absence of MCJ Promotes Cytokine Secretion

We used an unbiased metabolomics approach to investigate which metabolic pathways were regulated by MCJ in effector CD8$^+$ T cells. Metabolic profiling was obtained from equal numbers of WT and MCJ-deficient CD8$^+$ T cells after 2 days of activation and 4 hr of resting. Although no obvious phenotypic differences in terms of size or activation markers could be detected between the cell types, MCJ deficiency caused

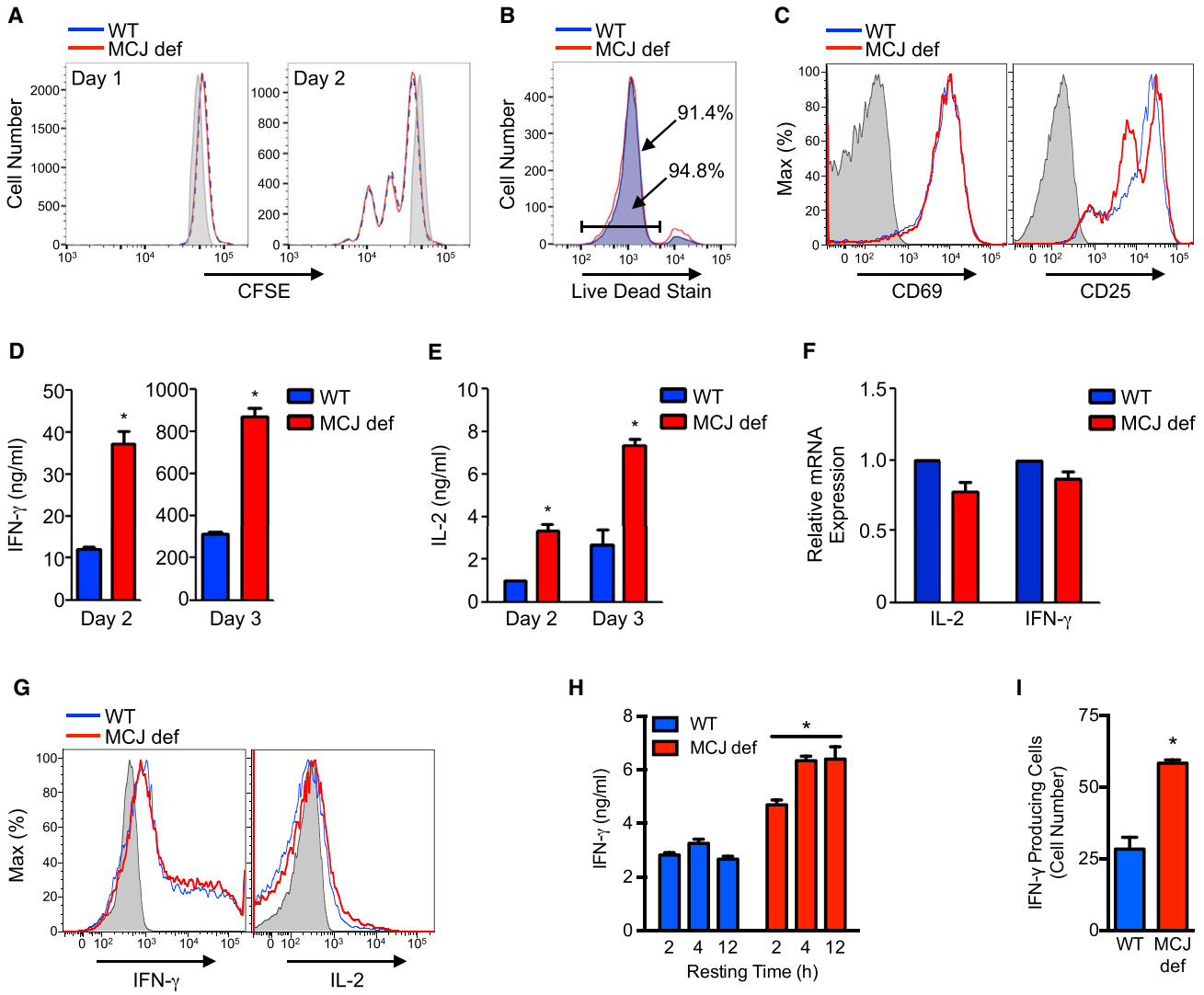

Figure 2. MCJ Deficiency Does Not Affect Effector CD8$^+$ T Cell Proliferation but Increases the Secretion of Cytokines

WT (blue) and MCJ-deficient CD8$^+$ T cells (MCJ def, red) were activated for 2 days with anti-CD3 and anti-CD28.

(A) Proliferation determined by CFSE staining. Grey histograms show unstimulated cells.

(B) Cell survival determined by Live Dead staining.

(C) Cell surface expression of CD69 and CD25. Grey histograms show unstained cells.

(D-E) Culture supernatants of activated cells were examined for (D) IFN-γ and (E) IL-2 by ELISA.

(F) IL-2 and IFN-γ mRNA expression determined by qRT-PCR.

(G) Intracellular staining for IFN-γ and IL-2. Grey histograms show unstained cells.

(H) Activated cells were washed and replated at equal numbers in medium alone. IFN-γ in the culture supernatants over time was determined by ELISA.

(I) Number of IFN-γ-producing cells determined by ELISpot assay. *$p < 0.05$ by unpaired t test. Avg ± SD ($n \geq 3$) shown. Results are representative of 2–3 experiments. See also Figure S2.

well-defined metabolic changes (Table S2). Similar to naive CD8$^+$ T cells, the absence of MCJ in activated CD8$^+$ T cells resulted in increased amounts of amino acids, but this increase was not restricted to essential amino acids (Figure 3A). In addition, a number of intermediate metabolites of the TCA and urea cycle pathways, two of the main mitochondrial pathways, were among the most elevated components in activated MCJ-deficient CD8$^+$ T cells relative to WT CD8$^+$ T cells (Table S2). Similar to naive CD8$^+$ T cells, succinate was also drastically increased in activated MCJ-deficient CD8$^+$ T cells, but fumarate, malate, and 2-hydroxyglutarate were also higher (Figure 3B). Citrulline and arginosuccinate, components of the urea cycle, were also increased (Figure 3C). Although there was no difference in proliferation, nucleotide pathways were also upregulated in the absence of MCJ (Figure 3D). Nucleotide synthesis is primarily cytosolic, however mitochondrial metabolic pathways feed into these pathways, as purine salvage reactions consume aspartate to produce fumarate and recover AMP upon deamination to IMP. Thus, an unbiased metabolic screening revealed increased mitochondrial activity in MCJ-deficient effector CD8$^+$ T cells.

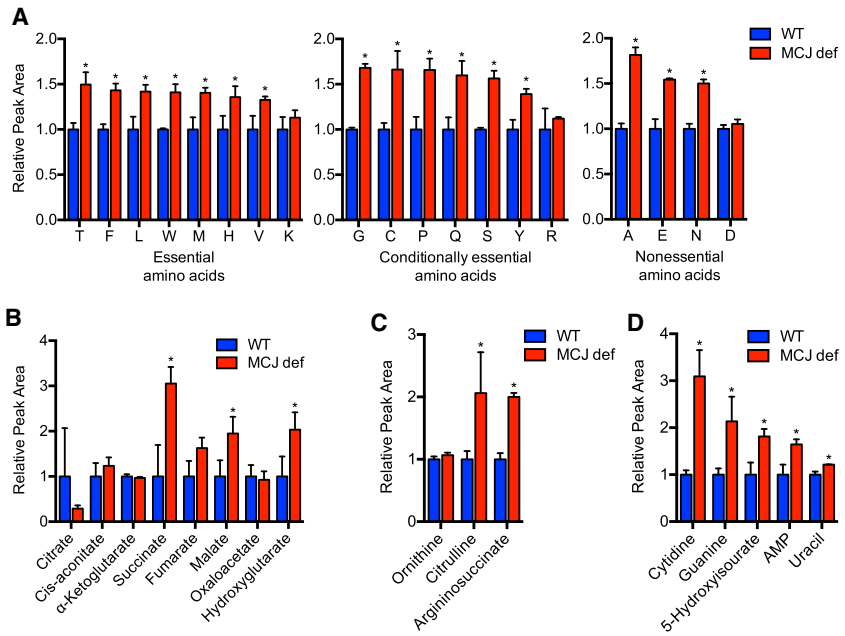

Figure 3. MCJ Deficiency Enhances Mitochondrial Metabolism in Effector CD8$^+$ T Cells

(A–D) WT (blue) and MCJ-deficient (MCJ def, red) CD8$^+$ T cells were activated for 2 days with anti-CD3 and anti-CD28, and metabolic profiles were determined by UPLC-MS. Relative peak areas of (A) amino acids and metabolites of the (B) TCA cycle, (C) urea cycle, and (D) nucleotide pathways shown. *$p < 0.05$ by unpaired t test. Avg ± SD (n = 3 mice) shown. See also Table S2.

Effector CD8$^+$ T cells are primarily glycolytic and use ATP from glycolysis instead of mitochondrial OXPHOS as the major source of energy. Because the absence of MCJ enhances overall mitochondrial activity, we examined intracellular ATP. Higher amounts of total ATP were present in MCJ-deficient CD8$^+$ T cells that were activated for 2 days and rested for 4 hr (Figure 4A). To determine whether this increased production of ATP resulted from increased mitochondrial respiration, we performed Seahorse MitoStress analysis. OCR was higher in activated MCJ-deficient CD8$^+$ T cells, as shown by the effect of oligomycin on baseline OCR (Figure 4B). These data indicate that the rate of ATP synthesis by mitochondria was increased in the absence of MCJ. In contrast, analysis of ECAR in response to glucose showed no difference between the two cell types (Figure 4C). Thus, loss of MCJ promotes mitochondrial respiration without altering the glycolytic rate of effector CD8$^+$ T cells.

The normal rate of glycolysis as determined by ECAR analysis correlated with the normal rate of proliferation and gene expression observed in MCJ-deficient CD8$^+$ T cells. While glycolysis-derived ATP represents the predominant source of energy and is sufficient for these processes in activated cells, mitochondrial-derived ATP could be essential for other CD8$^+$ T cell functions such as cytokine secretion. Due to the dynamic characteristics of mitochondria, this organelle could provide a subcellular microenvironment rich in ATP without the need to raise total cytosolic ATP. We investigated the presence of ATP-rich microdomains within activated CD8$^+$ T cells using a fluorescent probe used to identify ATP and ADP intracellular accumulation. Confocal microscopy of live cells showed only a few punctate ATP probe accumulations in activated WT CD8$^+$ T cells, while ATP puncta were abundant and prominent in MCJ-deficient CD8$^+$ T cells (Figure 4D). The subcellular ATP accumulation in MCJ-deficient CD8$^+$ T cells represented the mitochondrial-derived ATP pool since treatment with oligomycin prevented their formation (Figure S3A). Moreover, co-staining with the ATP probe and Mitotracker, a mitochondrial marker, revealed colocalization of the ATP puncta with mitochondria in activated MCJ-deficient CD8$^+$ T cells (Figure 4E). Thus, MCJ deficiency facilitates the formation of ATP-rich microdomains within activated CD8$^+$ T cells.

To address whether the increased secretion of IFN-γ found in MCJ-deficient CD8$^+$ T cells was mediated by increased mitochondrial ATP production, we activated CD8$^+$ T cells for 2 days and treated them with oligomycin during the last 4 hr of activation. Cells were then washed and incubated at equal numbers in medium alone for 4 hr. IFN-γ in the supernatants was determined by ELISA. Inhibition of mitochondrial ATP synthesis by oligomycin suppressed the enhanced secretion of IFN-γ by MCJ-deficient CD8$^+$ T cells (Figure 4F). In contrast, oligomycin did not reduce intracellular IFN-γ (Figure S3B). Thus, MCJ acts as an endogenous negative regulator of mitochondrial respiration, restricting the production of mitochondrial ATP and secretion of cytokines such as IFN-γ.

MCJ Attenuates Mitochondrial Metabolism during the Contraction Phase of Effector CD8$^+$ T Cells In Vivo

CD8$^+$ T cells reprogram their mitochondrial metabolism during the differentiation from naive to effector and from effector to memory stages. Memory CD8$^+$ T cells also have greater mitochondrial mass and maximum respiratory capacity (van der Windt et al., 2012). Because MCJ acts as an internal break for mitochondrial function in tissues with a high content of active mitochondria, we investigated MCJ expression during the contraction phase of effector CD8$^+$ T cells. To examine MCJ expression in individual cells, we used MCJ-deficient mice because they contain the β-galactosidase reporter gene inserted in the MCJ locus, and WT CD8$^+$ T cells served as negative controls (Figure S3C). We performed β-galactosidase activity assays by flow cytometry analysis in CD8$^+$ T cells that were freshly isolated, activated (effector), and rested in medium alone after activation (rested effector) to mimic the contraction phase of effector cells and development of memory cells. The frequency of MCJ-expressing cells was dramatically decreased in effector cells relative to naive cells (Figure 5A). We recently showed that Ikaros, a transcriptional repressor known to attenuate gene expression (John and Ward, 2011), binds the *Dnajc15* gene (encodes MCJ) promoter in macrophages to silence MCJ expression (Navasa et al., 2015b). Because Ikaros has been previously

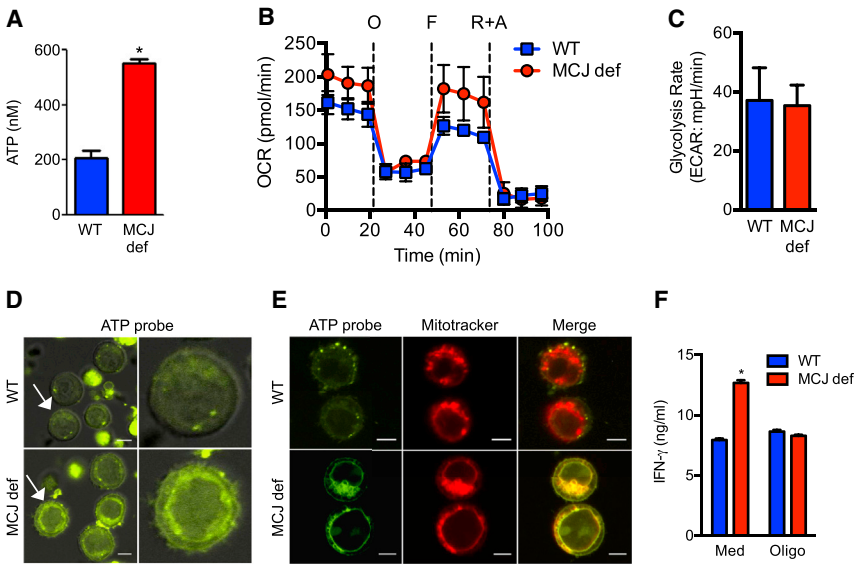

Figure 4. Increased Oxidative Phosphorylation in MCJ-Deficient Effector CD8$^+$ T Cells Facilitates IFN-γ Secretion

WT (blue) and MCJ-deficient CD8$^+$ T cells (MCJ def, red) were activated with anti-CD3 and anti-CD28 for 2 days.

(A) ATP concentration in cells rested in medium without stimuli for 4 hr.

(B) OCR of cells rested for 12 hr at baseline and in response to oligomycin (O), FCCP (F), and rotenone with antimycin (R+A) by Seahorse MitoStress assay.

(C) ECAR in cells after addition of glucose by Seahorse Glycolysis Stress assay.

(D) Live cells stained with ATP-probe (green) were visualized by confocal microscopy. Right panels show a magnification of the cells indicated by the white arrows.

(E) Live cells co-stained with ATP-probe (green) and Mitotracker (red) were visualized by confocal microscopy.

(F) Cells were incubated with oligomycin during the last 4 hr of activation and then rested for 4 hr. IFN-γ in the supernatants was determined by ELISA. *$p < 0.05$ by unpaired t test. Avg ± SD ($n \geq 3$) shown. Scale bar represents 10 nm. Results are representative of 2–3 experiments. See also Figure S3.

reported in CD8$^+$ T cells (O'Brien et al., 2014), we performed chromatin immunoprecipitation analysis (ChIP) to determine whether Ikaros also binds the *Dnajc15* promoter in CD8$^+$ T cells. Relative to naive CD8$^+$ T cells, greater Ikaros binding to the *Dnajc15* promoter was found in activated CD8$^+$ T cells (Figure 5B). Thus, MCJ is present in naive CD8$^+$ T cells as an additional checkpoint to restrict potential effector function.

The frequency of CD8$^+$ T cells expressing MCJ increased again when effector cells were rested in the presence of medium without additional stimuli (Figure 5A). During the contraction phase, effector CD8$^+$ T cells modulate their metabolism, become smaller and less active, and most die except for a few that survive to become memory cells (D'Cruz et al., 2009). We examined whether the observed re-acquisition of MCJ in resting effector CD8$^+$ T cells contributed to the attenuation of metabolism or cell survival in vitro during the contraction phase. CD8$^+$ T cells were activated for 2 days, washed, and then incubated in medium alone (without addition of cytokines). After 24 hr of resting, most WT and MCJ-deficient CD8$^+$ T cells remained alive (Figure 5C). However, after 48 hr only a few WT CD8$^+$ T cells remained alive, whereas many MCJ-deficient CD8$^+$ T cells were still viable even at 72 hr (Figure 5C). In addition, the surviving MCJ-deficient CD8$^+$ T cells maintain the "blastic cell stage" (large) reminiscent of effector cells (data not shown). Analysis of MMP in live cells after 48 hr of resting showed that a high proportion of WT CD8$^+$ T cells had low MMP (Figure 5D), similar to naive CD8$^+$ T cells (Figure S1A). In contrast, a large fraction of rested effector MCJ-deficient CD8$^+$ T cells displayed high MMP (Figure 5D). To determine whether the increased survival in rested MCJ-deficient CD8$^+$ T cells in vitro was due to their intrinsic metabolic state (high MMP) or due to increased IL-2 production that can promote cell expansion, a blocking anti-IL2 antibody was added during the resting period. No differences were detected in the survival of MCJ-deficient CD8$^+$ T cells after blocking IL-2 (Figure S3D). Furthermore, the addition of small amounts of recombinant IL-2 during the resting period resulted in increased expansion of both WT and MCJ-deficient CD8$^+$ T cells (Figure S3E). Thus, re-acquisition of MCJ in rested effector CD8$^+$ T cells contributes to the reduction of mitochondrial activity, restoration of a quiescent metabolic state and fitness impairment of effector CD8$^+$ T cells during the contraction phase in vitro.

To address the role of MCJ in the contraction phase of antigen-specific effector CD8$^+$ T cells in vivo, we crossed MCJ-deficient mice with OT-I TCR transgenic mice, which express a TCR that recognizes ovalbumin. MCJ deficiency did not affect the development of OT-I CD8$^+$ T cells (Figure S4A). Similar to polyclonal CD8$^+$ T cells, naive MCJ-deficient OT-I CD8$^+$ T cells also displayed high MMP relative to WT CD8$^+$ T cells (Figure 5E). CD8$^+$ T cells were purified from OT-I and MCJ-deficient OT-I mice, activated for 2 days in vitro, and then further expanded for 3 days. An equal number of cells from each genotype were combined and co-transferred into the same WT recipient mice (Figure 5F). After 2 weeks, donor cells present in LN and spleen of host mice were examined by flow cytometry using CD90.1 and CD90.2 markers (Figures S4B and S4C). Phenotypic characterization of the cells based on CD44 and CD62L (memory and homing markers) as well as KLRG1 and CD127 (markers that define subsets of long-lived effector and memory T cells; Jameson and Masopust, 2009; Kaech and Wherry, 2007; Sarkar et al., 2008) did not show differences between WT and MCJ-deficient CD8$^+$ OT-I T cells (Figures S4B and S4C). The overall percentage of cell recovery in both donors was comparable (data not shown). However, as determined by forward scatter (Figure 5G), only a few WT OT-I CD8$^+$ T cells showed a large blastic phenotype (Figure 5H). In contrast, a greater fraction of MCJ-deficient OT-I CD8$^+$ T cells displayed the large blastic phenotype (Figure 5H). Thus, in vivo MCJ does not seem to contribute to cell survival but does participate in the attenuation of metabolism during the transition from effector to rested effector cells.

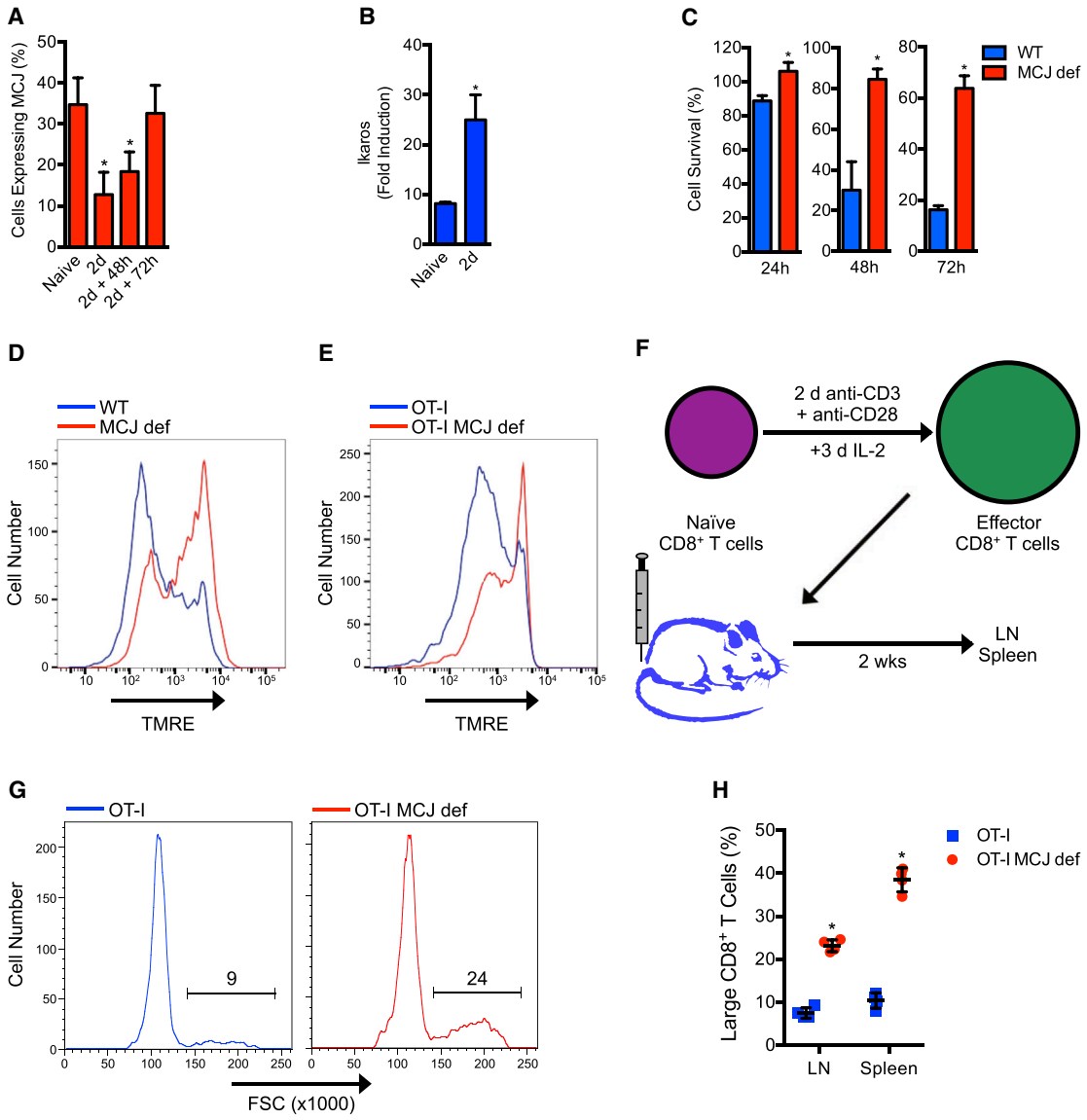

Figure 5. MCJ Deficiency Sustains the Metabolic Activity of Effector CD8$^+$ T Cells during the Contraction Phase

WT (blue) and MCJ-deficient CD8$^+$ T cells (MCJ def, red).

(A) Frequency of β-galactosidase$^+$ MCJ-deficient CD8$^+$ T cells that were naive, activated for 2 days with anti-CD3 and anti-CD28, or activated for 2 days and then rested in medium without stimuli for 48 hr (2 days + 48 hr) or 72 hr (2 days +72 hr) as determined by flow cytometry analysis.

(B) Ikaros binding to the *Dnajc15* gene (encodes MCJ) promoter in naive and activated (2 days) cells by ChIP assay. Fold increase over rabbit IgG immunoprecipitates relative to input shown.

(C) Cells were activated for 2 days, washed, and rested in medium. The number of live cells recovered relative to the initial number is shown.

(D) MMP was examined by TMRE staining in cells activated for 2 days and rested for 48 hr.

(E) MMP in freshly isolated OT-I and MCJ-deficient OT-I CD8$^+$ T cells.

(F–H) OT-I (CD90.1$^+$) and MCJ-deficient OT-I (CD90.1$^+$ CD90.2$^+$) CD8$^+$ T cells were activated for 2 days and then expanded with IL-2 for 3 days. Equal numbers of each cell type were then adoptively transferred into WT (CD90.2$^+$) recipient mice. LN and spleen of recipients were harvested after 2 weeks and analyzed for donor cells.

(G and H) Forward scatter of CD8$^+$ OT-I T cells as determined by flow cytometry analysis. *$p < 0.05$ by unpaired t test. Avg ± SD ($n \geq 3$) shown. Results are representative of 2–3 experiments. See also Figures S3 and S4.

MCJ Deficiency Enhances the Antiviral Protective Activity of Memory CD8$^+$ T Cells

Memory CD8$^+$ T cells are believed to play an important role in protection against influenza viral infection (La Gruta and Turner, 2014). Recent studies indicate that increased mitochondrial respiration in CD8$^+$ T cells results in increased memory activity (van der Windt et al., 2013). We investigated the role of MCJ in protective memory CD8$^+$ T cell responses using an influenza virus infection model. WT and MCJ-deficient mice were intranasally infected with a sublethal dose of influenza A/Puerto

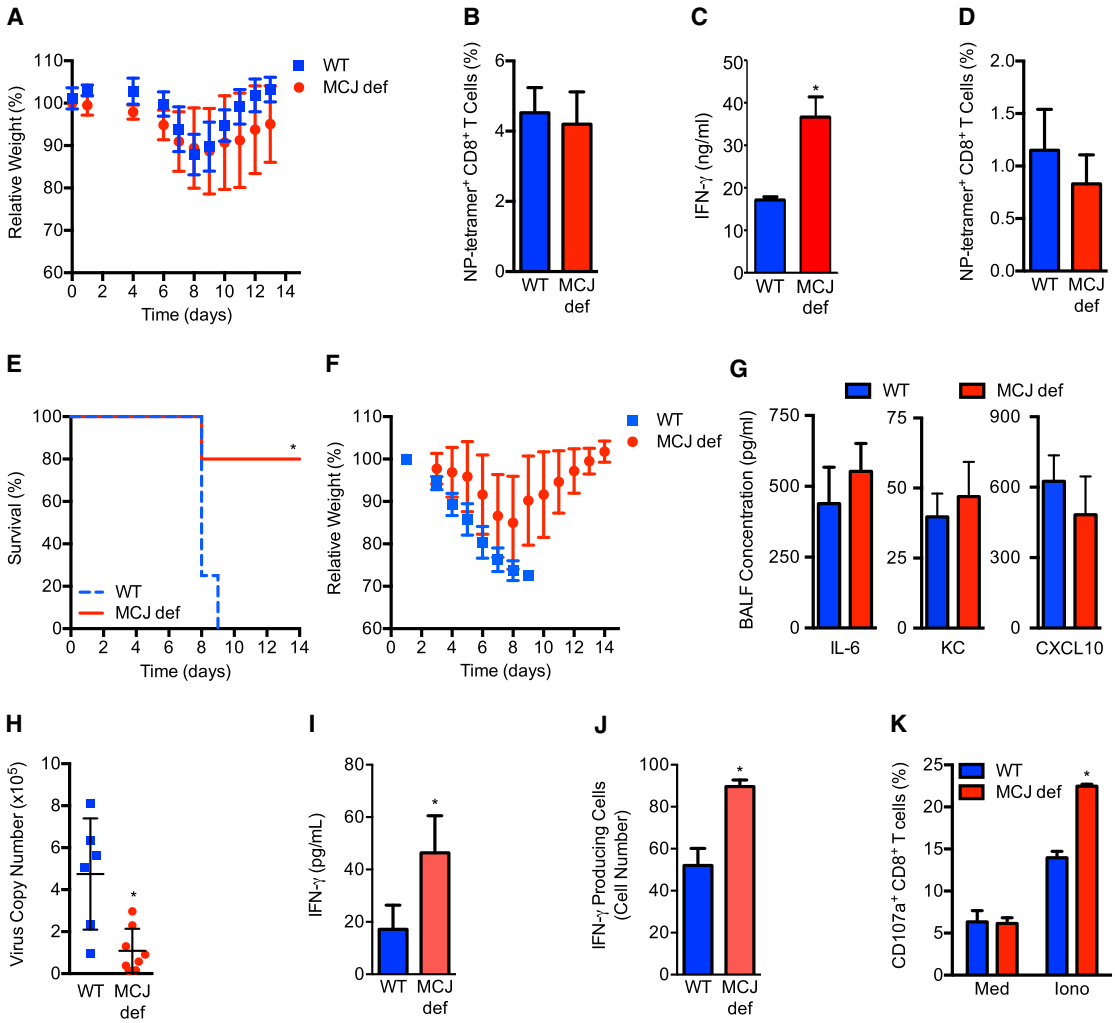

Figure 6. Loss of MCJ Confers Viral Protective Activity to Memory CD8$^+$ T Cells

WT (blue) and MCJ-deficient CD8$^+$ T cells (MCJ def, red).

(A–D) Mice were infected with a sublethal dose of PR8 virus (primary infection). (A) Percent weight loss over time. (B) Percentage of NP-tetramer$^+$ cells in the spleen 2 weeks post infection. (C) Ex vivo IFN-γ production of cells isolated from the spleen and MLN 2 weeks post infection by ELISA. (D) Percentage of NP-tetramer$^+$ cells from the spleen and MLN of mice 5 weeks post infection.

(E–K) Mice were infected with a sublethal dose of PR8 virus (primary infections). CD8$^+$ T cells were isolated 5 weeks post infection and adoptively transferred into naive WT recipients, which were then infected with a lethal dose of PR8 virus. (E) Survival and (F) percent weight loss over time. (G–K) Recipients were sacrificed 6 days post lethal infection. (G) BALF cytokines and chemokines. (H) Lung PR8 virus titer by qRT-PCR. (I) Ex vivo production of IFN-γ by MLN-CD8$^+$ T cells by ELISA. (J) IFN-γ secretion by lung CD8$^+$ T cells by ELISpot assay. (K) CD107a mobilization assay of MLN CD8$^+$ T cells cultured with (Iono) or without (Med) ionomycin. *$p < 0.05$ by log-rank test for Kaplan-Meier survival curve and by unpaired t test for all others. Avg ± SD ($n \geq 3$) shown. Results are representative of 2–3 experiments. See also Figures S5 and S6.

Rico/8/34 (PR8) H1N1 virus. As expected, based on the predominant role of innate immunity in primary infection with influenza virus, no significant differences were observed in weight loss and recovery or survival between infected WT and MCJ-deficient mice during primary infection (Figure 6A). Analysis of influenza NP-tetramer$^+$ CD8$^+$ T cells 2 weeks post-infection also showed a similar frequency between infected WT and MCJ-deficient mice (Figure 6B), indicating that the loss of MCJ did not affect the expansion of effector CD8$^+$ T cells in vivo, consistent with the in vitro studies. However, ex vivo analysis of IFN-γ production by CD8$^+$ T cells showed higher IFN-γ in the supernatants of MCJ-deficient CD8$^+$ T cells (Figure 6C). Thus, MCJ deficiency results in increased IFN-γ production by effector CD8$^+$ T cells in vivo during virus infection.

We then addressed whether the lack of MCJ could affect memory CD8$^+$ T cell development. Analysis of influenza NP-tetramer$^+$ CD8$^+$ T cells 3 and 5 weeks post-infection showed a lower percentage relative to 2 weeks post-infection as expected, but there was no difference in the frequency between WT and MCJ-deficient mice (Figures S5A and 6B). This further supported the finding that lack of MCJ does not affect cell survival during the generation of memory CD8$^+$ T cells from effector cells in vivo. Phenotypic analysis of NP-tetramer$^+$ CD8$^+$ T cells for CD44, CD62L, KLRG1, and CD127 showed no substantial difference

between WT and MCJ-deficient CD8$^+$ T cells (Figure S5B and data not shown). Lower CD27 expression was found in the MCJ-deficient CD8$^+$ T cell memory population (Figure S5B). CD27^{low} memory cells mediate rapid protective immunity against acute infection and manifest high cytolytic activity (Olson et al., 2013).

To investigate the protective capacity of memory MCJ-deficient CD8$^+$ T cells, we performed adoptive transfer of equal numbers WT and MCJ-deficient CD8$^+$ T cells obtained five weeks post-infection separately into WT recipient mice. Recipient mice were then infected with a lethal dose of PR8 virus. As expected, recipient mice that received cells from infected WT mice were not protected, did not recover their weight, and died between 8 and 9 days post lethal infection (Figures 6E and 6F). In contrast, most recipient mice that received cells from infected MCJ-deficient mice were protected and survived (Figure 6E). Mice receiving MCJ-deficient CD8$^+$ T cells lost weight initially, indicating that they had been infected, but they recovered to a healthy state (Figure 6F). Thus, the absence of MCJ in memory CD8$^+$ T cells confers greater protective capacity against influenza virus infection.

Death caused by some of the highly pathogenic influenza viruses (such as H5N1 influenza) is often associated with a strong systemic immune response and cytokine storm. To rule out that the death of the recipients of WT CD8$^+$ T cells was caused by an exuberant immune response, we examined cytokine production 6 days post-infection with the lethal dose. The concentration of inflammatory cytokines (IL-6, KC) and chemokines (CXCL10) in brochoalveolar lavage fluid (BALF) (Figure 6G) and serum (systemic) (Figure S6A) were comparable. These results indicate that the protection found in mice that received MCJ-deficient CD8$^+$ T cells was not due to an attenuated immune response relative to mice that received WT CD8$^+$ T cells.

To investigate whether the protective capacity of memory MCJ-deficient CD8$^+$ T cells was due to an improved effector function to clear virus, we examined PR8 virus titers in the lung of recipient mice 6 days post-infection with the lethal dose. Higher virus titers were present in host mice that received WT CD8$^+$ T cells (Figure 6H), indicating that memory MCJ-deficient CD8$^+$ T cells were more efficient in clearing influenza virus. To examine the effector function of memory MCJ-deficient CD8$^+$ T cells, we isolated CD8$^+$ T cells from the mediastinal LN (MLN) 6 days after the lethal infection and determined ex vivo IFN-γ production by culturing cells in medium without stimuli. IFN-γ was higher in MCJ-deficient CD8$^+$ T cells (Figure 6I); however, the NP-tetramer$^+$ cell frequency was not different (Figure S6B). Ex vivo IFN-γ production by MCJ-deficient CD8$^+$ T cells isolated from the lung was also increased (Figure S6C), as was the number of IFN-γ-secreting cells as determined by ELISpot assay (Figure 6J). However, the frequency of NP-tetramer$^+$ CD8$^+$ T cells in the lung was comparable (Figure S6D), showing a great secretory capacity of memory MCJ-deficient CD8$^+$ T cells.

Secretion of granules by exocytosis is dependent on both Ca^{2+} and ATP. We investigated whether increased mitochondrial ATP production in MCJ-deficient CD8$^+$ T cells could also facilitate an increase in exocytosis of cytotoxic granules present in effector cells by CD107a mobilization assay. CD8$^+$ T cells were isolated from the MLN 6 days after lethal infection and incubated in medium containing monensin with or without ionomycin to provide the Ca^{2+} signal. The frequency of CD107a$^+$ MCJ-deficient CD8$^+$ T cells treated with ionomycin was significantly higher than WT CD8$^+$ T cells (Figure 6K), indicating that MCJ-deficient CD8$^+$ T cells have a greater capacity to function as cytotoxic cells. Thus, increased mitochondrial respiration caused by the loss of MCJ in CD8$^+$ T cells results in increased antiviral protective activity during memory responses by enhancing the secretion both of effector cytokines as well as cytotoxic granules.

DISCUSSION

Mitochondria play a key role in balancing cellular metabolism primarily as the site for OXPHOS through the ETC and as a source of ATP. Recently, it has become clear that tight regulation of mitochondrial metabolism occurs during the reprograming of CD8$^+$ T cells. A number of molecules have been shown to be required for maximum efficiency of the ETC and OXPHOS. However, very little is known about negative regulatory mechanisms that restrict mitochondrial respiration. We have recently identified MCJ as one of the first known negative regulators of complex I activity through its effect on the formation of respiratory supercomplexes (Hatle et al., 2013). Our earlier studies demonstrated that the absence of MCJ prevents the development of steatosis by accelerating fatty-acid metabolism within the liver (Hatle et al., 2013). Here we have shown that MCJ restrains mitochondrial respiration in CD8$^+$ T cells. In the absence of this natural break, CD8$^+$ T cells have enhanced OXPHOS leading to increased secretion of cytokines by effector CD8$^+$ T cells. In addition, MCJ deficiency interferes with the metabolic adaptation during the contraction phase of effector CD8$^+$ T cells and results in greater antiviral protective activity of memory CD8$^+$ T cells.

Effector and memory CD8$^+$ T cells need ATP for effector functions in addition to cell growth and expansion. While CD8$^+$ T cells primarily use glycolysis instead of OXPHOS for proliferation (Frauwirth et al., 2002; Macintyre et al., 2011) other sources might provide the ATP required for processes with high ATP consumption. Production of some cytokines by effector CD8$^+$ T cells is not affected by strong inhibition of glycolysis (Cham et al., 2008), and cytotoxic activity can take place in the absence of glucose (MacDonald and Koch, 1977). Considering the dynamic aspect of mitochondria as organelles that can rapidly relocate in the cytosol, it is quite possible that mitochondria can create a microenvironment that is highly rich in ATP in specific locations without elevating overall cytosolic ATP. Mitochondria have been shown to relocate to the edge of lamellipodia and are critical for providing the energy for migration of cells (Morlino et al., 2014). Our studies revealed the presence of microenvironments where ATP and ADP accumulate in CD8$^+$ T cells located in the proximity of mitochondria. Here we have shown that increased mitochondrial respiration in CD8$^+$ T cells lacking MCJ had no effect on CD8$^+$ T cell proliferation or cytokine gene expression, but it enhanced the secretion of cytokines such as IFN-γ. Little is known about the mechanisms of cytokine secretion in T cells; however, secretion of intracellular components often is dependent on ATP (Jena, 2013; Monteleone et al., 2015) and the source of this ATP, whether mitochondrial or cytosolic, has yet to be

determined. Secretion of IFN-γ by CD8$^+$ T cells in the absence of MCJ is dependent on ATP derived from mitochondria. Thus, through OXPHOS mitochondria can regulate effector function of CD8$^+$ T cells independently of cell expansion.

The presence of respiratory supercomplexes in mammalian cells has been demonstrated in tissues such as heart. Respirasomes bring the individual complexes together to facilitate the efficient transfer of electrons between complexes while preventing electron leak and, thereby, production of ROS. Here we revealed the presence of supercomplexes in naive CD8$^+$ T cells and increased supercomplex formation in the absence of MCJ. Naive CD8$^+$ T cells primarily use mitochondria and OXPHOS relative to activated CD8$^+$ T cells; however, mitochondrial ROS are almost undetectable (Hatle et al., 2013). It is possible that the presence of supercomplexes prevents the formation of ROS and enhances survival of naive cells. Although increased MMP is normally associated with increased ROS, in MCJ-deficient CD8$^+$ T cells MMP is higher but ROS is not (Hatle et al., 2013). This is most likely due to abundance of supercomplexes in these cells. To date, there is no clear evidence that complex II (succinate dehydrogenase) is also recruited to supercomplexes. Because complex III receives electrons from both complex I and complex II, the recruitment of complex III to supercomplexes might cause an uncoupling of complex III from complex II. Therefore, the attenuation of complex II activity in the absence of MCJ could be a mechanism to prevent electron leakage since its corresponding acceptor, complex III, is sequestered, explaining the accumulation of succinate in MCJ-deficient CD8$^+$ T cells.

Memory CD8$^+$ T cells utilize mitochondrial respiration for both their generation and effector function. However, instead of using glucose to feed mitochondrial respiration through pyruvate, memory CD8$^+$ T cells perform β-oxidation of fatty acids. Recently, it has been shown that these cells utilize lipolysis to generate their own fuel (O'Sullivan et al., 2014). Pathways leading to increased mitochondrial respiration are associated with a superior memory CD8$^+$ T cell response. In our study, we have identified MCJ as an endogenous negative regulator of OXPHOS in CD8$^+$ T cells. Lack of MCJ sustained the active metabolism of effector CD8$^+$ T cells during the contraction phase and resulted in greater effector memory CD8$^+$ T cell responses to influenza virus. Although MCJ deficiency had an impact in the metabolic adaptation during the contraction phase of effector CD8$^+$ T cells, it did not seem to have a substantial effect on overall survival of those effector cells in vivo. MCJ deficiency appeared to provide a survival advantage to effector cells when these cells were rested in medium alone without additional cytokines in vitro. This is most likely due to the fact that during in vitro resting effector WT CD8$^+$ T cells undergo cytokine withdrawal. We also show here that WT memory CD8$^+$ T cells alone failed to provide protection against a lethal dose of influenza virus. Strikingly, MCJ-deficient memory CD8$^+$ T cells were highly protective against lethal infection with influenza. Using the LCMV infection model, it has been shown that CD4$^+$ T cells can rescue exhausted CD8$^+$ T cells during chronic viral infection (Aubert et al., 2011). We also observed that a small frequency of CD4$^+$ T cells was sufficient for WT memory CD8$^+$ T cells to provide protection against influenza virus infection (data not shown). Because MCJ deficiency results in enhanced CD8$^+$ T cell responses, it is not evolutionarily clear why MCJ is expressed in CD8$^+$ T cells. While CD8$^+$ T cells are key for protection, an exaggerated cytotoxic CD8$^+$ T cell response could cause non-specific tissue damage. We propose that MCJ was acquired in CD8$^+$ T cells as a strategy to restrain their metabolism and prevent a prolonged effector function that could be harmful.

EXPERIMENTAL PROCEDURES

Mice

Mouse strains used were C57BL/6J (WT), MCJ-deficient C57BL/6 (Hatle et al., 2013), OT-I TCR transgenic, and MCJ-deficient OT-I. All mice were maintained at the University of Vermont animal care facility and used under procedures approved by the University of Vermont Institutional Animal Care and Use Committee (IACUC).

Cell Preparation and Culture

Cells were purified by negative selection or positive selection using the MACS Cell Separation System (Miltenyi). Cytokine production was determined by ELISA. Detailed protocols are described in Supplemental Experimental Procedures.

Extracellular Flux Analysis

Oxygen consumption (OCR) and extracellular acidification rates (ECAR) were analyzed using a XF24 Extracellular Flux analyzer (Seahorse Bioscience). Detailed protocols are described in Supplemental Experimental Procedures.

Intracellular ATP Concentration

ATP concentration was determined using the ATPlite Luminescence Assay System and a TD-20/20 Luminometer. Detailed protocols are described in Supplemental Experimental Procedures.

Flow Cytometry Analyses

Flow cytometry analyses were performed using an LSRII Flow Cytometer (BD Biosciences). Cell proliferation, survival, and MMP were determined using CFSE, Live Dead Cell Viability Assay, and TMRE (Molecular Probes). β-galactosidase activity was determined using the FACS Fluorescent Blue lacZ β-Galactosidase Detection Kit (Marker Gene Technologies). Intracellular cytokine staining was performed without brefeldin A or monensin. CD107a mobilization assay was performed using monensin and anti-CD107a-PE (Biolegend) with or without ionomycin. Detailed protocols are described in Supplemental Experimental Procedures.

Chromatin Immunoprecipitation

ChIP assays were performed using the SimpleChip Enzymatic Chromatin IP Kit (Cell Signaling) with anti-Ikaros or rabbit IgG. Detailed protocols are described in Supplemental Experimental Procedures.

Influenza Infection and Analyses

Mice were infected intranasally with a sublethal dose of PR8 virus. CD8$^+$ T cells were isolated after 5 weeks, equal numbers of NP tetramer$^+$ cells were transferred to naive WT mice. Recipients were infected with a lethal dose and sacrificed 6 days later. CD8$^+$ T cells from the MLN and lung were examined for ex vivo IFN-γ production by ELISA and/or ELISpot and for effector and memory cell surface markers, NP-tetramer$^+$ cell frequency, and/or CD107a mobilization by flow cytometry. BALF and serum were analyzed by Luminex assay (Millipore). Lung was examined for PR8 virus titer by qRT-PCR for acid polymerase. Detailed protocols are described in Supplemental Experimental Procedures.

Confocal Microscopy

Cells were examined by confocal microscopy using ATP probe and/or Mitotracker and a Zeiss LSM 510 Meta Confocal Laser Scanning microscope (Carl Zeiss Microscopy). Detailed protocols are described in Supplemental Experimental Procedures.

Statistical Analyses

Statistical significance was determined by t test or long-rank test. Bars represent avg ± SD or SEM as indicated. $p < 0.05$ was considered statistically significant.

SUPPLEMENTAL INFORMATION

Supplemental Information includes six figures, two tables, and Supplemental Experimental Procedures and can be found with this article online at http://dx.doi.org/10.1016/j.immuni.2016.02.018.

AUTHOR CONTRIBUTIONS

D.P.C., K.A.F., A.D., T.M.T., R.Y., and J.A. conceived and designed experiments, acquired and interpreted data, and drafted and revised the manuscript. K.M.H., D.T., J.T.-C., and L.H. conceived and designed experiments and acquired and interpreted data. Y.W.J., K.H.A., and K.C.H. conceived and designed experiments. M.R. conceived and designed the study, acquired and interpreted data, and drafted and revised the manuscript.

ACKNOWLEDGMENTS

We thank the University of Vermont DNA Analysis Facility, Flow Cytometry and Cell Sorting Facility and Microscopy Imaging Center. We thank E. Atondo, I. Martín-Ruiz, P. Gummadidala, and B. Silverstrim for technical support. This work was supported by NIH grants AI110016 (M.R.) and GM103496 (M.R. and K.M.H.). J.A. was partially funded by the Spanish Ministry of Economy Plan Nacional grant SAF2012-34610. R.Y. was supported by an AAI Careers in Immunology Fellowship.

Received: September 4, 2015
Revised: February 18, 2016
Accepted: February 18, 2016
Published: May 24, 2016

REFERENCES

Acín-Pérez, R., Fernández-Silva, P., Peleato, M.L., Pérez-Martos, A., and Enriquez, J.A. (2008). Respiratory active mitochondrial supercomplexes. Mol. Cell *32*, 529–539.

Araki, K., Turner, A.P., Shaffer, V.O., Gangappa, S., Keller, S.A., Bachmann, M.F., Larsen, C.P., and Ahmed, R. (2009). mTOR regulates memory CD8 T-cell differentiation. Nature *460*, 108–112.

Aubert, R.D., Kamphorst, A.O., Sarkar, S., Vezys, V., Ha, S.J., Barber, D.L., Ye, L., Sharpe, A.H., Freeman, G.J., and Ahmed, R. (2011). Antigen-specific CD4 T-cell help rescues exhausted CD8 T cells during chronic viral infection. Proc. Natl. Acad. Sci. USA *108*, 21182–21187.

Carr, E.L., Kelman, A., Wu, G.S., Gopaul, R., Senkevitch, E., Aghvanyan, A., Turay, A.M., and Frauwirth, K.A. (2010). Glutamine uptake and metabolism are coordinately regulated by ERK/MAPK during T lymphocyte activation. J. Immunol. *185*, 1037–1044.

Cham, C.M., Driessens, G., O'Keefe, J.P., and Gajewski, T.F. (2008). Glucose deprivation inhibits multiple key gene expression events and effector functions in CD8+ T cells. Eur. J. Immunol. *38*, 2438–2450.

Chang, C.H., Curtis, J.D., Maggi, L.B., Jr., Faubert, B., Villarino, A.V., O'Sullivan, D., Huang, S.C., van der Windt, G.J., Blagih, J., Qiu, J., et al. (2013). Posttranscriptional control of T cell effector function by aerobic glycolysis. Cell *153*, 1239–1251.

D'Cruz, L.M., Rubinstein, M.P., and Goldrath, A.W. (2009). Surviving the crash: transitioning from effector to memory CD8+ T cell. Semin. Immunol. *21*, 92–98.

Frauwirth, K.A., Riley, J.L., Harris, M.H., Parry, R.V., Rathmell, J.C., Plas, D.R., Elstrom, R.L., June, C.H., and Thompson, C.B. (2002). The CD28 signaling pathway regulates glucose metabolism. Immunity *16*, 769–777.

Hatle, K.M., Neveu, W., Dienz, O., Rymarchyk, S., Barrantes, R., Hale, S., Farley, N., Lounsbury, K.M., Bond, J.P., Taatjes, D., and Rincón, M. (2007). Methylation-controlled J protein promotes c-Jun degradation to prevent ABCB1 transporter expression. Mol. Cell. Biol. *27*, 2952–2966.

Hatle, K.M., Gummadidala, P., Navasa, N., Bernardo, E., Dodge, J., Silverstrim, B., Fortner, K., Burg, E., Suratt, B.T., Hammer, J., et al. (2013). MCJ/DnaJC15, an endogenous mitochondrial repressor of the respiratory chain that controls metabolic alterations. Mol. Cell. Biol. *33*, 2302–2314.

Jameson, S.C., and Masopust, D. (2009). Diversity in T cell memory: an embarrassment of riches. Immunity *31*, 859–871.

Jena, B.P. (2013). Porosome: the secretory NanoMachine in cells. Methods Mol. Biol. *931*, 345–365.

John, L.B., and Ward, A.C. (2011). The Ikaros gene family: transcriptional regulators of hematopoiesis and immunity. Mol. Immunol. *48*, 1272–1278.

Kaech, S.M., and Wherry, E.J. (2007). Heterogeneity and cell-fate decisions in effector and memory CD8+ T cell differentiation during viral infection. Immunity *27*, 393–405.

La Gruta, N.L., and Turner, S.J. (2014). T cell mediated immunity to influenza: mechanisms of viral control. Trends Immunol. *35*, 396–402.

MacDonald, H.R., and Koch, C.J. (1977). Energy metabolism and T-cell-mediated cytolysis. I. Synergism between inhibitors of respiration and glycolysis. J. Exp. Med. *146*, 698–709.

Macintyre, A.N., Finlay, D., Preston, G., Sinclair, L.V., Waugh, C.M., Tamas, P., Feijoo, C., Okkenhaug, K., and Cantrell, D.A. (2011). Protein kinase B controls transcriptional programs that direct cytotoxic T cell fate but is dispensable for T cell metabolism. Immunity *34*, 224–236.

Monteleone, M., Stow, J.L., and Schroder, K. (2015). Mechanisms of unconventional secretion of IL-1 family cytokines. Cytokine *74*, 213–218.

Moreno-Lastres, D., Fontanesi, F., García-Consuegra, I., Martín, M.A., Arenas, J., Barrientos, A., and Ugalde, C. (2012). Mitochondrial complex I plays an essential role in human respirasome assembly. Cell Metab. *15*, 324–335.

Morlino, G., Barreiro, O., Baixauli, F., Robles-Valero, J., González-Granado, J.M., Villa-Bellosta, R., Cuenca, J., Sánchez-Sorzano, C.O., Veiga, E., Martín-Cófreces, N.B., and Sánchez-Madrid, F. (2014). Miro-1 links mitochondria and microtubule Dynein motors to control lymphocyte migration and polarity. Mol. Cell. Biol. *34*, 1412–1426.

Navasa, N., Martín, I., Iglesias-Pedraz, J.M., Beraza, N., Atondo, E., Izadi, H., Ayaz, F., Fernández-Álvarez, S., Hatle, K., Som, A., et al. (2015a). Regulation of oxidative stress by methylation-controlled J protein controls macrophage responses to inflammatory insults. J. Infect. Dis. *211*, 135–145.

Navasa, N., Martin-Ruiz, I., Atondo, E., Sutherland, J.D., Angel Pascual-Itoiz, M., Carreras-González, A., Izadi, H., Tomás-Cortázar, J., Ayaz, F., Martin-Martin, N., et al. (2015b). Ikaros mediates the DNA methylation-independent silencing of MCJ/DNAJC15 gene expression in macrophages. Sci. Rep. *5*, 14692.

O'Brien, S., Thomas, R.M., Wertheim, G.B., Zhang, F., Shen, H., and Wells, A.D. (2014). Ikaros imposes a barrier to CD8+ T cell differentiation by restricting autocrine IL-2 production. J. Immunol. *192*, 5118–5129.

O'Sullivan, D., van der Windt, G.J., Huang, S.C., Curtis, J.D., Chang, C.H., Buck, M.D., Qiu, J., Smith, A.M., Lam, W.Y., DiPlato, L.M., et al. (2014). Memory CD8(+) T cells use cell-intrinsic lipolysis to support the metabolic programming necessary for development. Immunity *41*, 75–88.

Olson, J.A., McDonald-Hyman, C., Jameson, S.C., and Hamilton, S.E. (2013). Effector-like $CD8^+$ T cells in the memory population mediate potent protective immunity. Immunity *38*, 1250–1260.

Pearce, E.L., Walsh, M.C., Cejas, P.J., Harms, G.M., Shen, H., Wang, L.S., Jones, R.G., and Choi, Y. (2009). Enhancing CD8 T-cell memory by modulating fatty acid metabolism. Nature *460*, 103–107.

Pearce, E.L., Poffenberger, M.C., Chang, C.H., and Jones, R.G. (2013). Fueling immunity: insights into metabolism and lymphocyte function. Science *342*, 1242454.

Sarkar, S., Kalia, V., Haining, W.N., Konieczny, B.T., Subramaniam, S., and Ahmed, R. (2008). Functional and genomic profiling of effector CD8 T cell subsets with distinct memory fates. J. Exp. Med. *205*, 625–640.

Schusdziarra, C., Blamowska, M., Azem, A., and Hell, K. (2013). Methylation-controlled J-protein MCJ acts in the import of proteins into human mitochondria. Hum. Mol. Genet. *22*, 1348–1357.

Shridhar, V., Bible, K.C., Staub, J., Avula, R., Lee, Y.K., Kalli, K., Huang, H., Hartmann, L.C., Kaufmann, S.H., and Smith, D.I. (2001). Loss of expression of a new member of the DNAJ protein family confers resistance to chemotherapeutic agents used in the treatment of ovarian cancer. Cancer Res. *61*, 4258–4265.

Strathdee, G., Davies, B.R., Vass, J.K., Siddiqui, N., and Brown, R. (2004). Cell type-specific methylation of an intronic CpG island controls expression of the MCJ gene. Carcinogenesis *25*, 693–701.

Strathdee, G., Vass, J.K., Oien, K.A., Siddiqui, N., Curto-Garcia, J., and Brown, R. (2005). Demethylation of the MCJ gene in stage III/IV epithelial ovarian cancer and response to chemotherapy. Gynecol. Oncol. *97*, 898–903.

van der Windt, G.J., and Pearce, E.L. (2012). Metabolic switching and fuel choice during T-cell differentiation and memory development. Immunol. Rev. *249*, 27–42.

van der Windt, G.J., Everts, B., Chang, C.H., Curtis, J.D., Freitas, T.C., Amiel, E., Pearce, E.J., and Pearce, E.L. (2012). Mitochondrial respiratory capacity is a critical regulator of CD8+ T cell memory development. Immunity *36*, 68–78.

van der Windt, G.J., O'Sullivan, D., Everts, B., Huang, S.C.-C., Buck, M.D., Curtis, J.D., Chang, C.H., Smith, A.M., Ai, T., Faubert, B., et al. (2013). CD8 memory T cells have a bioenergetic advantage that underlies their rapid recall ability. Proc. Natl. Acad. Sci. USA *110*, 14336–14341.

Wang, R., and Green, D.R. (2012). Metabolic reprogramming and metabolic dependency in T cells. Immunol. Rev. *249*, 14–26.

Wang, R., Dillon, C.P., Shi, L.Z., Milasta, S., Carter, R., Finkelstein, D., McCormick, L.L., Fitzgerald, P., Chi, H., Munger, J., and Green, D.R. (2011). The transcription factor Myc controls metabolic reprogramming upon T lymphocyte activation. Immunity *35*, 871–882.

Yang, R., Lirussi, D., Thornton, T.M., Jelley-Gibbs, D.M., Diehl, S.A., Case, L.K., Madesh, M., Taatjes, D.J., Teuscher, C., Haynes, L., and Rincón, M. (2015). Mitochondrial Ca^{2+} and membrane potential, an alternative pathway for Interleukin 6 to regulate CD4 cell effector function. eLife *4*, 4.

PLOS | PATHOGENS

RESEARCH ARTICLE

Enhanced control of *Mycobacterium tuberculosis* extrapulmonary dissemination in mice by an arabinomannan-protein conjugate vaccine

Rafael Prados-Rosales[1,2‡]*, Leandro Carreño[1,3], Tingting Cheng[1,4], Caroline Blanc[1,4], Brian Weinrick[1,5], Adel Malek[1,5], Todd L. Lowary[6], Andres Baena[7], Maju Joe[6], Yu Bai[6], Rainer Kalscheuer[8], Ana Batista-Gonzalez[1], Noemi A. Saavedra[1], Leticia Sampedro[2], Julen Tomás[2], Juan Anguita[2,9], Shang-Cheng Hung[10], Ashish Tripathi[10], Jiayong Xu[1,4], Aharona Glatman-Freedman[11,12], Williams R. Jacobs, Jr.[1,5], John Chan[1,4], Steven A. Porcelli[1], Jacqueline M. Achkar[1,4], Arturo Casadevall[1,13‡]

1 Department of Microbiology and Immunology, Albert Einstein College of Medicine, Bronx NY, United States of America, **2** CIC bioGUNE, Bizkaia Technology Park, Derio, Bizkaia, Spain, **3** Millennium Institute on Immunology and Immunotherapy, Programa Disciplinario de Inmunologia, Facultad de Medicina, Universidad de Chile, Santiago, Chile, **4** Department of Medicine, Albert Einstein College of Medicine, Bronx NY, United States of America, **5** Howard Hughes Medical Institute, Albert Einstein College of Medicine, Bronx NY, United States of America, **6** Alberta Glycomics Centre and Department of Chemistry, University of Alberta, Gunning-Lemieux Chemistry Center, Edmonton, Alberta, Canada, **7** Grupo de Inmunologia Celular e inmunogenetica, Universidad de Antioquia, Medellin, Colombia, **8** Institute for Medical Microbiology and Hospital Hygiene, Heinrich-Heine-University Duesseldorf, Duesseldorf, Germany, **9** Ikerbasque, Basque Foundation for Science, Bilbao, Bizkaia, Spain, **10** Genomics Research Center, Academia Sinica, Section 2, Nankang, Taipei, Taiwan, **11** Infectious Diseases Unit, Israel Center for Disease Control, Israel Ministry of Health, Tel Hashomer, Israel, **12** Department of Pediatrics, and Department of Family and Community Medicine, New York Medical College, Valhalla, NY, United States of America, **13** Department of Molecular Microbiology and Immunology, Johns Hopkins Bloomberg School of Public Health, Baltimore, MD, United States of America

‡ RPR and AC share senior authorship.
* rprados@cicbiogune.es

OPEN ACCESS

Citation: Prados-Rosales R, Carreño L, Cheng T, Blanc C, Weinrick B, Malek A, et al. (2017) Enhanced control of *Mycobacterium tuberculosis* extrapulmonary dissemination in mice by an arabinomannan-protein conjugate vaccine. PLoS Pathog 13(3): e1006250. https://doi.org/10.1371/journal.ppat.1006250

Editor: Padmini Salgame, New Jersey Medical School, UNITED STATES

Received: December 28, 2016

Accepted: February 17, 2017

Published: March 9, 2017

Data Availability Statement: All relevant data are within the paper and its Supporting Information files. Microarray data were deposited with the GEO NCBI database with the accession number GSE77711

Funding: This work was supported in part by grants from the National Institute of Health (NIH)/ National Institute of Allergy and Infectious Diseases (NIAID) AI105684 and AI096213-01 to JMA, the Aeras TB vaccine foundation and the Food and

Abstract

Currently there are a dozen or so of new vaccine candidates in clinical trials for prevention of tuberculosis (TB) and each formulation attempts to elicit protection by enhancement of cell-mediated immunity (CMI). In contrast, most approved vaccines against other bacterial pathogens are believed to mediate protection by eliciting antibody responses. However, it has been difficult to apply this formula to TB because of the difficulty in reliably eliciting protective antibodies. Here, we developed capsular polysaccharide conjugates by linking mycobacterial capsular arabinomannan (AM) to either Mtb Ag85b or *B. anthracis* protective antigen (PA). Further, we studied their immunogenicity by ELISA and AM glycan microarrays and protection efficacy in mice. Immunization with either Abg85b-AM or PA-AM conjugates elicited an AM-specific antibody response in mice. AM binding antibodies stimulated transcriptional changes in Mtb. Sera from AM conjugate immunized mice reacted against a broad spectrum of AM structural variants and specifically recognized arabinan fragments. Conjugate vaccine immunized mice infected with Mtb had lower bacterial numbers in lungs and spleen, and lived longer than control mice. These findings provide additional evidence that humoral immunity can contribute to protection against Mtb.

Drug Administration (FDA; 1U18 FD004012/01 to JMA). RK acknowledges support from the Juergen Manchot Foundation. TLL, MJ and YB acknowledge support from Alberta Glycomics Centre and the Bill and Melinda Gates Foundation. RP-R was supported in part by National Institutes of Health award 1R21AI115091. RPR is a 'Ramon y Cajal' fellow from the Spanish Ministry of Economy and Competitiveness. RPR acknowledge funding from the Ministry of Economy and Competitiveness SAF2016-77433-R. JA acknowledge support from the Ikerbasque, Basque Foundation for Science. The funders had no role in study design, data collection and analysis, decision to publish, or preparation of the manuscript.

Competing interests: The authors have declared that no competing interests exist.

Author summary

Vaccine design in the TB field has been driven by the imperative of attempting to elicit strong cell-mediated responses. However, in recent decades evidence has accumulated that humoral immunity can protect against many intracellular pathogens through numerous mechanisms. In this work, we demonstrate that immunization with mycobacterial capsular arabinomannan (AM) conjugates elicited responses that contributed to protection against Mtb infection. We developed two different conjugates including capsular AM linked to the Mtb related protein Ag85b or the Mtb unrelated PA from *B. anthracis* and found that immunization with AM conjugates elicited antibody populations with different specificities. These surface-specific antibodies could directly modify the transcriptional profile and metabolism of mycobacteria. In addition, we observed a prolonged survival and a reduction in bacterial numbers in lungs and spleen in mice immunized with Ag85b-AM conjugates after infection with Mtb and that the presence of AM-binding antibodies was associated with modest prolongation in survival and a marked reduction in mycobacterial dissemination. Finally, we show that AM is antigenically variable and could potentially form the basis for a serological characterization of mycobacteria based on serotypes.

Introduction

Mycobacterium tuberculosis (Mtb), the causative agent of TB, can establish latent or progressive infection despite the presence of a fully functioning immune system. The capacity of Mtb to avoid immune-mediated clearance reflects a necessary association with the human host that has led to an evolved and coordinated program of immune evasion strategies, including interference with antigen presentation to prevent and/or alter the quality of T-cell responses [1]. There is strong evidence to suggest that the mycobacterial cell envelope is of key importance for survival in the host [2]. The mycobacterial envelope consists of three major components: the plasma membrane, the cell wall, and an outermost capsule [2]. Bacterial capsules are protective structures important for the interaction with and successful colonization of the host [3]. Toxic substances have recently been found in the mycobacterial capsule, suggesting the contribution of this compartment to mycobacterial pathogenesis [4].

The mycobacterial capsule is loosely attached to the surface and is mainly composed of proteins and polysaccharides [2]. The major surface exposed capsule polysaccharides are a 120 kDa glycogen-like α-glucan, a 15 kDa arabinomannan (AM) and a 4 kDa mannan [5]. Both AM and mannan are structurally related to lipoarabinomannan (LAM), the major lipopolysaccharide of the mycobacterial cell wall. LAM is also known for having biological effects during its interaction with host cells, including immunosuppression of T cell responses or interference with macrophage activation [6]. LAM and AM can each elicit high antibody responses in infected hosts [7]. A low antibody to LAM response in children with TB was associated with disseminated mycobacterial disease [8]. That report concluded that a weak antibody response to LAM and other mycobacterial antigens increased the likelihood of dissemination [8]. Presumably, antibodies can also contribute to the host defense against Mtb by promoting the clearance of LAM [9]. In fact, several reports on AM or LAM-binding monoclonal antibodies have established their capacity to contribute to the clearance of mycobacteria from the host [10, 11].

In 2014, there were an estimated 9.4 million new cases of TB and 1.5 million people died from TB, including 1.1 million deaths among HIV-negative individuals and 0.4 million among

people who were HIV-positive [12]. Efforts to control the disease include the development of "point-of-care" tests, new TB drugs, the use of the Bacille Calmette-Guerin (BCG) vaccine and the development of new vaccines. Most of the new vaccine candidates against TB that have entered in clinical trials fall into one of the following groups: (I) live attenuated vaccines to replace BCG; (II) subunit vaccines to be given after initial BCG vaccination [13]; and (III) single immunodominant antigens, usually secreted, such as ESAT-6, Cfp10 and Ag85b along with other adjuvants [13]. These vaccine candidates were developed with the working assumption that immunity against TB relied solely on cellular defense mechanisms [14]. While there is no doubt that cell-mediated immunity is a major arm in the control of mycobacterial infection, there are now compelling data that certain antibodies are active against mycobacteria [9–11, 15].

In this study, we have generated two different polysaccharide conjugates made of capsular Mtb AM and proteins Ag85b (Ag85b-AM) from Mtb H37Rv and protective antigen (PA) (PA-AM) from *Bacillus anthracis*, aiming to create AM-specific humoral immunity prior to challenging mice with virulent mycobacteria via aerosol. Previous studies using similar approaches have shown that secreted AM or delipidated LAM-containing conjugates provided some protection against Mtb infection in mice, rabbit or guinea pigs [15, 16]. Here we report that capsular AM conjugates promote an AM-binding antibody response in mice that is associated with reduced bacterial numbers in lungs and spleen, and prolonged survival in immunized mice. Our study provides additional evidence for an important role for antibodies in protection against Mtb and suggests that polysaccharide antigens could be useful components of future vaccines to fight TB.

Results

Capsular arabinomannan conjugates

Mtb H37Rv was grown in minimal media without Tyloxapol, which is known to release capsule [4]. After 14 d cultures were harvested and an aliquot was submitted to transmission electron microscopy (TEM) analysis to examine bacterial cells for the presence of the capsule. An electron transparent zone was clearly visible surrounding Mtb cells (S1 Fig). Visualization of Mtb cells under the scanning electron microscope revealed that the capsule is a matrix composed of small spherical units of approximately 50 nm in diameter [17] (S1 Fig). Arabinomannan (AM) is a low molecular weight polysaccharide that can be recovered from the upper phase of a chloroform-methanol-water extraction step [18] and separated from the other low molecular weight polysaccharides after proteinase K treatment by size exclusion chromatography (S1 Fig). Three major peaks were obtained of molecular mass 20 kDa (peak a), 10 kDa (peak b) and 4 kDa (peak c). According to the glycosyl composition analysis of the pooled peaks, peak a consisted of two main glycosides, arabinose and mannose in a ratio (2:1). This result is consistent with mycobacterial capsular AM and other reported analysis in mycobacteria [5, 18]. In addition, only peak "a" showed binding to 9d8 an AM-specific monoclonal antibody (Mab) and not to 24c5, recognizing α-glucan (S1 Fig). AM, as many other polysaccharides are poorly immunogenic because they are T cell independent antigens; therefore, immunization with polysaccharides generally does not elicit IgG immune responses. We hypothesized that vaccine-induced AM antibodies had value in protecting against TB. For this, we conjugated Mtb capsular AM, corresponding to the purify fraction (peak a) to different protein carriers. We did not make conjugates to other fractions that did not correspond to AM, as that was not the scope of this work. We selected Ag85b as Mtb-related protein carrier to test whether inclusion of AM would boost its recognized protective properties as an immunogen. In addition, we also linked Mtb capsular AM to the protective antigen (PA) from

Bacillus anthracis as non-Mtb related antigen to set up a system where AM-binding immunity could be evaluated in an exclusive way. We developed Ag85b-AM and PA-AM conjugates using the cyanylating reagent CDAP as previously described [19, 20]. The conjugate products were separated by size exclusion chromatography on a Sephacryl S-200 (GE healthcare) (S2 Fig) in PBS. Ag85b-AM and PA-AM conjugates showed a protein-polysaccharide molar ratio of 1:8 and 1:7, respectively, as determined by Bradford and the phenol-sulphuric acid assays.

Antibody response of AM conjugates in mice

To test the immunological response of the different AM conjugates, mice were immunized with different amounts of Ag85b-AM or PA-AM conjugates (1, 5 and 10 μg) in 1% Alum. Alternatively, three different groups of mice received 1 μg of either Ag85b, PA or 10 μg of AM, also in 1% Alum. Each mouse was boosted twice every two weeks and serum samples were taken to determine the kinetics of specific antibodies (S3 Fig). No antibody response was detected in PBS, AM or 1% Alum alone-immunized mice. We determined that immunization with three doses of 10 ug of Ag85b-AM conjugate provided elevated levels of AM-specific Abs (1:3000) (S3 Fig). We believe that our regime of immunization provided sufficient and stable levels of Ag85b-specific T cells as it has been previously shown using similar immunization approaches [21].

We further analysed the IgG subclasses and IgM in sera isolated at day 45 after initial immunization (Fig 1A and 1B). Immunization with either Ag85b or PA induced high levels of protein-specific antibodies (1:6000, 1:4000) and no polysaccharide-specific antibodies as expected. Immunization with conjugates promoted an antibody response to both the protein and polysaccharide components of the conjugates, being the response to proteins very similar to that the immunization with protein alone. Ag85b-specific Ab response consisted on a mix of all subclasses being IgG2c the most prevalent with a three fold increase relative to the other groups. Immunization with PA alone induced a mix of IgM, IgG1 and IgG2c (Fig 1A and 1B). The AM-binding antibody response was very similar between the two conjugates in terms of diversity. A mix IgM, IgG1 and IgG2b was observed in AM-Ag85b immunized mice versus an exclusive IgG2b in AM-PA immunized mice.

Since AM is a mycobacterial capsular polysaccharide we considered whether AM polyclonal sera would recognize the outermost compartment of Mtb. However, any interpretation of the data needs to take into account the fact that AM and LAM share epitopes, suggesting that AM-immune serum might also label LAM. In fact, analysis of the specificity of AM-serum for binding to other Mtb cell wall components by ELISA revealed a cross reactivity with LAM, Man-LAM and LM and absence of binding to arabinogalactan (AG), mycolyl-arabinogalactan-peptidoglycan complex (mAGP) or trehalose deoxy mycolate (TDM) (S4 Fig). Notably, there is no Ab available to distinguish between AM and LAM. To explore the location of Ab binding we utilized immunogold TEM with AM-binding sera (Fig 1C and 1D and S5 Fig). We used encapsulated Mtb cells that were generated by growing mycobacteria in the absence of detergent. It is known that supplementation of the culture with detergent strips the mycobacterial capsule [22]. Grids containing sections of Mtb cells were labelled without any primary antibody (NP) as controls and no immunogold was detected. Similarly, no labelling was observed when the experiment was performed with a PA-binding serum, confirming the lack of cross reactivity of PA-binding antibodies to Mtb. We observed labelling in all conditions where AM-binding sera were used. The location of the immunogold particles in cells labelled with Ag85b-AM serum was not restricted to the surface but distributed all over the bacterial cell (Fig 1C). On the contrary, most of the immunogold labelling observed in grids treated with AM-PA serum was restricted to the bacterial surface. Since both conjugates were generated

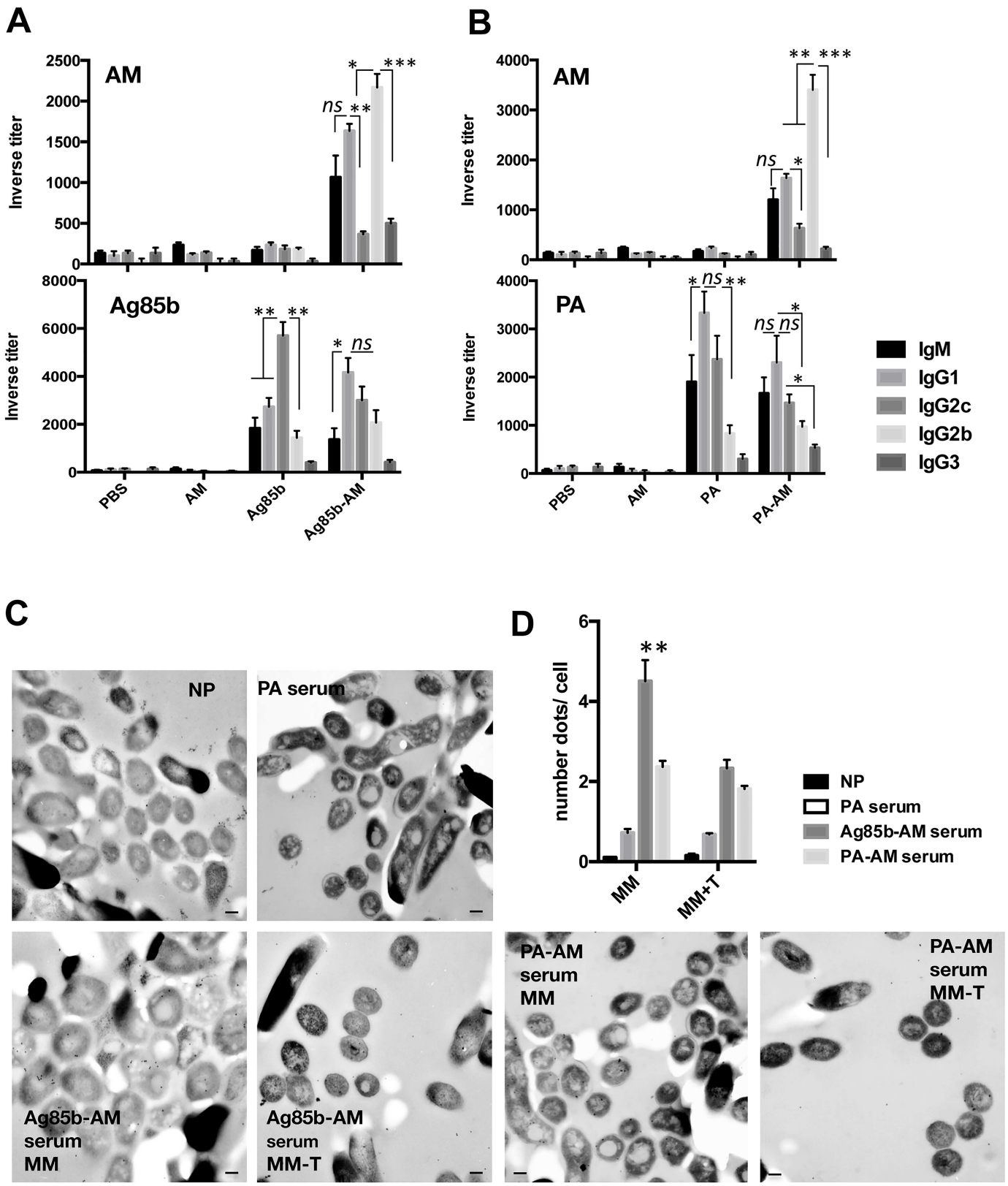

Fig 1. Antibody response to conjugate immunization in mice. (A) Titers of AM (Mtb) (top graph) or Ag85b (bottom graph)-specific antibodies measured by ELISA in serum from C57BL/6 mice ($n = 3$ per group) immunized with 10 μg of AM-Ag85b conjugate, 1 μg of Ag85b, 10 μg of AM or PBS.

(B) Titers of AM (Mtb) (top graph) or PA (bottom graph)-specific antibodies measured by ELISA in serum from C57BL/6 mice ($n = 3$ per group) immunized with 10 μg of AM-PA conjugate, 1 μg of PA, 10 μg of AM or PBS. The results are representative of three independent experiments performed in the same manner. **(C)** Immunogold electron microscopy of thin sections of Mtb H37Rv cells treated with immune sera specific for the indicated antigens and detected with a 6-nm IgG gold-labeled anti-mouse antibody. Immunolabeling was tested in Mtb grown in minimal medium with (MM-T) and without tyloxapol (MM). Scale bars: 100 nm. **(D)** Quantitative analysis of the immunobeling of immune sera by determining the number of gold particles per cell. Bars are mean +/- sem. NP, denotes No Primary antibody. $^{**}P < 0.01$ using one-way ANOVA. Data are mean +/- sem. *ns*, not significant.

https://doi.org/10.1371/journal.ppat.1006250.g001

with the same AM molecule, surface labelling is most probably due to AM or LAM. However, in the case of Ag85b-AM-immune serum, Abs to Ag85b could also be labelling this protein throughout the mycobacterial cell, explaining the broad distribution of the labelling that we observed.

When immunolabeling was performed on grids containing unencapsulated mycobacteria (grown in the presence of detergent) we observed a reduction on labelling, indicating that most of the material being recognized in encapsulated Mtb is not present in unencapsulated Mtb (Fig 1C and 1D). These results indicate that immunization with AM-conjugates induces a potent and specific antibody response primarily directed to the mycobacterial surface and specifically to the capsule.

Dissection of the AM-binding antibody response by glycan microarrays

AM is a neutral and heterogeneous capsular polysaccharide comprised of a mannan backbone substituted by a branched arabinan, further modified by mannose residues at the non-reducing end [23]. To gain insight into the specific differences in serum reactivity provided by the conjugates, we analyzed immune sera on glycan microarrays including 30 synthetic AM fragments (Fig 2 and S6 Fig). The synthetic AM fragments included on the array are representative of the motifs present in all three of these domains (S6 Fig). Selection of compounds for synthesis was based on the reported structure of AM.

Further, AM-arrays were probed with diluted sera from either AM-PA or AM-Ag85b conjugate-immunized mice. PA and Ag85b-immunized mice and the AM-binding monoclonal antibody (mAb) 9d8 were used as controls. We observed a more diverse repertoire of AM fragment recognized by conjugate sera relative to the control mAb 9d8 (Fig 2A). This is consistent with the response expected from a polyclonal serum versus a mAb. A reduced response was detected in arrays probed with the PA or Ag85b-serum for the majority of the epitopes. Notably, we observed a common reactivity profile between sera from both conjugate-immunize mice, indicating that the conjugated PS might have been modified similarly. More specifically, we observed a prevalent recognition for epitopes ranging from linear arabinose fragments including 4 to 8 sugar units (#24) to highly branched arabinose polysaccharides (#16, #17, #20, #23 and #24). (Fig 2A and 2B). The highest reactivity in AM-PA serum was observed for fragments 23, 24 and 22, whereas in AM-Ag85b serum was observed for fragments 16, 23, 24 and 20. All fragments represented linear or branched arabinose polysaccharides, except for fragment 22, which included the arabinan core of fragment 14 but highly mannosylated (three mannose residues) at both reducing ends. Fragments 5 and 6 were preferentially recognized by the mAb 9d8 and included structures with a short-branched arabinan core manosylated at both ends. Both conjugate sera shared reactivity of fragments 1, 10 and 12 with 9d8. These fragments included short and linear arabinose glycans (#1), short and branched arabinan molecules with low mannosylation (#12) and xylose-substituted at the mannose reducing end (#10). These results suggest that AM-binding antibody response is directed to a diverse set of glycans, mostly associated to the arabinan core and that the protective mAb 9d8 reacts to a reduced set of glycans including a less complex repertoire.

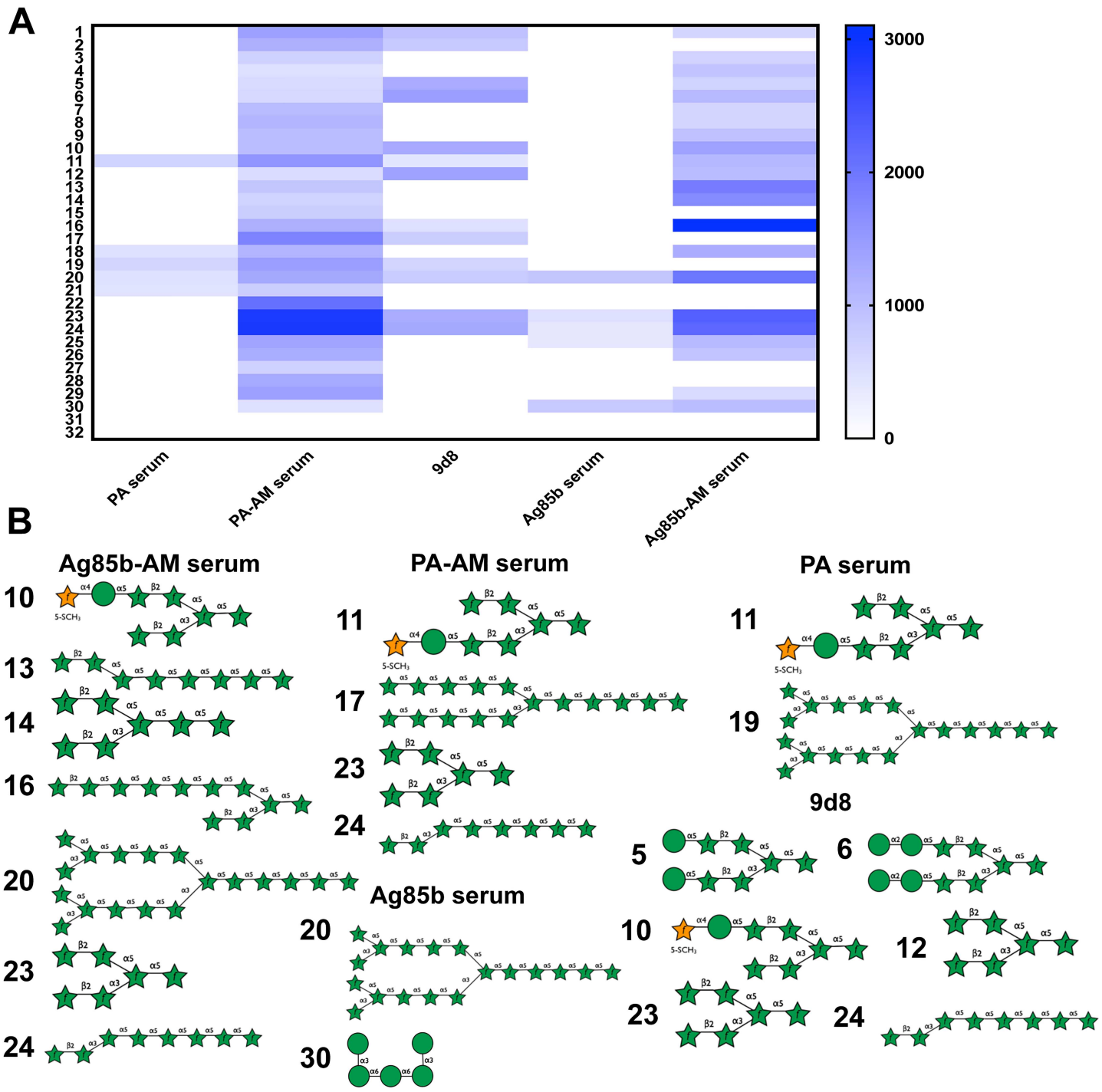

Fig 2. Assessment of the relative IgG-binding of AM immune sera the 29 printed AM fragments. (A) Heat map of AM glycan microarray data obtained after incubation with pooled murine sera diluted 1:400 followed by labeled anti-IgG. Data are mean of three independent spots. Values are relative fluorescence units. **(B)** AM fragments included in the glycan microarray representing the AM molecule recognized by the indicated serum. The numbers correspond to those in A and S6 Fig.

https://doi.org/10.1371/journal.ppat.1006250.g002

Transcriptional response of Mtb during AM-binding antibody interaction

Recently a new function for humoral immunity was described whereby the binding of specific antibodies to microbes triggered transcriptional responses that were associated with physiological changes [24, 25]. Consequently, we investigated whether capsular AM-binding antibodies elicited transcriptional changes in Mtb by incubating encapsulated Mtb with AM-PA serum for 4 h and comparing the changes in transcription with a condition including PA immune serum using microarrays (Fig 3). Microarray data was deposited with the GEO NCBI database with the accession number GSE77711.

We observed a consistent and significant upregulation of most of the *mce1* operon (Fig 3A and 3B), consisting of 13 genes encoding a putative ABC lipid transport system specialized in mycolic acids [26]. Upregulation of the *mce1* operon was also observed when Mtb is inside host cells [27]. Moreover, an Mtb mutant defective in the *mce1* operon was shown to be hypervirulent in mice and produce more mycolic acids [28, 29]. The fact that *umA*, a mycolic acid synthase, was downregulated lead us to hypothesize that upregulation of *mce1* operon could result in a reduction in the mycolic acid content of Mtb cells upon interaction with AM-binding immune serum. Indeed, when we measured fatty acids by TLC, we observed reduction in alpha, keto and methoxy mycolic acids levels (Fig 3C), establishing that antibody-induced transcriptional changes resulted in mycobacterial biochemistry changes.

We also observed upregulation in some of the *nuo* genes, which are involved in aerobic respiration (Fig 3A). Of note, the gene encoding for isocytrate lyase (*aceA*, *icl1*), which is known to be required for persistence in the mouse model, was downregulated in Mtb treated with AM-binding serum. Similarly, transcript levels of *cysD*, which encode a sulfate adenylyltransferase involved in sulphate metabolism, were reduced in AM-treated Mtb (Fig 3A and 3B). We could not explain why *lipF*, encoding a lipid esterase, appeared as downregulated in the microarray while this transcript showed a four-fold upregulation relative to untreated Mtb (Fig 3B). These results indicate that antiserum including antibodies with specificities for Mtb capsular AM can alter the lipid metabolism and the fitness of mycobacteria.

Protective efficacy of AM conjugates in mice

To separately test the ability of the two conjugates (Ag85b-AM and PA-AM) to modify the course of Mtb infection, mice were immunized three times with 10 μg of each conjugate and challenged with virulent tubercle bacilli by the respiratory route 4 weeks after the last immunization. Immunization controls included AM, PBS (1% Alum), and 1 x 10^6 BCG. At 4 weeks after challenge mice were sacrificed and bacterial loads were assessed in lung and spleen (Fig 4A and 4B). As Ag85b is a well known immunogenic and protective Mtb antigen [30], we initially tested whether AM-Ag85b conjugate could control bacterial replication more efficiently than Ag85b alone. An immunizing dose of Ag85b equivalent to that of included in the conjugate was used to generate Ag85b-immunized mice. Both conjugate and Ag85b-immunized mice showed similar reduction in mycobacterial numbers in the lung at 4 weeks (Fig 4A). Conversely, we noticed a more significant reduction in bacterial counts in spleen in AM-Ag85b immunized mice, similar to BCG-immunized mice (Fig 4B). Histological analysis revealed marked differences in tissue inflammation in mice immunized with AM, and adjuvant relative to those immunized with AM-Ag85b and Ag85b mice (Fig 4C), with the latter groups manifesting more intact lung morphology with less inflammation. We observed a major difference in the gross pathology of lungs from the AM-Ag85b-immunized mice compared to Ag85b-immunized mice, as evident by less diseased tissue. AM-Ag85b immunized mice showed a reduction in both the number of infiltrates and the percentage of diseased tissue, although these differences were not significant

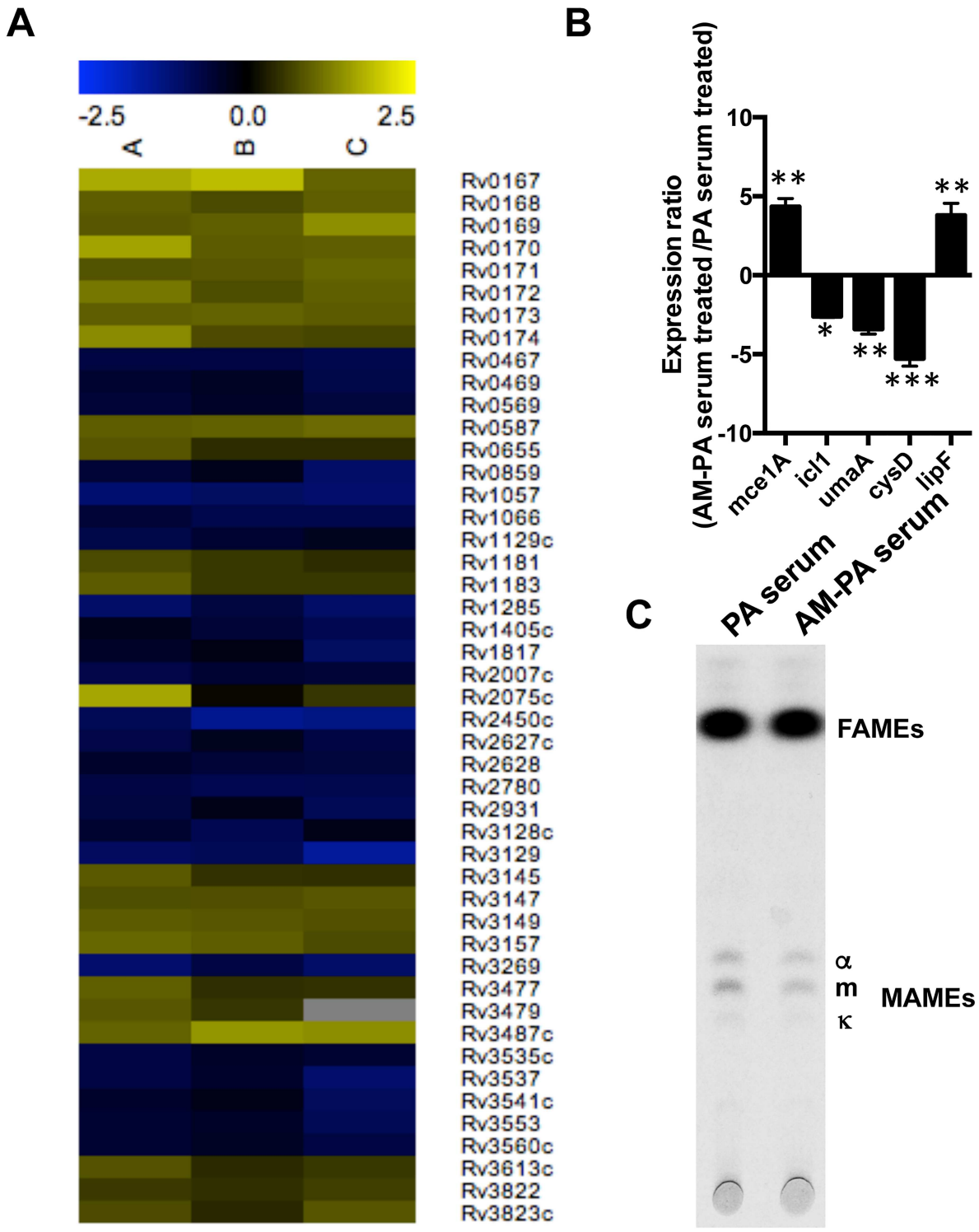

Fig 3. Effect of AM immune serum on the transcriptional profile of *M. tuberculosis*. **(A)** Transcriptomic profile of Mtb during treatment with AM-PA murine serum (1:400) compared to PA murine serum (1:400) for 4 h. The heat map shows transcriptional changes from three biologically independent replicates labelled as A, B and C. **(B)** Expression ratio of the indicated Mtb genes measured as the average relative expression of AM-PA serum vs PA serum-treated Mtb by quantitative real time PCR (qRT-PCR). (*$P < 0.05$, **$P<0.01$ ***$P < 0.001$, one-way ANOVA with Tukey post-test). **(C)** Analysis of fatty acid methyl esters (FAMEs) and mycolic acid methyl esters (MAMEs) in *M. tuberculosis* H37Rv labelled with ^{14}C-acetate for 22h prior to treatment with the indicated serum preparations for 5 h. Lipids were extracted and analyzed by TLC as described in Methods. The same amount of cpm was spotted for each sample.

https://doi.org/10.1371/journal.ppat.1006250.g003

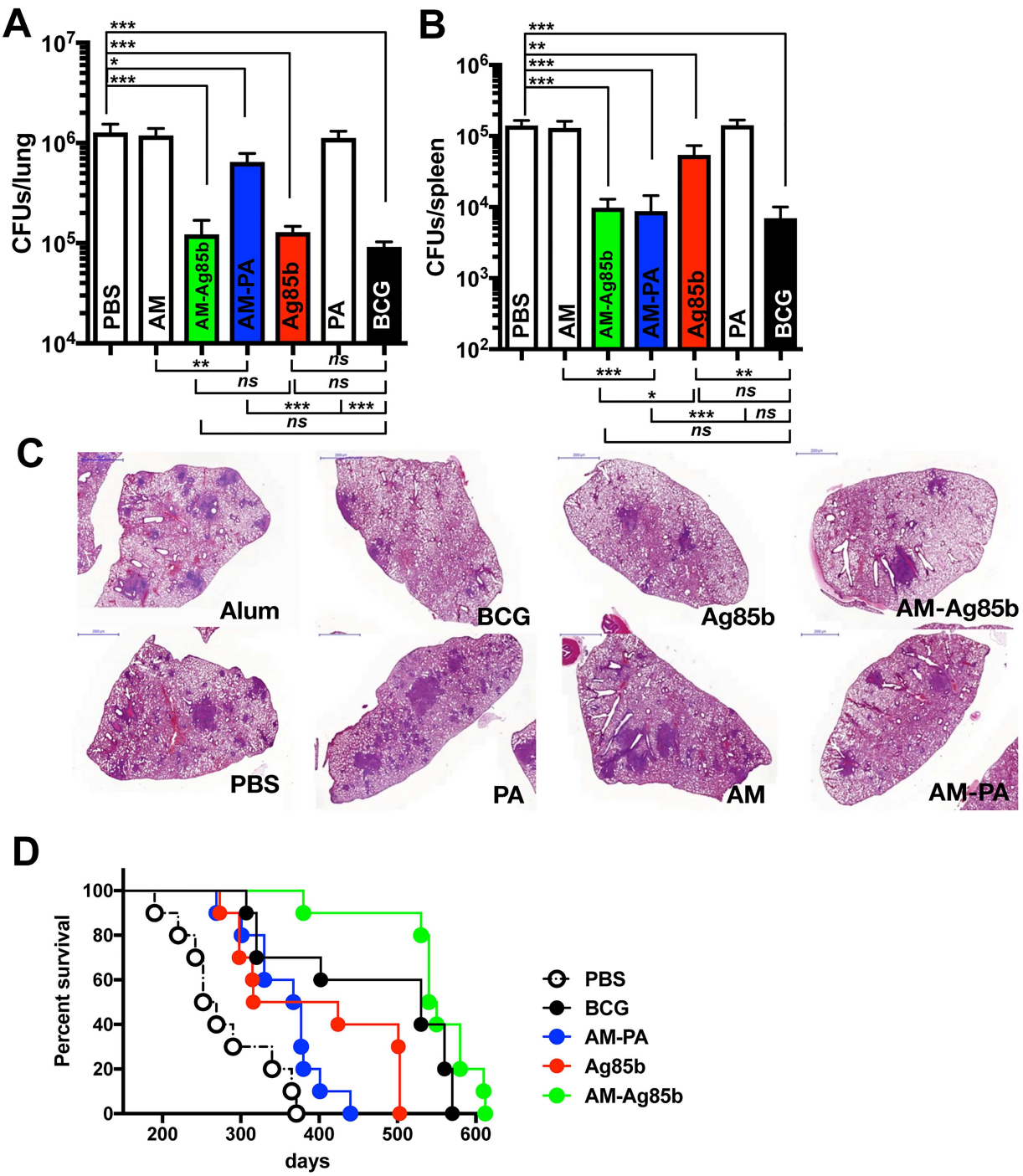

Fig 4. Immunization with conjugates protect against Mtb infection. (A,B) Bacterial load (CFUs) in the lungs **(A)** and spleen **(B)** of individual C57BL/6 mice, immunized with the indicated preparations was determined at 4 weeks after infection with a low dose of Mtb H37Rv via aerosol (approx. 100 CFUs). The results are pooled values from two similar and independent experiments. Experimental groups used 5 mice. (*$P < 0.05$, **$P<0.01$ ***$P < 0.001$, one-way ANOVA with Tukey post-test). **(C)** Representative H&E staining images from lungs of C57BL/6 mice immunized with the indicated preparations and aerosol infected with Mtb H37Rv for 4 weeks. A representative lung section for each treatment is shown. **(D)** Survival of mice immunized with PBS ($n = 10$), 1×10^6 CFU of BCG ($n = 10$), 10 μg of AM (Mtb)-Ag85b ($n = 10$), 10 μg of AM (Mtb)-PA conjugate ($n = 10$) or 1 μg of Ag85b ($n = 10$) and challenged with ~100 CFU of aerosolized Mtb H37Rv. All the immunized mice were significantly different from that of PBS-treated mice ($P < 0.001$, log-rank test for AM-Ag85b and BCG; $P = 0.0064$, log-rank test for Ag85b). No differences between the immunized groups were found except for Ag85b vs AM-Ag85b immunized mice ($P = 0.0166$). The survival curve for AM(Mtb)-PA was significantly different from that of PBS ($P = 0.049$, Gehan-Breslow-Wilcoxon test; $P = 0.057$, log-rank test). Survival studies were performed twice with similar results.

https://doi.org/10.1371/journal.ppat.1006250.g004

(S7 Fig). Next, we tested for the ability of these conjugate to influence the survival of mice challenged with a low dose of virulent tubercle bacilli via aerosol (Fig 4D). As a positive control, we included mice immunized with 1 x 10^6 BCG. All immunized mice, including BCG, Ag85b and conjugate immunized mice significantly lived longer than the non-immunized mice injected with adjuvant. No differences were observed between BCG and conjugate immunized mice. Mice immunized with AM-Ag85b lived significantly longer than Ag85b immunized mice ($P = 0.0166$) indicating that AM-binding antibodies contributed to prolonging the survival of infected mice. These results suggested that antibodies to Ag85b were also protective and could be masking any protective contribution of AM-binding immunity against Mtb whereas the longer survival in AM-Ag85b immunized mice suggested that AM-binding antibodies contributed to protection. Consequently, we analyzed the protective efficacy of AM-PA conjugates to assess the exclusive contribution of AM-binding immunity. Of note, a 0.42 log reduction ($P = 0.04$) in lung CFUs was observed in mice immunized with AM-PA conjugates (Fig 4A). Immunization with either AM and PA alone did not provide any protection and similar CFUs numbers as in 1% Alum-treated mice were counted in the lungs. When we analyzed bacterial loads in spleen we observed a significant reduction in CFUs in AM-PA immunized mice, similar to AM-Ag85b and BCG immunized mice, followed by Ag85b (Fig 4B). Consistent with the relatively weak ability of AM-PA conjugates to control bacterial replication in the lungs, we observed comparable lung pathology to non-immunized or PA and adjuvant-immunized mice (Fig 4C). Although we measured a mean of 5 infiltrates in lungs of PA-AM immunized mice versus 8 infiltrates in adjuvant-immunized mice, these differences were not significant. However we did measure a significant reduction in the percentage of diseased tissue (S7 Fig). AM-PA conjugate-immunized mice lived longer than adjuvant-treated mice (median survival 337 days vs 297; log-rank $P = 0.057$, GBW $P = 0.049$) and mice receiving BCG as a vaccine showed a survival mean time of 479 days ($p>0.001$) (Fig 4D). These results suggest that immunity directed to AM can contribute to reduced bacterial dissemination and lung inflammation, which in turn translated into prolonged survival of infected mice.

AM-binding antibodies contribute to control bacterial dissemination

To establish that the protection observed following conjugate immunization was due to humoral immunity we carried out a passive antibody transfer experiment using sera from immunized mice. Mtb bacterial counts were enumerated in lungs and spleens 4 weeks after challenge with a low dose of Mtb via aerosol (Fig 5A and 5B). We found that passive administration of sera from Ag85b and AM-Ag85b-immunized mice was associated with reduced bacterial CFUs in lung, as compared to adjuvant and naïve (PBS) mice (Fig 5A). In mice that received AM-PA-immune serum, there was a significant reduction in lung CFU of 0.4 log relative to PBS and adjuvant. Of note, although we observed a greater reduction in lung CFUs in mice that received Ag85b, this did not reach statistical significance relative to mice transferred with PA-AM-serum. Consistent with the ability of AM-PA and AM-Ag85b conjugates to control bacterial dissemination (Fig 4B), we observed that sera from conjugate-immunized mice significantly reduced the bacterial CFUs in spleen, with AM-Ag85b-immune serum being superior to AM-PA-immune serum (no statistically significant differences, $P = 0.054$) (Fig 5B). We observed no benefit from the transfer of serum from BCG immunized mice. These results strongly indicate that specific antibodies to AM and Ag85b contribute to control bacterial dissemination. The greater protective efficacy achieved by AM-Ag85b immune serum might be due to either synergistic or additive effects of antibodies to these two antigens.

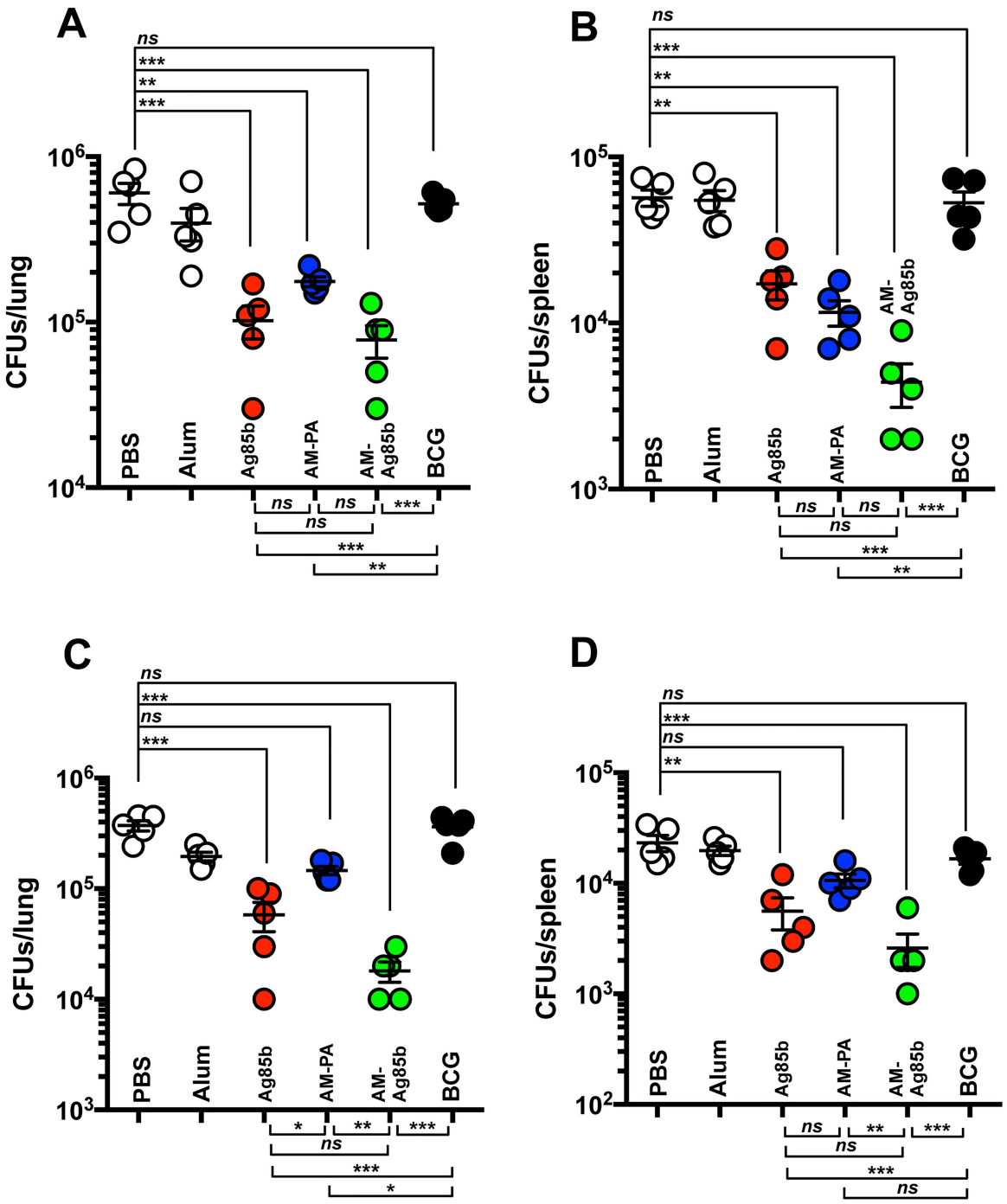

Fig 5. Passive transfer of immune serum and adoptive T cell transfer modify the course of mycobacterial infection. **(A,B)** Bacterial burden (CFUs) in the lungs **(A)** and spleen **(B)** at 4 weeks after infection with a low dose of Mtb H37Rv via aerosol (approx. 100 CFUs) of individual naïve C57BL/6 mice that previously received passively serum preparations. Results are representative of two similar and independent experiments. Experimental groups used 5 mice. (*$P < 0.05$, **$P<0.01$, one-way ANOVA with Tukey post-test). **(C,D)** Bacterial load (CFUs) in the lungs **(C)** and spleen **(D)** of individual naïve C57BL/6 mice adoptively transferred with 4 x 10^6 T cells from the indicated immunized mice were determined at 4 weeks after infection with a low dose of Mtb H37Rv via aerosol (approx. 100 CFUs). The results are representative of two similar and independent experiments. Experimental groups used 5 mice. (*$P < 0.05$, **$P<0.01$, one-way ANOVA with Tukey post-test).

https://doi.org/10.1371/journal.ppat.1006250.g005

T cells from AM-Ag85b mice mediate protection against *M. tuberculosis*

We next tested the ability of memory T cells from long-term immunized mice (S8 Fig) to protect naïve recipient mice against virulent Mtb by using a T-cell adoptive transfer protocol. Bacterial counts were enumerated in lungs and spleens 4 weeks after challenge with a low dose of Mtb via aerosol (Fig 5C and 5D). Remarkably, mice transferred with T cells from AM-Ag85b or Ag85b immunized mice showed significant reduction in CFU in the lung (Fig 5C) and spleen (Fig 5D), relative to PBS and Alum-mice. Mice receiving AM-PA-specific T cells did not show any capacity to control bacterial replication in lung and spleen (Fig 5C and 5D). The transfer of T cells from Alum or BCG-vaccinated mice did not translate into any protection. The later result is consistent with reports that transfer of BCG-induced immunity requires sublethal irradiation of recipients [31]. These data strongly suggests that the superior protection provided by AM-Ag85b conjugates is a combination of both AM and Ag85b-binding antibodies and Ag85b-specific T cells.

Antigenic variability of capsular AM

Some encapsulated variants of many bacterial clinical isolates are associated with higher rates of mortality and morbidity and consequently vaccine development is focused on the these serogroups [32]. Carbohydrate antigens exhibit tremendous structural variation that can translate into antigenic variation as demonstrated by the 13 different serogroups of *Neisseria meningitidis*, over 90 different serotypes in *Streptococcus pneumoniae* or the more than 80 serotypes in *Klebsiella* sp [33]. However, for Mycobacterial spp. the question of polysaccharide-related antigenic differences on the bacterial surface has not been investigated. We hypothesized that AM presents antigenic variability among Mtb isolates given that it is a variable structure comprising a mannan backbone substituted by a branched arabinan, which is further modified by mannose residues at the non-reducing end. To investigate AM antigenic variability we analyzed a panel of 17 strains, including Mtb H37Rv, representing the 6 known lineages of Mtb strains globally distributed [34] and tested for AM and α-glucan reactivity to the 9d8 mAb (AM) and 24c5 mAb (α-glucan), respectively (Fig 6). We could measure some statistically differences in Ab recognition between isolates form the same lineage. However, we also could establish some correlates. We observed that AM of isolates from L1, L5 and some from L3 showed the highest binding to 9d8 mAb. L6 showed the lowest binding with a reduction of an 80% relative to Mtb H37Rv. Isolates from L4 showed a 50% reduction in AM binding to 9d8. Of note, we did not find as much variability in the binding of α-glucan to mAb among the different isolates. Most of the isolates showed a reduction in binding relative to Mtb H37Rv, in the range of 50–60%. Only isolates from L4 and L5 showed a similar reactivity. These results suggest that AM is the main source of antigenic variability in the mycobacterial capsule and establish different antigenic groups among Mtb clinical isolates. However, we cannot rule out that the relative distribution of capsular polysaccharides may be relevant for their binding to specific Abs. To understand the antigenic variability contributed by AM would require a more extensive analysis, including more Mtb isolates.

AM-conjugate specific serum is opsonic to unencapsulated bacteria

Standard protocols for murine infection with Mtb use inoculum as a homogeneous bacterial suspension after growth in detergent. However, the generation of single cell suspensions using detergent to avoid clumping also can remove the capsular layer [2, 35]. Indeed, a recent study using Cryo-Electron microscopy (Cryo-EM) revealed that this layer is removed when cells are grown in the presence of detergent or agitation [4]. Since AM is part of the capsule we reasoned that capsular polysaccharide conjugate vaccines may be even more effective when the

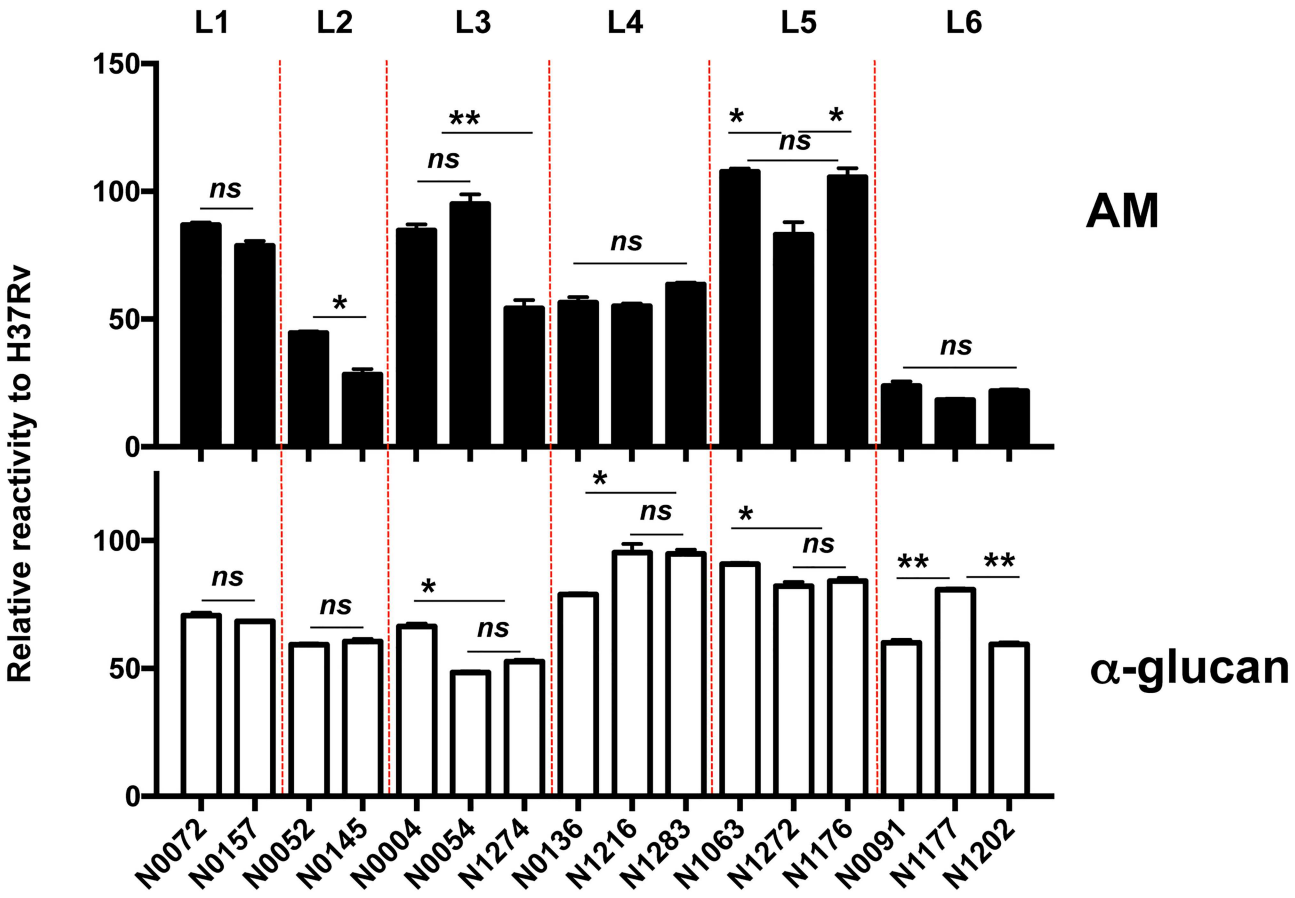

Fig 6. Antigenic variability of AM among Mtb isolates. Relative reactivity of Mtb isolates representing 6 of known lineages. The binding is shown as the percentage of reactivity compared to Mtb H37Rv. Data are mean +/- sem. Results are representative of two independent experiments. (*ns*, non significant, $*P < 0.05$, $**P<0.01$, one-way ANOVA with Tukey post-test).

https://doi.org/10.1371/journal.ppat.1006250.g006

capsule is present and were concerned whether the bacteria in the inoculum would bind antibody since these had been treated with detergent. To test whether there was antigen on the surface of such cells we performed macrophage infections with Mtb previously opsonized with conjugate (AM-PA) serum and a preimmune mouse serum. Bacterial counts were enumerated 2 h after infection (S9 Fig). The percentage of bacterial uptake by macrophage was significantly higher when bacteria were previously treated with conjugate serum relative to an untreated control or bacteria treated with a preimmune serum. Notably, we could measure a statistically significant difference in the macrophage uptake of encapsulated Mtb relative to unencapsulated Mtb. This result indicates that the conjugate-specific serum still retain the opsonic properties even though the capsule may have been removed, at least in part, by growth in media with detergent.

Discussion

Here, we demonstrate that immunization with mycobacterial capsular arabinomannan (AM) conjugates elicited responses that contribute to protection against Mtb infection. In this study we, (i) isolated capsular AM from the H37Rv strain of Mtb and developed conjugates with the Mtb related protein Ag85b and Mtb unrelated PA from *B. anthracis*; (ii) found that immunization with different AM conjugates elicited antibody populations with different specificities;

(iii) showed that surface-specific antibodies could directly modify the transcriptional profile and metabolism of mycobacteria; (iv) observed a prolonged survival and a reduction in bacterial numbers in lungs and spleen in mice immunized with Ag85b-AM conjugates after infection with Mtb; (v) observed that the presence of AM-binding antibodies was associated with modest prolongation in survival and a marked reduction in mycobacterial dissemination; (vi) and demonstrated that AM is antigenically variable and could potentially form the basis for a serological characterization of mycobacteria based on serotypes.

Our conjugates generated antibodies to cell-surface AM and LAM, given the overlapping structural motifs in these glycoconjugates. It is noteworthy that the vaccinated mice were challenged with bacteria grown in the presence of detergent, a condition that strips the mycobacterial polysaccharide capsule [22], and thus reduces AM epitopes. Consequently, the efficacy of these conjugates may be greater against encapsulated bacteria.

To our knowledge, this study represents the first effort to investigate a native mycobacterial capsular polysaccharide in a vaccine against pulmonary Mtb infection. Prior studies evaluating AM antigens in experimental conjugate vaccines have used either secreted AM [16] or delipidated LAM [15]. In the former report, mice were immunized with extracellular AM conjugates including the recombinant *Pseudomonas aeruginosa* exoprotein A (rEPA), with no adjuvant, and challenged intravenously with *M. tuberculosis* Erdman. A moderate reduction in lung CFU was observed early in the course of infection [16]. In the latter, AM oligosaccharides (AMOs) derived from LAM of Mtb H37Rv were isolated and covalently conjugated to tetanus toxoid (TT) or to Ag85b from Mtb. Ag85b conjugates were given to mice in Alum providing significant protection compared to sham immunized mice as estimated by long term survival against an intravenous challenge Mtb H37Rv [15]. AMOs-TT conjugates were given subcutaneously followed by nasal boost in the Eurocine L3 adjuvant providing a similar level of protection after a similar challenge with virulent *M. tuberculosis*. Remarkably, the protective efficacy was comparable to that of BCG vaccine. In guinea pigs, immunization with AMOs-Ag85b in Eurocine L3 adjuvant followed by an aerosol challenge with Mtb H37Rv showed an increased in survival and reduced pathology in lungs and spleens relative to non-immunized animals [15]. It is difficult to compare the efficacy of these vaccines as each was tested using different conditions that included the route of immunization, mode of infective challenge or animal model. In fact, only the study using AMOs-Ag85b immunization followed by an aerosol challenge [15] can be compared to our study even though it differs in the mouse strain used as experimental host. Nevertheless, each of these studies provide the consistent result that antibodies to AM modified the course of Mtb infection to the benefit of the host.

Animals immunized with the AM-Ag85b conjugate lived significantly longer than Ag85b-immunized mice, indicating that AM-specific immunity contributes to the protection. Also, we found a similar reduction in CFUs between AM-Ag85b conjugate- and Ag85b-immunized mice. Because Ag85b is a highly immunogenic antigen from Mtb that can elicit protective responses, it is difficult to assess the contribution of AM-specific immunity to the overall protection. Consequently, we also developed AM conjugates including the Mtb unrelated protein PA to study the specific contribution of antibodies to AM to the overall protection and found that circulating antibodies against AM reduced mycobacterial extrapulmonary dissemination in mice, as significant fewer CFUs were detected in spleens. Moreover, mice immunized with AM-PA conjugates manifested only a modest prolongation in survival compared to adjuvant-immunized mice. That the effect on CFU was antibody mediated was confirmed by passively transferring AM-specific serum to naïve mice and showing a similar reduction in CFUs in spleen after infection.

Considering that only zwtterionic polysaccharides can elicit T cell responses [36] and that AM is a neutral polysaccharide, it is extremely unlikely that a polysaccharide-specific T cell

response was responsible for the protective efficacy of the AM-PA conjugate. This fact is consistent with the finding that the transfer of AM-PA T cells does not confer any protection. We observed a trend to a superior protection of AM-Ag85b T cells relative to Ag85b-T cells. Although we do not have a clear explanation for this result we cannot rule out the possibility that the covalent conjugation of AM to Ag85b altered the processing of T cell epitopes in Ag85b to elicit enhanced T cell responses that could be translated into a better protection. A precedent for such an effect was reported in pneumococcal polysaccharide-protein conjugates where the type of polysaccharide altered the T cell response to protein epitopes [37]. Furthermore, conjugation of a PstS1 synthetic peptide to a branched polysaccharide, including a polylysine backbone and DL-alanine side chains elongated by glutamic acid, enhanced human T cell proliferation to peptide [38]. Cross-protection form heterologous unrelated antigen (heterologous immunity) has been reported in viral infection [39]. Experiments addressing the quality of Ag85b-specific responses, possibly involving tetramer analysis, will be of paramount importance to gain insight into this finding.

Our findings are consistent with and supportive of the view that antibodies can play a significant role in the overall protection against Mtb. In addition to the effects observed with antibodies to AM, we obtained evidence that Ag85b-specific antibodies contributed to the control of bacterial replication in lung and spleen as demonstrated by passive transfer experiments. The fact that bacterial numbers in spleens of mice transferred with AM-Ag85b-specific serum were lower relative to mice transferred with Ag85b-specific serum or AM-PA-specific serum, suggests a synergistic effect of antibodies to both the mycobacterial polysaccharide and protein conjugate components. It is noteworthy that Ag85b immunization was previously shown to induce protective responses against Mtb that were believed to be dependent only on cell-mediated immunity [40–44]. Our observations suggest that humoral responses to Ag85b could have also contributed to protection in those vaccine studies.

The specificity of antibodies elicited by AM conjugates was characterized using an array including a set of 30 fragments representing the AM molecule. The AM glycan microarray revealed an enhanced and more diverse response in mice immunized with Mtb AM conjugates than the AM-specific mAb 9d8. Surprisingly, the most reactive fragments included non-mannosylated arabinnan structures with variable grades of branching, indicating that the glycosydic determinant of AM antigenicity is the arabinnan and not mannose part. We observed weak binding of pooled sera from PA and Ag85b-immunized mice to some fragments. Although this binding was low and close to the limit of detection, we cannot rule out that these antigens elicited some weak cross-reactive antibody responses. The fact that AM might be antigenically variable suggests that the abundance or the features of this polysaccharide may be different from strain to strain. In fact, our finding that the reactivity of AM containing sera differed from strain to strain suggests a previously unknown antigenic variation at the mycobacterial surface. This result could have very important implications for vaccine design because it suggests the possibility that some of the variability of BCG and live vaccine candidates may have been the result of antigenic differences between immunizing and infecting strains. Furthermore, this antigenic variation implies that any vaccine attempting to target mycobacterial polysaccharides should include cocktails of polysaccharide or oligosaccharides to cover likely epitopes. In fact, such an approach has proven very successful in vaccination against pneumococcus.

Incubation of AM with mycobacteria resulted in altered metabolism of Mtb implying a direct effect of antibody on bacterial cells. This phenomenon was previously reported with fungi [24] and Gram positive bacteria [25] and is now extended here to mycobacteria. Upregulation of almost the entire *mce1* operon upon AM-specific antibody indicates a very specific response to immunoglobulin binding on the surface. This operon is highly induced when Mtb is inside the host and a *mce1* mutant has more intracellular fatty acids, including mycolic acids

[26, 27]. We found that upon upregulation of *mce1* operon, Mtb reduces the synthesis of mycolic acids. This finding raises the possibility that Mtb may become more susceptible to macrophages after interaction with AM-binding antibodies since mycolic acids strongly contribute to Mtb cell wall permeability and rigidity. The ability of AM-binding antibodies to modify Mtb metabolism opens a new door in our understanding of the potential of humoral immunity against mycobacteria. In addition, we have recently demonstrated that increased human serum IgG titers to capsular AM were associated with enhanced mycobacterial opsonophagocytosis, increased phagolysosomal fusion and intracellular growth reduction in human macrophages; data suggesting that these effects of antibodies to AM are FcR-mediated [45]. We thus hypothesize that some of the effects of the Abs induced by the AM conjugate vaccine are FcR-mediated, while some of the Mtb transcriptional changes could reflect a more direct growth reducing effect on Mtb. Functional *in vitro* and *in vivo* studies with monoclonal Abs are needed to further elucidate the specific effects by which Abs to AM and its oligosaccharide epitopes contribute to the defense against Mtb infection.

Vaccine design in the TB field has been driven by the imperative of attempting to elicit strong cell-mediated responsive while disregarding humoral immunity against Mtb. This view was fueled by overwhelming evidence for an important role for cell-mediated immunity while the role for humoral immunity was considered inconsistent at best. Further fueling this emphasis was the notion that since Mtb is an intracellular pathogen, immunoglobulins as extracellular molecules cannot reach this pathogen. However, that two-dimensional view has been supplanted by the realization that humoral immunity can protect against many intracellular pathogens through numerous mechanisms [46, 47]. Moreover, recent studies have shown that immunoglobulins can have direct effects on microbes including triggering signal transduction and modulating their physiology [48]. The difficulty of assigning a functional role for Abs against Mtb was recently uncovered as being due to the heterogeneity of the Ab response [49]. In addition, human Mtb-specific IgAs have superior capacity to inhibit Mtb growth than IgG antibodies [50], indicating that mucosal immunity should be highly considered. In this regard, we could not measure AM and Ag85b-specific IgAs in serum and BALs, suggesting that the lack of protection provided by the PA-AM conjugate in the lung might be due to the absence of this Isotype.

Although the mechanism of action of antibodies to AM has not been determined, there are a number of possibilities by which these antibodies can mediate protection based on precedents from other systems. AM-binding antibodies could: (i) promote the ingestion by phagocytic cells and increased intracellular killing through FcR-mediated phagocytosis [45, 51]; (ii) alter the inflammatory response thus reducing host-damaging effects on the immune response [52]; iii) promote the clearance of polysaccharide antigens from tissues thus removing immunomodulatory antigens with deleterious effects on the immune response; and/or iv) modulate the metabolism of Mtb to make it more susceptible to host defense mechanisms [53]. Vaccines that elicit AM-binding antibodies may have the potential to recruit humoral immunity for host defense, which could achieve synergy with cellular immune mechanisms.

In summary, our findings are consistent with role of AM-binding antibodies in defense against Mtb infection and suggest that vaccines that elicit both humoral and cell-mediated immunity may be more protective than those that elicit either. These data suggest that antibody-mediated immunity can make an important contribution to the outcome of mycobacterial infection and provide a new impetus for developing vaccines that harness this arm of the immune system.

Methods

Strains and reagents

M. bovis BCG Pasteur and Mtb H37Rv were grown in minimal medium (MM) [KH_2PO_4 1 g/l, Na_2HPO_4 2.5 g/l, asparagine 0.5 g/l, ferric ammonium citrate 50 mg/l, $MgSO_4 \times 7\ H_2O$ 0.5 g/l, $CaCl_2$ 0.5 mg/l, $ZnSO_4$ 0.1 mg/l, 0.1% (v/v) glycerol, and with or without Tyloxapol 0.05% (v/v; Sigma), pH 7.0] or in Middlebrook 7H9 supplemented with 10% (v/v) OADC enrichment (Becton Dickinson Microbiology Systems, Spark, MD), 0.5% (v/v) glycerol and with or without Tyloxapol 0.05% (v/v) for 14 days in a 5% CO_2 incubator at 37˚C. Mtb lineages were a gift from Sebastien Gagneux. Mtb lineages were systematically grown in MM supplemented with 30 mM pyruvate.

Recombinant Ag85b was obtained from AERAS Tb vaccine Foundation (Rockville, MD). Recombinant PA (Protective Antigen from *Bacillus anthracis*) was obtained from David Axelrod Institute, Albany, NY). The 1-cyano-4-dimethylaminopyridinium tetrafluoroborate (CDAP) and the other reagents used during the conjugation reaction were purchased from Sigma. The CS-35 monoclonal antibody recognizing LAM and AM, was obtained from BEI resources (Manassas, VA). The monoclonal antibody 9d8 specifically recognizes mycobacterial capsular AM [10, 54]. The monoclonal antibody 24c5 specifically recognizes mycobacterial capsular α-glucan [55]. Alhydrogel was purchased from InvivoGen (San Diego, US).

Polysaccharide isolation

Capsular polysaccharides were isolated as described, with some modifications [5, 18]. Briefly, cells were pelleted from cultures at 3,450 x g for 15 min at 4˚C. Five mg of glass beads (4 mm, Fisher) per g of cells were added and the mixture was gently shaken by vortex for 1 min. A volume of 50 ml of distilled water was added per g of disrupted cells and centrifuged at 8000 x g for 10 min at 4˚C. The supernatant was recovered, clarified in a 0.22 μm filter unit (Millipore) and lyophilized. To separate the capsular arabinomannan (AM) from the rest of capsular polysaccharides, the capsule residue was resuspended in 4 ml of distilled water and subjected to a chloroform:methanol:water extraction (1:1:0.9). The upper phase was recovered and incubated in a rotavapor at 40˚C overnight. Proteinase K (Sigma) was added at 10 mg/ml in a 50 mM Tris-HCl pH 7.5, 10 mM $CaCl_2$ buffer and incubated overnight at 37˚C. The deproteinated solution was dialyzed for 3 d at 4˚C in distilled water, lyophilized and chromatographed on a column (90 cm x 1.8 cm) of Bio-Gel P-10 (Bio-Rad) using 0.1 M NaCl in 0.1% acetic acid. Collected fractions of 4 ml were assayed for carbohydrate content by the phenol-sulfuric acid assay. Pooled fractions were dialyzed in water and lyophilized. The concentration of protein was determined on each isolation step by Bradford.

Conjugates

Mycobacterial AM-PA and AM-Ag85b conjugates were prepared as described [19, 56]. Briefly, 6 mg of AM was dissolved in 1 ml of borate buffer pH 9.0 and 60 μl of 100 mg/ml 1-cyano-4-dimethylaminopyridinium tetrafluoroborate (CDAP) was added and mixed with agitation for 10 min at room temperature. Then 6 mg of recombinant PA or Ag85b was added in 0.5 ml of 0.15 M HEPES pH 7.5, and the mixture was incubated for 1 h. The reaction was stopped with 100 μl of 0.15 M ethanolamine and incubated for 1 h. The mixture was then dialyzed in PBS for 2 days. To isolate the conjugates from the non-bound AM and PA or Ag85b, the dialyzed conjugated reaction was separated by FPLC on a Sephacryl SH200 (GE Healthcare) in PBS. Each fraction was then assayed for polysaccharide and protein content by the phenol-sulfuric acid assay and Bradford assay, respectively.

Immunization

C57BL/6 female mice between 6 to 8 weeks old were purchased from Jackson Laboratories (Bar Harbor, MN). Animals were maintained in a specific pathogen-free animal facility under animal biosafety level-2 conditions for all experiments except for those involving infection with virulent Mtb for which animal biosafety level-3 conditions were used. Animals were immunized intraperitoneally (i.p) three times with 10 μg of Ag85b-AM or PA-AM conjugates including 1% (w/v) Alum, 1 μg of Ag85b or PA alone including 1% (w/v) Alum. Immunizations were given every two weeks. Control mice received i.p. injections of PBS or 10 μg of AM including 1(w/v) Alum. Alternatively, mice were vaccinated subcutaneously with 1 million BCG as a positive control in protection efficacy experiments or survival studies.

Murine infections

Aerogenic challenge was done using a whole-body exposure aerosol chamber (Mechanical Engineering Workshop) custom fitted to a class III biosafety cabinet (Baker) to deliver approximately 100 CFU per animal of Mtb (H37Rv). Immunized mice were infected four weeks after the last immunization and eight weeks after BCG immunization. Mice were euthanized at 15 and 30 d after challenge. Lungs of individual mice were aseptically removed and homogenized separately in 5 ml normal saline plus 0.05% Tyloxapol using a Seward Stomacher 80 blender (Tekmar). The homogenates were diluted serially and plated on Middlebrook 7H11 agar to determine CFU of Mtb. Dilutions 10^{-2} and 10^{-3}, and 10^{-2} and 10^{-1} were platted when counting CFUs in lungs and spleens, respectively.

In bacterial loads studies, animals infected with Mtb H37Rv were observed at least twice daily until they died or became moribund and were euthanized.

Macrophage infection

J774 macrophages (ATCC TIB 67) were plated in 96-well plates in complete DMEM. The cells were washed with DMEM and infected with Mtb, previously grown in MM with or without Tyloxapol, at an MOI of 10:1 for 2 h at 37˚C. Before infection bacteria were opsonized with 20 μg/ml of pre-immune serum or H37Rv-conjugate serum for 30 min. Cell lysates were prepared by removing the medium and lysing with 0.05% SDS. Serial dilutions of the lysate were plated on 7H11 agar, and incubated at 37˚C for 21 days before counting CFUs.

Transmission electron microscopy

Cells of *M. bovis* BCG Pasteur and *M. tuberculosis* H37Rv were grown in minimal medium and fixed with 2% glutaraldehyde in 0.1 M cacodylate at room temperature for 2 h, and then incubated overnight in 4% formaldehyde, 1% glutaraldehyde, and 0.1% PBS. After fixation the samples were stained for 90 min in 2% osmium tetraoxide, then serially dehydrated in ethanol and embedded in Spurrs epoxy resin. Thin sections were obtained on an Ultracut UCT (Reichert) and stained with 0.5% uranyl acetate and 0.5% lead citrate (Reichart, Depew, NY, USA). Immunogold TEM (IEM) was performed as previously described with a polyclonal murine immune serum diluted 1:300 or monoclonal murine IgG2a 9d8 antibody (10 μg ml^{-1}) and then immunogold stained using 6 nm goat α-mouse gold (Electron Microscopy Sciences). Samples were viewed on a JEOL 100CXII or JEOL 1200EX at 80kV.

Scanning electron microscopy

Cells of *M . bovis* BCG Pasteur and *M. tuberculosis* H37Rv were fixed with 2.5% glutaraldehyde, 0.1 M sodium cacodylate, 0.2 M sucrose, 5 mM $MgCl_2$ pH 7.4 and dehydrated through a

graded series of ethanol solutions. Critical point dry was accessed using liquid carbon dioxide in a Toumisis Samdri 795 Critical Point drier (Rockville,MD, USA). Sputter was coated with gold-palladium in a Denton Vacuum Desk-2 Sputter Coater (Cherry Hill, NJ, USA). Samples were examined in a Zeiss Supra Field Emission Scanning Electron Microscope (Carl Zeiss Microscopy, LLC North America), using an accelerating voltage of 5 kV.

ELISA

Two types of ELISA were used in this study. In one assay polystyrene microtiter plate wells were coated with 50 μl of AM (5 μg/ml) in carbonate buffer (0.015 M Na_2CO_3, 0.035 M $NaHCO_3$, 0.003 M NaN_3; pH 9.8) or with 1 μg of recombinant proteins (PA or Ag85b) in PBS by incubating the plates 2 h at room temperature. The wells were then blocked by adding 200 μl of 2% BSA in TBS and incubated at 37˚C for 1 h. Serum from conjugate-immunized mice, PBS-injected mice or recombinant Ag85b or PA-injected mice were added to the wells and incubated for 1 h at 37˚C. The plates were then washed and 50 μl of a 1 μg/ml solution of Goat anti-mouse-alkaline phosphatase (GAM-AP) IgG1, IgG2b, IgG2c, IgG3 or IgM antibody (Southern Biotechnologies) for 1 h at 37˚C. The ELISA plates were washed and developed by using *p*-nitrophenylphosphate substrate. Results are presented as inverse titers, what means the inverse of the greatest dilution that still gives a positive result, after removing the background (2 times OD from control serum). Isolated AM from KZN clinical isolates was also tested for reactivity to mAb 9d8 and AM-immune serum following the above protocol.

Whole cell ELISA was used to measure the relative reactivity of monoclonals Ab 9d8 and 24c5 to different clinical isolates. For this ELISA, mycobacterial cells were killed by heating to 80˚C for 2 h. Bacterial cells were dispersed by drawing up and expelling the bacterial suspension 10 times through a 25-gauge needle attached to a 1-ml syringe. The suspension was then allowed to settle in a transparent 1.5-ml microcentrifuge tube, and the supernatant was removed, leaving 100 μl of settled bacteria. The number of bacteria used was standardized according to the amount of protein in a 100-μl volume of sedimented bacteria. Coated plates were blocked as above and incubated with either a-glucan-specific mAb 24c5 or AM-specific mAb 9d8. The plates were then washed and 50 μl of a 1 μg/ml solution of goat anti-mouse-alkaline phosphatase (GAM-AP) IgG antibody was added to each well for 1 h at 37˚C. The ELISA plates were washed and developed by using *p*-nitrophenylphosphate substrate.

AM microarray

A panel of 30 AM fragments (corresponding to motifs at the non-reducing terminus of the molecule, which have previously been shown to be recognized by anti-AM/LAM Abs) [57–59] were synthesized, and coupled to BSA via a squarate-linker [60]. Arrays were printed and used as described [61]. Briefly, after blocking with 3% BSA/PBS, AM microarrays were incubated with diluted mouse sera (1:400), or the murine IgG2a mAb 9d8 (known to recognize only Mtb AM) [62], followed by incubation with goat anti-mouse biotin-labeled IgG (Southern Biotech, AL; Jackson Immunoresearch, PA) and incubation with a Streptavidin probe tagged with Sure-Light-P3 Cy5 (Cayman Chemicals, MI). The slides were scanned using the GenePix 4000 Microarray scanner system (Molecular Devices, CA). Images were analyzed by the image-processing software Spotfinder (http://www.tm4.org/spotfinder.html), which measured median pixel intensity (MPI) and neighboring background pixel intensity (BPI) of individual spots. The median fluorescent reactivity (MFI), representing AM-epitope specific Ab responses, was the MPI subtracted by the BPI. The minimum value of pixel intensity was determined by the MFI of the spots with low quality, which was determined by the software quality control score

for each spot depending on signal-to-noise ratio and spot shape. The final MFI was averaged from the triplicates. The symbolic nomenclature used is that recommended by the Consortium for Functional Glycomics. Green circles = mannose; Green stars = arabinose; orange stars = 5-thiomethyl-xylose; white ovals = inositol. The linkage position and stereochemistry between the monosaccharides is indicated over the line connecting them. 3P5 = a phosphate linkage between O3 of the inositol and O5 of an arabinose residue [63].

Microarray analysis

M. tuberculosis was grown in MM with detergent for 6 days and then subcultured in fresh MM without detergent for 5 days. Cultures were harvested and submitted to a syringe and gentle sonication to breakdown the clumps. Bacterial cells were further incubated with AM-PA and PA immune sera (1:200 dilution) for 4 h. After treatment cell were washed once on PBS and resuspended in Trizol (Ambion, Carlsbad, CA). Cells were disrupted by mechanical lysis in a FastPrep-24 instrument (MP Biomedicals, Santa Ana, CA) in Lysing Matrix B tubes and RNA was purified with the Direct-zol RNA miniprep kit (Zymo Research, Irvine, CA). cDNA probes were prepared and hybridized to DNA microarrays (Microarrays, Inc. Huntsville, AL), which were scanned and analyzed as described previously [64]. Briefly, slides were scanned on a GenePix 4000A scanner (Molecular Devices, Sunnyvale, CA) and processed with the TM4 software suite (http://www.TM4.org). TIGR Spotfinder was used to grid and quantify spots. TIGR MIDAS was used for Lowess normalization, standard deviation regularization and in-slide replicate analysis, with all quality control flags on and one bad channel tolerance policy set to generous. Results were analysed in MeV with Significance Analysis of Microarrays (SAM) and hierarchical clustering algorithms. Microarray data was deposited with the GEO NCBI database with the accession number GSE77711.

For quantitative PCR (qPCR) experiments, diluted cDNA was used as a template at 50 ng per reaction for real-time PCR reactions containing primer sets designed by Primer 3 and SYBR Green PCR Master Mix (Applied Biosystems) in accordance with the manufacturers' instructions. qRT-PCR reactions were performed on an ABI 9700HT real-time PCR cycler (Applied Biosystems).

Fatty acid analysis

M. tuberculosis was grown in MM with detergent for 6 days and then subcultured in fresh MM without detergent for 5 days. Cultures were harvested and submitted to a syringe and gentle sonication to breakdown the clumps. Bacterial cells were further labeled with ^{14}C-acetate (10μCi in 10ml culture) for 22h and incubated with AM-PA and PA immune sera (1:400 dilution) for 10 h. Bacterial pellets were treated with 20% tetrabutylammonium hydroxide at 100˚C overnight. Cell suspensions were further methylated with methyl iodide (0.1ml) in dichloromethane (2ml) for 1h and the organic phase was washed twice and dried [65]. Fatty acids were analyzed by TLC (hexane/ethyl acetate; 95/5; 3 elutions).

Histology

Lungs were removed and fixed in 10% neutral buffered formalin (Fisher Scientific, Fair Lawn, NJ). Tissues were embedded with paraffin, sectioned at 5 μm thickness, and stained with haematoxylin and eosin stain. Five different lung sections per mouse were analyzed. Slides were scanned with a Perkin Elmer P250 High Capacity Slide Scanner (Waltham, Massachusetts) at 2,000 dots per inch (dpi). Digitized images were then analyzed using ImageJ software to calculate the total disease area occupied by granuloma and the percentage of lung surface affected by pneumonia as well as the number of infiltrates per lung. The total disease area for the entire

lung section was calculated by adding the values for each lesion. The total percentage of diseased tissue was calculated by dividing the total disease area by the entire lung section and multiplying by 100, using image J software.

Passive serum transfer experiments

Blood was collected from the retro-orbital plexus from C57BL/6 mice immunized three times with either 10 μg of Ag85b-AM conjugate, 1 μg of Ag85b, 10 μg of PA-AM conjugate, 1 μg of PA in 200 μl of 1% (w/v) Alum. Vaccines were administered at two weeks intervals. Control sera were obtained from mice that received i.p. injections of PBS, 1% (w/v) Alum or 1 million of bacteria of BCG (subcutaneously). Sera were collected after clarification by centrifugation of clotted blood and stored at −80˚C until use. Two hundred μl of immune and control sera were administered i.p. 4h before infection with 100 CFU of *M*. *tuberculosis* H37Rv. Four weeks after infection mice CFUs were assessed in lung and spleen.

Adoptive T cell transfer experiments

Total T cell populations were isolated from spleens from C57BL/6 mice immunized three times with 10 μg of Ag85b-AM conjugate, 1 μg of Ag85b, 10 μg of PA-AM conjugate, 1 μg of PA in 200 μl of 1% (w/v) Alum. Control T cells were obtained from mice that received i.p. injections of PBS, 1% (w/v) Alum or 1 million of bacteria of BCG (subcutaneously). Spleens were homogenized and treated with RBC lysis buffer (Sigma–Aldrich, St. Louis, MO). Splenic T cells were purified using the Pan T cell isolation kit (Miltenyi Biotec, Germany). An aliquot of isolated T cells was stimulated with 1 μg ml^{-1} of the synthetic peptide antigens (Invitrogen): FQDAYNAAGGH-NAVF (Ag85B-P25; residues 240–254 of MTb/BCG Ag85B, I-Ab restricted); and 5 μg ml-1 of PA from *Bacilllus anthracis* to assess their specificity. Unstimulated wells served as negative controls in naive mice. Samples were combined with 1 μg ml^{-1} soluble antibody to mouse CD28 (clone 37.51; eBioscience) and 1 μg ml^{-1} soluble antibody to mouse CD49d (clone 9F10; eBioscience). After 2 h at 37˚C, 10 μg ml^{-1} of brefeldin A (Sigma) 10 μg ml^{-1} of monensin (Sigma) were added to all samples, followed by incubation for 6 h at 37˚C. Cells were stained with blue LIVE/DEAD viability dye (Invitrogen) followed by antibody to FcγRII/III (clone 2.4G2; American Type Culture Collection), with fluorochrome-conjugated monoclonal antibodies for surface staining: antibody to CD3ε (clone 145-2C11; eBioscience), antibody to CD8α (clone 53–6.7; BD Bioscience), antibody to CD4 (clone GK1.5; BD Bioscience), and antibody to CD45R (B220) (clone RA3-6B2; BD Bioscience). Cells were fixed with 2% (vol/vol) paraformaldehyde, washed with permeabilization buffer (PBS with 1 mM Ca^{2+}, 1 mM Mg^{2+}, 1 mM HEPES [N-2-hydroxyethylpiperazine-N′-2-ethanesulfonic acid], 2% [vol/vol] FCS, and 0.1% [wt/vol] saponin) and then blocked in permeabilization buffer plus 5% (vol/vol) normal mouse serum (Jackson ImmunoResearch Laboratories). Intracellular cytokines were detected with fluorochrome-conjugated antibodies to IL-2 (clone JES6-5H4; eBioscience), IFN-γ (clone XMG1.2), TNF-α (MP6-XT22) (both from BD Biosciences). Data were acquired on an LSR II flow cytometer (BD Biosciences), and data analysis was performed using FlowJo software v.10 (Tree Star).

C57BL/6 mice were injected i.p with 4 mg/mouse of cyclophosphamide to partially deplete lymphocytes and promote engraftment of transferred cells [66], and 2 days later received adoptive transfer of 4×10^6 isolated total T cells. Twenty-four h later the recipient mice were subjected to a low dose (50–100 CFU) aerosol challenge with Mtb H37Rv. Lungs and spleens were harvested for CFU counts 4 weeks after infection.

Statistical analysis

Standard one-way ANOVA followed by Tukey's multiple comparison test of the means was used to determine statistical significance of immune responses and protective efficacies of the conjugates. $P<0.05$ was considered statistically significant.

Survival data were analyzed by comparing Kaplan-Meier survival curves with a log-rank test (GraphPad Prism); after the log-rank test, a Grehan-Breslow-Wilcoxon modification of the log-rank test was used in an exploratory manner to apply more weight to early events in experiments where larger differences in early survival were observed.

Ethics statement

Mouse studies were performed in accordance to National Institutes of Health guidelines using recommendations in the Guide for the Care and Use of Laboratory Animals. The protocols used in this study were approved by the Institutional Animal Care and Use Committee of Albert Einstein College of Medicine (Protocols #20120110; #20150110).

Supporting information

S1 Fig. Isolation of capsular AM. (A) Electron micrograph of Mtb H37Rv cells grown in minimal media without detergent. Notice the capsule surrounding the cells. Scale bar is 100 nm. **(B)** Scanning electron micrograph of Mtb H37Rv cells grown in minimal media without detergent. Arrow denotes the polysaccharide capsule. Scale bar 1 μm. **(C)** Gel chromatography of light Mtb capsular polysaccharides on a PD-10 size exclusion column. Fractions of 4 ml were taken and the carbohydrate content was estimated by phenol-sulphuric acid method. "Vo" means void volume. The pooled fractions are indicated by letters. **(D)** Binding of 9d8 (anti-AM) (top graph) and 24c5 (anti-α-glucan) (bottom graph) monoclonal antibodies at various concentrations of the indicated PD-10 fractions. The diagram indicates the ELISA configuration. PS, Polysaccharide fraction; AP, alkaline phosphatase; GAM, goat anti-mouse. Capsular polysaccharide isolation was performed up to four times using the same experimental conditions. The results are representative of three independent experiments.
(PDF)

S2 Fig. Purification of AM-conjugates. (A,B) Separation of the conjugate reactions AM-Ag85b **(A)** or AM-PA **(B)** on Sephacryl S-200 size exclusion column in PBS. Fractions were monitored by on-line measurements of protein content at 280 nm (dotted line) and post-column by measurement of carbohydrate content (straight line) by phenol sulphuric acid method.
(PDF)

S3 Fig. Kinetics of AM-binding antibodies after immunization with AM-Ag85b conjugates. Inverse titers (total IgG) of AM-binding antibodies measured by ELISA in serum from C57BL/6 mice ($n = 3$ per group) immunized with different amounts of AM-Ag85b conjugate. Mice were immunized every two weeks twice after initial immunization. Measurements were performed at 2, 4 and 8 weeks after the initial immunization.
(PDF)

S4 Fig. Specificity of AM-immune serum. Inverse titers of Abs from AM-Ag85b conjugate serum for binding to different components of mycobacterial cell surface measured by ELISA in serum from C57BL/6 mice ($n = 3$ per group). Mice were immunized three times with 10 μg of AM-Ag85b conjugate. The results are representative of three independent experiments performed in the same manner. AM, arabinomannan; AG, arabinogalactan; LAM, lipoarabinomannan; LM, lipomannan; ManLAM, mannose capped LAM; TDM, trehalose deoxy mycolate; mAGP,

mycolate arabinogalactan peptidoglycan. complex
(PDF)

S5 Fig. Immunogold electron microscopy of thin sections of Mtb H37Rv cells treated with immune sera specific for the indicated antigens and detected with a 6-nm IgG gold-labeled anti-mouse antibody. Mtb cells were grown in the presence (MMT) or in the absence of detergent (MM). Scale bar 100 nm.
(PDF)

S6 Fig. AM fragments included in the glycan microarray representing the AM molecule. The symbolic nomenclature used is that recommended by the Consortium for Functional Glycomics. Green circles = mannose; Green stars = arabinose; orange stars = 5-thiomethyl-xylose; white ovals = inositol. The linkage position and stereochemistry between the monosaccharides is indicated over the line connecting them. 3P5 = a phosphate linkage between O3 of the inositol and O5 of an arabinose residue [63].
(PDF)

S7 Fig. Morphometric analysis of lung histopathology by assessing the number of infiltrates per lung (bottom graph) and the percentage of diseased tissue (top graph) ($^{*}P < 0.05$, $^{**}P<0.01$ $^{***}P < 0.001$, one-way ANOVA with Tukey post-test); *ns*, not significant.
(PDF)

S8 Fig. Specificity of the isolated T cells. Mice were immunized with AM conjugates, PA and Ag85b in Alum and after 4 weeks T cells were isolated. Specificity of $CD4^{+}$ T cells was assessed by intracellular cytokine staining after stimulation with the indicated antigens (PA, p25). Data are mean +/- sem. Results are representative of two independent experiments.
(PDF)

S9 Fig. Phagocytosis of opsonized Mtb by J774 macrophages. J774 macrophages were infected with unencapsulated (uncap) or encapsulated (encap) *M. tuberculosis* H37Rv, which were previously opsonized with conjugate (H37Rv) serum (CS), pre-immune mouse serum or untreated at an MOI of 10:1, and CFU counts were obtained 2 h after infection. Data shown are representative of 2 independent and similar experiments ($^{*}p < 0.05$).
(PDF)

Acknowledgments

AB acknowledges Estrategia de Sostenibilidad, Universidad de Antioquia.

Author Contributions

Conceptualization: RPR AC.

Data curation: RPR LC TC CB BW.

Formal analysis: RPR TC CB BW.

Funding acquisition: RPR AC JA JMA SAP WRJ JC.

Investigation: RPR LC TC CB BW AM AB RK ABG NAS LS JT JA JX.

Resources: AGF SCH AT YB MJ TLL.

Supervision: RPR AC.

Validation: RPR.

Visualization: RPR TC TLL.

Writing – original draft: RPR AC JMA.

Writing – review & editing: RPR AC.

References

1. Baena A, Porcelli SA. Evasion and subversion of antigen presentation by Mycobacterium tuberculosis. Tissue Antigens. 2009; 74(3):189–204. Epub 2009/07/01. PubMed Central PMCID: PMC2753606. https://doi.org/10.1111/j.1399-0039.2009.01301.x PMID: 19563525
2. Daffe M, Etienne G. The capsule of Mycobacterium tuberculosis and its implications for pathogenicity. Tuber Lung Dis. 1999; 79(3):153–69. Epub 2000/02/03. https://doi.org/10.1054/tuld.1998.0200 PMID: 10656114
3. Guo H, Yi W, Song JK, Wang PG. Current understanding on biosynthesis of microbial polysaccharides. Curr Top Med Chem. 2008; 8(2):141–51. Epub 2008/02/22. PMID: 18289083
4. Sani M, Houben EN, Geurtsen J, Pierson J, de Punder K, van Zon M, et al. Direct visualization by cryo-EM of the mycobacterial capsular layer: a labile structure containing ESX-1-secreted proteins. PLoS Pathog. 2010; 6(3):e1000794. PubMed Central PMCID: PMC2832766. https://doi.org/10.1371/journal.ppat.1000794 PMID: 20221442
5. Ortalo-Magne A, Dupont MA, Lemassu A, Andersen AB, Gounon P, Daffe M. Molecular composition of the outermost capsular material of the tubercle bacillus. Microbiology. 1995; 141 (Pt 7):1609–20. Epub 1995/07/01.
6. Briken V, Porcelli SA, Besra GS, Kremer L. Mycobacterial lipoarabinomannan and related lipoglycans: from biogenesis to modulation of the immune response. Molecular microbiology. 2004; 53(2):391–403. Epub 2004/07/02. https://doi.org/10.1111/j.1365-2958.2004.04183.x PMID: 15228522
7. Yu X, Prados-Rosales R, Jenny-Avital ER, Sosa K, Casadevall A, Achkar JM. Comparative evaluation of profiles of antibodies to mycobacterial capsular polysaccharides in tuberculosis patients and controls stratified by HIV status. Clinical and vaccine immunology: CVI. 2012; 19(2):198–208. Epub 2011/12/16. PubMed Central PMCID: PMC3272928. https://doi.org/10.1128/CVI.05550-11 PMID: 22169090
8. Costello AM, Kumar A, Narayan V, Akbar MS, Ahmed S, Abou-Zeid C, et al. Does antibody to mycobacterial antigens, including lipoarabinomannan, limit dissemination in childhood tuberculosis? Trans R Soc Trop Med Hyg. 1992; 86(6):686–92. Epub 1992/11/01. PMID: 1287946
9. Glatman-Freedman A, Mednick AJ, Lendvai N, Casadevall A. Clearance and organ distribution of Mycobacterium tuberculosis lipoarabinomannan (LAM) in the presence and absence of LAM-binding immunoglobulin M. Infection and immunity. 2000; 68(1):335–41. Epub 1999/12/22. PubMed Central PMCID: PMC97139. PMID: 10603406
10. Teitelbaum R, Glatman-Freedman A, Chen B, Robbins JB, Unanue E, Casadevall A, et al. A mAb recognizing a surface antigen of Mycobacterium tuberculosis enhances host survival. Proc Natl Acad Sci U S A. 1998; 95(26):15688–93. PubMed Central PMCID: PMC28105. PMID: 9861031
11. Hamasur B, Haile M, Pawlowski A, Schroder U, Kallenius G, Svenson SB. A mycobacterial lipoarabinomannan specific monoclonal antibody and its F(ab') fragment prolong survival of mice infected with Mycobacterium tuberculosis. Clin Exp Immunol. 2004; 138(1):30–8. Epub 2004/09/18. PubMed Central PMCID: PMC1809178. https://doi.org/10.1111/j.1365-2249.2004.02593.x PMID: 15373902
12. 2015 GTC. WHO. Geneva, Switzerland: WHO, 2015.
13. Kaufmann SH. Future vaccination strategies against tuberculosis: thinking outside the box. Immunity. 2010; 33(4):567–77. Epub 2010/10/30. https://doi.org/10.1016/j.immuni.2010.09.015 PMID: 21029966
14. Glatman-Freedman A. The role of antibody-mediated immunity in defense against Mycobacterium tuberculosis: advances toward a novel vaccine strategy. Tuberculosis (Edinb). 2006; 86(3–4):191–7.
15. Hamasur B, Kallenius G, Svenson SB. Synthesis and immunologic characterisation of Mycobacterium tuberculosis lipoarabinomannan specific oligosaccharide-protein conjugates. Vaccine. 1999; 17 (22):2853–61. Epub 1999/08/07. PMID: 10438056
16. Glatman-Freedman A, Casadevall A, Dai Z, Jacobs WR Jr., Li A, Morris SL, et al. Antigenic evidence of prevalence and diversity of Mycobacterium tuberculosis arabinomannan. J Clin Microbiol. 2004; 42 (7):3225–31. PubMed Central PMCID: PMC446310. https://doi.org/10.1128/JCM.42.7.3225-3231.2004 PMID: 15243086
17. Antoine AD, Tepper BS. Characterization of glycogens from mycobacteria. Arch Biochem Biophys. 1969; 134(1):207–13. PMID: 4981255

18. Ortalo-Magne A, Andersen AB, Daffe M. The outermost capsular arabinomannans and other manno-conjugates of virulent and avirulent tubercle bacilli. Microbiology. 1996; 142 (Pt 4):927–35. Epub 1996/04/01.
19. Lees A, Nelson BL, Mond JJ. Activation of soluble polysaccharides with 1-cyano-4-dimethylaminopyridinium tetrafluoroborate for use in protein-polysaccharide conjugate vaccines and immunological reagents. Vaccine. 1996; 14(3):190–8. Epub 1996/02/01. PMID: 8920699
20. Lees A, Sen G, LopezAcosta A. Versatile and efficient synthesis of protein-polysaccharide conjugate vaccines using aminooxy reagents and oxime chemistry. Vaccine. 2006; 24(6):716–29. Epub 2005/10/20. https://doi.org/10.1016/j.vaccine.2005.08.096 PMID: 16233938
21. Lindenstrom T, Agger EM, Korsholm KS, Darrah PA, Aagaard C, Seder RA, et al. Tuberculosis subunit vaccination provides long-term protective immunity characterized by multifunctional CD4 memory T cells. J Immunol. 2009; 182(12):8047–55. https://doi.org/10.4049/jimmunol.0801592 PMID: 19494330
22. Stokes RW, Norris-Jones R, Brooks DE, Beveridge TJ, Doxsee D, Thorson LM. The glycan-rich outer layer of the cell wall of Mycobacterium tuberculosis acts as an antiphagocytic capsule limiting the association of the bacterium with macrophages. Infection and immunity. 2004; 72(10):5676–86. PubMed Central PMCID: PMCPMC517526. https://doi.org/10.1128/IAI.72.10.5676-5686.2004 PMID: 15385466
23. Daffe M, Brennan PJ, McNeil M. Predominant structural features of the cell wall arabinogalactan of Mycobacterium tuberculosis as revealed through characterization of oligoglycosyl alditol fragments by gas chromatography/mass spectrometry and by 1H and 13C NMR analyses. The Journal of biological chemistry. 1990; 265(12):6734–43. Epub 1990/04/25. PMID: 2108960
24. McClelland EE, Nicola AM, Prados-Rosales R, Casadevall A. Ab binding alters gene expression in Cryptococcus neoformans and directly modulates fungal metabolism. The Journal of clinical investigation. 2010; 120(4):1355–61. PubMed Central PMCID: PMCPMC2846037. https://doi.org/10.1172/JCI38322 PMID: 20335660
25. Yano M, Gohil S, Coleman JR, Manix C, Pirofski LA. Antibodies to Streptococcus pneumoniae capsular polysaccharide enhance pneumococcal quorum sensing. mBio. 2011; 2(5). PubMed Central PMCID: PMCPMC3171983.
26. Dunphy KY, Senaratne RH, Masuzawa M, Kendall LV, Riley LW. Attenuation of Mycobacterium tuberculosis functionally disrupted in a fatty acyl-coenzyme A synthetase gene fadD5. The Journal of infectious diseases. 2010; 201(8):1232–9. PubMed Central PMCID: PMCPMC3225055. https://doi.org/10.1086/651452 PMID: 20214478
27. Casali N, White AM, Riley LW. Regulation of the Mycobacterium tuberculosis mce1 operon. J Bacteriol. 2006; 188(2):441–9. PubMed Central PMCID: PMCPMC1347267. https://doi.org/10.1128/JB.188.2.441-449.2006 PMID: 16385033
28. Shimono N, Morici L, Casali N, Cantrell S, Sidders B, Ehrt S, et al. Hypervirulent mutant of Mycobacterium tuberculosis resulting from disruption of the mce1 operon. Proceedings of the National Academy of Sciences of the United States of America. 2003; 100(26):15918–23. PubMed Central PMCID: PMCPMC307668. https://doi.org/10.1073/pnas.2433882100 PMID: 14663145
29. Forrellad MA, McNeil M, Santangelo Mde L, Blanco FC, Garcia E, Klepp LI, et al. Role of the Mce1 transporter in the lipid homeostasis of Mycobacterium tuberculosis. Tuberculosis (Edinb). 2014; 94(2):170–7. PubMed Central PMCID: PMCPMC3951760.
30. Kaufmann SH. Tuberculosis vaccines—a new kid on the block. Nat Med. 2011; 17(2):159–60. Epub 2011/02/08. https://doi.org/10.1038/nm0211-159 PMID: 21297606
31. Orme IM, Collins FM. Protection against Mycobacterium tuberculosis infection by adoptive immunotherapy. Requirement for T cell-deficient recipients. The Journal of experimental medicine. 1983; 158(1):74–83. PubMed Central PMCID: PMCPMC2187069. PMID: 6602861
32. Kalin M. Pneumococcal serotypes and their clinical relevance. Thorax. 1998; 53(3):159–62. PubMed Central PMCID: PMC1745174. PMID: 9659348
33. Weintraub A. Immunology of bacterial polysaccharide antigens. Carbohydr Res. 2003; 338(23):2539–47. PMID: 14670715
34. Coscolla M, Gagneux S. Consequences of genomic diversity in Mycobacterium tuberculosis. Semin Immunol. 2014; 26(6):431–44. PubMed Central PMCID: PMCPMC4314449. https://doi.org/10.1016/j.smim.2014.09.012 PMID: 25453224
35. Schwebach JR, Casadevall A, Schneerson R, Dai Z, Wang X, Robbins JB, et al. Expression of a Mycobacterium tuberculosis arabinomannan antigen in vitro and in vivo. Infection and immunity. 2001; 69(9):5671–8. Epub 2001/08/14. PubMed Central PMCID: PMC98683. https://doi.org/10.1128/IAI.69.9.5671-5678.2001 PMID: 11500443
36. Kalka-Moll WM, Tzianabos AO, Wang Y, Carey VJ, Finberg RW, Onderdonk AB, et al. Effect of molecular size on the ability of zwitterionic polysaccharides to stimulate cellular immunity. J Immunol. 2000; 164(2):719–24. PMID: 10623815

37. McCool TL, Harding CV, Greenspan NS, Schreiber JR. B- and T-cell immune responses to pneumococcal conjugate vaccines: divergence between carrier- and polysaccharide-specific immunogenicity. Infection and immunity. 1999; 67(9):4862–9. PubMed Central PMCID: PMCPMC96820. PMID: 10456942

38. Wilkinson KA, Hudecz F, Vordermeier HM, Ivanyi J, Wilkinson RJ. Enhancement of the T cell response to a mycobacterial peptide by conjugation to synthetic branched polypeptide. European journal of immunology. 1999; 29(9):2788–96. https://doi.org/10.1002/(SICI)1521-4141(199909)29:09<2788::AID-IMMU2788>3.0.CO;2-4 PMID: 10508253

39. Shen ZT, Nguyen TT, Daniels KA, Welsh RM, Stern LJ. Disparate epitopes mediating protective heterologous immunity to unrelated viruses share peptide-MHC structural features recognized by cross-reactive T cells. J Immunol. 2013; 191(10):5139–52. PubMed Central PMCID: PMCPMC3844262. https://doi.org/10.4049/jimmunol.1300852 PMID: 24127554

40. Teixeira FM, Teixeira HC, Ferreira AP, Rodrigues MF, Azevedo V, Macedo GC, et al. DNA vaccine using Mycobacterium bovis Ag85B antigen induces partial protection against experimental infection in BALB/c mice. Clinical and vaccine immunology: CVI. 2006; 13(8):930–5. PubMed Central PMCID: PMCPMC1539111. https://doi.org/10.1128/CVI.00151-06 PMID: 16893994

41. Ko HJ, Ko SY, Kim YJ, Lee EG, Cho SN, Kang CY. Optimization of codon usage enhances the immunogenicity of a DNA vaccine encoding mycobacterial antigen Ag85B. Infection and immunity. 2005; 73 (9):5666–74. PubMed Central PMCID: PMCPMC1231050. https://doi.org/10.1128/IAI.73.9.5666-5674.2005 PMID: 16113284

42. Kamath AT, Feng CG, Macdonald M, Briscoe H, Britton WJ. Differential protective efficacy of DNA vaccines expressing secreted proteins of Mycobacterium tuberculosis. Infection and immunity. 1999; 67 (4):1702–7. PubMed Central PMCID: PMCPMC96517. PMID: 10085007

43. Lozes E, Huygen K, Content J, Denis O, Montgomery DL, Yawman AM, et al. Immunogenicity and efficacy of a tuberculosis DNA vaccine encoding the components of the secreted antigen 85 complex. Vaccine. 1997; 15(8):830–3. PMID: 9234526

44. Aagaard C, Hoang T, Dietrich J, Cardona PJ, Izzo A, Dolganov G, et al. A multistage tuberculosis vaccine that confers efficient protection before and after exposure. Nat Med. 2011; 17(2):189–94. https://doi.org/10.1038/nm.2285 PMID: 21258338

45. Chen T, Blanc C, Eder AZ, Prados-Rosales R, Souza AC, Kim RS, et al. Association of Human Antibodies to Arabinomannan With Enhanced Mycobacterial Opsonophagocytosis and Intracellular Growth Reduction. The Journal of infectious diseases. 2016.

46. Achkar JM, Casadevall A. Antibody-mediated immunity against tuberculosis: implications for vaccine development. Cell host & microbe. 2013; 13(3):250–62. Epub 2013/03/19.

47. Casadevall A, Pirofski LA. Immunoglobulins in defense, pathogenesis, and therapy of fungal diseases. Cell host & microbe. 2012; 11(5):447–56. Epub 2012/05/23. PubMed Central PMCID: PMC3360875.

48. Casadevall A, Pirofski LA. A new synthesis for antibody-mediated immunity. Nature immunology. 2012; 13(1):21–8. Epub 2011/12/20. PubMed Central PMCID: PMC3589717.

49. Lu LL, Chung AW, Rosebrock TR, Ghebremichael M, Yu WH, Grace PS, et al. A Functional Role for Antibodies in Tuberculosis. Cell. 2016; 167(2):433–43 e14. https://doi.org/10.1016/j.cell.2016.08.072 PMID: 27667685

50. Zimmermann N, Thormann V, Hu B, Kohler AB, Imai-Matsushima A, Locht C, et al. Human isotype-dependent inhibitory antibody responses against Mycobacterium tuberculosis. EMBO Mol Med. 2016; 8 (11):1325–39. https://doi.org/10.15252/emmm.201606330 PMID: 27729388

51. Mukherjee J, Scharff MD, Casadevall A. Protective murine monoclonal antibodies to Cryptococcus neoformans. Infection and immunity. 1992; 60(11):4534–41. Epub 1992/11/01. PubMed Central PMCID: PMC258199. PMID: 1398966

52. Nimmerjahn F, Ravetch JV. The antiinflammatory activity of IgG: the intravenous IgG paradox. The Journal of experimental medicine. 2007; 204(1):11–5. Epub 2007/01/18. PubMed Central PMCID: PMC2118416. https://doi.org/10.1084/jem.20061788 PMID: 17227911

53. Glatman-Freedman A, Casadevall A. Serum therapy for tuberculosis revisited: reappraisal of the role of antibody-mediated immunity against Mycobacterium tuberculosis. Clinical microbiology reviews. 1998; 11(3):514–32. Epub 1998/07/17. PubMed Central PMCID: PMC88894. PMID: 9665981

54. Glatman-Freedman A, Martin JM, Riska PF, Bloom BR, Casadevall A. Monoclonal antibodies to surface antigens of Mycobacterium tuberculosis and their use in a modified enzyme-linked immunosorbent spot assay for detection of mycobacteria. Journal of clinical microbiology. 1996; 34(11):2795–802. Epub 1996/11/01. PubMed Central PMCID: PMC229406. PMID: 8897185

55. Schwebach JR, Glatman-Freedman A, Gunther-Cummins L, Dai Z, Robbins JB, Schneerson R, et al. Glucan is a component of the Mycobacterium tuberculosis surface that is expressed in vitro and in vivo.

Infection and immunity. 2002; 70(5):2566–75. Epub 2002/04/16. PubMed Central PMCID: PMC127896. https://doi.org/10.1128/IAI.70.5.2566-2575.2002 PMID: 11953397

56. Shafer DE, Toll B, Schuman RF, Nelson BL, Mond JJ, Lees A. Activation of soluble polysaccharides with 1-cyano-4-dimethylaminopyridinium tetrafluoroborate (CDAP) for use in protein-polysaccharide conjugate vaccines and immunological reagents. II. Selective crosslinking of proteins to CDAP-activated polysaccharides. Vaccine. 2000; 18(13):1273–81. Epub 2000/01/29. PMID: 10649629

57. Kaur D, Lowary TL, Vissa VD, Crick DC, Brennan PJ. Characterization of the epitope of anti-lipoarabinomannan antibodies as the terminal hexaarabinofuranosyl motif of mycobacterial arabinans. Microbiol-Sgm. 2002; 148:3049–57.

58. Rademacher C, Shoemaker GK, Kim HS, Zheng RB, Taha H, Liu C, et al. Ligand specificity of CS-35, a monoclonal antibody that recognizes mycobacterial lipoarabinomannan: A model system for oligofuranoside—protein recognition. J Am Chem Soc. 2007; 129(34):10489–502. https://doi.org/10.1021/ja0723380 PMID: 17672460

59. Murase T, Zheng RB, Joe M, Bai Y, Marcus SL, Lowary TL, et al. Structural Insights into Antibody Recognition of Mycobacterial Polysaccharides. Journal of Molecular Biology. 2009; 392(2):381–92. https://doi.org/10.1016/j.jmb.2009.06.074 PMID: 19577573

60. Kamath VP, Diedrich P, Hindsgaul O. Use of diethyl squarate for the coupling of oligosaccharide amines to carrier proteins and characterization of the resulting neoglycoproteins by MALDI-TOF mass spectrometry. Glycoconjugate journal. 1996; 13(2):315–9. PMID: 8737256

61. Campbell CT, Zhang Y, Gildersleeve JC. Construction and use of glycan microarrays. Current protocols in chemical biology. 2010; 2(1):37–53. Epub 2010/03/01. https://doi.org/10.1002/9780470559277.ch090228 PMID: 23836542

62. Navoa JA, Laal S, Pirofski LA, McLean GR, Dai Z, Robbins JB, et al. Specificity and diversity of antibodies to Mycobacterium tuberculosis arabinomannan. Clinical and diagnostic laboratory immunology. 2003; 10(1):88–94. Epub 2003/01/11. PubMed Central PMCID: PMC145285. https://doi.org/10.1128/CDLI.10.1.88-94.2003 PMID: 12522045

63. Varki A, Cummings RD, Aebi M, Packer NH, Seeberger PH, Esko JD, et al. Symbol Nomenclature for Graphical Representations of Glycans. Glycobiology. 2015; 25(12):1323–4. PubMed Central PMCID: PMCPMC4643639. https://doi.org/10.1093/glycob/cwv091 PMID: 26543186

64. Vilcheze C, Weinrick B, Wong KW, Chen B, Jacobs WR Jr. NAD+ auxotrophy is bacteriocidal for the tubercle bacilli. Mol Microbiol. 2010; 76(2):365–77. PubMed Central PMCID: PMC2945688. https://doi.org/10.1111/j.1365-2958.2010.07099.x PMID: 20199601

65. Vilcheze C, Jacobs WR. Isolation and analysis of Mycobacterium tuberculosis mycolic acids. Curr Protoc Microbiol. 2007;Chapter 10:Unit 10A 3.

66. Salem ML, Al-Khami AA, El-Naggar SA, Diaz-Montero CM, Chen Y, Cole DJ. Cyclophosphamide induces dynamic alterations in the host microenvironments resulting in a Flt3 ligand-dependent expansion of dendritic cells. J Immunol. 2010; 184(4):1737–47. PubMed Central PMCID: PMCPMC3066076. https://doi.org/10.4049/jimmunol.0902309 PMID: 20083664

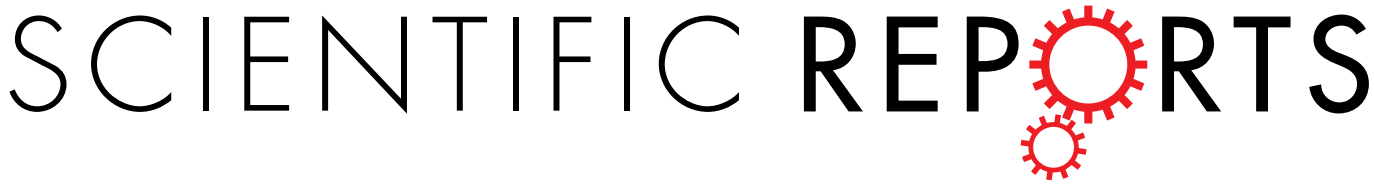

OPEN

Ikaros mediates the DNA methylation-independent silencing of *MCJ/DNAJC15* gene expression in macrophages

Received: 08 April 2015
Accepted: 04 September 2015
Published: 30 September 2015

Nicolás Navasa[1,2], Itziar Martin-Ruiz[2], Estíbaliz Atondo[2], James D. Sutherland[2], Miguel Angel Pascual-Itoiz[2], Ana Carreras-González[2], Hooman Izadi[1], Julen Tomás-Cortázar[2], Furkan Ayaz[1], Natalia Martin-Martin[2], Iviana M. Torres[1,†], Rosa Barrio[2], Arkaitz Carracedo[2,3,4], Elias R. Olivera[5], Mercedes Rincón[6] & Juan Anguita[1,2,3]

MCJ (DNAJC15) is a mitochondrial protein that regulates the mitochondrial metabolic status of macrophages and their response to inflammatory stimuli. CpG island methylation in cancer cells constitutes the only mechanism identified for the regulation of *MCJ* gene expression. However, whether DNA methylation or transcriptional regulation mechanisms are involved in the physiological control of this gene expression in non-tumor cells remains unknown. We now demonstrate a mechanism of regulation of MCJ expression that is independent of DNA methylation. IFNγ, a protective cytokine against cardiac inflammation during Lyme borreliosis, represses MCJ transcription in macrophages. The transcriptional regulator, Ikaros, binds to the MCJ promoter in a Casein kinase II-dependent manner, and mediates the repression of *MCJ* expression. These results identify the *MCJ* gene as a transcriptional target of IFNγ and provide evidence of the dynamic adaptation of normal tissues to changes in the environment as a way to adapt metabolically to new conditions.

MCJ (Methylation-Controlled J protein), also known as DNAJC15, is a small protein (147 aa) that contains a highly conserved 70 aa J domain at the C-terminus, an unusual transmembrane domain, and an N-terminal region with no homology to any other known protein[1–3]. The *MCJ* gene originated as a gene-duplication from the related gene *DnaJC19*, already present in flies[2]. MCJ is located in the inner mitochondrial membrane where it interacts with Complex I of the electron transport chain (ETC), interfering with the formation of supercomplexes composed of complexes I, III and IV[4,5]. MCJ is the first described endogenous negative regulator of Complex I that has also been associated with the TIM23 translocase and the import of pre-proteins to the mitochondria[3]. Silencing MCJ expression does not affect cell survival or proliferation[5]. However, loss of MCJ results in augmented mitochondrial membrane potential, increased oxidative respiration and mitochondrial ATP[5]. Although MCJ deficiency has no harmful effects under physiological conditions, increased mitochondrial metabolism in the absence of MCJ *in vivo* prevents the pathological accumulation of lipids in the liver during starvation or high cholesterol diet, and the development of liver steatosis[5]. MCJ is thus a modulator of mitochondrial

[1]Department of Veterinary and Animal Sciences. University of Massachusetts Amherst. Amherst, MA 01003. [2]CIC bioGUNE. 48160 Derio, Bizkaia, Spain. [3]Ikerbasque, Basque Foundation for Science. 48011 Bilbao, Bizkaia, Spain. [4]Biochemistry and Molecular Biology Department, University of the Basque Country (UPV/EHU), P. O. Box 644, E-48080 Bilbao, Spain. [5]Department of Molecular Biology, Veterinary School, University of León. 24071 León, Spain. [6]Department of Medicine. University of Vermont College of Medicine. Burlington, VT 05405. [†]Present address: Department of Microbiology and Immunology, Dartmouth School of Medicine, Hanover, NH 03755. Correspondence and requests for materials should be addressed to J.A. (email: janguita@cicbiogune.es)

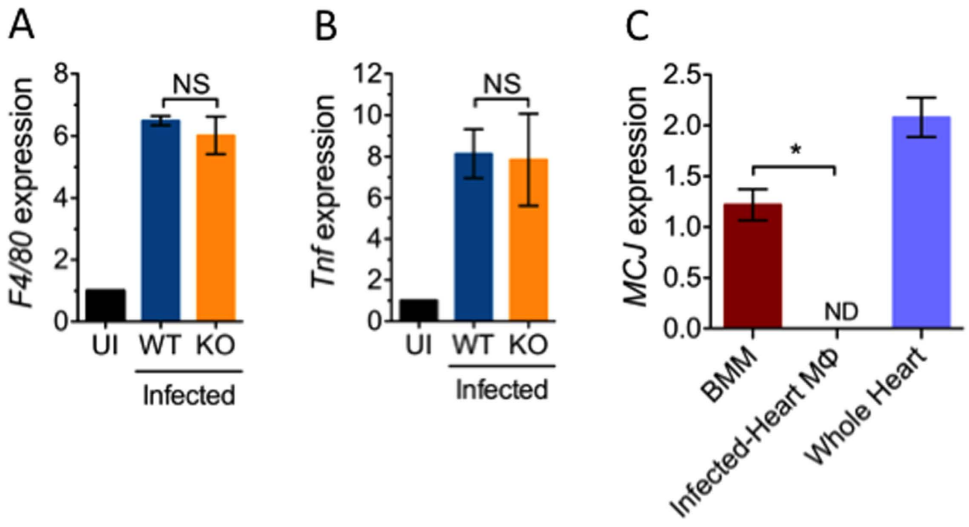

Figure 1. Heart-infiltrating macrophages do not express MCJ upon infection with *B. burgdorferi*. The base of the hearts of 3 week infected and uninfected (UI) mice were used to extract RNA and assess macrophage infiltration and TNF expression levels by qRT-PCR using primers specific for *F4/80* (**A**) or *TNF* (**B**). NS; Not significant. (**C**) Macrophages were purified from the hearts of 3-week infected B6 mice and used to extract RNA. qRT-PCR was then performed to detect *MCJ* mRNA levels, compared to bone marrow-derived macrophages (BMM). As a control, MCJ mRNA levels were also determined in whole heart tissue of 3-week infected mice. The data shown correspond to 5 mice per group and are presented as the mean ± SE. *; Student´s t test, $p < 0.05$.

metabolism that acts as a break to attenuate mitochondrial metabolism during adaptation to metabolic stress conditions.

MCJ was initially identified as a gene expressed in some but not all ovarian cancer cell lines and primary ovarian cancer tumors[6]. MCJ is expressed in breast and uterine cancer cells that are sensitive to different chemotherapeutic drugs, but not in those that are multidrug resistant[2,6]. In normal human and murine tissues, MCJ is highly expressed in heart, liver and kidney and within the immune system, in $CD8^+$ T cells and macrophages[2,7]. DNA methylation constitutes the only mechanism associated with the regulation of MCJ expression. In ovarian cancer cells, the presence of high levels of CpG island methylation within the first exon of the *MCJ* gene is associated with loss of expression and correlates with a diminished response to chemotherapy and poor survival[1,6,8–10]. However, the mechanisms that regulate MCJ expression in normal tissues and cells are not known.

We have shown that MCJ modulates macrophage responses to a variety of proinflammatory insults[7]. Short-term induction of inflammation by infection with *Staphylococcus aureus* or injection with LPS prevented TNF production *in vivo* and the development of acute fulminant hepatitis in mice in the absence of MCJ[7]. MCJ is therefore, a potential therapeutic target under conditions of persistent inflammation. Here, we report that IFNγ regulates the expression of MCJ in macrophages through a mechanism that involves the transcriptional regulator, Ikaros. These data demonstrate a novel mechanism of *MCJ* gene expression regulation that is independent of DNA methylation.

Results and Discussion

Loss of MCJ expression in heart-infiltrating macrophages during infection with *B. burgdorferi*. During short-term *in vivo* inflammatory conditions, MCJ regulates the response of macrophages to *Staphylococcus aureus* as well as LPS treatment in mice sensitized with galactosamine [7]. In order to determine the role of MCJ on the local macrophage response during an infectious process that requires a more complex and long lasting interaction between the pathogen and the host, we infected MCJ KO and WT mice with *Borrelia burgdorferi*. After 3 weeks of infection, macrophage infiltration was not significantly different in infected MCJ KO mice and WT animals (Fig. 1A). In addition, the amount of TNF expressed in the cardiac tissue upon infection was not altered in the absence or presence of MCJ (Fig. 1B). We also assessed the level of expression of MCJ in heart-infiltrating macrophages at the peak of infection with the spirochete. Surprisingly, in contrast to bone marrow-derived macrophages (BMMs), real time RT-PCR failed to detect appreciable levels of *MCJ* mRNA in macrophages infiltrating the hearts (Fig. 1C). The downregulation of MCJ expression during infection was selective of macrophages since total heart *MCJ* expression levels were readily detected in the infected mice (Fig. 1C). The histological analysis of infected joint and heart tissue showed that the degree of cardiac inflammation was not affected by the lack of the *MCJ* gene (Fig. S1A,B). Furthermore, the levels of spirochetal DNA were similar in

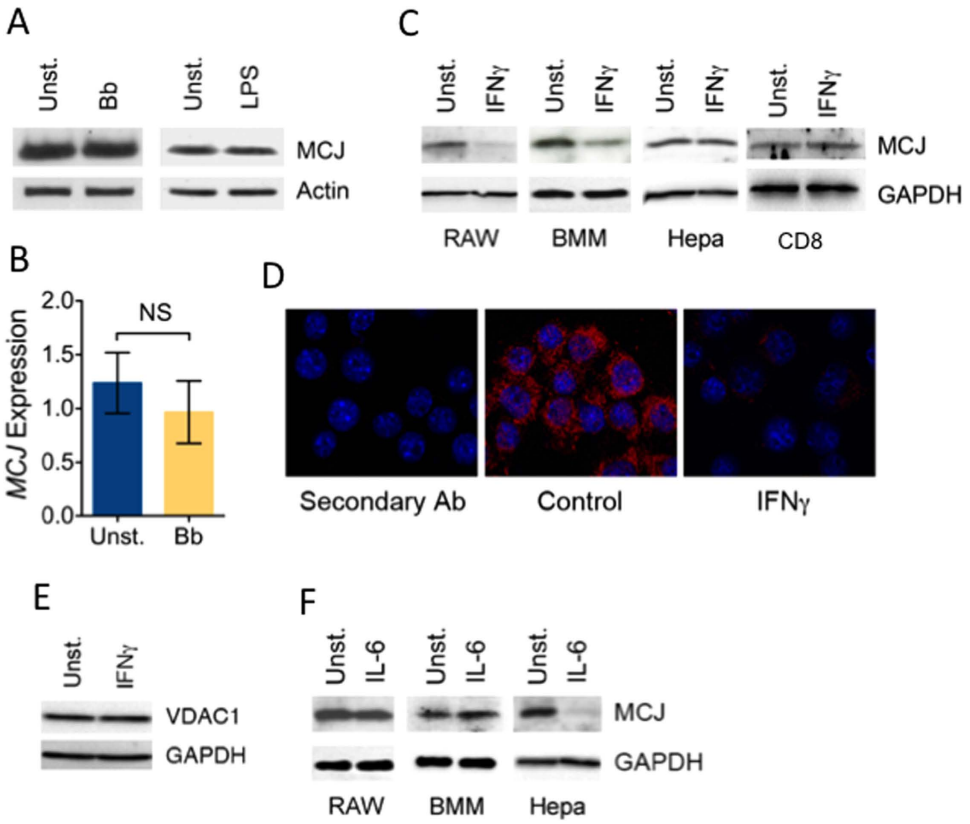

Figure 2. IFNγ induces the repression of MCJ in macrophages. (**A**) RAW cells were stimulated with live *B. burgdorferi* (m.o.i = 25) or 100 ng/mL of LPS for 16 h and analyzed by immunoblotting for MCJ protein levels. Actin levels were determined to ensure equal loads. (**B**) BMMs were stimulated with live *B. burgdorferi* for 16 h and analyzed for *MCJ* mRNA levels by qRT-PCR. The data shown correspond to the mean ± SE of 3 points per group. (**C**) RAW cells (RAW), BMMs, Hepa 2–7 cells (Hepa) or $CD8^+$ T cells (CD8) were stimulated with 100 ng/mL of IFNγ for 24–48 h, followed by the analysis of MCJ protein levels by immunoblotting. GAPDH levels were determined to ensure equal protein loads. (**D**) RAW cells were stimulated for 72 h with 100 ng/mL of IFNγ in 8-well chamber slides, washed and stained for intracellular MCJ. The slides were analyzed by ApoTome fluorescence microscopy. (**E**) RAW cells stimulated with IFNγ were analyzed for the levels of the mitochondrial protein, VDAC1, by immunoblotting. (**F**) RAW, BMMs and Hepa cells were stimulated with 100 ng/mL of IL-6 for 24 h, followed by their analysis for MCJ protein content by immunoblotting.

WT and MCJ KO mice (Fig. S1C). These results suggested that upon infection with *B. burgdorferi*, *MCJ* expression is repressed specifically in macrophages infiltrating the heart.

MCJ expression in macrophages is selectively downregulated by IFNγ. In order to determine whether the interaction of macrophages with bacterial products results in reduced levels of MCJ, we stimulated RAW cells and BMMs with live *B. burgdorferi* and assessed the levels of MCJ. Stimulation with the spirochete did not affect MCJ protein (Fig. 2A) or mRNA (Fig. 2B) levels. LPS stimulation also failed to alter the levels of MCJ in macrophages (Fig. 2A). These data indicate that the regulation of the expression of MCJ occurs independently of pattern-recognition receptor (PRR) stimulation, including TLR4, TLR1/2 and other PRRs stimulated by the interaction of live *B. burgdorferi* with macrophages[11–15]. Since IFNγ is a major contributor to macrophage function during cardiac infection with *B. burgdorferi*[16,17], we stimulated macrophages with IFNγ. Treatment with IFNγ resulted in lower levels of MCJ protein in both RAW cells and BMMs (Fig. 2C,D). Because MCJ is localized in mitochondria, we examined the effect of IFNγ on mitochondrial mass; however, no difference was observed as determined by levels of the mitochondrial protein, VDAC1 (Fig. 2E). The effect of IFNγ was selective of macrophages, because it did not affect MCJ levels in the murine tumor cell line, Hepa 1–6 or primary $CD8^+$ T cells (Fig. 2C). IL-6 has been shown to downregulate MCJ levels in breast cancer cell lines[2]. Similarly, we found that IL-6 induced the downregulation of MCJ in Hepa liver cancer cells (Fig. 2F). However, IL-6 failed to downregulate MCJ expression in RAW cells or BMMs (Fig. 2F). These results show that *MCJ* expression in macrophages is selectively silenced by IFNγ.

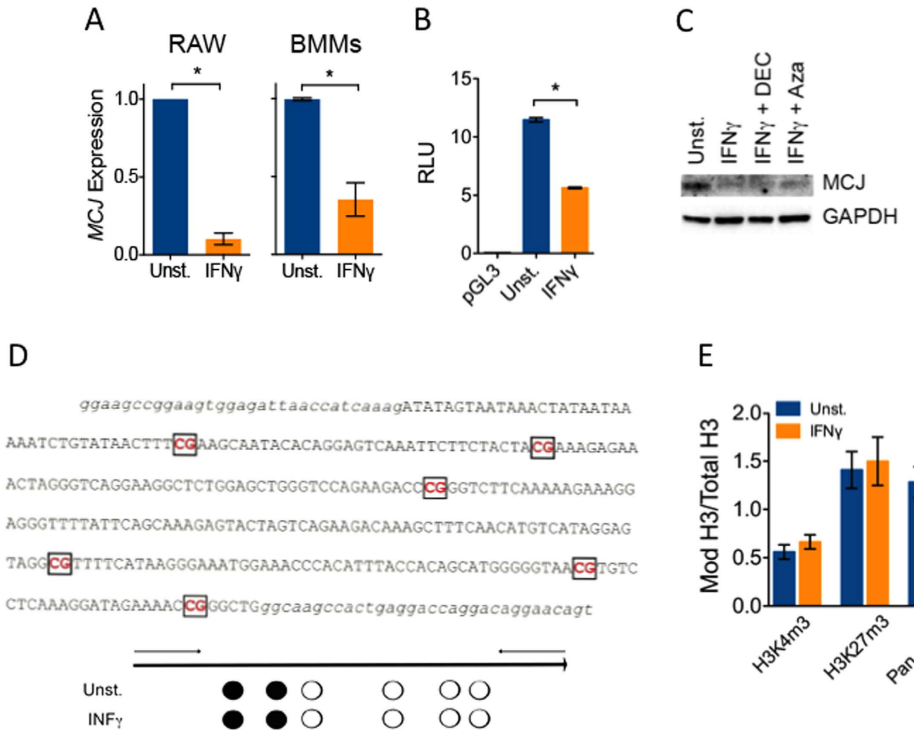

Figure 3. IFNγ represses *MCJ* gene expression independently of DNA methylation. (**A**) RAW cells and BMMs were stimulated for 20 h with IFNγ and analyzed by qRT-PCR for *MCJ* mRNA levels. The results correspond to the average of 3 independent experiments. *; Student´s t test, $p < 0.05$. (**B**) RAW cells were co-transfected with plasmids containing the luciferase gene under the influence of the 1 kb proximal promoter region of the *MCJ* gene or the Renilla luciferase gene under the influence of the SV40 promoter. After 4 h, the cells were stimulated with 100 ng/mL of IFNγ or left unstimulated. Dual luciferase activity was assessed after 16 h of incubation. The promoterless vector, pGL3 was used as a control. *; Student´s t test, $p < 0.05$. (**C**) BMMs were left unstimulated or stimulated with 100 ng/mL of IFNγ in the absence or presence of 1 μM of decitabine (DEC) or Azacitidine (Aza). After 48 h, the cells were tested by Western blotting for the presence of MCJ. GAPDH levels were determined to ensure equal loading. (**D**) CpG-rich region in the MCJ gene analyzed by bisulfite sequencing. The primers used for amplification are noted in lower case. The percentage of methylated CpG residues in BMMs stimulated with 100 ng/mL of IFNγ or left untreated is marked in each of the 6 CpG residues. Black circles indicate 100% of the samples contained these residues methylated, while white circles represent 0%. The analysis corresponds to BMMs isolated from 6 mice. (**E**) CHIP analysis of BMM DNA immunoprecipitated with antibodies against the H3 marks corresponding to trimethylation of Lys 4 (H3K4m3) and 27 (H3K27m3) or H3 pan-acetylation (Pan Ac-H3). The binding leves are relative to total H3. The results correspond to the average ± SE of 3 independent experiments.

IFNγ inhibits *MCJ* gene transcription independently of DNA methylation. To determine if the downregulation of MCJ protein levels by IFNγ in macrophages was due to an effect on MCJ gene expression, we assessed *MCJ* mRNA levels in macrophages stimulated with IFNγ. The treatment with IFNγ resulted in a significant decrease in *MCJ* mRNA levels in RAW cells and BMMs (Fig. 3A). No previous studies have characterized the human or mouse *MCJ* gene promoter region and addressed transcriptional regulation. We identified a 1 kb region upstream of the start initiation site of the murine *MCJ* gene (Fig. S2A), that was capable to mediate high levels of transcription in RAW cells in luciferase reporter assays (Fig. 3B). Treatment with IFNγ caused a pronounced decrease in the transcriptional activity of this region of the *MCJ* promoter (Fig. 3B).

The only described mechanism of regulation of *MCJ* involves the methylation of CpG rich regions of the gene[9]. Thus, we addressed whether IFNγ could silence *MCJ* expression through DNA methylation. BMMs were treated with IFNγ in the presence of the methylation inhibitors, decitabine (DEC) and 5-azacitidine (Aza). Both DEC and Aza failed to prevent the downregulation of *MCJ* expression by IFNγ (Fig. 3C). We also analyzed by bisulfite sequencing the methylation status of CpG residues present in the gene region identified as distinctively methylated between $CD8^+$ T and B cells[18] and that correlates with the level of expression of MCJ in these cells[5,7]. Six CpG residues were identified in this region (Fig. 3D). Of these, the first two were methylated in 100% of the BMMs samples analyzed (Fig. 3D). Importantly, the stimulation of BMMs with IFNγ did not affect the methylation of these CpG residues (Fig. 3D), indicating that IFNγ effect is independent of DNA methylation mechanisms. We further analyzed the

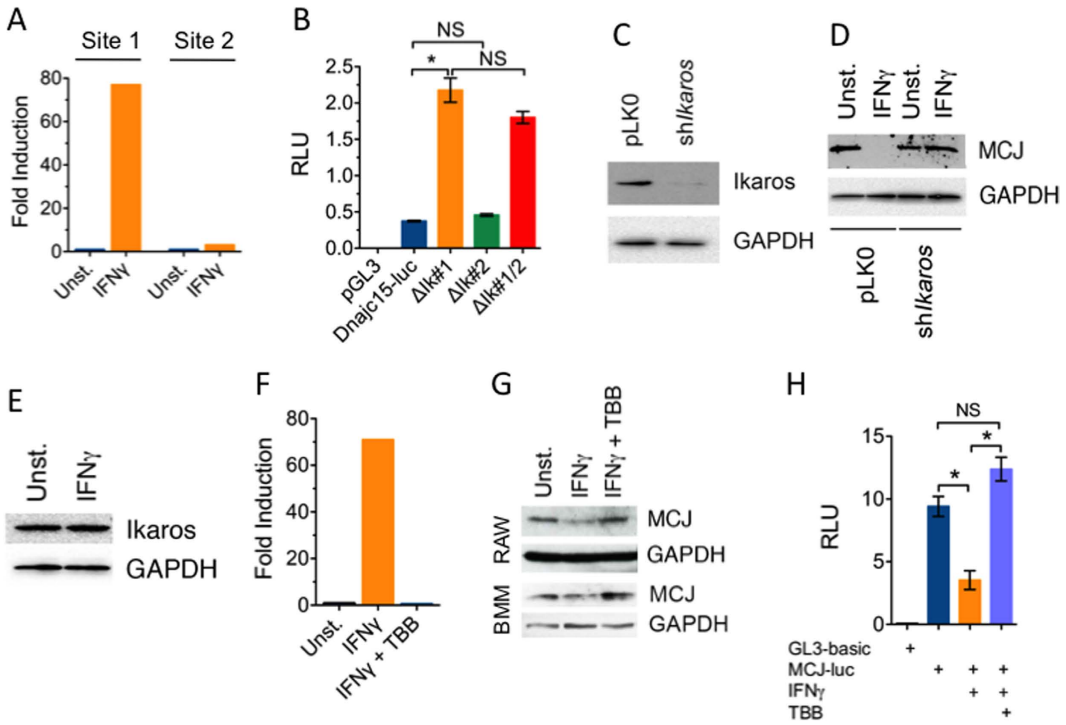

Figure 4. IFNγ induces the binding of Ikaros to the *MCJ* promoter through the activation of CK2. (**A**) Chromatin immunoprecipitation using an antibody specific for Ikaros. BMMs were stimulated with 100 ng/mL of IFNγ for 16 h or left unstimulated. Chromatin was processed and immunoprecipitated as described in Experimental Procedures. The values presented correspond to one experiment of 2 with similar results. (**B**) Luciferase activity driven by the 1 kb MCJ proximal promoter (MCJ-luc) and deletion mutants corresponding to Site 1 (ΔIk#1), Site 2 (ΔIk#2) or double mutants (ΔIK#1/2). The values correspond to the mean ± SE of triplicates and represent at least 3 independent experiments. *; Student´s T test, $p < 0.05$; NS; not significant. (**C**) Western blot showing silencing of Ikaros in RAW cells stably transduced with lentiviral particles containing a short hairpin (sh) specific for the Ikaros gene (sh*Ikzf1*). GAPDH levels were determined to ensure equal loads. (**D**) sh*Ikaros* cells and pLK0-transduced control cells were stimulated with 100 ng/mL of IFNγ or left stimulated for 24 h. The levels of MCJ were then determined by immunoblotting. (**E**) Levels of Ikaros in BMMs unstimulated or stimulated with 100 ng/mL of IFNγ for 24 h. The cells were l tested by immunoblotting using specific Ikaros antibodies. GAPDH levels were determined to ensure equal loads. (**F**) BMMs were stimulated with IFNγ in the presence or absence of TBB as before, and Ikaros binding was determined by chromatin immunoprecipitation. The values correspond to 1 of 2 experiments performed with similar results. (**G**) RAW cells and BMMs were stimulated with 100 ng/mL of IFNγ in the presence or absence of 50 μM of the CK2 inhibitor, 4,5,6,7-Tetrabromobenzotriazole (TBB), for 24 h, followed by MCJ protein level determination by immunoblotting. (**G**) RAW cells were co-transfected with the plasmids pGL3-MCJ-Luc plus pSV40-RenillaLuc. Four h later, the cells were stimulated with 100 ng/mL of IFNγ in the presence or absence of 50 μM TBB and 16 h later, assessed for luciferase levels. The values correspond to luciferase activity relative to Renilla luciferase in triplicate (mean ± SE) and represent one of at least 4 experiments performed. *; Student´s T test, $p < 0.05$; NS; not significant.

effect of IFNγ treatment on histone H3 marks associated with the activation and repression of gene expression (ref. 31). The treatment of BMMs with IFNγ did not affect the binding of thrimethylated H3 at Lys 4 and Lys 27 or acetylated H3 to the *MCJ* promoter (Fig. 3E). These data revealed that transcriptional regulation is an alternative mechanism of *MCJ* expression modulation that is independent of DNA methylation or alteration on histone marks.

Ikaros is an inducible repressor of MCJ gene transcription. To identify the specific mechanism by which IFNγ represses *MCJ* gene transcription, we performed a search for potential transcription factor binding sites within the 1kb region of the mouse *MCJ* gene promoter using the tool TFSearch[19]. Two consensus binding sites for Ikaros (−350 to −361 and −706 to −717) were identified (Fig. S2A). Ikaros is known to act primarily as a repressor of gene expression[20]. To demonstrate whether Ikaros binds to these putative binding sites in the *MCJ* promoter and address whether binding was regulated by IFNγ, we performed chromatin immunoprecipitation (ChIP) assays in BMMs. Binding of Ikaros to both sites was almost undetectable in untreated BMMs (Fig. 4A). However, Ikaros binding to Site 1 (the most proximal

to the transcription start site; Fig. S2A) was highly induced in cells treated with IFNγ (Fig. 4A). Ikaros binding to Site 2 (Fig. S2A), however, was not induced by IFNγ (Fig. 4A).

To further analyze the contribution of both putative Ikaros binding sites to the regulation of MCJ gene expression, we generated deletion mutants of both binding sites, as well as a double deletion mutant lacking both binding sites. The deletion of Site 1 resulted in significantly increased transcriptional activation in reporter assays (Fig. 4B) suggesting that this site is bound under basal conditions to a negative gene expression regulator. However, the deletion of Site 2 did not affect the expression activity of the promoter (Fig. 4B). Furthermore, the deletion of both sites resulted in transcriptional activity that was equivalent to that observed with the deletion of Site 1 (Fig. 4B). Overall, these data suggest that Ikaros binds to Site 1 upon induction with IFNγ and displaces a weaker negative regulator of gene expression.

To demonstrate the role of Ikaros in the IFNγ-dependent repression of *MCJ* gene expression, we generated stable lentiviral transductants containing a short hairpin sequence (shRNA) specific for the *IKFZ1* gene encoding Ikaros. Transduction with sh*IKFZ1* in RAW cells caused a prominent reduction of Ikaros levels (Fig. 4C). Importantly, while IFNγ downregulated MCJ levels in control cells, it did not affect MCJ levels in sh*IKFZ1*-transduced cells (Fig. 4D). These results demonstrate that silencing of MCJ expression by IFNγ is mediated by Ikaros and reveal this repressor as a key factor in the alternative mechanism regulating MCJ expression.

We then assessed whether IFNγ upregulates Ikaros expression. The stimulation with IFNγ did not affect Ikaros levels in macrophages (Fig. 4E), suggesting that the increased binding to the *MCJ* promoter region was due to post-translational modifications induced by IFNγ. Ikaros activity is regulated by phosphorylation mediated by Casein Kinase 2 (CK2)[21]. It has also been reported that IFNγ regulates the expression of a subset of genes through the activation of CK2[21,22]. To investigate whether IFNγ promotes Ikaros binding through CK2, cells were treated with IFNγ in the presence of a CK2 specific inhibitor, 4,5,6,7-tetrabromobenzotriazole (TBB)[23]. CHIP analysis demonstrated that the pretreatment with TBB abrogated IFNγ-induced binding of Ikaros to the *MCJ* promoter (Fig. 4F).

We then investigated whether silencing of MCJ expression by IFNγ was mediated by CK2. Pretreatment of macrophages with the CK2 inhibitor prevented downregulation of MCJ expression by IFNγ (Fig. 4G). In addition, inhibition of CK2 also prevented IFNγ from suppressing *MCJ* promoter transcriptional activity (Fig. 4H). Together, these results show that IFNγ represses *MCJ* gene transcription in macrophages by promoting CK2-dependent DNA binding of Ikaros to the proximal region of the MCJ promoter.

Our studies identify a novel mechanism of regulation of *MCJ* gene expression that is independent of the well-established DNA methylation pathway described in several tumors. MCJ/DnaJC15 is emerging as an important regulator of mitochondrial activity and cellular function *in vitro* and *in vivo*[5,7]. Therefore, the control of MCJ transcription constitutes a mechanism to regulate cellular responses to environmental changes. As opposed to DNA methylation, which is considered a long-term mechanism to silence gene expression[24], the transcriptional control of *MCJ* gene expression by Ikaros may allow normal tissues to adapt dynamically to a changing environment. Here, we demonstrate that Ikaros represses *MCJ* expression in response to IFNγ in macrophages. Similar mechanisms could be used to alter MCJ levels in other cells or tissues in response to changes in the environment as a way to adapt metabolically to new conditions.

Our results identify *MCJ* gene expression as a transcriptional target of the cytokine IFNγ, contributing to the regulation of their inflammatory output[7]. Our data also reinforces the role of IFNγ as a cytokine that exerts a protective effect during infection with *B. burgdorferi*[16,17,25]. Overall, we hypothesize that the combined effect of IFNγ, including the regulation of MCJ expression, results in a more efficient elimination of the bacteria from the infected tissue without a concomitant increase in the inflammatory damage.

Methods

Mice. MCJ-deficient mice in a C57Bl/6 (B6) background[5] and wild type B6 mice were bred at UMass Amherst and CIC bioGUNE. The Institutional Animal Care and Use Committees at UMass Amherst and CIC bioGUNE approved all procedures involving animals.

Infections. Groups of WT and KO mice were infected by subcutaneous injection with 10^5 *Borrelia burgdorferi* 297 in the midline of the back. The mice were sacrificed after 3 weeks of infection and analyzed for inflammatory symptoms in joints and hearts stained with hematoxilin and eosin. Signs of arthritis and carditis were determined blindly as described[26]. The number of spirochetes in heart tissue was determined by real-time PCR, using primers specific for the *recA* gene (Table S1) standardized to μg of total DNA with primers corresponding to Glyceraldehyde 3-Phosphate Dehydrogenase, *GAPDH*, (Table S1)[17].

Cells. Infiltrating cardiac macrophages were isolated from 3-week infected B6 mice. Hearts were perfused with cold Hank´s balanced salt solution (HBSS, Lonza, Anaheim, CA) and cut into small pieces, followed by digestion with 1 mg/mL of collagenase/dispase (Roche) and homogenization in a Dounce homogenizer. The digest was passaged through a 16" gauge syringe to obtain single cell suspensions. The cellular suspension was layered on top of a 3 mL layer of Ficoll (GE Healthcare, Piscataway, NJ) and centrifuged at 400 × g for 40 min without brakes. Monocytes were then purified from the interphasic

cellular fraction using a one-step discontinuous Percoll gradient (46%) under isosmotic conditions[27]. Monocytes were used for RNA extraction.

Bone marrow-derived macrophages were generated as described[17] using 30 ng/mL of M-CSF (Miltenyi Biotec, Bergisch Gladbach, GE). Macrophages were allowed to differentiate in 100 mm × 15 mm petri dishes (Fisher Scientific, Pittsburgh, PA) for 8 days. Non-adherent cells were then eliminated and adherent macrophages were scraped, counted and resuspended in serum-free RPMI medium 2 h prior to use.

$CD8^+$ T cells were purified by positive selection from the spleens of B6 mice using biotinylated anti-CD8 (BD Biosciences, San Diego, CA), anti-biotin microbeads and the MACS system (Miltenyi Biotec, Auburn, CA).

Lentiviral particles containing shRNA targeting Ikaros (*Ikzf1* gene, Sigma Chemical Co, St. Louis, MO) were produced as described[28]. Supernatants containing the virus were used to infect RAW 264.7 cells, followed by incubation with puromycin at 2 μg/mL to generate stable lines. Cells containing the empty vector, pLK0.1, were used as a control.

***In vitro* stimulation.** Cells were incubated with 100 ng/mL of murine IFNγ or human IL-6 for the indicated time periods. In some instances, the following inhibitors were used 1 h prior to stimulation: decitabine (DEC, 1mM), 4,5,6,7-tetrabromobenzotriazole (TBB, 1 μM; Tocris Bioscience, Bristol, UK), 5-Aza-2-Deoxycytidine (Aza, 1 μM; Sigma Chemical Co.). Stimulations with *B. burgdorferi* (m.o.i. = 25) or LPS (100 ng/mL) were performed for 4–6 h.

Real-time RT-PCR. RNA from isolated cells or cardiac tissue was extracted by the thioisocyanate method (Amresco, Solon, OH), treated with DNase I (Qiagen), and reverse transcribed using the SuperScript VILO cDNA synthesis kit (Life Technologies). Real-time PCR was then performed using SYBR Green PCR Master Mix (Life Technologies) on a BioRad CFX96 Real-Time System (Bio-Rad, Hercules, CA). Fold induction of the genes was calculated relative to actin, using the $2^{-\Delta\Delta Ct}$ method. The primers used are listed in Table S1.

Western blot. Five to 20 μg of protein were run on SDS-PAGE, transferred to nitrocellulose membranes and tested with antibodies specific for MCJ[5], VDAC1 (D-16) and Ikaros (M-20, Santa Cruz Biotechnology, Dallas, TX). Equal loading was determined using antibodies against GAPDH (6C5) or actin (I-19) from Santa Cruz Biotechnology.

Epifluorescence (Apotome) microscopy. Cells were grown in 8-well chamber slides (Nunc Thermo Scientific, Waltham, MA). Upon incubation with 100 ng/mL of IFNγ (eBioScience, San Diego, CA) for 3 days, the cells were processed as described[29] using anti-MCJ Abs, followed by an anti-rabbit IgG conjugated to Alexa Fluor 594.

Cloning of the proximal 1 kb MCJ promoter and luciferase assays. The proximal 1 kb promoter of the murine *MCJ* gene was cloned into pGL3 using the primers in Table S1. Deletion mutants corresponding to the putative Ikaros binding sites of the *MCJ* promoter (Fig. S2) were generated using the QuickChange Site-Directed Mutagenesis kit (Stratagene, La Jolla, CA) and the primers listed in Table S1. 1.9 μg of these constructs plus 0.1 μg of pSVL40 plasmid were cotransfected into RAW cells using the X-TremeGene HP DNA tranfection reagent (Roche). After 6h, the cells were treated with IFNγ in the presence or absence of the specific inhibitor, TBB. After 20 hr incubation, the cells were lysed in lysis buffer (Promega, Madison, WI) and Firefly and Renilla luciferase activities were determined by the Dual Luciferase reporter system (Promega).

Bisulfite sequencing. DNA was extracted from BMMs treated with IFNγ and controls, denatured and subjected to bisulphite conversion as described by Clark and colleagues[30]. The resultant product was PCR amplified using the primers in Table S1, corresponding to the region in the *MCJ* gene described by Meissner and colleagues[18].

Chromatin immunoprecipitation. Fifteen million BMMs were stimulated with 100 ng/mL of IFNγ in the presence or absence of TBB for 16h. CHIP assays were performed using the SimpleChip Enzymatic Chromatin IP kit-Magnetic beads (Cell Signaling, Beverly, MA) following the manufacturer´s instructions using anti-Ikaros, anti-H3K4m3, anti-H3K27m3, anti-pan acetylated H3 antibodies and anti-H3 (Cell Signaling) or normal rabbit IgG as negative control. The immunoprecipitated DNA was subjected to q-PCR using primers encompassing the two putative Ikaros binding sites (Table S1). The results are presented as fold induction over rabbit IgG immunoprecipitates or total H3 relative to input (percent input method), following the formula: $\frac{100x2^{(Adjinput-Ct_{TEST})}}{100x2^{(Adjinput-Ct_{IgG})}} = 2^{-\left(Ct_{TEST}-Ct_{IgG}\right)}$, where AdjInput = Adjusted input to 100%; Ct_{TEST} = Ct of test samples; Ct_{IgG} = Ct of samples control.

Statistical Analysis. Results are presented as means ± SE. Significant differences between means were calculated with the Student's t test. P values of 0.05 or less were considered statistically significant.

References

1. Lindsey, J. C. *et al.* Epigenetic inactivation of MCJ (DNAJD1) in malignant paediatric brain tumours. *Int J Cancer* **118,** 346–352 (2006).
2. Hatle, K. M. *et al.* Methylation-controlled J protein promotes c-Jun degradation to prevent ABCB1 transporter expression. *Mol Cell Biol* **27,** 2952–2966 (2007).
3. Schusdziarra, C., Blamowska, M., Azem, A. & Hell, K. Methylation-controlled J-protein MCJ acts in the import of proteins into human mitochondria. *Human molecular genetics* **22,** 1348–1357 (2013).
4. Roy, A. *et al.* Mitochondria-dependent reactive oxygen species-mediated programmed cell death induced by 3,3′-diindolylmethane through inhibition of F0F1-ATP synthase in unicellular protozoan parasite Leishmania donovani. *Mol Pharmacol* **74,** 1292–1307 (2008).
5. Hatle, K. M. *et al.* MCJ/DnaJC15, an endogenous mitochondrial repressor of the respiratory chain that controls metabolic alterations. *Mol Cell Biol* **33,** 2302–2314 (2013).
6. Shridhar, V. *et al.* Loss of expression of a new member of the DNAJ protein family confers resistance to chemotherapeutic agents used in the treatment of ovarian cancer. *Cancer Res* **61,** 4258–4265 (2001).
7. Navasa, N. *et al.* Regulation of oxidative stress by methylation-controlled j protein controls macrophage responses to inflammatory insults. *J Infect Dis* **211,** 135–145 (2015).
8. Strathdee, G. *et al.* Demethylation of the MCJ gene in stage III/IV epithelial ovarian cancer and response to chemotherapy. *Gynecol Oncol* **97,** 898–903 (2005).
9. Strathdee, G., Davies, B. R., Vass, J. K., Siddiqui, N. & Brown, R. Cell type-specific methylation of an intronic CpG island controls expression of the MCJ gene. *Carcinogenesis* **25,** 693–701 (2004).
10. Ehrlich, M. *et al.* Hypomethylation and hypermethylation of DNA in Wilms tumors. *Oncogene* **21,** 6694–6702 (2002).
11. Alexopoulou, L. *et al.* Hyporesponsiveness to vaccination with *Borrelia burgdorferi* OspA in humans and in TLR1- and TLR2-deficient mice. *Nature Medicine* **8,** 878–884 (2002).
12. Behera, A. K. *et al. Borrelia burgdorferi* BBB07 interaction with integrin alpha3beta1 stimulates production of pro-inflammatory mediators in primary human chondrocytes. *Cell Microbiol* **10,** 320–331 (2008).
13. Behera, A. K. *et al.* Identification of a TLR-independent pathway for *Borrelia burgdorferi*-induced expression of matrix metalloproteinases and inflammatory mediators through binding to integrin alpha 3 beta 1. *J Immunol* **177,** 657–664 (2006).
14. Cervantes, J. L. *et al.* Phagosomal signaling by *Borrelia burgdorferi* in human monocytes involves Toll-like receptor (TLR) 2 and TLR8 cooperativity and TLR8-mediated induction of IFN-{beta}. *Proc Natl Acad Sci USA* **108,** 3683–3688 (2011).
15. Petzke, M. M., Brooks, A., Krupna, M. A., Mordue, D. & Schwartz, I. Recognition of *Borrelia burgdorferi*, the Lyme disease spirochete, by TLR7 and TLR9 induces a type I IFN response by human immune cells. *J Immunol* **183,** 5279–5292 (2009).
16. Brown, C. R., Blaho, V. A., Fritsche, K. L. & Loiacono, C. M. Stat1 deficiency exacerbates carditis but not arthritis during experimental lyme borreliosis. *J Interferon Cytokine Res.* **26,** 390–399 (2006).
17. Olson, C. *et al.* Local Production of IFN-gamma by Invariant NKT Cells Modulates Acute Lyme Carditis. *Journal of Immunology* **182,** 3728–3734 (2009).
18. Meissner, A. *et al.* Genome-scale DNA methylation maps of pluripotent and differentiated cells. *Nature* **454,** 766–770 (2008).
19. Kast, C., Wang, M. & Whiteway, M. The ERK/MAPK pathway regulates the activity of the human tissue factor pathway inhibitor-2 promoter. *J Biol Chem* **278,** 6787–6794 (2003).
20. John, L. B. & Ward, A. C. The Ikaros gene family: transcriptional regulators of hematopoiesis and immunity. *Mol Immunol* **48,** 1272–1278 (2011).
21. Cho, S. J., Huh, J. E., Song, J., Rhee, D. K. & Pyo, S. Ikaros negatively regulates inducible nitric oxide synthase expression in macrophages: involvement of Ikaros phosphorylation by casein kinase 2. *Cell Mol Life Sci* **65,** 3290–3303 (2008).
22. Harris, S. M., Harvey, E. J., Hughes, T. R. & Ramji, D. P. The interferon-gamma-mediated inhibition of lipoprotein lipase gene transcription in macrophages involves casein kinase 2- and phosphoinositide-3-kinase-mediated regulation of transcription factors Sp1 and Sp3. *Cell Signal* **20,** 2296–2301 (2008).
23. Qaiser, F. *et al.* Protein kinase CK2 inhibition induces cell death via early impact on mitochondrial function. *J Cell Biochem* **115,** 2103–2115 (2014).
24. Raynal, N. J. *et al.* DNA methylation does not stably lock gene expression but instead serves as a molecular mark for gene silencing memory. *Cancer Res* **72,** 1170–1181 (2012).
25. Bockenstedt, L. K. *et al.* $CD4^+$ T helper 1 cells facilitate regression of murine Lyme carditis. *Infect Immun* **69,** 5264–5269 (2001).
26. Hawley, K. *et al.* Macrophage p38 Mitogen-Activated Protein Kinase Activity Regulates Invariant Natural Killer T-Cell Responses During *Borrelia burgdorferi* Infection. *Journal of Infectious Diseases* **206,** 283–291 (2012).
27. Fincato, G., Polentarutti, N., Sica, A., Mantovani, A. & Colotta, F. Expression of a heat-inducible gene of the HSP70 family in human myelomonocytic cells: regulation by bacterial products and cytokines. *Blood* **77,** 579–586 (1991).
28. Garcia-Cao, I. *et al.* Systemic elevation of PTEN induces a tumor-suppressive metabolic state. *Cell* **149,** 49–62 (2012).
29. Hawley, K. L. *et al.* CD14 cooperates with complement receptor 3 to mediate MyD88-independent phagocytosis of *Borrelia burgdorferi*. *Proceedings of the National Academy of Sciences of the United States of America* **109,** 1228–1232 (2012).
30. Clark, S. J., Statham, A., Stirzaker, C., Molloy, P. L. & Frommer, M. DNA methylation: bisulphite modification and analysis. *Nat Protoc* **1,** 2353–2364 (2006).
31. LB Ivashkiv *et al.* Epigenetic regulation of macrophage polarization and function. *Trends in Immunology* **34:** 216–222.

Acknowledgements

We thank JM Iglesias-Pedraz for technical support. Supported by grants from the National Institutes of Health (AI-078277 to JA, and CA-127099 to MR), the Spanish Ministry of Economy Plan Nacional (SAF2012-34610 to JA, BFU2011-25986 to RB and JDS), Basque Government Depts. of Industry, Tourism and Trade (Etortek to AC), Health (2012111086 to AC) and Education (PI2012-03 to AC, and PI2012/42 to RB and JDS), Instituto de Salud Carlos III (PI10/01484 and PI13/00031 to AC), Marie Curie (277043 to AC), and ERC (336343 to AC). AC is supported by a Ramón y Cajal Award. N.M.M. is supported by the Spanish Association Against Cancer (AECC).

Author Contributions

N.N., I.M.M., E.A., J.D.S., M.A.P.I., A.C.G., H.I., J.T.C., F.A. and I.M.T. performed the experiments. N.M.M. and A.C. helped with lentiviral production and transduction experiments. R.B., A.C., E.R.O. and

M.R. provided reagents and helped in the analysis of the data. N.N., M.R. and J.A. wrote the manuscript. J.A. designed the study.

Additional Information

Supplementary information accompanies this paper at http://www.nature.com/srep

Competing financial interests: The authors declare no competing financial interests.

How to cite this article: Navasa, N. *et al.* Ikaros mediates the DNA methylation-independent silencing of *MCJ/DNAJC15* gene expression in macrophages. *Sci. Rep.* **5**, 14692; doi: 10.1038/srep14692 (2015).